SAINT PETERSBURG STATE UNIVERSITY

*Manuscript copyright*

Torilov Sergey Yurievich

# Cluster degrees of freedom in nuclei

Scientific specialty 1.3.15. – Physics of atomic nuclei and elementary particles, high energy physics

Dissertation for the degree of
Doctor of Physical and Mathematical Sciences
Translation from Russian

Saint Petersburg
2025

# Contents

Introduction . . . . . 3
Chapter 1. Methods of description and study of cluster states . . . . . 20
1.1. Model of binding $\alpha$-particles . . . . . 21
1.1.1. Geometric model . . . . . 22
1.1.2. Chain configurations . . . . . 30
1.1.3. Bose-Einstein condensate in nuclei . . . . . 35
1.2. Two-particle model . . . . . 41
1.2.1. Tunneling . . . . . 42
1.2.2. Potential model in an elastic channel . . . . . 43
1.3. Reactions . . . . . 50
1.3.1. Elastic scattering . . . . . 50
1.3.2. Transfer reactions . . . . . 56
1.3.3. Quasi-free scattering . . . . . 59
1.3.4. Processes of decay of an excited system . . . . . 61
Chapter 2. Experimental methods . . . . . 62
Chapter 3. Spectroscopy of light neutron-rich nuclei . . . . . 66
3.1. Isotopes of helium . . . . . 66
3.1.1. Aims and Methods of the Study . . . . . 66
3.1.2. Results obtained. . . . . 72
3.2. Beryllium isotopes . . . . . 72
3.2.1. Aims and Methods of the Study . . . . . 75
3.2.2. Results obtained . . . . . 79
3.3. Carbon isotopes . . . . . 79
3.3.1. Aims and Methods of the Study . . . . . 80
3.3.2. Results obtained . . . . . 83
3.4. Oxygen isotopes . . . . . 83
3.4.1. Aims and Methods of the Study . . . . . 86
3.4.2. Results obtained . . . . . 87
3.5. Isotopes of neon . . . . . 88
3.5.1. Aims and Methods of the Study . . . . . 90

3.5.2. Results obtained . . . . . 96
3.6. Magnesium . . . . . 98
3.7. Silicon and Sulfur . . . . . 111
3.8. Argon . . . . . 111
3.9. Calcium . . . . . 113
3.10. Heavy nuclei and clusters . . . . . 120
Chapter 4. Cluster transfer in elastic scattering . . . . . 129
4.1. Reaction $^{16}$O+$^{20}$Ne . . . . . 130
4.2. Reaction $^{10,11}$B+$^{15}$N . . . . . 132
Chapter 5. Reactions with heavy cluster escape . . . . . 136
Chapter 6. Systematics of interaction of heavy clusters within the framework of a potential model . . . . . 150
6.1. Elastic interaction . . . . . 150
6.2. Model . . . . . 151
6.3. Analysis . . . . . 157
Chapter 7. Fusion reactions in the cluster approximation . . . . . 160
7.1. Cluster states in astrophysics problems . . . . . 160
7.2. Reactions in Nuclear Astrophysics . . . . . 163
7.3. Interaction Potential . . . . . 165
7.4. Description of quasi-bound states in the framework of the potential model . . . . . 171
7.5. Rotational bands in the heavy ion system . . . . . 173
7.6. Determination of the astrophysical $S$-factor for the cluster approximation in the framework of the rectangular potential well model . . . . . 177
Conclusion . . . . . 185
Bibliography . . . . . 188
Appendix . . . . . 222

# Introduction

## The relevance of the topic

The two simplest of the existing nuclear models assume diametrically opposite approaches to the description of the structure of the nucleus and the properties of nuclear matter. On the one hand, a good description of such collective properties of the nucleus as, for example, the binding energy, is given by the droplet model, which assumes a strong interaction between the nucleons composing the nucleus. On the other hand– the simplest microscopic model of the nucleus, assuming the motion of non-interacting nucleons in a self-consistent nuclear field. This model was constructed by analogy with the Bohr model of the atom and can satisfactorily describe some properties of low-lying states, explain the appearance of magic numbers, etc.

Attempts to improve both models, endowing one with elements of the other, often lead to an increasing number of parameters requiring additional definition (as, for example, shell corrections in the drop model) or lead to significant complications of calculations when trying to describe a wide class of phenomena associated with the appearance of multiparticle configurations. As follows directly from the shell model, the two-particle forces must lead to local correlations in the distribution of nucleons that are not accounted for by the central field approximation.

One of the formal possibilities to take into account the action of residual forces is to divide the considered nuclear system into a set of clusters – interacting objects whose internal structure is neglected, which leads to the possibility of explaining and predicting a number of phenomena in the physics of the nucleus. The importance of considering cluster degrees of freedom in describing the structure of nuclei is demonstrated by the fact that one of the first models of the nucleus assumed a quasicrystalline structure, where $\alpha$-particles were considered as constituent elements (the very first model of this kind appeared before the discovery of the neutron!). The reason for the appearance of such a model was both data on the $\alpha$-decay of heavy elements and purely energetic, based on the analysis of binding energies of the light nuclei known at that time, considerations.

Indeed, the $\alpha$-particle is a very stable nucleus due to the simple configuration of its constituent nucleons – they are in the same spatial state but in different spin and charge states. The $\alpha$-particle has large nucleon binding energies and the energy of the first excited state. All this makes the $\alpha$-particle an ideal candidate for the role of a structureless cluster. In addition, the increased stability of self-conjugate nuclei (i.e., nuclei in which the number of protons is even and equal to the number of neutrons) is also observed.

Thus, the assumption that it is possible (and even necessary) to take into account the $\alpha$-cluster component when discussing the structure of the nucleus led Wheeler in 1937 to the creation of one of the first cluster models. The fact that larger structures than nucleons were used in the description of nuclei was reflected in the title of the paper, indicating a molecular-like description: `Molecular Viewpoints in Nuclear Structure` [1]. Since it was already clear at that time that the Pauli principle does not allow the presence of $\alpha$-particles in the high-density region at the center of the nucleus, where the antisymmetrization effects lead to the nucleons, in general, occupying a certain state in accordance with the nuclear shell model, a mechanism was needed to circumvent this condition. According to Wheeler's proposal, $\alpha$-particles in the nucleus can be considered as quasi-stable formations, i.e., there is a high probability of finding a group of nucleons localized in some region of space and sufficiently distant from other such groups. In this model, an important notion of *bonding* between $\alpha$-particles was introduced. In the simplest case, if one considers a fixed arrangement of $\alpha$-particles in space, the number of bonds is the number of shortest distances between $\alpha$-particles along which their interaction takes place. The model seemed promising and soon, in collaboration with Teller, it was extended to describe the rotational properties of nuclei [2]. Further, an contribution from of neutron excess (deficiency) was proposed. The model was proposed by Hafstad and Teller and was already called `The Alpha-Particle Model of the Nucleus` [3]. Figure 1 shows a plot of the bonding energy versus bond number obtained in [3]. The calculations were performed by the authors for the nuclei known at that time, and the geometrical structure was determined from the conditions of close-packing of $\alpha$-particles, which, in the first approximation, corresponded to a quasi-crystalline structure

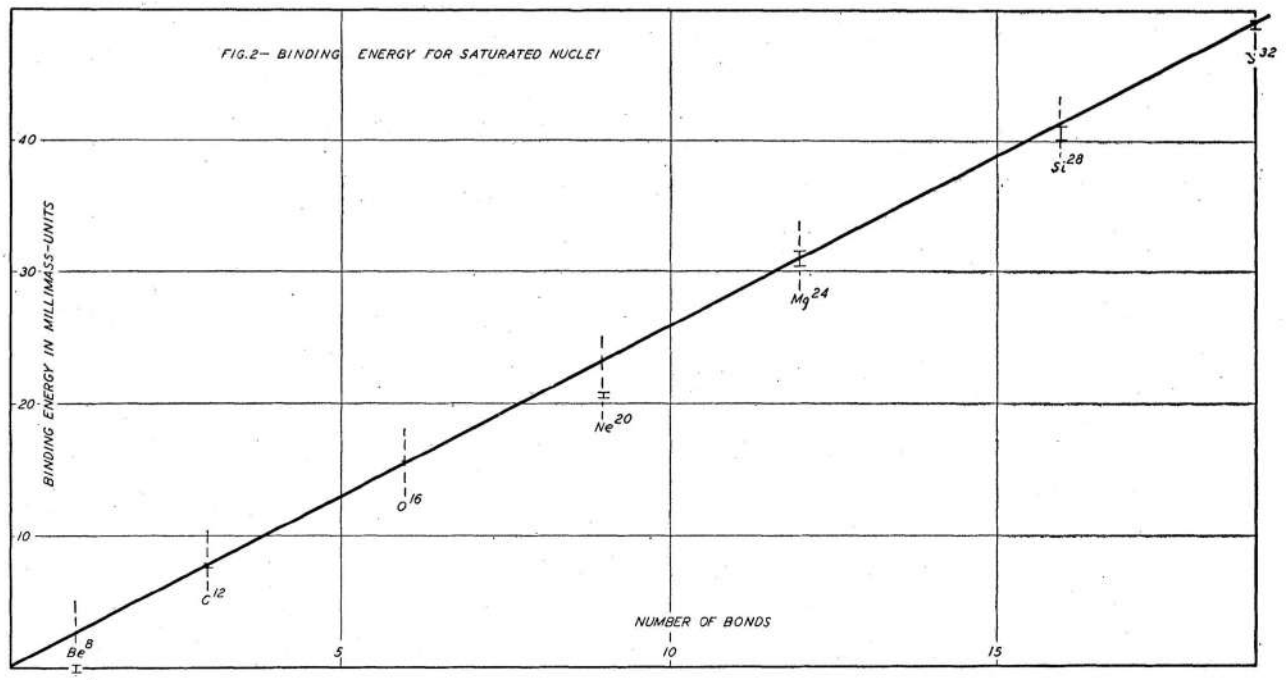


FIG. 2. Binding energy for saturated nuclei.

Figure 1. Binding energy of self-conjugated nuclei from work [3].

based on tetrahedrons. Further this question will be considered in more detail.

The success of the development of the shell model, and especially the emergence of the generalized nuclear model, led to a decline in interest in cluster models for some time.

The second period of increased interest in the $\alpha$-cluster model began after 1960. It was at this time that a number of classical experiments important for understanding the internal structure of the nucleus were performed, the construction of effective "cluster" theories began, and approaches to resolving the contradictions of the cluster and shell approaches were outlined.

To date, as the atomic nucleus (and especially the properties of light nuclei) is being studied, interest in the cluster model has gradually revived again, at this time not as a basic model, but as a model to describe some set of phenomena not explained by the shell approach. For example – we can consider self-conjugated nuclei or nuclei containing $\alpha$-particle as a well-formed cluster (lithium nuclei, halo nuclei, rotational bands in some nuclei). But by far the most promising was the attempt to search for and describe within the framework of this model a variant of *quasimolecular states*. In the most general case, such states are understood

as systems consisting of atomic nuclei interacting by means of nuclear forces, but with relatively low energy, so that the interaction process does not affect the internal structure of these nuclei and, consequently, they can be assumed to be structureless. In addition to predicting new, often rather unusual, states, this point of view allows to simplify considerably the process of microscopic description of the system, since it contains a relatively small number of constituent elements. Obviously, in this approach the $\alpha$-particle is the first and most optimal building block of the cluster model – large values of the binding energy and the first excited level, as well as zero spin and isospin. The mechanism of formation of such constituent clusters, similar to the one described in Wheeler's work [1], is based on the idea of spin-dependent attractive forces between nucleons. As a result, Wheeler's pioneering work led to the creation of the effective theory of the Resonating Group Method [4]. Other theories that emerged at that time include the Generator Coordinate Method [5] and the Orthogonality Condition Method [6].

Since this paper is devoted specifically to the experimental study of cluster degrees of freedom, we will mention only the simplest variants of the models, which are convenient to use in planning the experiment, as well as for obtaining systematics. From this point of view, the currently existing $\alpha$-cluster models can be conditionally divided into two large groups.

The first is when one $\alpha$-particle (more rarely, two) interacts with a core, which is also considered to be structureless, or the $\alpha$-particle itself is a core (lithium, halo nuclei).

The second, when the whole nucleus is considered to consist of $\alpha$-particles – the maximal $\alpha$-particle model.

A good illustration of such approaches is the *Ikeda diagram* [7] – the systematics of admissible cluster states, which plays a central role in the considered approach to the description of the structure of the nucleus (see Fig. 2).

From the point of view of the cluster model, each element of the Ikeda diagram must correspond to a state in the level spectrum of the corresponding self-conjugate nuclei (the so-called *threshold rule*). The first "diagonal" of the diagram corresponds to the ground states of nuclei with no cluster characteristics

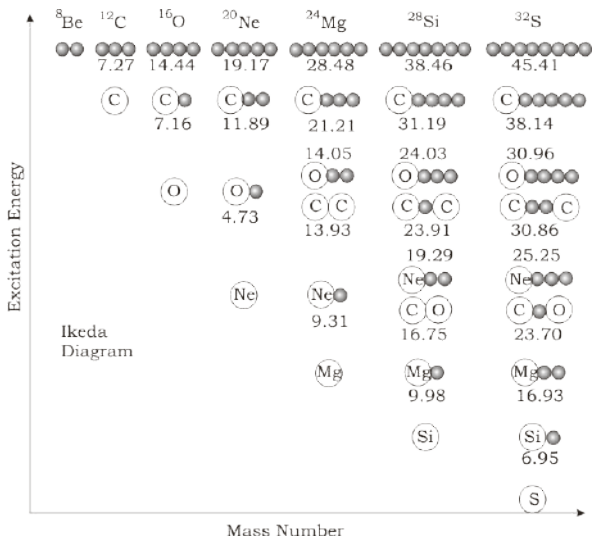


1

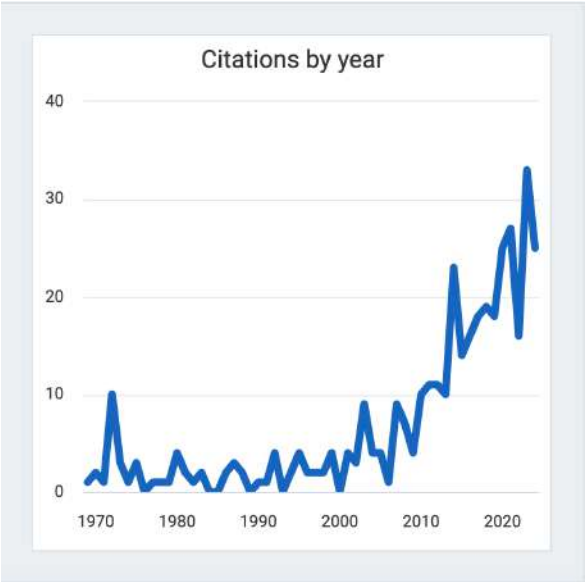


2

Figure 2. 1. Ikeda diagram [7] (modified to take into account currently known data), 2. Citation of work [7] by year [8]

in the first approximation, the second to states of the form "cor+$\alpha$-particle", the third to "cor+2$\alpha$-particles", etc. The topmost line thus corresponds to the state where the whole nucleus is split into $\alpha$-particles. In addition, the diagram may contain more complex states, such as $^{12}$C+$^{16}$O, corresponding to heavier clusters. The numbers under each element correspond to the reaction threshold for that partition, that is, they indicate the *approximate* position of the level in the spectrum of excited states. The Ikeda model developed in the mid-sixties turned out to be such a convenient method of working with cluster states that, as can be seen from the figure 2, even today it is, if not the main, then extremely important apparatus for working with the cluster approximation, especially in the case of experimental work.

Recently, it has been possible to extend the approach discussed above to nuclei with neutron excess. In the works of von Oertzen [9, 10], the "extended Ikeda diagram" was proposed. It is based on a similar principle and includes states corresponding to the structure "cor+$\alpha$-particle+covalent neutrons". Such configurations, strongly separated in energy space, are called *molecular* in the modern literature. As follows from this approximation, the excitation energy with increasing complexity of the configuration grows very rapidly, so that in the experiment we usually see only the most "simple" states corresponding to the excitation of one or two clusters, i.e., belonging to the theories of the first group.

The most successful and simple description of such states is obtained in the framework of the potential model. This model was developed by B. Buck [11–13] on the basis of the work on the introduction of the convolution potential for self-conjugate nuclei [14], which had a great influence on the development of the physics of the study of cluster states. The model was based on the introduction of an optical potential that reproduced the cluster states as levels of the corresponding rotational bands. The resulting wave functions of the states under consideration are similar to those computed in the framework of methods using group theory [11], and the application of a simple relation to exclude forbidden states reduces the calculations to the solution of the Schrödinger equation for bound and quasi-bound states. The model gives an intuitive picture of the relative motion of the cluster-core system and does not require cumbersome calculations (e.g., work [13]). Advantages of this approach include the possibility of systematizing (or unifying) the cluster-core potential, and thus the ability to compute features such as decay widths, decay intensities, or using the potential to reproduce the angular distributions of nuclear reactions. Inversely, it is possible to apply the potential extracted from experimental data to determine approximate positions of cluster states.

Another variant of considering "one-particle" cluster states was proposed by Horiuchi and Ikeda [15,16]. This approach was very different from the "potential" approach discussed above, although it was originally applied to the same $^{16}$O and $^{20}$Ne nuclei that had always been considered key to cluster computing. The model introduced the notion of *inverse doublet* for negative and positive parity states. In spite of the fact that a similar doublet appeared in the previous model, here its nature was different, the two types of states in the rotational bands appeared as a consequence of tunneling of the $\alpha$-particle "through" the nucleus, which led to a split in energy depending on the parity of the state. Initially, this model proved to be of little use. Despite its good qualitative description and simplicity of application (the WKB method could be used to construct wave functions), the model was used only to describe the parity splitting in the $^{16}$O and $^{20}$Ne nuclei. The discovery of similar doublets in heavy nuclei and the systematics of the "strain potential" have revived interest in this model.

Since both models play a key role in the presented thesis, they will be discussed in more detail below.

Of course, there are many models based on more complex theories, but in this paper we will only mention the description within the framework of the Antisymmetrized Molecular Dynamics (AMD) [17] approach, with the results of which we will compare the obtained data. In spite of the fact that in this model the degrees of freedom of the nucleons in the nucleus are considered independently, without assuming the presence of clustering, this approach is particularly popular for the description of cluster degrees of freedom. This is made possible by incorporating the Bloch-Brink cluster wave function from the above-mentioned Coordinate Generator method into the AMD model space.

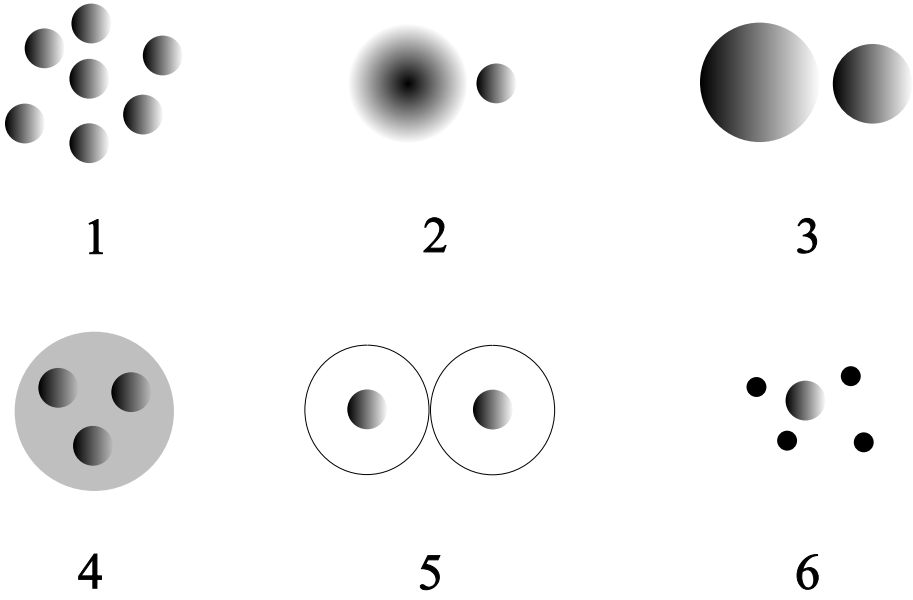


Figure 3. The types of systems considered in this paper (see text for explanation).

The figure 3 schematically shows the types of systems considered in this paper that exhibit clustering. 1) A system of bound (or weakly bound) clusters, usually $\alpha$-particles (Chapters 1, 5), 2) A cluster (usually a $\alpha$-particle) in the nucleus-core field (Chapters 1, 3, 4, 5), 3) Heavy clusters forming a binary system (Chapters 4, 6, 7), 4) Clusters ($\alpha$-particles) that can be considered, as correlations in systems of nucleons weakly interacting with other nucleons (Chapter 3), 5) similar to the previous point, but nucleons form orbitals ($\pi$, $\sigma$), by analogy with electrons in molecules (Chapter 3), 6) a nucleus being a core in a halo-nucleus system (Chapter 3). The methods of investigation of such systems are described in Chapters 1 and 2.

One of the problems of further development of this field is a significant deficit of experimental data and new interpretations for the existing ones. It is to the solution of this problem that the present work is mainly devoted. Nuclei belonging to the light and medium mass groups, including those with significant neutron excess, have been studied experimentally. The figure 4 shows the nuclei and clusters studied in this work.

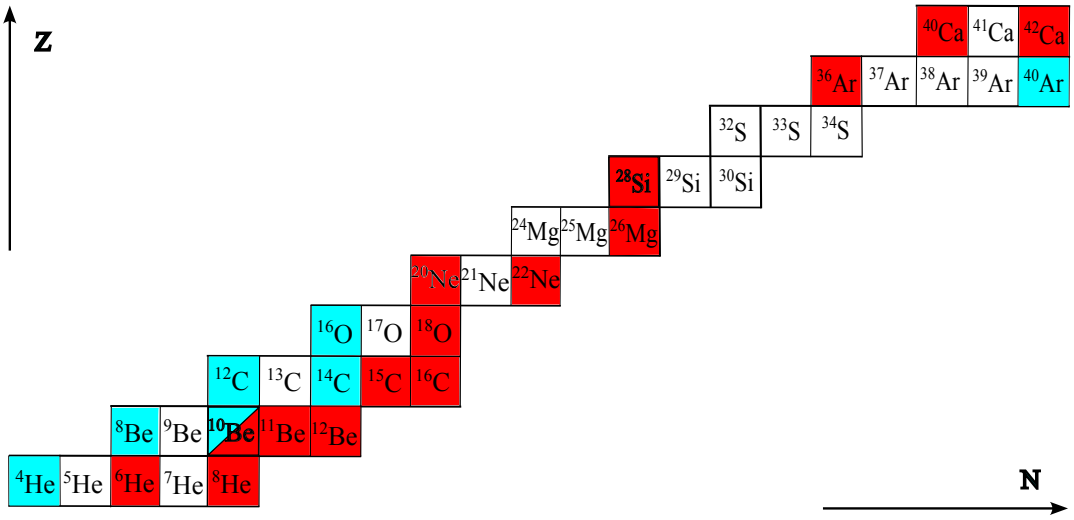


Figure 4. Isotopes studied in this paper. Isotopes whose cluster characteristics were investigated in the considered experiments are marked in red. The clusters under consideration are highlighted in blue.

Also, our results are examined in the framework of clustering approaches in order to understand how well they can be described. The good agreement of theoretical results with experimental results can be considered as an additional argument in favor of the cluster nature of the observed phenomena.

To date, there is a considerable number of reviews on the problem of clustering in nuclei. Let us mention here the most recent ones [18–22]. The fundamental monograph containing theoretical approaches to the cluster description of the structure of the nucleus and to date is the work [23].

It should not be assumed that the main field of application of the considered approaches belongs to low energies. The currently actively developing experimental methods at high energies develop similar approaches. Thus, in the paper [24] the flight of heavy clusters in unstable states at energies of the order of $A$ GeV is considered, a problem similar to the one solved in this paper for low energies. We should also mention the BECQUEREL [25] experiment, which studies fragmentation into $\alpha$-clusters at relativistic energies. The cluster structure as a correlation

of $\alpha$-particles as $^{8}$Be resulting from fragmentation of $^{16}$O, $^{22}$Ne, $^{28}$Si nuclei is also considered at relativistic energies [26], as in this paper.

Finally, significant progress has been made in the study of nuclear matter fragmentation in relativistic ion collisions at the NICA/Nuclotron collider in the study of processes important from the point of view of high-energy astrophysics [27].

The relevance of this research is also confirmed by the large number of international conferences and annual reviews devoted to the topic discussed in this paper. The interest in this topic is growing every year, which can be seen, among other things, from the growth of references to Ikeda's work (Fig. 2), which is fundamental in this issue. At the same time, it should be noted that most of such works are theoretical in nature and are related to the reinterpretation of previously obtained results, including for simpler variants of the cluster approximation. Thus, there is a significant shortage of experimental data that could confirm (or refute) the predictions of the currently existing models.

One of the factors determining the considerable interest in new experimental data in this field is, among others, the possibility of transition from the description of finite nuclei studied in the laboratory to the description of such objects as neutron stars [28]. This, in turn, requires the study of possible correlations in neutron systems, in order to adequately account for them in the equation of state of nuclear matter [29]. However, to date, the question of correlations has not been completely resolved. Recent experiments in this field have actually repeated the result of the present work [30].

Another example is the advances in the AMD approach. A recent review devoted to the problems of clusters in light nuclei [31] suggests a scheme for augmenting AMD with methods from quantum chromodynamics and artificial intelligence to solve the problems at hand. And, it is worth noting that the review focuses specifically on experimental work in this area. Examples of problems (including those solved in this work) are: ambiguity of determination of angular momenta of states, difficulties of studying high-spin states in light nuclei, difficulties of work at low energies. As can be seen, the above problems refer us specifically to the problems of experimental investigation.

In another review of AMD modeling [32], not only is there a significant deficit

of experimental values for beryllium isotopes, but also a figure for the $^{22}$Ne nucleus, which has predictions almost twenty years old and was last updated with our results.

Below, this state of affairs will be illustrated by the example of the $^{18}$O nucleus, for which, to date, there are diametrically opposite (!) experimental results, as pointed out in the review on the history of clusters [33]. In addition, the possibility of studying the properties (including cluster properties) of nuclei near the stability boundary has been obtained relatively recently, so that any new experimental result in this area can be useful both for developing theoretical approaches and for planning new experiments.

The importance of studying the cluster structure of nuclei from the point of view of astrophysics is well illustrated in the review [34].

**The goal** of this series of works is to:

1. Experimental study of cluster degrees of freedom in self-conjugated and neutron-excess nuclei.
2. Description of the experimental results obtained within the framework of the cluster model to obtain the necessary systematics.
3. Experimental study of rotational bands of cluster nature in nuclei. The analysis of high-spin states in nuclei of light and medium mass groups detected in our experiments.
4. Experimental study of neutron-excess isotopes near the neutron stability boundary, study of the influence of neutron excess on clustering in nuclei.
5. Consideration of possible exotic states due to clustering.
6. Experimental study of the emission of heavy clusters of beryllium and carbon.
7. Study of the influence of cluster transfer in reactions with heavy ions.
8. Obtaining systematics for the description within the two-particle model of low-energy interaction of heavy ions, important from the point of view of astrophysics.

**Structure of the work**.

The dissertation consists of Introduction, 7 chapters, Conclusion and Appendix. The full volume of the dissertation is 233 pages, including 79 figures and 30 tables. The bibliography contains 317 titles. The Introduction briefly formulates the purpose of the presented cycle of work and the relevance of this research, the main results. The provisions of the defense are indicated and the list of conferences at which the main results obtained in the work were highlighted.

In Chapter 1, the main provisions of the $\alpha$-particle model, taking into account the known, to date, experimental data, used in the work to prepare for the execution of the experiment, or in its analysis. In addition, the main types of reactions used in this work are listed, and their characteristic features are indicated with respect to the goals and objectives of this work. It is shown that the results obtained agree well both with calculations based on other models and with existing experimental results.

Chapter 2 briefly reviews the main methods of experimental study of the properties of nuclei used in this work. The main characteristics of the experimental setups used are given.

Chapter 3 summarizes the main results of the spectroscopy study of the nuclei indicated in the figure 4. In addition, for $^{6}$He and $^{8}$He nuclei the obtained cluster momentum distributions are indicated and the research setup is given. The procedure for obtaining experimental results is briefly described. The results for resonant scattering of $\alpha$-particles and heavy clusters in the inverse geometry method with a thick target are discussed.

Chapter 4 summarizes the results of the study of quasi-elastic transfer of $\alpha$-particles in reactions with oxygen, neon, boron, and nitrogen nuclei.

In Chapter 5, the results of the experiment with the flight of heavy clusters in the form of $^{12}$C* and $^{8}$Be nuclei are discussed. It is shown how this result can be interpreted in the framework of the occurrence of Bose-Einstein condensates in the nuclei.

In Chapter 6 we present a systematics for nuclei of intermediate mass group, in the framework of the cluster approach. The case of elastic scattering of $^{12}$C+$^{16}$O nuclei is considered, pointing out the main difficulties in studying the quasi-

molecular states arising in such a heavy system.

In Chapter 7, the case of the potential model is considered and compared with experiment, based on which a description of the resonance-like structure arising at the excitation function is given. Finally, a systematics for other reaction variants important from an astrophysical point of view is given.

The Conclusion summarizes the main results and acknowledgments.

The Appendix contains a list of the author's publications related to the topic of the dissertation.

**Theoretical and practical significance**

In the present work, cluster states in nuclei have been investigated. A distinctive feature of this topic is the possibility of applying the results obtained in a wide variety of fields of research on the atomic nucleus and elementary particles. This, in turn, determines the significance, both from a practical and theoretical point of view, of the results of the work performed. Let us enumerate the main points.

In this work, we studied the cluster properties of nuclei using the method of inverse geometry. This method is currently undergoing rapid development, since it makes it possible to study nuclear exotics near and even beyond the stability boundary. Thus, the results of work with such systems are very useful for scientific groups engaged in the experimental study of the properties of nuclei. In particular, the methods developed in our work allow us to greatly simplify the study of reactions at low energies, coming close to the energies typical of stellar nucleosynthesis. Such works are very important from the point of view of modern astrophysics. In addition, the evaluation of the obtained cross sections for ion fusion in the low energy region will allow us to better understand the mechanisms of reactions occurring in stars.

In our work on the study of neutron-excess nuclei, a new method of charge collection time registration was applied to identify the decay products. A distinctive feature of this method is the undemanding nature of the detector parameters, which allows us to significantly reduce the cost of the work. The separation of flying particles is carried out without the use of the $\Delta E$ part, which will avoid the use of an expensive thin detector or a gas system that adversely affects the

vacuum. It was shown to be possible to separate $^{4}$He and $^{6}$He nuclei.

The practical usefulness can also include the methods we are developing for analyzing the nuclear fusion cross section in the low energy region. The small number of free parameters and the absence of the need to solve the Schrödinger equation allow us to work with a large amount of experimental data at once. This allows us to find universal regularities important for extrapolation of cross section values to the low energy region.

The experimental results obtained in this work are of interest for the work of international scientific groups. They are included in databases and have been independently verified. The theoretical approaches used allow a simple and fast evaluation of the effect of the first approximation. Despite the use of low energies in this work, the results of the present work, as indicated above, can be used in modern facilities for studying the behavior of superband nuclear matter in heavy ion collisions.

**Methodology and Research Methods**

In this work, the most modern equipment for conducting experiments was used. In particular, these are magnetic spectrometers, systems of particle identification by time of charge collection and methods of inverse geometry and thick target. The potential model, the tunneling model, and the calculation of reaction parameters within the framework of the Born distorted-wave approximation were used to process the data obtained. Given the importance of these techniques for understanding the results obtained, the theoretical approaches used are discussed in more detail in Chapter 1, and the experimental methods are discussed in Chapter 2.

**Reliability and Evaluation of results**

The reliability of the obtained results is due to their reproducibility in experiments performed in other scientific groups, as well as agreement with theoretical calculations performed by other authors based on the information presented in the articles with the materials of this dissertation.

The experiments described in the present work were performed by us at LNL (Legnaro, Italy), HMI (Berlin, Germany), GSI (Darmstadt, Germany), JYFL (Jyvaskyla, Finland), the Cyclotron Laboratory of the University of Warsaw (War-

saw, Poland), and at the gas pedal of the National Laboratory of Nazarbayev University (Astana, Kazakhstan).

The main results of this work were obtained for the first time. A number of results were later used by various international research groups.

The results obtained in this work were published in international scientific journals. The Appendix contains the main list of publications on this thesis in journals and proceedings of international conferences – 44 titles.

Of the main works on the topic of the dissertation, 15 works were published in journals from the HAC list, 27 works are contained in the scientometric databases Scopus and Web of Science.. The experimental results obtained were indexed in EXFOR and XUNDL–international databases of experimental results in nuclear physics.

The results of the work were presented at international conferences on nuclear physics:

– NUCLEUS 2005 (St. Petersburg, Russia)

– NUCLEUS 2006 (Sarov, Russia)

– NUCLEUS 2007 (Moscow, Russia)

– NUCLEUS 2009 (Cheboksary, Russia)

– NUCLEUS 2010 (St. Petersburg, Russia)

– NUCLEUS 2011 (Sarov, Russia)

– NUCLEUS 2012 (Voronezh, Russia)

– NUCLEUS 2015 (St. Petersburg, Russia)

– NUCLEUS 2017 (Alma-ata, Kazakhstan)

– NUCLEUS 2020 (St. Petersburg, Russia)

– NUCLEUS 2021 (St. Petersburg, Russia)

– NUCLEUS 2022 (Moscow, Russia)

– 4th International Conference on Exotic Nuclei and Atomic Masses 2004 (Pine Mountain, USA)

– 5th Conference on Nuclear and Particle physics 2005 (Cairo, Egypt)

– Sandanski Coordination Meeting on Nuclear Science 2005 (Albena, Bulgaria)

– Current Problems in Nuclear Physics and Atomic Energy 2006 (Kyiv,

Ukraine)

– Exon 2004 (St. Petersburg, Russia)

– 7th Conference on Nuclear and Particle Physics 2009 (Sharm El-Sheikh, Egypt)

They were also reported at seminars at St. Petersburg University (St. Petersburg, Russia), Heavy Ion Institute (GSI) (Darmstadt, Germany), Hahn-Meitner Institute (HMI) (Berlin, Germany) and Nazarbayev University (Astana, Kazakhstan).

**Thesis defense key points**

1. The momentum distributions of clusters in $^{6}$He and $^{8}$He halo nuclei are obtained.

2. A number of new cluster states in neutron-deficient isotopes of beryllium, carbon, oxygen, and neon, as well as in self-conjugated argon and calcium nuclei belonging to rotational bands have been discovered.

3. On the basis of the maximal $\alpha$-cluster model we consider ways of describing exotic states of nuclear matter – chain configurations and Bose-Einstein condensate. This result allows us to explain some regularities of heavy cluster departure, which we found in the experiment.

4. A systematics for rotational bands with the $\alpha$+cor structure is proposed.

5. New data on the molecular states arising in the interaction reactions $^{12}$C+$^{14}$C, $^{12}$C+$^{16}$O.

6. New data on quasi-elastic cluster transfer in reactions with carbon, oxygen, neon, boron, and nitrogen nuclei are obtained.

7. Systematics of data for heavy ion fusions important from the point of view of astrophysics is proposed.

**Main scientific results**

The materials of the dissertation are a generalization of the author's work on the topic of the research topic. The results presented in the thesis were obtained by the author personally, or in co-authorship with direct participation. The author

has made a significant contribution both in setting the problems solved in the work, and in conducting experiments, performing processing and analysis of the experimental data and preparation of research results for publication in scientific publications.

1. The states in neutron-excess nuclei of beryllium, carbon, neon, and magnesium have been studied. The results obtained allowed us to detect a number of new states with cluster structure, as well as high-spin states belonging to rotational bands. In the works [35–39] the problem formulation, data processing and preparation of publications were carried out by the author personally. In [40], the author analyzed the data on the reaction $^{12}$C+$^{14}$C. In [41–45], the author's contribution to data processing and analysis is 60%.

2. For helium isotopes the momentum distribution in cluster knockout reactions was obtained. Conclusions about the possible configuration of valence neutrons and the possibility of the formation of exotic neutron clusters have been drawn. Calculations for the momentum distribution of clusters in the considered nuclei and obtaining the experimental distribution in the work [46] were performed personally by the author.

3. The case of $\alpha$-particle clusters – $^{12}$C* and $^{8}$Be – flying out of the nucleus is considered. A decrease in the energy carried away from the nucleus in this case was found, which allowed us to conclude further on the possible Bose-Einstein condensation of these nuclei. Calculations of the energy balance for the departing clusters $^{12}$C and $^{12}$C* and obtaining experimental values for them in the work [47] were performed personally by the author.

4. A systematics of reactions important from the point of view of astrophysics in the framework of the potential model has been carried out. A satisfactory description of the excitation function for fusion reactions in the case of one free parameter has been obtained. The author's personal contribution to the work [48–50] is at least 80%. In the work [51], the author performed data processing within the framework of the optical model.

5. The elastic and inelastic scattering reactions of heavy ions – carbon, oxygen, boron, nitrogen, and neon – are considered. The importance of considering

resonance states and cluster transfer is shown. The contribution to experimental data acquisition and information processing in the work [52] is at least 60%. The author's contribution to the problem formulation, experimental data acquisition and results in the paper [53] at least 80%.

6. A systematics for the predictions of the cluster model is obtained, allowing simple estimates for nuclei in exotic states. The author's contribution to the work [54–60] is at least 80%.

7. systematics within a potential model for rotational bands is obtained. The author's contribution [61–63] is at least 80%. The work [64,65] was completed in its entirety by the author. In [66], the processing of experimental data and characterization of cluster excited states were performed by the author.

# Chapter 1. Methods of description and study of cluster states

In this chapter, we briefly review the main approaches that allow us to estimate, to a first approximation, the possible effect of the manifestation of the cluster structure of the nucleus and the experimental methods used in this work to study the cluster degrees of freedom in nuclei. Conventionally, they can be divided into two groups – spectroscopic and those related to the study of nuclear reactions.

From a historical point of view, one of the first and most important reasons for the development of a model of the cluster structure of the nucleus (in this case – $\alpha$-cluster structure) is the result of the study of the natural $\alpha$-radioactivity of heavy nuclei. After Rutherford established that $\alpha$-particles correspond to $^4$He nuclei, and Gamow constructed a theory of $\alpha$-decay, a legitimate question arose about the presence of "ready" $\alpha$-particles in the nucleus. Despite the existence of much more accurate models, the experimental study of $\alpha$-radioactivity is still an urgent task and provides new information on the properties and structure of heavy nuclei from the cluster point of view. In this case, the nuclear wave function is considered as the sum of the "shell" part for the residual nucleus and the "cluster" part for the escaping $\alpha$-particle:

$$\Psi = \Psi(shell) + \Psi(cluster), \tag{1}$$

where the cluster wave function can be written as the antisymmetrized product of the internal wave functions (of the residual nucleus $\Phi_c$ and the $\alpha$-particle $\Phi_\alpha$) and the wave function of their relative motion $\phi$:

$$\Psi(cluster) = \mathcal{A}[\Phi_c(\xi_c)\Phi_\alpha(\xi_\alpha)\phi(R)]. \tag{2}$$

Assuming that the decay can be described using the Gamow wave function, the $\alpha$-particle is well described by the oscillatory wave function for the $1s$ state, and the basis for the shell states is reproduced by diagonalizing the corresponding Hamiltonian. In this model, the decay width and the probability of forming a $\alpha$-particle can be calculated. For most heavy nuclei, this value lies in the range 0.3-0.6 [67].

Another important way to directly observe the cluster structure is to study the $\alpha$-particle knockout reaction from the nucleus, e.g. $(p, \alpha)$. It is not difficult to extend this model to the case of choosing an arbitrary cluster. At energies when the contribution from compound-nucleus formation no longer prevails, the analysis of direct processes allows one to draw important conclusions about the probability of cluster formation.

Although, as indicated in the Introduction, the cluster model originally considered primarily light nuclei, experimental confirmation of the large clustering contribution for them proved to be a much more difficult task than for heavy nuclei, remaining for a long time a concept rather related to energetic considerations than to the manifestation in reactions. The reaction leading to the $^{8}$Be residual nucleus can perhaps be considered an exception. The reaction $^{7}\mathrm{Li}(p, \alpha)\alpha$ studied by Rutherford unambiguously pointed to the prevailing character of the cluster structure of this nucleus.

The next important evidence of the cluster nature of light nuclei was the experimental confirmation of the assumption made by Hoyle about the existence in the $^{12}$C nucleus of a level near the threshold of the collapse into three $\alpha$-particles. Despite the considerable time that has elapsed since the discovery of the Hoyle state and its enormous importance for astrophysical models, its structure is still an object of study, including experimental research.

The further history of the study of $\alpha$-cluster states was mainly connected with the Ikeda diagram (see Fig. 2) and later with the molecular states from the extended diagram proposed by von Oertzen. From the experimental point of view, there was a significant complication of the equipment used, the interaction energies increased (although not very significantly compared to other areas of nuclear physics), the kinematics became more complicated, and the need to register three-particle states became more frequent. However, the general principles remained the same. Let us briefly consider the main provisions.

### 1.1. Model of binding $\alpha$-particles

In this section we will consider a variant of the "maximal" $\alpha$-particle model, when the whole nucleus is split into a system of interacting $\alpha$-particles, taking

into account the condition of "virtuality" of their existence in the nucleus. The first result – the calculation of the binding energy of nuclei as a function of the number of bonds is shown in Fig. 1. As can be seen, there is good agreement with experimental data for the nuclei known at that time. Thus, we reproduce the fragmentation energy corresponding to the topmost states of the Ikeda diagram. The success of the model led to attempts to more consistently conceptualize the notion of "configuration" (i.e., mutual arrangement in space) for the $\alpha$-particles in the nucleus, since this is how the notion of "bonding" can be defined.

### 1.1.1. Geometric model

Let us restrict ourselves to the consideration of self-conjugate nuclei. The simplest configuration of the $^{8}$Be nucleus is two $\alpha$-particles. Given that the nucleus is unbound and exhibits good rotational properties (ground state band), consistent with the assumption of a $\alpha$-particle structure, this structure seems self-evident. A configuration corresponding to an equilateral triangle has been proposed for the $^{12}$C nucleus, $^{16}$O – a tetrahedron. Further addition of $\alpha$-particles corresponded to the construction of a quasi-crystalline structure based on tetrahedrons. A similar model for the description of liquid properties was, in due time, developed by Bernal [68]. Two points should be noted:

1) Tetrahedrons do not allow to continuously "cover" the whole three-dimensional space.

2) For some nuclei, the number of bonds was smaller than that obtained by adding a "tetrahedrally packed" $\alpha$-particle.

Thus, the geometrical structure obtained within the limit model allowed certain discrepancies, depending on the conditions underlying the construction of configurations. For example, for the $^{28}$Si nucleus, two configurations with different types of symmetry can be assumed. The basic geometrical structures used at an early stage were considered by Hafstad and Teller [3]. Later, similar structures were obtained by Brink [5]. The interaction potential of $\alpha$-particles in the considered works was chosen in the Van der Waals form, i.e., repulsion at small distances and attraction at large distances. Its depth was determined from agreement with experimental data. This is a typical potential for molecular interactions.

Hodgson formulated the fundamental questions of the $\alpha$-cluster model as fol-

lows [67]:

1) Is there evidence for the presence of $\alpha$-clusters in the nucleus?

2) If such clusters do exist, how long do they live?

3) What is their distribution in the nucleus?

4) What are their energy and direction of motion?

5) Are they different from free $\alpha$-particles?

6) What is the probability that a given nucleon will form part of a $\alpha$-particle?

7) How do the answers to these questions depend on the size of the nucleus, its shape, and its excitation energy?

To present the state of the art for the model under consideration, we ask two questions.

1) What can be a general algorithm for constructing spatial configurations?

2) For what values of mass numbers can we continue to construct such configurations, for example, for self-conjugate nuclei?

Note that the very assumption of the existence of "virtual" clusters does not impose any restrictions on their mutual arrangement. Moreover, even extending our approach to construct the corresponding wave functions [5], we cannot reach an unambiguous conclusion. As stated above, several attempts have been made to point the way to an algorithm for constructing spatial configurations on the basis of general reasoning (Poling, Bernal). However, the result has been rather ambiguous. A possible reason for this is too "classical" consideration of such a quantum problem. Therefore, in our consideration we will not rely on quasi-classical analogies from other areas of physics, but will construct the algorithm only on the basis of the problem of minimization of the potential energy of interacting particles [54].

Consider a three-dimensional grid of small (compared to the size of the $\alpha$-particle) step, place a $\alpha$-particle in some cell and set some sufficiently smooth molecular interaction potential (e.g., the Lennard-Jones potential) so that the minimum occurs at a distance of the order of 3 fermi. Let's add a second $\alpha$-particle. For their interaction energy to be minimized, the second particle must be placed in a position with a minimum value of the potential. We continue adding $\alpha$-particles by calculating the value of the potential at each node of the

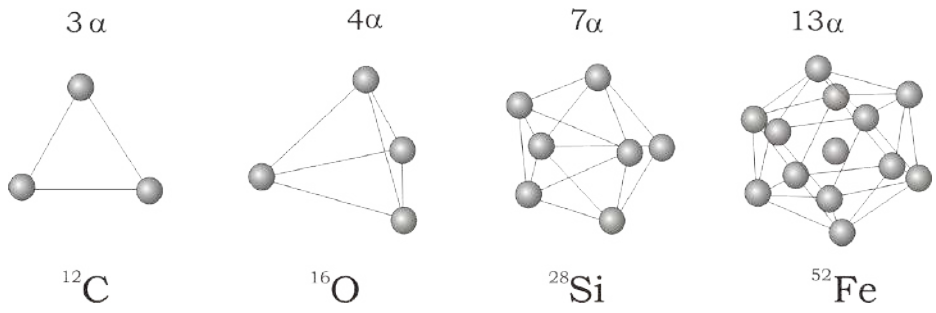


Figure 5. 3 $\alpha$-particles, 3 bonds, 4 $\alpha$-particles, 6 bonds, 7 $\alpha$-particles, 16 bonds, 13 $\alpha$-particles, 42 bonds [54].

grid and placing a new $\alpha$-particle there. Thus, for step $i$, the effective potential for particle $i$+1, will be:

$$V^i = \sum_{j=1}^{i} V(\mathbf{r_{i+1}} - \mathbf{r_j}). \tag{3}$$

As we have shown in [55, 57], correcting for tcorehe impossibility of tight packing within tetrahedral configurations, we will obtain approximately the same configurations for a wide class of molecular potentials (Ali-Bodmer, Lennard-Jones, Morse, Yukawa with repulsive core). For 3, 4, 7, and 13 $\alpha$-particles, we have the configurations shown in the Figure 5.

The answer to the question of the limit of applicability should, in our opinion, be decided primarily by the constraints on the fit to the experimental data. From the point of view of theory, to date, a number of works have been done, the authors of which, in the framework of the quantum-mechanical approach, have tried to determine the limits of applicability of the maximal $\alpha$-particle model (e.g., [69–73]). It is generally assumed that for light nuclei where the $LS$ coupling scheme applies, the model under consideration works well, while in the region $A$¿40, where the $jj$ coupling scheme becomes important, limitations arise, depending on the type of calculations.

Therefore, in this paper we propose to use the "toy" model we proposed in [56]. Consider the nucleus as a set of protons and neutrons with random coordinate values within a sphere of radius $1.2A^{\frac{1}{3}}$ fermi. Restricting ourselves to self-conjugate nuclei, we assign a spin projection to each nucleon such that the total spin of the nucleus is 0. What will be the rms radius of a random correlation of the form $(p\uparrow p\downarrow n\uparrow n\downarrow)$? This problem is not difficult to solve by Monte

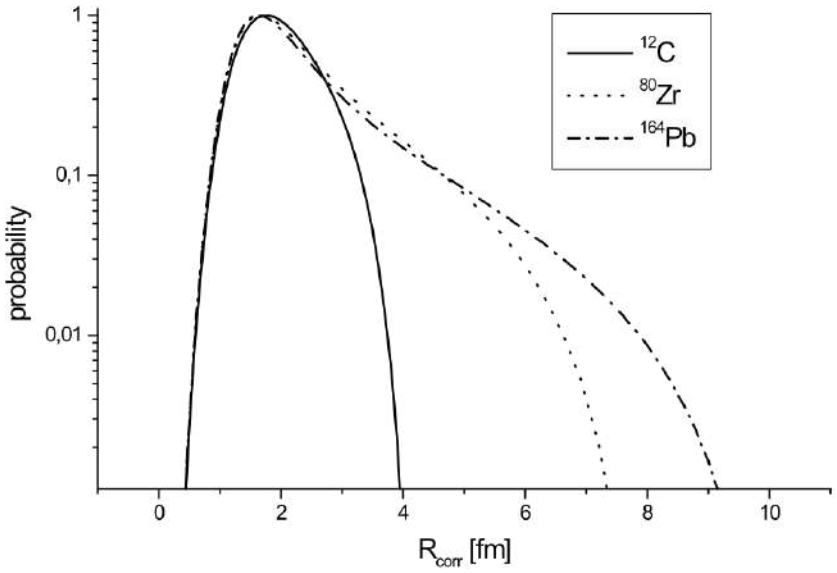


Figure 6. Probability distribution of the mean-square radii of random correlations of the form $(p\uparrow p\downarrow n\uparrow n\downarrow)$ in self-conjugate nuclei [59].

Carlo method and the graph of the dependence of the conditional probability on the correlation radius is shown in the Figure 6. As can be seen, in all cases the probability for the rms radius of the "antisymmetrized four nucleons" has a sharp peak in the region of 1.8 fm, so that even for a hypothetical $^{164}$Pb nucleus the probability of finding four particles in the desired charge-spin state is quite large. The correlation radius is close to the value of the radius of the $\alpha$-particle.

Thus, if we assume that the clustering-inducing correlation of four nucleons has an interaction radius of the order of 3 fm, then the cluster structure should indeed be observed in light nuclei, and gradually decrease due to "widening", as can be seen in the figure. If for the case of independent motion in the $^{12}$C nucleus only 7% of the nucleons in the required spin-isospin state are located at a distance greater than the correlation distance, then in the $^{80}$Zn nucleus the fraction of such nucleons is already 23%. The data obtained can be considered as a "lower bound" for the degree of correlation of nucleons in the nucleus.

Of course, such a simplified model gives only an approximate solution, so it is necessary to compare the predictions of the considered $\alpha$-particle model with experimental data.

As it is supposed, at present we can consider self-conjugated nuclei up to values $Z$=52. The above described model of the formation of $\alpha$-particle nuclei

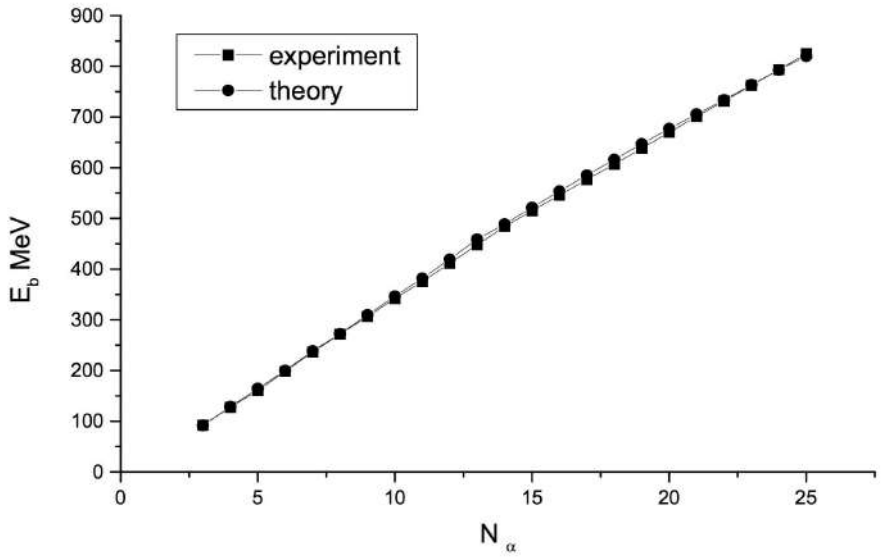


Figure 7. Experimental and theoretical binding energies of nuclei as functions of the number of $\alpha$-particles [54].

allows us to construct, in general, systems of unlimited size. At the same time, the obtained binding energy, in the case of a number of short-range potentials, turns out to be approximately the same. The binding energy of the nucleus in the framework of the considered model can be estimated by the formula [54]:

$$E_B = F_0(6N_\alpha + n_\alpha) + C. \tag{4}$$

Here $F_0$ – defines the interaction energy (a fitting parameter of the model), $n_\alpha$ – the number of bonds between $\alpha$-particles, $N_\alpha$ – the number of $\alpha$-particles in the nucleus, and $C$ – the Coulomb energy.

$$C = \frac{3}{5}\frac{e^2 Z(Z-1)}{r_0 A^{1/3}}, \tag{5}$$

here $r_0$=1.2 fm.

Table 1 shows the values calculated from the geometric theory of the bonding number and extracted from the formula (4) by substituting the experimental values. In Figure 7, the results presented above are summarized as a plot of the dependence of binding energy on the number of $\alpha$-particles. As can be seen, there is good agreement between theory and experiment in the whole range of nuclei considered. Subsequently, similar results were later obtained in [74].

The disadvantage of this approach is the problem of choosing the “bond

Table 1. Comparison of the number of connections obtained within the geometric model with experimental data [54].

| Nucleus | Number of $\alpha$-particles | Binding energy MeV | Number of bonds exp. | Number of bonds theor. |
|---|---|---|---|---|
| $^{12}$C | 3 | 92.1 | 3.00 | 3 |
| $^{16}$O | 4 | 127.6 | 5.69 | 6 |
| $^{20}$Ne | 5 | 160.7 | 8.14 | 9 |
| $^{24}$Mg | 6 | 197.2 | 11.54 | 12 |
| $^{28}$Si | 7 | 236.5 | 15.74 | 16 |
| $^{32}$S | 8 | 271.8 | 19.33 | 19 |
| $^{36}$Ar | 9 | 306.7 | 23.04 | 23 |
| $^{40}$Ca | 10 | 342.1 | 27.06 | 27 |
| $^{44}$Ti | 11 | 375.5 | 30.84 | 31 |
| $^{48}$Cr | 12 | 411.5 | 35.36 | 36 |
| $^{52}$Fe | 13 | 447.7 | 40.09 | 42 |
| $^{56}$Ni | 14 | 484.0 | 45.01 | 45 |
| $^{60}$Zn | 15 | 515.0 | 49.01 | 49 |
| $^{64}$Ge | 16 | 545.9 | 53.15 | 53 |
| $^{68}$Se | 17 | 576.4 | 57.37 | 57 |
| $^{72}$Kr | 18 | 607.1 | 61.79 | 61 |
| $^{76}$Sr | 19 | 638.1 | 66.42 | 66 |
| $^{80}$Zr | 20 | 669.8 | 71.36 | 71 |

length". For the tetrahedral approximation, the value of $F_0$ is of the order of 4.8 MeV [54]. As mentioned above, due to the impossibility of tight packing of the tetrahedral character, the distance between $\alpha$-particles is not discrete, as we have shown in [54].

Thus, to estimate the binding energy of nuclei heavier than $^{52}$Fe it is necessary to change the calculation procedure by excluding the number of bonds from the (4) formula. This can be done by calculating the binding energy by direct enumeration of $\alpha$-particles, summing their interactions (by analogy with the formula (3)). In this case, a weak dependence of the binding energy of nuclei on the type of potential [55, 57] is observed. Since the discrepancies between the experimental and theoretical values are very small, a plot of the dependence of the specific binding energy of $\alpha$-particles should be used. Figure 8 shows the corresponding dependence on the number of $\alpha$-particles in the nucleus for different types of potential.

This result shows that, as it was suggested earlier, a satisfactory description can be achieved using almost any molecular-type potential after an appropriate fit-

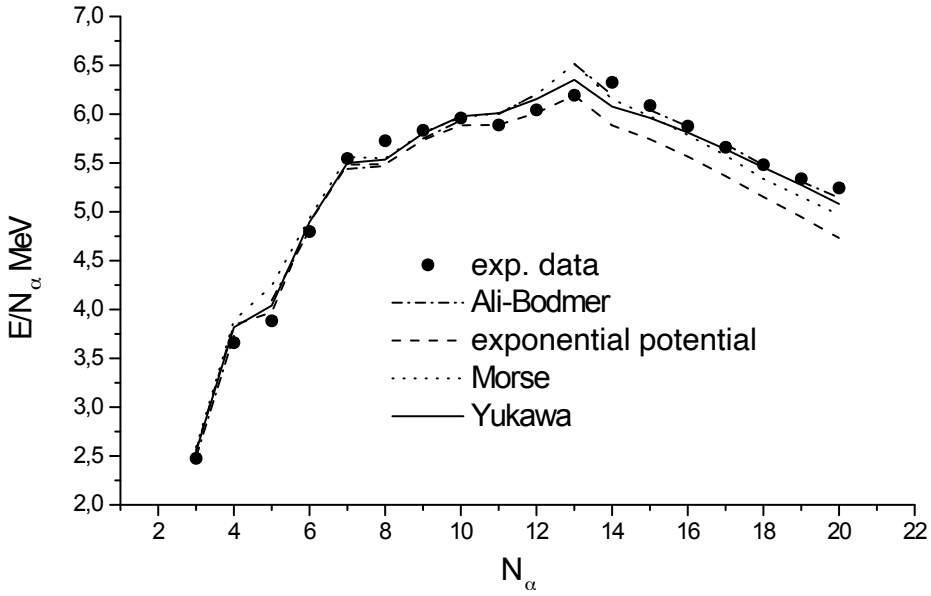


Figure 8. The binding energy per $\alpha$-particle from the number of $\alpha$-particles in the nucleus for different potentials [54].

ting of the parameters. For calculations of the binding energy from the $\alpha$-particle coordinates obtained in the model under consideration, the repulsive cor is taken into account automatically, so that the class of potentials under consideration can be extended. Thus, for example, the Yukawa potential [56] gives the best result when fitting to all available experimental data:

$$V(r) = -V_0 \exp(-\gamma r)/r, \tag{6}$$

when $V_0$=106.7 MeV, and the parameter $\gamma$ is equal to the inverse of the $\pi^0$ wavelength lumped meson. Since in this case we are no longer bound to calculate the Coulomb energy of the nucleus as a whole, we can introduce the Coulomb potential for each particle separately. For the calculations we have used the potential [55]:

$$V_C(r) = 4e^2 \mathrm{erf}(0.6r)/r. \tag{7}$$

Of course, this "classical" approach to such an essentially quantum object as the nucleus requires a little more justification than simply stating that the results obtained coincide with experimental data. Certainly we think of the $\alpha$-particle correlation as a quantum-mechanical particle and should use the system of Hartree-Fock equations to explain the behavior of such a system. But if we take into account that such a correlation is not a "real" particle, but only a math-

ematical concept – the center of mass of a system consisting of two protons and two neutrons (bound by a strong interaction), the picture changes dramatically. The average momenta of such $\alpha$-particle correlation are rather small compared to the momenta of the nucleons "composing" the particle. Thus, the problem is reduced to the classical version.

As a conclusion, we note the following interesting features. When analyzing the number of bonds in Table 1, we see that the largest errors are obtained for $^{20}$Ne and $^{52}$Fe nuclei. In the former case, as shown in [75,76], one can assume a structure other than tetrahedral. On the other hand, when describing the binding energy by the molecular potential, the largest errors occur in the description of $^{32}$S and $^{56}$Ni nuclei, which is quite natural. In this case, a new $\alpha$-particle is added "over the top" of the closed configuration (see Figure 5), which should underestimate the binding energy compared to the more symmetric distribution.

It is not difficult to extend the formula (4) to the case of neutron-excess nuclei, as shown in our work [54]. However, a more consistent approach is the introduction of covalent bonds and the corresponding extension of the Ikeda diagram. An interesting consequence of the considered model may be an attempt to estimate the binding energies of nuclei with excess neutrons in the region of superheavy nuclei [54]. In this case, at a certain number of $\alpha$-particles, an increase in the number of "short" bonds is observed, which corresponds to the filling of a new "envelope". This occurs for the number of $\alpha$-particles $N_\alpha$=60-62 [58] ($Z$=120-122). Of course, such a nucleus is not bound, but it can be stabilized by an appropriate neutron excess, so that the mass number (from extrapolation of the neutron number to a given charge region) will be of the order of 310. It should be noted that some time ago statements were made about the discovery of superheavy nuclei with charge $Z$=120 [77]. At the same time, we do not observe any increase in the binding energy for fullerene-like nuclei [54], which may be an inaccuracy of the model under consideration.

So, we have performed systematics based on the early work of Wheeler, Teller and Hafstad. How realistic is the model discussed above and are its results applicable? Strangely enough, the present results show a very high degree of applicability of such a simple geometrical approach, at least for light nuclei. Recent studies,

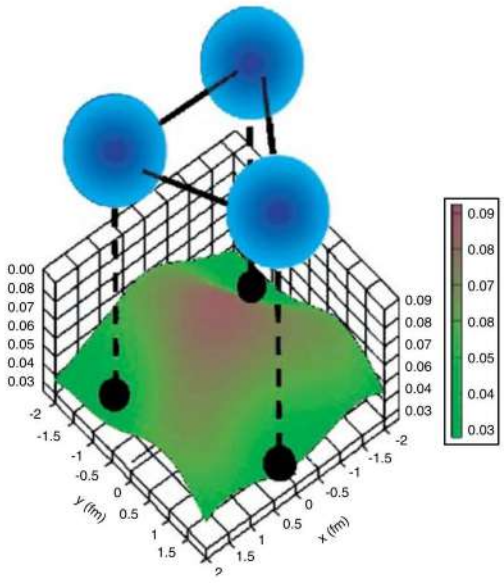


Figure 9. Cluster states in the $^{14}$C nucleus obtained in [80]. The valence neutron density distribution is also shown.

both theoretical and experimental, show the need to take into account the tetrahedral character for the $^{16}$O nucleus( [78] and references in this paper). Similar results are obtained for the carbon [79] nuclei. Figure 9 from the [80] paper shows the spatial distribution of $\alpha$-particles for the $^{14}$C nucleus.

Next, we will look at some other implications of this model.

### 1.1.2. Chain configurations

In 1956 Morinaga suggested [81], on the possibility of the existence of so-called *chain configurations*. Based on the $\alpha$-cluster model, he suggested that at a certain excitation energy in nuclei, $\alpha$-particles can line up in a line, so that a very highly deformed nucleus is obtained – a chain configuration, since it corresponds to minimization of the Coulomb repulsion between the fragments that make up the chain. The first structure we can thus construct is the $^{8}$Be nucleus.

The mechanism of origin of such configurations can be roughly described as breaking a number of bonds so that the $\alpha$-particles in the line remain bound. It is not difficult to see that for $^{12}$C one bond must thus be broken, for $^{16}$O – 3 bonds, etc. From here it is not difficult to calculate the excitation energy required to create such a configuration, and, as is obvious, the $0^+$ state for it lies under the threshold of fragmentation into $\alpha$-particles. Although this model

is rather approximate, Morinaga concluded that, at least for $^{12}$C and $^{16}$O nuclei, such states do not exist. Subsequently, a number of papers on the quasi-molecular structure of nuclei were published, confirming Morinaga's assumption about the possibility of such configurations, but they were supposed to be searched for above the fragmentation threshold (i.e., above the top row of the Ikeda diagram). In addition to quasi-molecular methods, there are at least two approaches to date that allow us to conclude that chain configurations are admissible. First, is the description of the nucleon system in the framework of a deformed oscillatory pit [82]. Second, an unexpectedly good fit with the cluster model was obtained by analyzing the energy surface in the framework of the liquid drop model. In particular, it was shown in [83] that for $^{20}$Ne and $^{24}$Mg nuclei there is a minimum corresponding to such a degree of deformation that the state can be considered as a chain state. This approach is usually cited in reviews on chain configurations as justification for their existence. Given that the model includes shell corrections, the coincidence of the predictions of highly deformed states with the oscillatory approximation is not surprising.

Let us consider the situation from the position of the $\alpha$-cluster model [56]. To calculate the energy, instead of the bond-breaking method proposed by Morinaga, we used the direct method with fixed coordinates. Consider a chain of $\alpha$-particles interacting with each other by means of potentials (6) and (7). This will allow us to calculate the binding energy of this system $E_b$. Then, the required excitation energy $E^*$ to produce the chain configuration can be calculated by knowing the fragmentation energy $E_{fr}$ of the nucleus into $\alpha$-particles (as is clear, in this case all bonds are broken). In other words:

$$E^* = E_{fr} - E_b. \tag{8}$$

Since in this approach we are no longer bound by the need to calculate the number of broken bonds and the fragmentation energy is taken from experimental data, the only parameter of the model is the radius of the $\alpha$-particle $R_\alpha$, which we have chosen to be 1.52 fm. This value is close to the available experimental data and determines the position of $\alpha$-particles in the chain at dense "linear" packing. This, in turn, allows us to calculate the binding energy of the chain configuration

by summing the nuclear (6) and Coulomb (7) potentials for all $\alpha$-particles, and from the formula (8) obtain the excitation energy and the moment of inertia of the $\Theta$ chain configuration. Two quantities – $E^*$ and $\Theta$, completely determine the position of the rotational band levels. Table 2 lists the excitation energies obtained from this approach, together with the energies from the work [83] obtained from the microscopic-macroscopic approach, for the minima on the energy surface corresponding to states with deformation close to chain states. Also in the table are the values of the energies of fragmentations of nuclei into $\alpha$-particles.

Table 2. Excitation energies obtained for states with $\omega$-type $N_\alpha$:$N_\alpha$:1 deformation in the framework of the $\alpha$-bound particle model [56] and in the liquid drop [83] model. The fragmentation energy $E_{fr}$ is indicated.

| Nucleus | Number $\alpha$-particles | Model of binding $\alpha$-particles (MeV) | Liquid drop model (MeV) | $E_{fr}$ (MeV) |
|---|---|---|---|---|
| $^{12}$C | 3 | 3.0 | 1.0 | 7.27 |
| $^{16}$O | 4 | 8.98 | 9.0 | 14.44 |
| $^{20}$Ne | 5 | 12.99 | 13.0 | 19.17 |
| $^{24}$Mg | 6 | 21.87 | 20.0 | 28.48 |

Since the chain configuration rotates around its center of mass and consists of spinless particles, it is invariant with respect to reflection, so that the rotational band will contain only states with even values of angular momenta and with positive parity. Strictly speaking, the moment of inertia of such a band is not necessarily a constant value; moreover, as will be discussed below, it can both increase and decrease with increasing angular momentum. In addition, as the excitation energy increases, the contribution from vibrational degrees of freedom [84] must be taken into account. But in this case we will assume, as a simplification, that the moment of inertia of the rotational band of the chain configuration is constant. In the classical approximation, it is easy to calculate it by the formula:

$$\Theta = \sum_{i=1}^{N} M_\alpha a_i^2 + \frac{2}{5} M_\alpha R_\alpha^2, \tag{9}$$

here $N$ is the number of $\alpha$-particles, $M_\alpha$ is the mass of $\alpha$-particle and $a_i$ is the distance from $\alpha$-particle to the center of mass of the chain configuration. Because of the small radius of the $\alpha$-particle, the second term is usually neglected. The excitation energies for the rotational band levels are calculated by the formula:

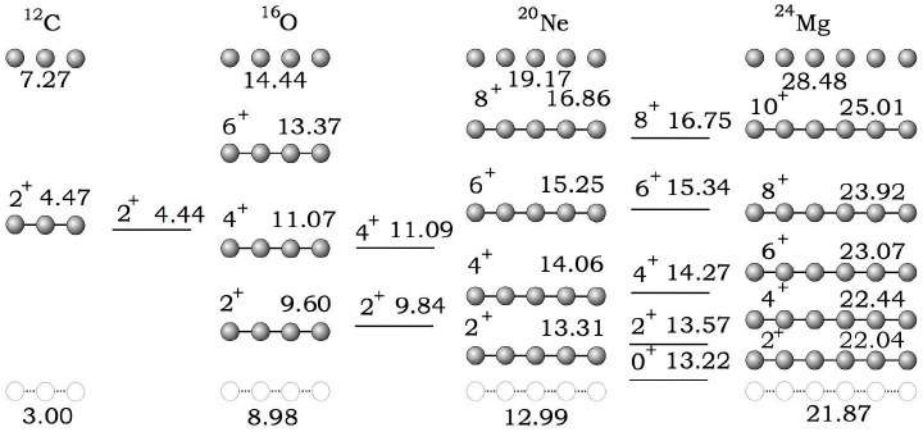


Figure 10. Theoretical (circles) and experimental (lines) energies for the rotational bands of the chain configurations of $^{12}$C, $^{16}$O, $^{20}$Ne, and $^{24}$Mg nuclei [56]. The lower levels marked with dashed lines correspond to the head levels of the rotational bands, the upper levels correspond to the fragmentation energies.

$$E_J = \frac{J(J+1)\hbar^2}{2\Theta} + E^*. \tag{10}$$

The resulting levels for the nuclei from Table 2 are shown in Figure 10, where the upper states correspond to the upper states of the Ikeda diagram (Figure 2). The states below the fragmentation energy are considered because we cannot accurately estimate the maximum angular momentum in the system in this simple model. An approximate estimate can be obtained from the following considerations. We define the angular frequency of the rotating deformed nucleus as:

$$\omega = \frac{\hbar(J(J+1))^{1/2}}{\Theta}. \tag{11}$$

Let us assume that the adiobaticity conditions are satisfied and in this model $\omega_{rot} \ll \omega_{osc}$. As was shown in [85], the maximum angular momentum of the hyperdeformed core $^{152}$Dy is of the order of 100. According to the calculations performed in [86], this value is in good agreement with the predictions based on the liquid drop model. Assuming that the nuclear radius is proportional to $A^{1/3}$ and calculating the corresponding radius for chain configurations, we can obtain that for the nuclei $^{12}$C, $^{16}$O,$^{20}$Ne, at the corresponding strains, the maximum angular momentum will be of the order of 3.5 and 7, respectively. More accurate calculations within such a simplified model are inadmissible.

As can be seen from Figure 10, in agreement with Morinaga's conclusions,

there are no levels corresponding to $0^+$ states of the chain configurations for the $^{12}$C and $^{16}$O nuclei. For the $^{12}$C nucleus, agreement is observed for the $2^+$ states, which must be recognized as coincidental since the $2^+$ structure at 4.44 MeV is well studied, and it is shown to be well described by a shape close to a right triangle [87]. In addition, as seen in Table 2, there is poor agreement between the predictions of the cluster model and the liquid drop model for the $^{12}$C nucleus. Thus, we can consider that if chain states exist in the $^{12}$C nucleus, they lie well above the fragmentation energy.

Similarly, for $^{16}$O nuclei, no states corresponding to $0^+$ states of chain configurations are observed. As can be seen, such a level would have to have an energy on the order of 9 MeV. This energy region in this nucleus is quite well investigated and it appears that even a strong overlap with the $2^-$ level with energy 8.87 MeV could not mask the corresponding $0^+$ state. Of the levels claiming to be higher spin states, there are only the rather low-lying 9.84 MeV $2^+$ and 11.09 MeV $4^+$ states with relatively small widths.

Much more interesting, from the point of view of the model under consideration, is the comparison for the known levels of the $^{20}$Ne nucleus. As can be seen from Table 2, the results of the excitation energy estimation for the core level of the strongly deformed state for the cluster model and the liquid drop model almost coincide. This core is characterized by a significant number (at least 7) of rotational bands of different structure. The initial and most reliable distribution of levels over the bands was performed in [88] (5 bands), further work was continued in [89]. The levels shown in Figure 10 are not reliably assigned to any rotational bands (see Table 20.20 in [89]). A list of levels with widths is given in Table 3.

Table 3. Proposed $K^+_8$ rotational band in the $^{20}$Ne nucleus [56].

| J | $E^*$ (MeV) | $\Gamma$ (keV) |
|---|---|---|
| 0 | 13.22 | 40 |
| 2 | 13.53/13.57 | 61/12 |
| 4 | 14.27 | 92 |
| 6 | 15.35 | - |
| 8 | 16.75 | 160 |

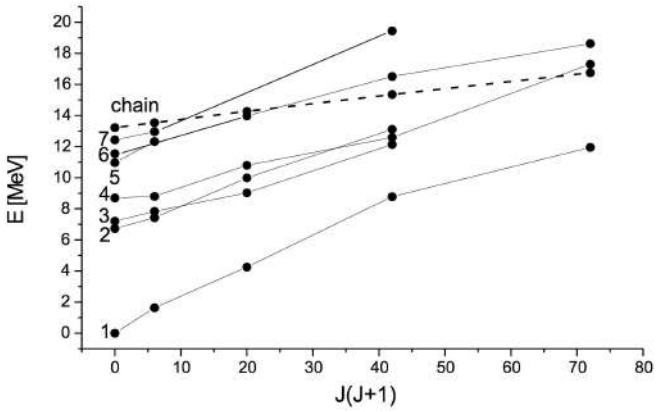


Figure 11. Rotational bands of the $^{20}$Ne nucleus. The dotted line shows the predicted chain state [56].

For the level corresponding to the state with angular momentum $J$=2, there are two possible candidates, differing slightly in energy. A comparison of this band with the reference data from the work [89] is presented in Figure 11.

As a conclusion on this issue, we note that in the literature the $^{24}$Mg nucleus is usually used to illustrate the possibility of describing chain states in the framework of the liquid drop model (see paper [18], Figure 6). It can be seen from Table 2 that the predictions of the cluster and droplet models are still close and that the head level of such a state should be nearly 7-8 MeV below the $\alpha$-particle collapse threshold. Nevertheless, the energy of this level is already large enough to allow unambiguous comparisons with the available experimental data (EXFOR data end at excitation energies on the order of 17 MeV). A similar situation with the $^{16}$O nucleus was considered in [90].

### 1.1.3. Bose-Einstein condensate in nuclei

So far we have considered approximations with a sufficiently strong "classical" component. Now we assume a transition to essentially quantum phenomena, which requires sufficient justification. Although this section is included as applications of the limit $\alpha$-particle model, it differs significantly from the approximations considered earlier. Although the formula (4) includes the binding energy of the $\alpha$-particle (6 bonds analogous to inter $\alpha$-particle bonds), nevertheless, as indicated, such $\alpha$-particles are virtual and this summand could, in principle, be replaced by some fitting quantity. However, such an approach at this stage would lead to unnecessary complication that has no connection with the fundamental processes.

This is described in detail in [91].

In this case, although we break the nucleus into its constituent $\alpha$-particles, but the latter are already analogs of free particles, and a phenomenon similar to Bose-Einstein condensation [91] is realized, accompanied not only by a change in the internal structure of the nucleus, but also in its size. From the perspective of quantum mechanics, the phenomenon itself, as well as the rationale for its possibility in nuclei, is detailed in the articles [92–94].

Let us first consider some experimental corollaries. They are usually related to the already mentioned above phenomenon of the increase of the nucleus size at the corresponding phase transition.

For example, when studying the scattering of $\alpha$-particles on the $^{12}$C nucleus, the condensation phenomenon leads to the appearance of a structure associated with the Airy minimum in the picture of the angular distribution [95]. Another manifestation of condensation was found in our experiment to study the levels of the $^{40}$Ca [63] nucleus. When studying the evaporation spectra of the $^{12}C^*$ nucleus in the $0_2^+$ state, we found an underestimation of the average energy carried away by such a nucleus from the compound [47] nucleus (these experiments will be discussed below). The explanation was obtained exactly in the framework of the condensation phenomenon approach, when a "loose" nucleus with a large radius has a higher probability of passing under the Coulomb barrier at a given energy [96]. A number of other important manifestations of the phenomenon of Bose-Einstein condensation in nuclei can be found in the review [97].

Since it is assumed that it is not possible to find any other explanation for the observed phenomena, we need methods to describe condensation in nuclei. One of the most interesting proposed methods in this direction is the approach developed in [94] by Yamada and Schuck. The condensate behavior was analyzed on the basis of the Gross-Pitaevskii and Hill-Wheeler equations. This approach has great generality, but is associated with significant computational difficulties. Therefore, in the works [59, 60] we developed a different approach based on the reduction of the problem to the problem of particle motion in some mean field, with the subsequent solution of the Schrödinger equation.

Let us consider the nucleus as a system of interacting $\alpha$-particles. In the

simplest case of a $^8$Be nucleus (two $\alpha$-particles), there is a resonance with energy $E^*$=92 keV. The magnitude of the de Broglie wavelength, in this case, becomes very large and thus we can require a large (compared to the size of the nucleus) wavelength of the constituent particles. On the other hand, the approximate distance between these clusters can be estimated from the dependence of the rotational band levels on the angular momentum. Calculating the moment of inertia of such a two-cluster configuration, one can obtain that the average density of the $^8$Be nucleus roughly corresponds to one third of the average observed density for most nuclei. Knowing the nucleon density distribution in the nucleus (from electron scattering data), one can estimate the energy at which a cluster state close in properties to Bose-Einstein condensation arises. And vice versa – at a known energy of occurrence of the cluster condensate, one can estimate the corresponding density. Note that the obtained result agrees well with Brink [5]'s prediction about the occurrence of clustering when the nuclear density decreases approximately threefold from the central one. As is well known, the dependence of nuclear density on radius is described by a function with "diffusion" at the boundary, and, figuratively speaking, light nuclei consist solely of "surfaces". Thus, one can justify the nuclear matter$\rightarrow\alpha$-cluster transition in light nuclei.

Let the function $\rho_0(r) \rightarrow \rho(E, r)$ specify the distribution of the nucleon density in the nucleus and be some function of the excitation energy. We calculate the function $\rho(r)$ corresponding to a threefold lower nucleon density (assuming the number of particles is conserved). Then, based on the convolution equation [98], we can calculate the distribution of the cluster density in such a nucleus.

$$\rho(r) = \int \rho_{cl}(r')\rho_\alpha(r - r')d^3r'. \tag{12}$$

Here, $\rho_{cl}$(r′) is the cluster density distribution, $\rho_\alpha$(r) is the nucleon density distribution in the $\alpha$-particle. This distribution was taken from scattering work in the form of the Fermi distribution:

$$\rho_\alpha(r) = (1 + wr^2/c)/\left(1 + \exp\frac{r - c}{a}\right). \tag{13}$$

The constants were chosen according to the work [11] as $c$=1.01 fm, $a$=0.372 fm, $w$=0.445 fm. The result is to obtain the cluster density for the ground state

of the nucleus and for the excited state corresponding to 1/3 of the density. It should be noted that the cluster density distribution, in this case, is not a "final" solution of the problem. For example, for a number of nuclei, the solution of such a problem leads to the appearance of negative densities at the Satchler-Love [98] transformation and it should be considered as intermediate, passing directly to the potential. For this purpose, the obtained value of the cluster density should be substituted into the convolution equation defining the interaction potential:

$$V(r) = \int \rho_{cl}(r')V_{\alpha}(r - r')d^3r'. \tag{14}$$

Here $V_{\alpha}$(r) – specifies the interaction potential between $\alpha$-particles. In this case, the Yamada-Schuck potential from the paper [94] was used. This potential belongs to the class of soft-core potentials and was found from fulfillment of two conditions:

1) A sufficiently fast decreasing wave function at zero. This is an analogue of the antisymmetrization condition.

2) The ground state, for the interaction of two $\alpha$-particles, should correspond with high accuracy to the case of the $^8$Be nucleus (reproducing the experimentally known width and energy of the resonance).

The obtained one-particle potential can be used to find the states corresponding to the cluster phase transition under the assumption of independent motion of the $\alpha$-particle in the mean field $V(r)$. Substituting it into the Schrödinger equation, we have the value of the single-particle state energy $E_{Sch}$, so that the phase transition energy for a nucleus consisting of $N_{\alpha}$ $\alpha$-particles can be calculated in the form [59]:

$$E_{BEC} = E_{Sch}(N_{\alpha} - 1). \tag{15}$$

This result allows us to plot the density dependence of the phase transition energy. As mentioned above, we must take into account that in the $^8$Be nucleus the averaged density is about three times smaller than the density at the center of the middle mass group nuclei, as well as the positions of the experimentally observed cluster states in the $^{12}$C and $^{16}$O nuclei. The result is presented in Figure 12. It shows the dependence of the single-particle energy, obtained from the solution of the Schrödinger equation with the potential found above, as a function of the

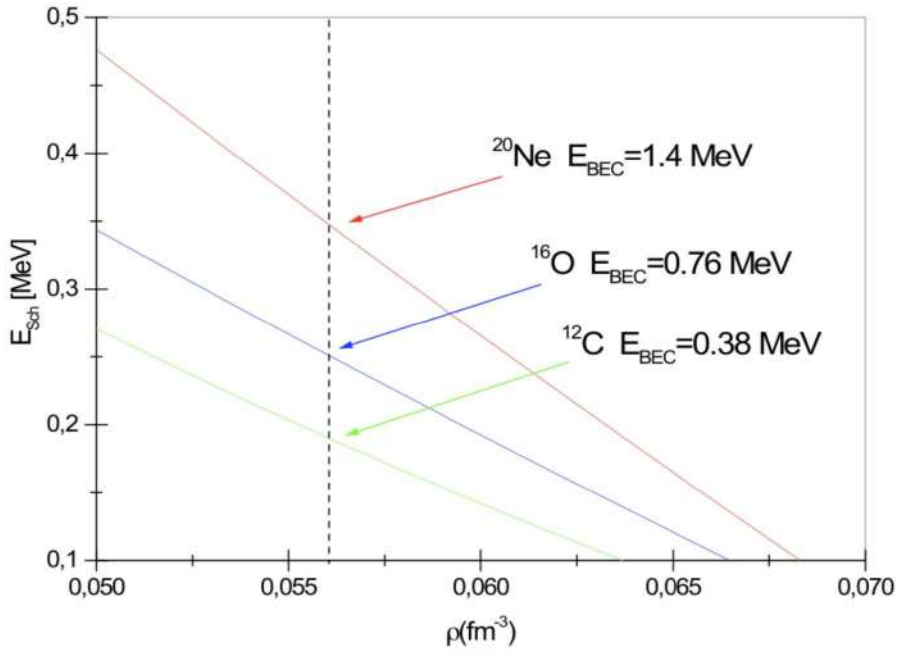


Figure 12. Energies for cluster states [59].

nuclear matter density for the three nuclei. The dotted line shows the value of the density corresponding to one third of the mean nuclear density. As can be seen, the excitation energy decreases monotonically with increasing nuclear density.

Table 4 shows the values of the obtained energies of transitions to the condensed state (measured from the threshold of disintegration into constituent clusters), as well as the values of the root-mean-square radii of such nuclear systems.

Table 4. Energies and root-mean-square radii of light nuclei during the transition to the Bose-Einstein condensation state [59].

| Number of $\alpha$-particles | Energy above threshold (MeV) | RMS radii (fm) |
|---|---|---|
| 2 | 0.092 | 2.9 |
| 3 | 0.38 | 3.5 |
| 4 | 0.76 | 3.8 |
| 4 | 1.4 | 4.1 |
| 6 | 3.6 | 4.3 |
| 7 | 6.4 | 4.7 |

Figure 13 shows the behavior of the obtained excitation energies and the values of the root-mean-square radii of the ground and excited states for nuclei with different masses. It should be noted that the radii increase significantly during the phase transition, which is in good agreement with the assumption of the occurrence of a Bose-Einstein condensate in the nuclear system.

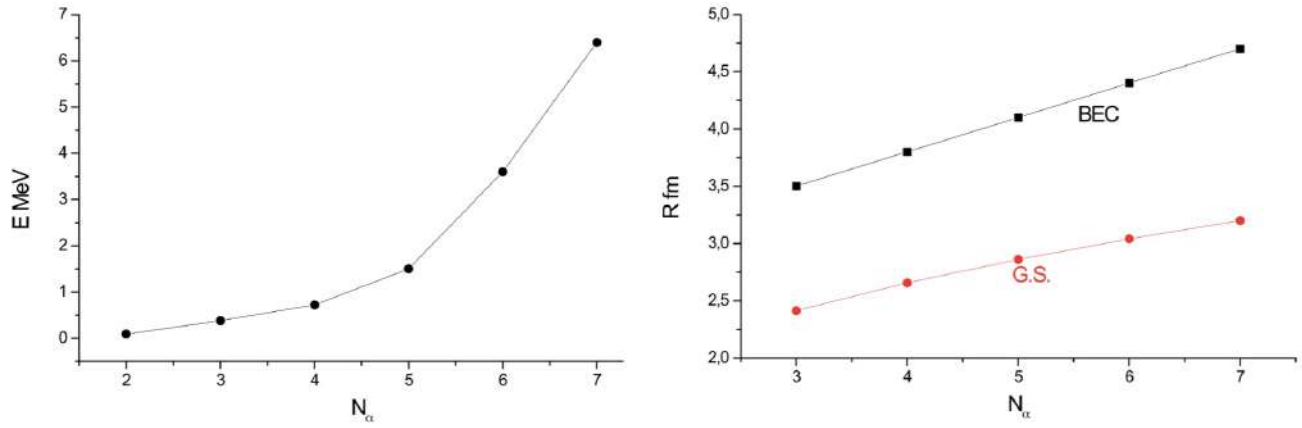


Figure 13. Excitation energy values (left) and comparison of the radii of the ground and excited states (right) of nuclei [59].

Assuming that the considered phase transition leads to a significant contribution of the cluster configuration to the wave function of the nucleus, one can expect a significant contribution of decay channels with cluster escape, as well as the appearance of rotational bands.

In this chapter, the case of the maximal $\alpha$-particle model has been considered. It has been shown that the interpretation proposed in [3] continues to hold for all nuclei known to date [54, 55, 57].

It has been shown that the cluster model gives good agreement with calculations based on the drop model with Nilsson-Strutinsky corrections for strongly deformed states of the $^{20}$Ne nucleus [56, 60]. Candidates for such states from the available experimental data are proposed. The possibility of existence of subthreshold chain states is shown [56].

It was shown that in the framework of the limit cluster model, by analogy with the shell model, a transition to the description of the nucleus as a system of $\alpha$-particles moving in some mean field is possible [59]. The results of this approach coincide with the results of calculations based on the Hill-Wheeler and Gross-Pitaevskii equations [59].

## 1.2. Two-particle model

As it was pointed out in the previous section, in spite of the considerable simplicity of the maximal $\alpha$-cluster model, there are some difficulties associated

with the transition to the quantum mechanical description. Moreover, such a transition can take place directly only in the case of exotic states of the nucleus, such as Bose-Einstein condensation. However, this is not a serious problem, since a number of other approaches have been developed, among which, recently, the AMD method has been emphasized.

At the same time, the approach in which the system is split into two parts – a cluster (not necessarily a $\alpha$-particle) and a cor, proved to be not only a clear and simple model, but also allowed quantitative evaluations in the framework of quantum mechanical calculations. As stated in the introduction, such a partitioning of the system is necessary to reduce the variables and to reduce the problem to the easily solvable case of two-particle interaction.

Let us consider the most typical examples.

1) Helium isotopes. In this case, the $\alpha$-particle plays the role of a core. Moreover, despite the fact that the excess neutrons do not agree well with the concept of a structureless, well-localized cluster, nevertheless this is also a variant of the cluster degree of freedom, which allows one to reduce the number of variables to solve structural problems very effectively. For example, for the $^6$He nucleus, the problem reduces to three-body instead of six-body. And, in spite of the fact that stochastic methods currently allow to work with systems of 6 or more particles, this transition significantly simplifies the description of the system.

2) The $^6$Li and $^7$Li nuclei. These nuclei turned out to be very convenient to consider as a $\alpha$-particle plus a deuteron or, respectively, a triton. Owing to the low energy of collapse into these components, the use of these nuclei in the transmission reaction opened a new chapter in the study of $\alpha$-particle states in heavier nuclei.

3) The $^8$Be nucleus. This is the first unstable self-conjugate nucleus. It exists only as a resonance with energy 92 keV, decaying into two $\alpha$-particles. Nevertheless, this is one of the most important cases of clustering, allowing us to study this phenomenon effectively. This nucleus has already been mentioned in the section on chain configurations and Bose-Einstein condensation. It is also necessary to note important corollaries such as:

- The presence of a rotational band, which allows us to estimate the distance

between the $\alpha$-particles composing the nucleus, and to use this value as a measure of clustering [18, 41, 59]. This point will be described in more detail below.

- Information on resonance states has contributed to the emergence of $\alpha$-$\alpha$ interaction potentials that greatly facilitate the description of cluster degrees of freedom within the potential model [99–103]. One of such potentials was used above in the description of the $\alpha$-particle condensate in nuclei, the Yamada-Schuck [94] potential.

- Because of the above properties, an important indicator of the cluster content in the excited states of nuclei is the departure of the $^{8}$Be nucleus in reactions proceeding through compound-nucleus [47] formation. The experiment performed by us will be described in the corresponding section.

- This nucleus proved to be crucial for checking the position of a number of exact quantum mechanical models that do not contain clustering explicitly [17].

4) The $^{12}$C and $^{16}$O nuclei. At first glance, reducing these nuclei to the two-particle version contradicts the previously discussed models with a "geometric" approach. However, especially for the oxygen nuclei, this approach has greatly clarified their structure, resulting in the confirmation of the correctness of the geometric approaches [104].

5) The $^{20}$Ne and $^{44}$Ti nuclei. These nuclei are "canonical" in describing the cluster degrees of freedom within the potential model. Populating two protons and two neutrons in a new shell above the magic number promotes clustering on the one hand, making "pure" shell calculations difficult on the other [76]. For a long time, this approach was the only way to describe the rotational bands in these nuclei arising from the $\alpha$-particle transfer.

### 1.2.1. Tunneling

A number of the examples discussed above are united by the appearance of well-structured rotational bands. This is not the only manifestation of the cluster nature of these nuclei, but it is one of the most obvious and well describable.

To explain the appearance of rotational bands in the $^{16}$O nucleus, the manifestation of the cluster structure of this nucleus in the form of $^{12}$C+$\alpha$ was considered in [15]. Such a structure leads to a noticeable octupole deformation. The latter can have a minus or plus sign, but energetically these states are degenerate. Then

the new state can be described as their superposition in the form $\Psi^{\pm}=\langle^{12}\mathrm{C}\otimes\alpha\rangle \pm \langle\alpha\otimes^{12}\mathrm{C}\rangle$. The plus corresponds to even and the minus to odd states. If the Hamiltonian of the $H$ system allows mixing between them (the possibility of a tunnel transition between these two deformations), then the splitting $\Delta E=\langle\Psi^{-}H\Psi^{-}\rangle$-$\langle\Psi^{+}H\Psi^{+}\rangle$ will occur between the states with positive and negative parity. This will cause the band with even values of states to be lower than the band with odd values.

$$\begin{array}{ll} E_{+}(J) = E_0 - \frac{\Delta E}{2} + \frac{\hbar^2 J(J+1)}{2\Theta^{+}} & K{=}0^{+}, \\ E_{-}(J) = E_0 + \frac{\Delta E}{2} + \frac{\hbar^2 J(J+1)}{2\Theta^{-}} & K{=}0^{-}. \end{array} \tag{16}$$

At the same time, their moments of inertia $\Theta^{+}$ and $\Theta^{-}$ almost the same.

The model turned out to be very successful in terms of a visual explanation of the phenomenon, but unfortunately it was difficult to parameterize, taking into account that for heavier nuclei the splitting value turns out to be a function of the spin of the state (or excitation energy). Below we will consider in detail the contribution of such a mechanism in the case of the $^{40}$Ca nucleus.

### 1.2.2. Potential model in an elastic channel

Much more successful, from this point of view, was the potential model in which the cluster was in the core field.

The basic ideas for this approach are the results obtained from resonance scattering, namely, the observation of sufficiently narrow resonance states forming one or more rotational bands with approximately linear dependence of the excitation energy on the square of the angular momentum. As in the case of the quasi-classical approximation for a deformed nucleus, the level system of the rotational band can be described, in the first approximation, by the formula (10), so that the problem is reduced to the determination of the excitation energy of the head level $E^{*}$ and the moment of inertia.

For the moment of inertia, it is easiest to consider the case of two spherical nuclei – cluster $A_1$ and core $A_2$, so that the formula (9) can be rewritten as:

$$\Theta = N_0 \left[\frac{2}{5}(A_1^{5/3} + A_2^{5/3}) + [A_1 A_2/(A_1 + A_2)](A_1^{1/3} + A_2^{1/3})^2\right] \cdot r_0^2, \tag{17}$$

where $N_0$ is a parameter and $r_0$ ∼1.3 fm. In particular, in the work [105], a value of $0.0104 \cdot 10^{-42}$MeV·c$^2$ was chosen for $N_0$. In the following, when analyzing our results, we will use a simplified version of this formula as a criterion for the possibility of a cluster description of the bands.

For the case of heavy clusters, in the considered phenomenological approximation, the excitation energy for the head level can be chosen as $E^* = E_B + E_C$, where $E_B$ is the binding energy for the considered cluster-core system, and $E_C$ is the Coulomb interaction, which is a correction for the threshold state in the Ikeda diagram. It can be chosen in the form [105]:

$$E_C = 1.21 Z_1 Z_2 [r_0(A_1 + A_2)](A_1^{1/3} + A_2^{1/3}) + 0.5]^{-1}. \quad (18)$$

In spite of the fact that this approach, as will be shown below, allows us to describe the rotational states for "good" cluster nuclei quite accurately, it has significant disadvantages inherent in all phenomenological approaches – poor definition of the limits of applicability of the approach and difficulty of including the obtained results in the quantum-mechanical description of the structure of the nucleus.

The simplest variant of the extension of this problem is the quantum-mechanical solution for the system of two bodies interacting by means of some potential. Let us briefly consider the main provisions of the potential model. As mentioned in the introduction, the main contribution to its development was made by Bak [11–13] on the basis of analyzing the applicability of the convolution potential for cluster states [14]. As usual, in the quantum mechanical two-body problem, the Hamiltonian is divided into parts corresponding to the relative motion and the motion of the center of mass. For the problem of relative motion of the cluster with mass $A_1$ and the core with mass $A_2$, the Schrödinger equation must be solved:

$$\hat{H}\psi(\mathbf{r}) = \left[\frac{\hbar^2}{2\mu}\nabla^2 + V(\mathbf{r})\right]\psi(\mathbf{r}) = E\psi(\mathbf{r}), \quad (19)$$

where $\mu = \frac{A_1 A_2}{A_1 + A_2}$ is the reduced mass, and $V(\mathbf{r})$ is the interaction potential of the cluster and the core. Further, the problem is reduced to solving the radial equation:

$$\left[-\frac{\hbar^2}{2\mu}\frac{d^2}{dr^2}+\frac{\hbar^2 L(L+1)}{2\mu r^2}+V(r)\right]\varphi_{nL}(r)=E_{nL}\varphi_{nL}(r) \tag{20}$$

and the potential is taken as the sum of the nuclear and Coulomb interactions:

$$V(r)=V_N(r)+V_C(r). \tag{21}$$

The Coulomb term, unless otherwise specified, is written as:

$$V_C(r)=\begin{cases}\frac{Z_1Z_2e^2}{2R_C}\left[3-\left(\frac{r}{R_C}\right)^2\right] & r\le R_C;\\ \frac{Z_1Z_2e^2}{r} & r>R_C.\end{cases} \tag{22}$$

Another variant of the notation, via the error function $\mathrm{erf}(ar)/r$, was used by us, as mentioned above, in the calculations of the condensation state.

Thus, the problem is, for the most part, reduced to the choice of the nuclear potential $V_N$. In describing the maximal $\alpha$-cluster model, we have used set of the molecular potentials, which is consistent with the main idea of the cluster [18] approach. This type of potential can be roughly divided into attractive and repulsive regions. The latter, in our case, corresponds to the Pauli principle by preventing a strong cluster-core overlap when cluster destruction will occur due to antisymmetrization. This approach has also been implemented when trying to describe the $\alpha$-$\alpha$ interaction [103]. There have been more or less successful attempts at a general description of cluster-core type systems with an impermeable wall [106] (as a variant, with a soft core, when the wave function decreases rapidly enough at zero [94]). On the other hand, for the case of nuclear interactions, it would have been preferable to go to well-established optical potentials, such as Woods-Saxon. However, a serious problem in this case was the presence of so-called *unphysical states* in such potentials. This was especially important when directly solving the equation (20) with a sufficiently deep potential. Of the resulting spectrum of bound states, only some corresponded to the experimentally observed levels. The rest appeared to be forbidden due to the Pauli principle. The problem was solved by introducing a condition on the number of nodes, which can be found from Wildermuth's formula [11]:

$$2N + L \geq \sum_{j=1}^{n_c} (2n_j + l_j). \tag{23}$$

Here $N$ and $L$ are the principal quantum number and orbital momentum of the cluster, and $n$ and $l$ are the corresponding quantum numbers of the nucleons in the cluster containing $n_c$ nucleons. Usually, for calculations of the main rotational bands in this formula, the number of nodes of the ground state wave function is chosen so that the equality is satisfied. This approach allows one to exclude unphysical states, but imposes a number of requirements.

(1) As shown by Ohkubo in [107], the formula (23) is applicable only if, if the condition of strong overlap with the oscillatory wave functions $u_{NL}(r)$ is satisfied for the wave functions of the forbidden states $\varphi_{NL}(r)$, i.e., the value $\langle \varphi_{NL}(r) | u_{NL}(r) \rangle^2$ is close enough to unity. In particular, it is shown in [107] that the potential proposed by Pilt [108] and well describing the level distribution for the $^{44}$Ti nucleus does not possess such a condition.

2) In the case of sufficiently heavy clusters, it is sometimes difficult to calculate the right-hand side of the formula (23), not to mention the fact that it has only the character of a restriction. Moreover, the problem of cluster selection is not always self-evident. This problem was successfully solved by Buck [109].

It should be noted that such an approach is valid only in the case of the local potential model under consideration. The microscopic approach within the resonating group method or algebraic approaches may yield a different number of nodes. Thus, for example, for the case $\alpha$+$^{12}$C in the orthogonal conditions method and the resonating groups method, the head state of the rotational band $K = 0^+$ (at an excitation energy of 6. 6 MeV) is described by a wave function with three nodes ($2N + L$=6) [110], while the potential model and the model based on $SU(3)$ symmetry assume 4 nodes ($2N + L$=8) [111].

Hence, one of the central problems of this approach is the choice of potential. We mainly use form factors for potentials of the following kind:

-Woods-Saxon $WS$.

$$f(r) = \frac{1}{\left(1 + \exp\left(\frac{r-R}{a}\right)\right)} \tag{24}$$

-Square Woods-Saxon $WS^2$.

$$f(r) = \frac{1}{\left(1 + \exp\left(\frac{r-R}{a}\right)\right)^2} \tag{25}$$

-Potential developed by the Oxford group *cosh*.

$$f(r) = \frac{1 + \cosh(R/a)}{\cosh(r/a) + \cosh(R/a)} \tag{26}$$

-Combination $WS + WS^3$.

$$f(r) = \frac{x}{1 + \exp\left(\frac{r-R}{a}\right)} + \frac{1-x}{\left[1 + \exp\left(\frac{r-R}{3a}\right)\right]^3} \tag{27}$$

-Potentials of single $F1$

$$f(r) = \int \rho_{cl}(r')V_\alpha(r - r')d^3r' \tag{28}$$

or double $F2$ folding.

$$f(r) = \int\int \rho_{cl(1)}(r_1)\rho_{cl(2)}(r_2)V_\alpha(s)d^3s \tag{29}$$

here $\mathbf{s} = |\mathbf{r} + \mathbf{r_1} - \mathbf{r_2}|$.

All the above potentials will be further considered in a more general case, when describing reactions in the framework of the optical model. In this case, we add an imaginary part to the interaction potential, usually in the form $WS$, so that the total interaction potential can be written as:

$$U(r) = -V(r) + \mathrm{i}W(r), \tag{30}$$

where $V(r) = V \cdot f_1(r)$ and $W(r) = W \cdot f_2(r)$, $V, W$ are the depths of the real and imaginary parts, and $f_{1,2}$ are the form factors of the real and imaginary parts, respectively. This approach allows us to successfully describe the angular distribution of elastic scattering of particles and ions, and the permeability coefficient calculated for a given potential allows us to calculate the fusion cross section.

The following criteria for "successful" application of the selected potential can be specified:

1) Describe the distribution of rotational band levels.

2) Reproduce the widths of the resonance states.

3) Reproduce the intensities of electromagnetic transitions between states.

4) The potential can be used as a real part in describing the angular distribution of elastic scattering of a nucleus-cluster on a nucleus-core to determine the cross section (or correctly reproduce phase shifts) or to describe reactions with particle redistribution (e.g., to determine the permeability coefficient in the Hauser-Feshbach model).

In some cases, the problems may be supplemented by requirements to reproduce the mean radius or momentum distribution.

In part, such problems for the "canonical" nuclei $^{20}$Ne and $^{44}$Ti, as well as for $^{8}$Be, were solved by Buck in [76, 101, 112].

In addition, the rotational bands can be analyzed in the framework of form [113] isomerism, in analogy to the states found in the actinide region. Such predictions, obtained for a number of self-conjugated nuclei in the $p$ and $sd$ shell region, allow one to link low-lying low-spin states whose cluster structure is established, for example, from the study of transfer reaction or elastic scattering mechanisms and high-spin states found from the study of $\gamma$ spectra.

Further extensions of the model are usually associated with group theory calculations. One of the main reasons for the necessity of such an extension is the difficulty (or impossibility) of describing the experimentally observed phenomenon of fragmentation of cluster states, when several closely spaced states with the same spin are observed. Within the potential model the description of this phenomenon can be given only qualitatively, while the group approach for light nuclei allows a detailed comparison for most levels. The basis for this approach is the idea of the formation of molecular states arising from the interaction of nuclei, so that some similarity between rotational and vibrational states should be observed, as is the case in two-atomic molecules. By introducing the vibrational quantum number $n_0$ as an additional degree of freedom, along with the angular momentum, a relatively simple formula for describing the spectrum of excited states [114] (an extension of the formula (10)) can be obtained:

$$E_{L,n_0} = -D + A\left(n_0 + \frac{1}{2}\right) - B\left(n_0 + \frac{1}{2}\right)^2 + CL(L+1), \tag{31}$$

where $A, B, C, D$ are the fitting parameters. The number of fitting parameters can be reduced within an anharmonic vibration-rotation model approach that takes into account the quadrupole nature of the vibration component, as was done in [115].

All this convincingly shows the importance of taking into account the cluster states for the above nuclei. It should be noted that even for them the problem is far from being solved [116, 117]!

Another significant gap in the description of the cluster degrees of freedom is the weak study (both experimental and theoretical) of light nuclei with neutron excess. It is to fill this gap that Chapter 3 is devoted.

The potential model can be extended to the inelastic channel. In this case, the problem is reduced to the calculation of the reaction cross section using the formula:

$$\sigma(E) = \frac{\pi}{k^2}\sum_L (2L+1)(1 - |\eta(E)|^2), \tag{32}$$

where $\eta(E)$ – is defined in terms of the phase shift for a given potential. In the most general case, this approach requires the imaginary part of the potential or the imposition of boundary conditions on the wave function used. To date, this method has worked well when used in conjunction with the coupled channel method. Nevertheless, this variant already implies a departure from the clustering ideas considered in this paper, so the variant with cross-section computation based on (32) will be considered in the last chapter as an analog of the cluster case for the potential model. In this case (32) can be rewritten as:

$$\sigma(E) = \frac{\pi}{k^2}\sum_L (2L+1)T_L, \tag{33}$$

where $T_l$ is the permeability coefficient for partial wave $L$ at energy $E$. The simplest but very useful case of the potential is the rectangular pit model. Let us consider only the case of a pit of radius $R$, where the potential outside is defined only by the sum of the Coulomb (22) and centrifugal $V_L = L(L+1)\hbar^2/(2\mu R^2)$

potentials. In this case, the permeability coefficient is written in the form:

$$P_L(kR) = \frac{1}{F_L(kR)^2 + G_L(kR)^2}. \tag{34}$$

here $F_l$ and $G_l$ are regular and irregular Coulomb wave functions, respectively. This quantity is often encountered in nuclear reaction physics. In Chapter 7, an extension of this model to the complex potential and the description of fusion reactions will be discussed.

## 1.3. Reactions

Below is a brief overview of the main reaction types used in this work.

### 1.3.1. Elastic scattering

The simplest reaction to infer a significant contribution of the $\alpha$-cluster state is the elastic scattering of $\alpha$-particles. In this case, information on the properties of the levels can be extracted from the phase analysis of the angular distribution. Unfortunately, such a procedure becomes rather complicated as the level density grows, especially given our increased interest in levels with large reduced widths, i.e., with a high contribution from configurations of the $|\alpha\otimes\mathrm{Cor}\rangle$ form.

Nevertheless, it was the resonance scattering experiments that provided initial insights into the manifestation of $\alpha$-cluster states. For this purpose, measurements of the energy dependence of the elastic scattering cross section of $\alpha$-particles were carried out, and the excitation function had to be known in a sufficiently wide range but with a small energy step. Then, if the energy of the $\alpha$-particle-target system corresponded to some level of the constituent nucleus, a significant increase in the cross section, of the order of several barns, was observed. Significant progress in the study of this reaction has been made since the advent of tandems – optimal gas pedals for studying excitation functions with good accuracy. However, if the range of energies is too large and there are no accurate predictions for the positions of the relevant levels, the work of scanning the relevant region requires a Herculean effort. This is evident from the results obtained in the study of the spectra of $^{16}$O and $^{20}$Ne nuclei at the University of Madison-Wisconsin under the direction of Prof. Richards [118–121].

The quantum description of the scattering of a zero-spin particle is well understood and described in the relevant sections of scattering theory. For simplicity we will restrict ourselves to the case of spinless particles. Consider a system of two interacting particles described by the Schrödinger equation (19). At a large distance from the scattering center and under the condition of spherical symmetry of the potential and its boundedness in space, the solution can be written as a superposition of the incident plane wave and the scattered spherical wave:

$$\psi = \mathrm{e}^{\mathrm{i}kz} + f(\theta)\frac{\mathrm{e}^{\mathrm{i}kr}}{r}. \tag{35}$$

Here $k = \sqrt{2\mu E}/\hbar$, and $f(\theta)$ is the scattering amplitude. In the case of elastic scattering, it can be shown that the following equality holds for the cross section magnitude:

$$\frac{d\sigma}{d\Omega} = |f(\theta)|^2. \tag{36}$$

By passing to the radial wave $\varphi(r)$ functions for the Schrödinger equation and using the spherical wave decomposition of the incident plane wave from (35), we can obtain an expression for the scattering amplitude (the Faxen-Holtsmark formula):

$$f(\theta) = \frac{1}{2\mathrm{i}k}\sum_{L}(2L+1)(\exp(2\mathrm{i}\delta_L) - 1)P_L(\cos\theta). \tag{37}$$

where $\delta_L$ is the magnitude of the phase shift and $P_L(\cos\theta)$ is a Legendre polynomial of order $L$.

Consider an isolated level in the nucleus excited by interaction with a beam particle. Then, the excitation energy can be written as:

$$E^* = E + S, \tag{38}$$

where $E$ is the channel energy equal to the energy of the colliding particle in the center-of-mass system, and $S$ is the binding energy of the particle in the compound nucleus. By analogy with an oscillator with friction, the amplitude of oscillations of which, under the action of a forcing force, depends on the frequency of its influence on the oscillator, we can rewrite the expression for the wave function of

a decaying quantum system:

$$\psi \sim \exp(-\mathrm{i}Et/\hbar)\exp(-\Gamma t/(2\hbar)). \tag{39}$$

This gives an exponential decay of the quantity $||\psi_l|^2$ with lifetime $\tau = \hbar/\Gamma$. Such a state can be constructed as a superposition of states with a small difference in energy:

$$\psi \sim \int_{-\infty}^{+\infty} A(E)\exp(-\mathrm{i}Et/\hbar)dE, \tag{40}$$

where $A(E)$ denotes the amplitude of states with energy $E$. Since the cross section is proportional to the square of the amplitude, after the Fourier transform, we can write:

$$\sigma \sim \frac{1}{(E-E_0)^2 + \frac{1}{4}\Gamma^2}. \tag{41}$$

The proportionality factor can be determined from a phase space analysis for the reaction under consideration [122], so that, for a reaction in which $x$ denotes the input channel and $y$ denotes the output channel, we have:

$$\sigma_{xy} = \frac{\pi}{k^2}(2L_x+1)\frac{\Gamma_x\Gamma_y}{(E-E_0)^2 + \frac{1}{4}\Gamma^2}, \tag{42}$$

which is a variant of the Breit-Wigner formula for spinless particles.

Taking into account the phase shift value introduced earlier in (37), the elastic scattering cross section from formula (36) can be written as:

$$\sigma_L(E) = \frac{4\pi}{k^2}(2L+1)\sin^2\delta_L, \tag{43}$$

In this case, the Breit-Wigner cross section is reproduced when the equality $\tan\delta_L = \Gamma/(2(E_0 - E)$ is satisfied. It follows that at the resonance energy, i.e., when $(E_0 - E)$=0, the phase shift is $\delta_L = \frac{1}{2}\pi$.

More generally, in order to reproduce the behavior of the cross section between two resonances, both resonance scattering ($\beta_L$) and potential scattering (scattering on a rigid sphere) processes $\phi_L$ are taken into account in the phase shift. Then $\delta_L = \beta_L - \phi_L$ and the resonance condition:

$$\beta_L = \arctan \frac{\Gamma}{2(E_0 - E)} \tag{44}$$

and the elastic interaction cross section can be written as:

$$\sigma_L(E) = \frac{4\pi}{k^2}(2L+1) \left| \frac{\frac{1}{2}\Gamma}{E_0 - E - \frac{1}{2}\mathrm{i}\Gamma} - \exp(\mathrm{i}\phi_L)\sin(\phi_L)) \right|^2 . \tag{45}$$

Analysis of the scattering of $\alpha$-particles on the basis of this theory led to some curious conclusions. It turned out that levels with a significant contribution of states with the $\alpha\otimes$Cor structure are very common in nuclei. This result was somewhat unexpected, since there were difficulties in explaining it in the framework of the shell model. The continued search for similar states at higher excitation energies or in heavier nuclei was hampered by the imperfection of the experimental procedure. Indeed, it was necessary to scan a very large area with a small step, and a considerable time was required to set the appropriate statistics.

As can be seen from the formulas (36) and (37), the differential cross section for elastic scattering includes the square of the Legendre polynomial. Thus, the maximum of the cross section will be observed at angles 0° and 180°. However, there is interference with the potential scattering discussed above, which negatively affects the observation of resonances. Assuming that the potential scattering has a smooth dependence on the angular momentum, and that the even and odd Legendre polynomials have different signs when scattering by 180° and the same when scattering by 0°, we obtain that the potential scattering is large under 0°and small under 180°. Thus, with backward scattering we have optimal conditions for studying resonances.

The Inverse Geometry and Thick Target Method (IGTT) is devoid of the above disadvantages (the need to scan a wide energy region with a small step and the unattainability of the angle 180°). In this case, a beam of heavy ions from the gas pedal enters a scattering chamber filled with gas containing light nuclei (hydrogen, helium). At the same time, the beam energy, taking into account losses in the thin entrance window and gas pressure, is chosen so that the beam stops completely in the chamber. In the case of interaction of beam particles with a gas target, light recoil nuclei with a much longer range can be registered by

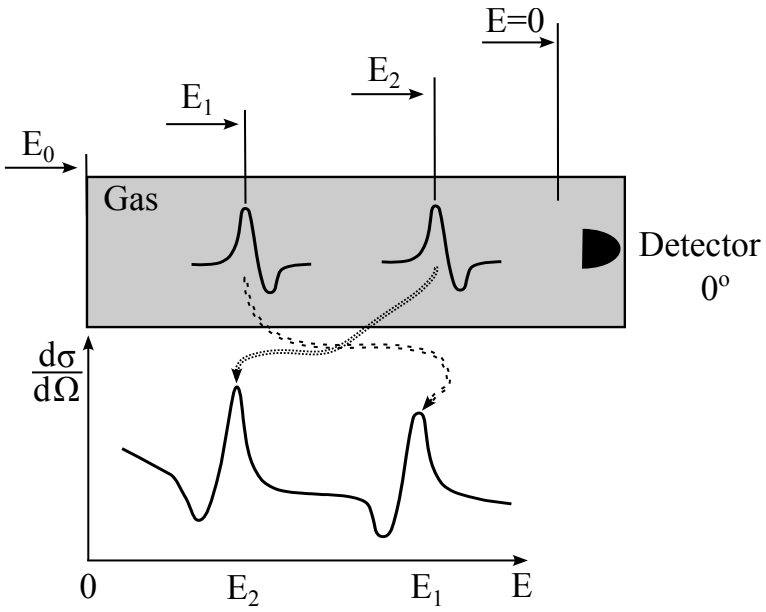


Figure 14. Inverse geometry method with a thick target

.

detectors located on the chamber wall, including at an angle of 0°, corresponding to an angle of 180° for the "usual" geometry. Another important advantage of this scheme is the possibility of scanning a large range of energies (from the energy that the beam has immediately after passing the window to zero) in "one pass", i.e., without changing the energy of the accelerated ions. This makes it possible to use a cyclotron with a sufficiently high beam intensity as a gas pedal. It should also be noted the possibility of working with heavy ions, experiments with which are difficult in the case of direct geometry (gases or radioactive isotopes). The disadvantages of the method include the difficulty of obtaining the angular distribution in a fairly wide range of angles due to the problem of determining the point at which the interaction of the beam ion with the nucleus of the gas target occurred and, as a consequence, the "integrity" of the cross section, which grows rapidly with increasing angle, as well as the difficulty of separating the elastic and inelastic components.

A schematic diagram illustrating such an approach is shown in Figure 14. The yield function for the reaction under consideration for the energy range $E = (E_1 - E_2)$ will be described as [123]:

$$Y(E) = I(E) \int_{E-\Delta E/2}^{E+\Delta E/2} \frac{\sigma(E_i)}{\epsilon(E_i)} dE_i, \tag{46}$$

where $\Delta E$ is the energy channel width, $I(E)$ is the number of beam particles, and $\epsilon(E)$ is the beam braking cross section in the gas target.

This method was very effective in studying the resonance scattering of $\alpha$-particles on both self-conjugated nuclei and neutron-excess nuclei with excitation of levels having $\alpha$-cluster nature. Figure 15 shows an example of the excitation function we obtained for the scattering of $\alpha$-particles on such nuclei. The experiment was performed on a DC-60 cyclotron (Astana, Kazakhstan). The time-of-flight separation method was used as an identification method. A detailed description of the performed work is presented in the article [124]. Comparison of the results obtained by us with abstracts shows high efficiency of the method. These results are important not only for the study of cluster degrees of freedom, but also for nuclear astrophysics problems.

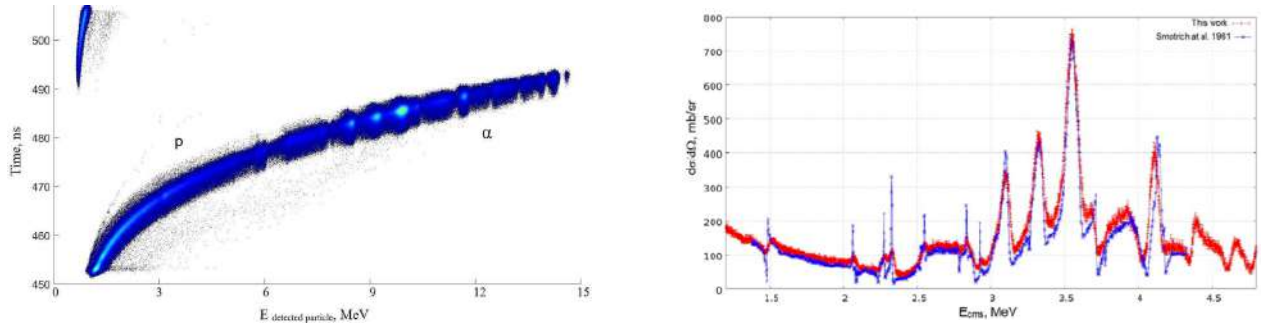


1 2

Figure 15. 1. Time-span spectrum for the products of the interaction of the $^{15}$N nucleus with $\alpha$-particles. 2. The elastic scattering excitation function of $\alpha+$ $^{15}$N obtained in this work (red line). A comparison with the results obtained in the traditional geometry (blue line) [124] is shown.

Finally, it is possible to study the manifestation of cluster configurations formed by the scattering of heavier ions, where a significant number of molecular resonances can be observed. This is the case, for example, in the systems $^{12}$C+$^{12}$C, $^{16}$O+$^{12}$C, $^{16}$O+$^{16}$O, $^{24}$Mg+$^{24}$Mg, $^{28}$Si+$^{28}$Si [125]. But the currently available experimental data for these nuclei are scarce enough that the corresponding rotational bands cannot be clearly distinguished. Despite the importance of the problem – determination of molecular states in the heavy ion system – to date there is no approach that allows one to unambiguously distinguish such states in experiment. Thus, for the most interesting from this point of view system $^{16}$O+$^{12}$C, about half a dozen states that can be considered as quasi-molecular are known so far. The main experimental approaches here can be considered to be:

1) Analysis of the angular distribution for energies corresponding to a resonance-like change of the cross section with energy. It is assumed that in this case the summation in the formula (37) is dominated by the summand for the angular momentum $L$, so that the contribution $|P_L(\cos\theta)|^2$ in the angular distribution will be significant. Obviously, this method requires an angular distribution in the maximum available angular range and performs poorly both at very low energies (because of the significant Coulomb contribution) and at very high energies (because of the very high level density and strong oscillations). Further this approach will be analyzed in more detail.
2) Analysis of the oscillations of the merger cross section, with assignment of angular momenta to the peaks, according to the assumption of a linear dependence of the excitation energy as a function of $L(L+1)$. A significant disadvantage of this approach is the considerable ambiguity in determining the magnitude of the angular momentum of the system. It is sometimes assumed that it is close to the grazing angular momentum at a given energy, which can be used as a first approximation.
3) The angular correlation method for three particles in the output channel. The reaction used in this case has the form $A(B, C+D)E$, where $C+D$ is the system under study, in which molecular resonances are assumed to exist. The cross section of such a reaction also has a dependence $|P_L(\cos\theta)|^2$. The advantage of this method is the very high selectivity of the response to the states under study, as well as the possibility to work without changing the beam energy. The disadvantage of this approach is the strong contribution of the continuous spectrum to the oscillatory spectrum, which often leads to ambiguity in the determination of the angular momentum.

### 1.3.2. Transfer reactions

The resonance scattering method discussed above has limited sensitivity at low energies due to the strong influence of Coulomb scattering. Since the elastic scattering amplitude is a coherent sum of the Coulomb and resonance contributions, there are difficulties in observing resonance peaks in the near-threshold region. On the other hand, the transmission reaction allows one to populate both bound and resonant states, the cross sections for which will be proportional to

the spectroscopic factor.

Let us make a more detailed comparison of these methods. The width $\Gamma$ that can be obtained in the case of elastic resonance scattering described above is related to the value of the reduced width $\gamma^2$ as follows:

$$\Gamma = 2kRP_L(kR)\gamma^2, \tag{47}$$

here $k$ is the wave vector, and $R$ is the channel radius, and the value of $P_L(kR)$ is determined from the expression (34). In this case, the spectroscopic particle transmission factor can be determined from the DWBA description of the angular distribution of the transmission response, as the ratio of the experimental cross section to the theoretical cross section:

$$S = \left(\frac{d\sigma}{d\Omega}\right)_{\text{exp}} \Bigg/ \left(\frac{d\sigma}{d\Omega}\right)_{\text{DWBA}}. \tag{48}$$

Then the relation between the obtained spectroscopic factor and the value of the reduced width is defined as:

$$\gamma^2 = \frac{3\hbar^2}{2\mu R^2} S. \tag{49}$$

Thus, transfer reactions can be useful for studying states in the neighborhood of the threshold where the observed value of $\Gamma$ is very small but the value of $\gamma^2$ is large.

Consider a reaction in which the nucleus $c_2$ interacts with the nucleus $a_1$, consisting of the core $c_1$ and the particle $t$. In the reaction under consideration, $t$ is transferred to the nucleus $c_2$, forming the nucleus $a_2$.

$$\underbrace{(c_1 + t)}_{a_1} + c_2 \rightarrow c_1 + \underbrace{(c_2 + t)}_{a_2}. \tag{50}$$

The differential cross section for this process can be written as:

$$\frac{d\sigma}{d\Omega} = \frac{m_i m_f}{(2\pi\hbar^2)^2} \frac{k_f}{k_i} \frac{1}{(2a_1+1)(2c_2+1)} \sum_{\alpha_1,\alpha_2,\gamma_1,\gamma_2} |T_{\alpha_1,\alpha_2,\gamma_1,\gamma_2}|^2, \tag{51}$$

where $m_1$,$m_2$ are the reduced masses of the nuclei in the input and output chan-

nels, $k_i$,$k_f$ are their wave numbers, $a_1$, $c_2$ are the spin values of the corresponding nuclei, and $\alpha_1$,$\alpha_2$,$\gamma_1$,$\gamma_2$ are the corresponding spin components. The amplitude of $T_{\alpha_1,\alpha_2,\gamma_1,\gamma_2}$ can be written within the DWBA approximation:

$$T_{\alpha_1,\alpha_2,\gamma_1,\gamma_2} = \langle \chi^-_{f,c_1,\gamma_1,a_2,\alpha_2} | \Delta V | \chi^+_{i,a_1,\alpha_1,c_2,\gamma_2} \rangle, \tag{52}$$

where $\chi^-_f(\boldsymbol{r}_f)$ and $\chi^+_i(\boldsymbol{r}_i)$ are distorted waves, with an expression of the form $|a_1\alpha_1\rangle$ giving the full wave function for the $a_1$ nucleus (for others – analogously). Interaction can be described in two ways, POST and PRIOR:

$$\begin{aligned} \Delta V^{POST} &= V_{c_1 t} + V_{c_1 c_2} - U^{OPT}_{c_1 a_2}, \\ \Delta V^{PRIOR} &= V_{c_2 t} + V_{c_1 c_2} - U^{OPT}_{c_2 a_1}. \end{aligned} \tag{53}$$

In this case, $U^{OPT}_{c_1 a_2}$ and $U^{OPT}_{c_2 a_1}$ are the potentials (optical and Coulomb) used in the calculation of distorted waves $\chi_f$ and $\chi_i$. $V_{c_1 t}$ , for example, describes the interaction between the core $c_1$ and the transmitted particle $t$, with the Coulomb potential taken into account in describing all interactions.

From the perspective, considered in the present work, of the problem of studying cluster states in nuclei, the transfer reactions with lithium ions play a special role for this type of reactions. Like deuterons, the work with which led to the development of the theory of transfer reactions, lithium nuclei are relatively weakly bound, and, as indicated by theoretical and experimental studies, they have a pronounced quasi-molecular structure. Thus, lithium isotopes with mass numbers 6 and 7, can be represented as: $^6$Li=$\alpha + d$, $^7$Li=$\alpha + t$. This structure leads to an increased probability of transfer of the $\alpha$-cluster in reactions ($^6$Li,$d$),($^7$Li,$t$), as is the case for reactions of the type $(d, p)$,$(d, n)$. This leads to preferential populating of those states of the nucleus-product that possess a cluster structure. In this case, the formulas considered above (on the example of the reaction $^{12}$C($^6$Li,$d$)$^{16}$O) can be rewritten in the following form. The contributions to the potential describing the transfer for the POST and PRIOR cases will be $V_{\alpha d}$ and $V_{\alpha^{12}C}$, respectively. Then the transition amplitude can be written in the form:

$$T = \int \chi^*_{d^{16}\mathrm{O}}(k_d, r) \langle \varphi_d \varphi_{^{16}\mathrm{O}} | V | \varphi_{^6\mathrm{Li}i} \varphi_{^{12}\mathrm{C}} \rangle \chi_{^{12}\mathrm{C}^6\mathrm{Li}i}(k_{^6\mathrm{Li}i}, r) dr. \tag{54}$$

The expression in angle brackets describes the form factor for this reaction.

The reaction with $\alpha$ transfer is also possible for heavier nuclei. This process is related not only to the molecular states discussed above, but also to the manifestation of the $\alpha$-cluster structure of these nuclei. To make this approach more explicit, we can consider the resonance scattering process of nuclei of the form ($A$+two protons and two neutrons)+($A$). The first nucleus can be considered as having the structure ($A$+ $\alpha$), so that the $\alpha$-particle can be transmitted to the second nucleus, introducing distortions in the elastic scattering amplitude due to the indistinguishability of the output channels.

Of course, the class of transfer reactions (pickup) of the $\alpha$-particle is much broader than mentioned above. Let us mention here only our work on the study of the transition from collective to single-particle degrees of freedom in strontium [126]

In the present work, this type of reaction was used to study the states in neutron-deficient isotopes of beryllium and carbon, as well as to study the contribution from elastic cluster transfer in heavy ion scattering.

### 1.3.3. Quasi-free scattering

The third type of reaction used in this paper is the knockout reaction. Compared to two-particle reactions, this type of reaction leads to the appearance of three particles in the exit channel, which leads to a significant complication of the description of kinematics, when instead of two independent variables (energy in the center-of-mass system and angle) there are five variables. In this case, a different choice of a set of such variables is possible, for example, the total energy in the center-of-mass system, three angles in the center-of-mass system determining the direction of two departing particles, and the energy in the center-of-mass system of one of the particles.

In the case when the relative energies of the colliding particle and the target greatly exceed the binding energy of the constituent elements (beam or target), we can neglect this binding and consider the collision as quasi-free. Let us consider the case when the colliding particle is considered as a structureless object $a$, and the target consists of a weakly bound core $b$ and a particle $x$ (or a group of particles). The reverse case (weakly coupled beam particles and structureless

target particles) can be described within the framework of the inverse kinematics discussed above.

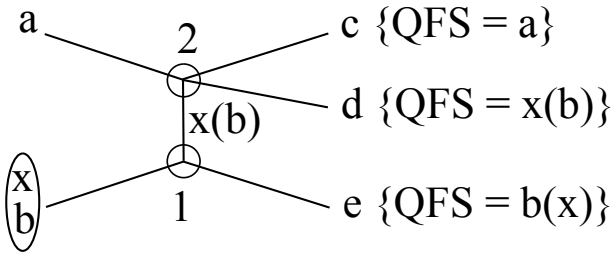


Figure 16. Diagram of a reaction with a three-particle state in the output channel. The products in the output channels for quasi-free scattering QFS are indicated

.

In general, the interaction of such systems leads to a three-particle state in the output channel – particles $c, d, e$, which can be viewed as a two-particle interaction of particle $a$ with core $b$ or particle $x$. Figure 16 shows the general case of the diagram for a three-particle reaction. In the case of quasi-free scattering, we have particles $a, b$ and $x$ in the exit channel, as shown in Figure 16 on the right. Such a process, in the simplest case, can be described by plane waves in the Born approximation, where all particles are treated as free except for the initial bound state $bx$, whose wave function we can describe as $\psi(\mathbf{r}_b - \mathbf{r}_x)$. Thus, the problem is reduced to the computation of the amplitudes of the processes occurring in vertices 1-2. In the case of the lower vertex (1), we need to extract the factor corresponding to the Fourier transform of the above wave function for the bound state $bx$, since it is this quantity that determines the transferred momentum at scattering $b$, so that $\psi(\mathbf{p}_b) = \int\int \exp(\mathrm{i}\mathbf{p}_b\mathbf{r})\psi(\mathbf{r})d\mathbf{r}$. The opposite vertex corresponds to the amplitude of the Born approximation for the reaction $a + x(b) \to a + b(x)$. Then, in the simplest case, for the magnitude of the cross section, we can write:

$$d\sigma = K\left(\frac{T_i^{cm}}{T_f^{cm}}\right)^{\frac{1}{2}}\left(\frac{d\sigma}{d\Omega}\right)_{cm}|\psi(\mathbf{p_b})|^2 \times vol. \tag{55}$$

Here $K$ is the kinematic factor, which includes the necessary constants, the spectroscopic reaction factor, and the masses. The relative kinetic energies can be written as $T_f^{cm} = \mu_{cd}(\mathbf{v}_c - \mathbf{v}_d)^2/2$ and $T_i^{cm} = \mu_{ab}(\mathbf{v}_a - \mathbf{v}_b)^2/2$ for the case of scattering on a light fragment, $vol$ is the phase space element.

We used this type of reaction when studying the nuclei of $^6$He and $^8$He.

### 1.3.4. Processes of decay of an excited system

Except for the $\alpha$-decay process mentioned in the introduction, the methods of studying cluster degrees of freedom discussed above assume the presence of a cluster in the input channel of the reaction. At the same time, the presence of clustering processes in light nuclei can also be inferred from the processes associated with the decay of the resulting compound system. This is especially true for nuclei with neutron excess, when certain excited levels can be considered as molecular states. In most cases, the evidence of such states is not the decay into the corresponding clusters, but the correspondence of the obtained data (binding energies, level scheme, angular distribution of reaction products, etc.) to the calculations performed under the assumption of clustering, especially if the obtained results contradict the calculations based on the single-particle model. Effective methods for studying such states are, for example, multinucleon transfer reactions, heavy ion fusion reactions with the formation of high-spin states followed by $\gamma$-decay (excitation of rotational bands), and cluster knockout reactions. These types of reactions will be used in the analysis of heavy cluster departure.

# Chapter 2. Experimental methods

Let us briefly review the experimental methods that were used in our experiments. As can be seen from the models described above, we need to carry out the registration and determination of the charges and masses of nuclei, starting from $\alpha$-particles, in a wide range of angles, at relatively low energies. With the exception of the work on helium isotopes (this experimental setup will be described in the corresponding chapter), such registration has mainly been carried out by the $\Delta E - E$ technique. In this case, the particle is registered by two detectors: a thin detector in which it loses a small fraction of energy $\Delta E$ and a thick detector in which the particle completely loses the remaining energy $E$, so that the total energy is $E_{tot} = \Delta E + E$. From the Bethe-Bloch law we know that in this case for nuclei with charge $Z$ and mass $A$ the condition:

$$\frac{\Delta E}{\Delta X} \sim \frac{Z^2 A}{E}, \tag{56}$$

where $\Delta X$ is the thickness of the thin detector. Then the registered nuclei with a given value of $Z^2A$ appear to be located on a hyperbola in the coordinates $E$ on the ordinate scale and $\Delta E$ on the abscissa scale. As can be seen, the energy of the detected particle must be at least as large as the loss in a thin detector, which imposes severe limitations due to the complexity and cost of very thin silicon detectors. For example, a silicon $\Delta E$ detector with a thickness of 20 $\mu$m completely stops $\alpha$-particles with energies on the order of 4 MeV. For this reason, we used such $\Delta E$ detectors only in the case of $\alpha$-particles of sufficiently high energies (when studying nuclei heavier than $^{32}$S). To cover the largest area, we used the ISIS [127] setup (thickness of $\Delta E$ and $E$ parts 130 $\mu$m and 1 mm, respectively, for $^{40,42}$Ca nuclei).

To record heavy ions and $\alpha$-particles of low and intermediate energies, we used ICARE [128] gas telescope systems and position-sensitive assemblies based on proportional counters [129]. In the latter case, each assembly was a gas $\Delta E$ part and 10 PIN diodes for the $E$ part. The sensing area was 18 cm$^2$. The thickness of the sensitive layer of PIN-diodes was 380 $\mu$m, which made it possible to measure the spectra of particles with maximum energies: p – 7 MeV, d – 9

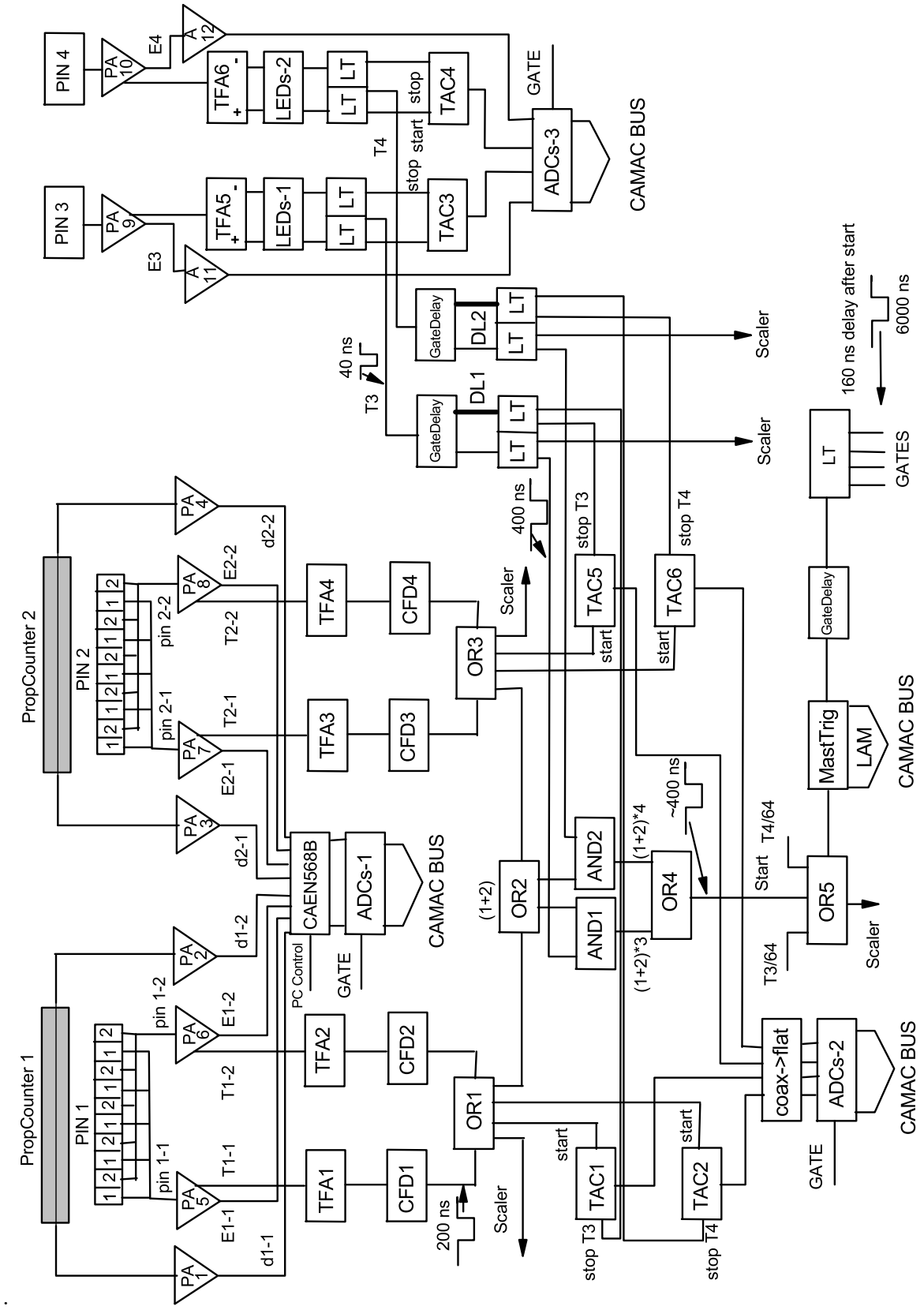


Figure 17. Lock diagram of the experimental setup

.

MeV, t – 11 MeV, $^3$He – 25 MeV, $\alpha$ – 28 MeV.

The gas $\Delta E$ part was a proportional chamber, with a single high impedance electrode (33 kOhm) at the center of the chamber, which allowed us to obtain the magnitude of the charged particle energy loss in the gas and the X coordinate values. The depth of the chamber was 1 cm. The entrance window of the chamber was Mylar, 2$\mu$m thick (with wire amplification). The detector was filled with a gas mixture of Ar+10% $CH_4$ at a pressure of 400 mbar. Thus, labeling the signals from both ends of the electrode as $A_1$ and $A_2$, the loss and coordinate information can be obtained as:

$$\Delta E = C * (A_1 + A_2), \tag{57}$$

$$X = l * \frac{A_1 - A_2}{A_1 + A_2}. \tag{58}$$

Here $C$ is the normalization constant, which is found during detector calibration, and $l$ is the electrode length (12 cm). The resolution for $\alpha$-particles at maximum energy was 70 keV and 65 keV for the $E$ and $\Delta E$ parts, respectively.

Another variant, used for registration of low-energy charged particles, represented the detector inclusion according to the scheme of analysis of charge collection time in the semiconductor detector $T_{ch}$ [130]. In this case, event selection was performed on a two-dimensional plot of $E$ vs $T_{ch}$. In contrast to gas telescopes, this method was able to confidently separate $\alpha$-particles and $^6$He nuclei. Figure 17 shows an example of the general scheme we used for experiments on $^{18}$O, $^{22}$Ne, and $^{26}$Mg nuclei. The circuit shows the preamplifiers for the position-sensitive part of the proportional cameras (P1–P4), the preamplifiers for the detectors turned on in the charge collection time analysis mode, (P5,P10) with the amplifiers of the corresponding time filters (TFA1–TFA4), and the electronic logic circuits. Figure 18 shows an example of detector assembly operation for the position-sensitive detector (PropCounter) when $^{11}$B nuclei are registered. In Figure 19, we present two-dimensional spectra obtained by studying the contribution of the cluster configuration of the $^6He\otimes$Kor species in the $^{26}$Mg nucleus, and the level groups corresponding to the excited states of the $^{20}$Ne nucleus are clearly

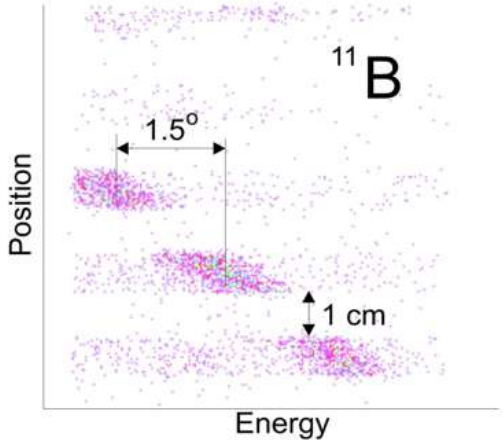


Figure 18. Registration of $^{11}$B nuclei by the $\Delta E - E$ gas telescope

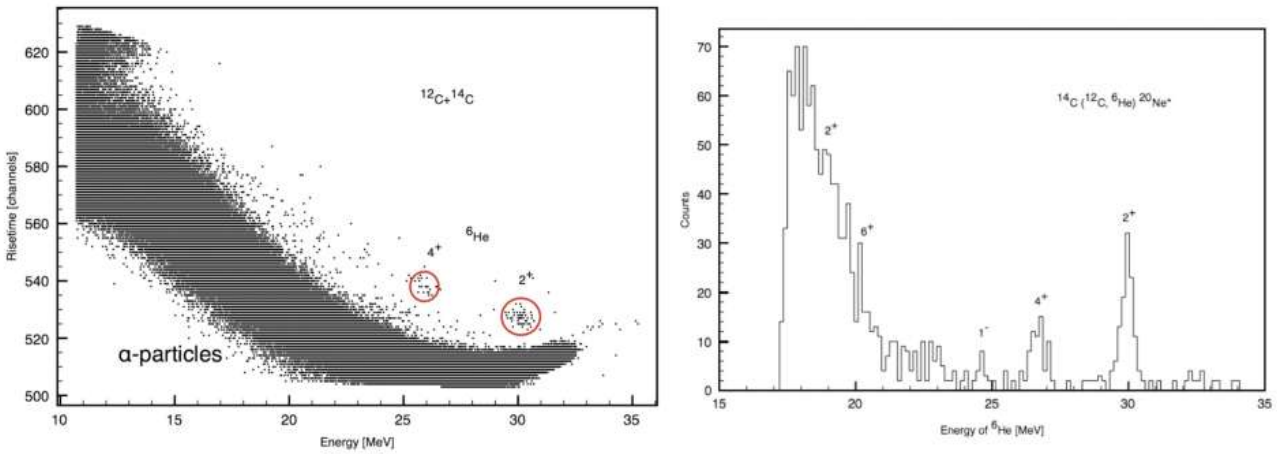


Figure 19. Left is a two-dimensional spectrum of detectors operating in charge time collection analysis mode. The spectra of $\alpha$-particles and $^{6}$He are shown, on the right the spectrum of the $^{14}$C($^{12}$C, $^{6}$He)$^{20}$Ne reaction.

visible.

In addition, we used a Q3D [131] magnetic spectrometer consisting of a quadrupole and three dipoles to study the neutron-depleted isotopes of beryllium and carbon. The angular axeptance of the setup was $\pm 3°$. Particle registration, similar to the previous setup, was carried out by gas wire chambers operating in the $\Delta E$-detector mode. The $E$-detector was designed as a scintillation counter. The $TOF$-information was obtained from the start signal from this detector and the stop signal from the gas pedal high frequency generator.

The data were processed in the ROOT [132] package.

# Chapter 3. Spectroscopy of light neutron-rich nuclei

## 3.1. Isotopes of helium

One of the most impressive discoveries in nuclear physics at the end of the last century was the discovery of halo nuclei, where one or two particles are removed from the core – the strongly bound core of the nucleus. In the context of the question of the $\alpha$-cluster structure of the nucleus, the $^6$He and $^8$He nuclei are of particular interest. Their structure is not only the simplest variant of the cluster degree of freedom, but also an important source of information about the nuclear forces. The need for an experimental study of the properties of these nuclei is due, among other things, to the ambiguity and complexity of theoretical predictions. One of the most interesting questions in this field is the question of the "geometric" arrangement of excess neutrons [133]

### 3.1.1. Aims and Methods of the Study

A quasi-free proton scattering experiment on $^6$He and $^8$He nuclei was performed to study the $(p, pn)$, $(p, p\alpha)$, and $(p, p\ ^6\text{He})$ [46] processes. The study was carried out with relativistic $^6$He and $^8$He beams in inverse kinematics. The work was performed at the Institute for Heavy Ion Research (GSI), Darmstadt, Germany. After fragmentation of a $^{18}$O beam with energies of 820 MeV/A and 730 MeV/A on a beryllium target, secondary beams of $^6$He and $^8$He with energies of 717 and 671 MeV, respectively, were selected by an analyzing magnet and directed onto a proton target. The experimental setup is shown in Figure 20.

The secondary beam was passed through two scintillators ($S_1$,$S_2$) to analyze the $\delta E$ loss and time-of-flight. The beam position was determined by position-sensitive proportional counters ($p_1$,$p_2$), and the polar and azimuthal angle of the fragment by counters ($p_3$,$p_4$). Protons scattered at an angle larger than 70° were then selected by $\delta E$ and time-of-flight ($p_5$,$p_6$) into the first hodoscope. The fragments were analyzed by the ALADIN magnetic spectrometer and fell into the second yearoscope.

The processing of the obtained information was based on the kinematics of quasi-free scattering described in the first chapter, when the conservation law is

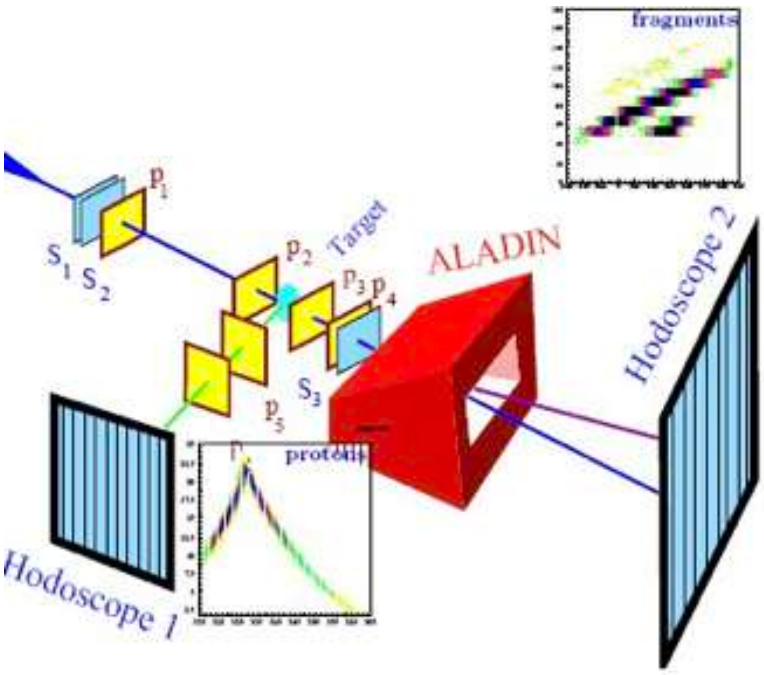


Figure 20. Experimental setup.

satisfied:

$$p_0 + P = Q + q_0 + q_1, \tag{59}$$

where $p_0 = (\mathbf{p}_0, \omega_0)$ and $q_0 = (\mathbf{q}_0, E_0)$ are the momentum of the particle (proton) before and after scattering, respectively. $P = (\mathbf{P}, \omega_P)$ and $Q = (\mathbf{Q}_0, E_Q)$ are the initial and final momentum of the helium nucleus and $q_1 = (\mathbf{q}_1, E_1)$ – the momentum of the cluster knocked out of the nucleus, as shown in Figure 21.

In the momentum approximation, the condition $p_e = P - Q = q_0 + q_1 - p_0$ is satisfied for the reaction (59), as seen in Figure 21. The redispersed and knocked-out particles ($q_0$ and $q_1$) must be strictly correlated. Consider the correlation between the polar angles of the particles involved in the reaction. This correlation is similar to the elastic scattering correlation, but is distorted, as mentioned above, by the motion of the cluster inside the nucleus. The correlation between their azimuthal angles will be more characteristic.

From the conservation law for point 2 in Figure 21 we can find that $p_0 + p_1 = q_0 + q_1$. In the laboratory system (—$p_0$—=0), so the angle between the momentum vector $q_1$ and $q_0 \times P$, which is perpendicular to the plane of reaction, will be defined as:

$$\cos\theta = \hat{n}_0 \cdot \hat{n}_1, \tag{60}$$

here

$$\hat{n}_0 = \frac{P \times q_0}{|p \times q_0|} \tag{61}$$

$$\hat{n}_1 = \frac{q_1}{|q_1|}. \tag{62}$$

From the expression $p_1 = q_0 + q_1$ we obtain that:

$$\cos\theta = \frac{(p_1 - q_0)}{|q_1|} \cdot \frac{P \times q_0}{|p \times q_0|} = \frac{p_1(P \times q_0)}{|q_1||P \times q_0|} = \frac{p_1\hat{n}_1}{|q_1|} = \frac{Q_{tr}}{|q_1|}. \tag{63}$$

Thus, for the value $Q_{tr}$ we have:

$$Q_{tr} = |q_1|\cos\theta = |q_1|\hat{n}_0 \cdot \hat{n}_1 = \frac{q_1(P \times q_0)}{|P \times q_0|}. \tag{64}$$

Let us choose the beam direction along the $z$ axis, so that $P = (0, 0, P_z)$. Then:

$$Q_{tr} = \frac{1}{|p||q_0|\sin(\widehat{Pq_0})}\begin{vmatrix} q_1^x & q_1^y & q_1^z \\ p^x & p^y & p^z \\ q_0^x & q_0^y & q_0^z \end{vmatrix} = \frac{q_1^y p^z q_0^x - q_0^y p^z q_1^x}{|p||q_0|\sin(\widehat{pq_0})} = \frac{q_1^y q_0^x - q_0^y q_1^x}{|q_0|\sin\theta}. \tag{65}$$

Let us introduce the notation: $\theta_1 = (\widehat{zq_1})$, $\varphi_1 = (\widehat{xq_1})$, $\varphi_0 = (\widehat{xq_0})$. Then:

$$\begin{aligned} q_1^x &= |q_1|\sin\theta_1\cos\varphi_1, \\ q_1^y &= |q_1|\sin\theta_1\sin\varphi_1, \end{aligned} \tag{66}$$

$$\begin{aligned} q_0^x &= |q_0|\sin\theta_0\cos\varphi_0, \\ q_0^y &= |q_0|\sin\theta_0\sin\varphi_0. \end{aligned} \tag{67}$$

And finally for the value $Q_{tr}$ we have:

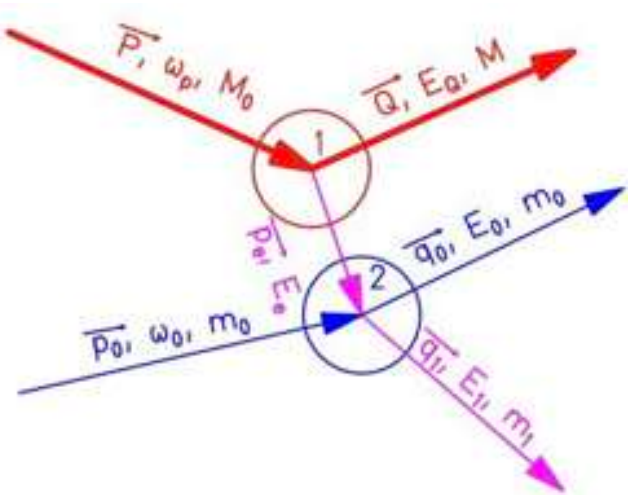


Figure 21. Feynman diagram for quasi-free scattering.

$$Q_{tr} = |q_1|(\sin\theta_1 \sin\varphi_1 \cos\varphi_0 - \sin\varphi_0 \sin\theta_1 \cos\varphi_1) = \\ = |q_1| \sin\theta_1 \sin(\varphi_1 - \varphi_0), \quad (68)$$

$$\cos\theta = \frac{(\mathbf{q}_1(\mathbf{q}_0 \times \mathbf{P}))}{|\mathbf{q}_1||\mathbf{q}_0 \times \mathbf{P}|} = \sin\vartheta_c \sin(\varphi_c - \varphi_p) = \frac{Q_{tr}}{\mathbf{q}_1}, \quad (69)$$

here $Q_{tr}$ is the component of the cluster momentum in the nucleus perpendicular to the reaction plane, $\vartheta_c$ is the polar angle of the knocked-out cluster, $\varphi_p$ and $\varphi_c$ are the azimuthal angles for the scattered proton and cluster, respectively.

The scattered particle in this reaction is the proton, and the cluster can be the $\alpha$-particle (for $^6$He or $^8$He beams) or $^6$He (for $^8$He beam). Figure 22 shows an example for the correlation between the angles of the scattered proton and $\alpha$-particle in the $p$+$^6$He reaction. Panel 1 shows the correlation between the polar angles $\vartheta_p$ and $\vartheta_\alpha$, resembling the shape of a butterfly, while panel 2 shows the correlation between the azimuthal angles $\varphi_p$ and $\varphi_\alpha$. The first panel clearly shows the separation of events into two distinct groups – weak correlations (bottom group) and strong correlations (top group). In the second panel, this fact appears in the form of a homogeneous distribution for the poorly correlated events, while the events with strong correlation are concentrated at the angle $\varphi_p - \varphi_\alpha \approx 180°$.

Having obtained the data on the distribution of $Q_{tr}$ value based on the formula (69), we can make a comparison with the model calculations based on the

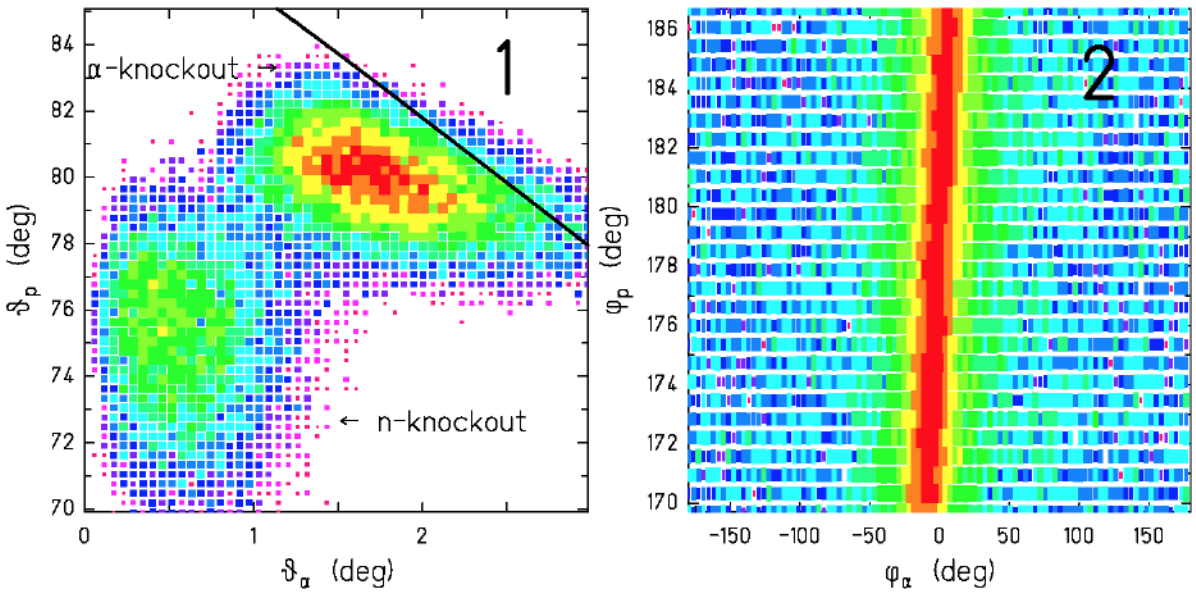


Figure 22. Correlation between the angles of a scattered particle and a cluster.

cluster wave function representation [134, 135]. Figure 23, shows the momentum distribution for clusters of different types:

1) The case of $\alpha$-cluster knockout from the $^6$He nucleus.

2) The case of knocking out a $\alpha$-cluster from the $^8$He nucleus.

3) The case of knocking out the $^6$He cluster from the $^8$He nucleus.

The obtained distributions can be analyzed in the framework of the potential model under the two-particle approximation. As has been shown in [136–138], the theoretical and experimental study for $^6$He and $^8$He nuclei applies, at least in a first approximation, the approaches used in the transfer reaction when the nucleus is split into a cluster and a cor interacting by means of a two-particle optical potential. The choice of a particular type of potential is certainly a problem for such exotic nuclei [139], but it has been shown that the problems involved in obtaining the momentum distribution of clusters in a nucleus are not too sensitive to the form of the potential as long as the binding energy is not too small. For the distributions we have considered, the binding energies are:

$^6$He=$\alpha$+2$n$ binding energy $S_{2n}$=-0.975 MeV

$^8$He=$\alpha$+4$n$ binding energy $S_{4n}$=-3.1 MeV

$^8$He=$^6$H+2$n$ binding energy $S_{2n}$=-2.125 MeV

In [46], the simplest case of a rectangular potential well was used to analyze the momentum distribution. At the same time, with a slight complication of calculations, it is acceptable to use the Woods-Saxon potential (24) $WS$, which, at

the same time, allows one to avoid possible artifacts, to use the obtained potentials for transmission reactions with exotic nuclei, and to apply known systematics.

We choose a Woods-Saxon potential (24), in the form $V_0 \cdot f(r)$ with diffusivity $a$=0.65 fm, radius [138] $R$=1.25$A^{1/3}$ ($A$-core mass), and vary the depth until the indicated binding energies are reached. In addition, the constraints imposed by the condition (23) must be considered. The value of $2N + L$ was 2 for the first and third distributions and 3 for the second. The calculations were performed by the analytical solution of the Schrödinger equation with a given potential and subsequent integration by the Fox-Goodwin method [140]. As a result, the depths of the potentials were:

$^6$He=$\alpha$+2$n$, $V_0$=65.39 MeV

$^8$He=$\alpha$+4$n$, $V_0$=118.03 MeV.

$^8$He=$^6$H+2$n$ $V_0$=53.77 MeV

The momentum distribution was obtained from the Fourier transform of the wave functions found with the above parameters and the results for the rectangular well and the potential $WS$ coincide. Note that such an approach cannot well describe the distribution far away from zero [46], as can be seen from the presented Figures 23. The red line shows the expected distribution of the corresponding cluster ($\alpha$-particle or $^6$He). As can be seen, we describe the distributions well when a dineutron is considered as a cluster, but poorly for the case $^8$He=$\alpha$+4$n$ (blue line). Lowering the binding energy to a value of 8 MeV, we obtain the depth of potential as above, $V_0$=118.03 MeV. As can be seen from the Figure, in this case a much better agreement with the experimental resolution is obtained (red line). This suggests either the possibility of the existence of resonance at 5 MeV energy in a four-neutron (tetraneutron) system, or it is a reflection of the strong internal correlation of four neutrons in the $^8$He wave function.

The case of a four-neutron cluster has been repeatedly considered in the literature [141–143] as well as the existence of heavier neutron clusters [144]. The present result can be considered as an indirect indication of this possibility. However, so far there is no unambiguous confirmation of this extremely interesting fact. Recent work has confirmed the resonant character of this phenomenon [30].

To test these assumptions, one could use the $d(^8\mathrm{He},4n)^6\mathrm{Li}$ reaction proposed

in [139], using the potentials given here to describe the bound states. In any case, to date, the study of the properties of helium isotopes is one of the most rapidly developing areas of nuclear physics, which is greatly facilitated by studies with radioactive beams.

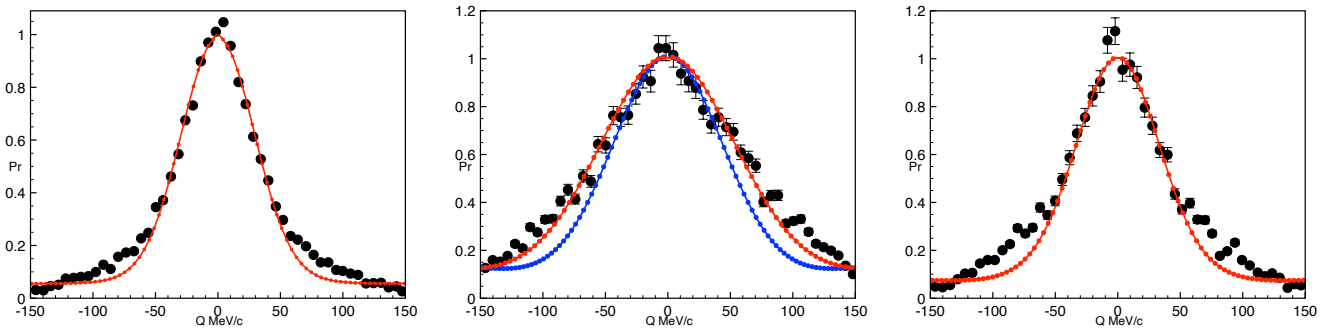


Figure 23. Distribution of transverse momenta of clusters in the reaction of their knockout ( [46], see description in text). 1) Knocking out a $\alpha$-particle from $^6$He. 2) Knocking out a $\alpha$-particle from $^8$He. 3) Knocking $^6$He out of $^8$He.

### 3.1.2. Results obtained.

The main result of this work can be considered as:

- Proof of the dominance of the quasi-free scattering mechanism due to the independence of the fragment momentum distribution from the beam energy.

- For the first time the momentum distribution of complex clusters inside $^6$He and $^8$He nuclei was measured.

- The dominant contribution of the $^6$He+2$n$ configuration in the $^8$He nucleus was shown.

- An estimate of the detachment energy of the $\alpha$-particle from $^8$He indicates either a resonance in the tetraneutron system or a correlation of valence neutrons in the $^8$He wave function.

## 3.2. Beryllium isotopes

In the Introduction it has already been pointed out how important, from the point of view of studying cluster degrees of freedom, is the $^8$Be nucleus. Hence a natural question immediately arises – whether the manifestation of cluster properties is preserved with increasing number of excess neutrons or not. To answer

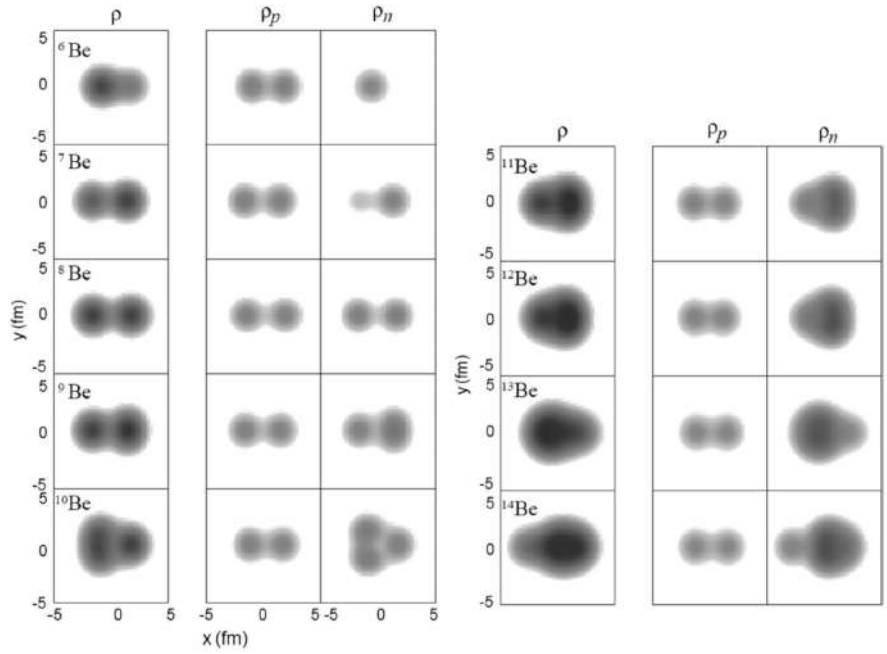


Figure 24. Density distribution in beryllium isotopes within the AMD model [153]. The first column gives the total density of nucleons, the second - the density distribution of protons, the third - neutrons.

this question, we have performed a series of experiments [41, 42, 44, 45]. In this chapter, we will only consider the structure of beryllium isotopes.

Neutron-excess isotopes of beryllium are of extreme interest from the position of studying their properties – both $\alpha$-cluster and quasi-molecular, where the added neutrons end up on the corresponding covalent molecular orbitals [145]. As stated above, in the ground state $^8$Be – are two $\alpha$-particles 3-4 fm apart. Given the rms radius for the $\alpha$-particles, it is clear from the formula (13) that they are almost touching each other. This agrees well with the density distribution in the $^8$Be nucleus obtained in the framework of the GFMC (Green's function Monte Carlo calculation) [146] model.

For the ground state of the $^9$Be nucleus, calculations performed also on the basis of the two-center model [147], AMD [148], and the coordinate generator method [149], predict the appearance of a potential energy minimum for the distance between $\alpha$-particles of the order of 3.0-3.4 fm, in agreement with the properties known from experiment. An estimate of the moment of inertia of the rotational band of the ground state ($K$=3/2$^-$) gives a similar value. All this makes the $^9$Be nucleus an excellent example of a stable nuclear molecule.

Cluster and molecular properties are also demonstrated by heavier isotopes

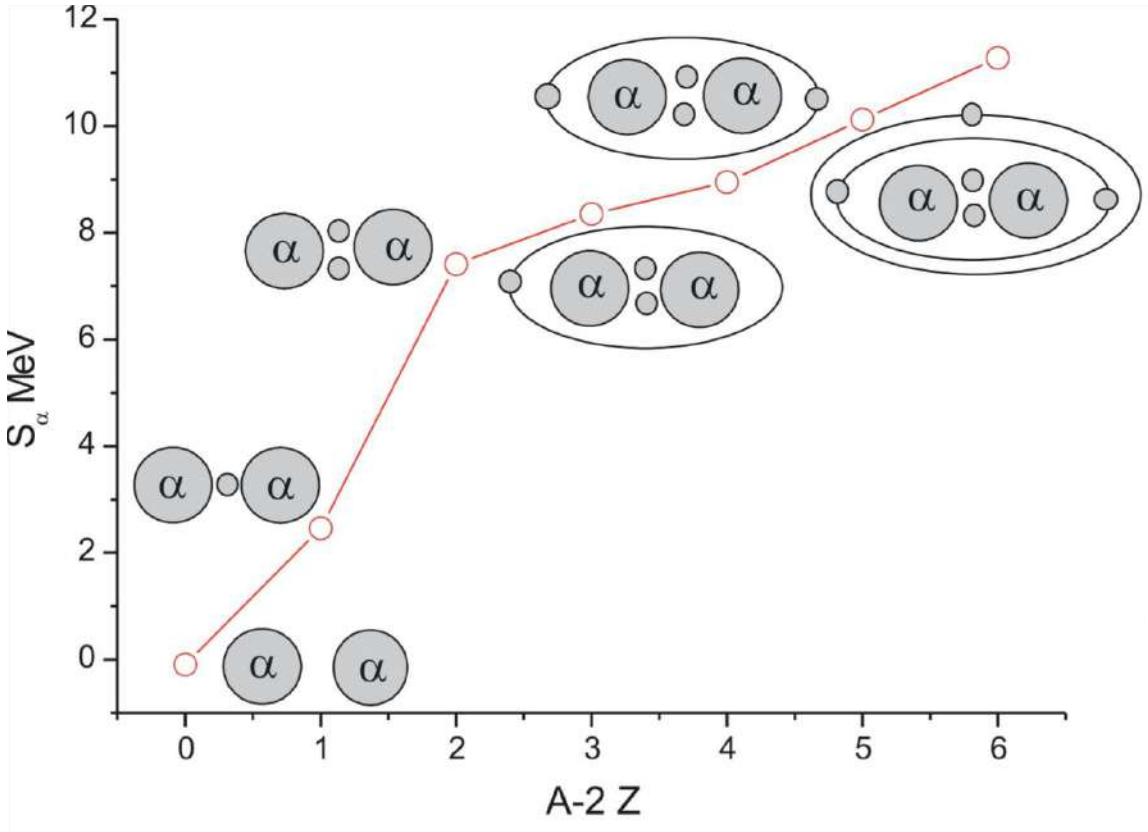


Figure 25. Graph of the dependence of the separation energy of the $\alpha$-particle for beryllium isotopes.

($A$=10-12) [150–152]. Theoretical calculations within the AMD approach from the paper [153] are presented in Figure 24. As can be seen, throughout the mass range, beryllium retains pronounced signs of octupole deformation, which should result in well-fragmented band(s). However, information on these is incomplete. There is no clear understanding of the structure of the different states – estimating the degree of single-particle contributions and core excitation, and there is ambiguity in assigning spin values to some states. For example, there is ambiguity in determining the spin of low-lying states in the $^{11}$Be nucleus at excitation energies of 3.41, 3.89, and 3.96 MeV. The latter state is especially important because it is considered as the head state for the molecular rotational band $K^\pi$=3/2$^-$ [145,150], while an estimate of 5/2$^-$ [154] is found in the literature. All this suggests the urgent need for additional experimental studies.

Figure 25 presents a plot of the detachment energy of the $\alpha$-particle as a function of mass number for the currently known beryllium isotopes. The excess neutrons shown in the plot are for illustrative purposes only and do not characterize their orbitals.

The graph clearly shows a kink at the point corresponding to the $^{10}$Be nucleus. This again indicates the preference for studying multineutron transfer when $^{9}$Be is used as the target nucleus.

### 3.2.1. Aims and Methods of the Study

In our study of the structure of neutron-excess beryllium isotopes, we used the one-, two-, and three-neutron transfer reactions of the $^{9}$Be target. Additionally, the one and two neutron transfer reactions of the $^{10}$Be target were studied. This allowed the structure of $^{10}$Be, $^{11}$Be, and $^{12}$Be nuclei to be studied.

The measurements were carried out using the Q3D magnetic spectrometer of the Hahn-Meitner Institute (HMI), Berlin, Germany. The beam energy was 15-30 MeV/A. The reactions studied were:

$^{9}$Be($^{14}$N,$^{13}$N)$^{10}$Be at an energy of 217.9 MeV.

$^{9}$Be($^{13}$C,$^{11}$C)$^{11}$Be at energy 379 MeV.

$^{9}$Be($^{15}$N,$^{12}$N)$^{12}$Be at an energy of 240 MeV.

$^{10}$Be($^{14}$N,$^{13}$N)$^{11}$Be at energy 217.9 MeV.

$^{10}$Be($^{14}$N,$^{12}$N)$^{11}$Be at an energy of 216 MeV.

A BeO target was used as the $^{10}$Be target.

In the above reactions, we can, to a first approximation, consider the target as a core for the neutron configurations of the final states. However, we can expect certain differences in the final result, due to the fact that the $^{9}$Be nucleus has a much more pronounced $2\alpha$ configuration, while the states of the heavier isotopes are more complex (see Figure 24, 25).

The above differences can be clearly seen when comparing the experimental spectra obtained. Figure 26 shows the spectra for the transfer of one, two, and three neutrons to the $^{9}$Be nucleus. The departing particles were recorded in the range 2.0°-5.9°. As a result, the spectra identified [42]:

$^{10}$Be: 8 states up to excitation energies of 15. 34 MeV.

$^{11}$Be: 15 states up to excitation energies of 25.0 MeV.

$^{12}$Be: 7 states between 5.5 and 21.7 MeV (low-lying levels did not seen in the focal plane).

As expected, most of our observed states exhibited a linear dependence of the excitation energy on the value of $J(J+1)$, a manifestation of the basic property

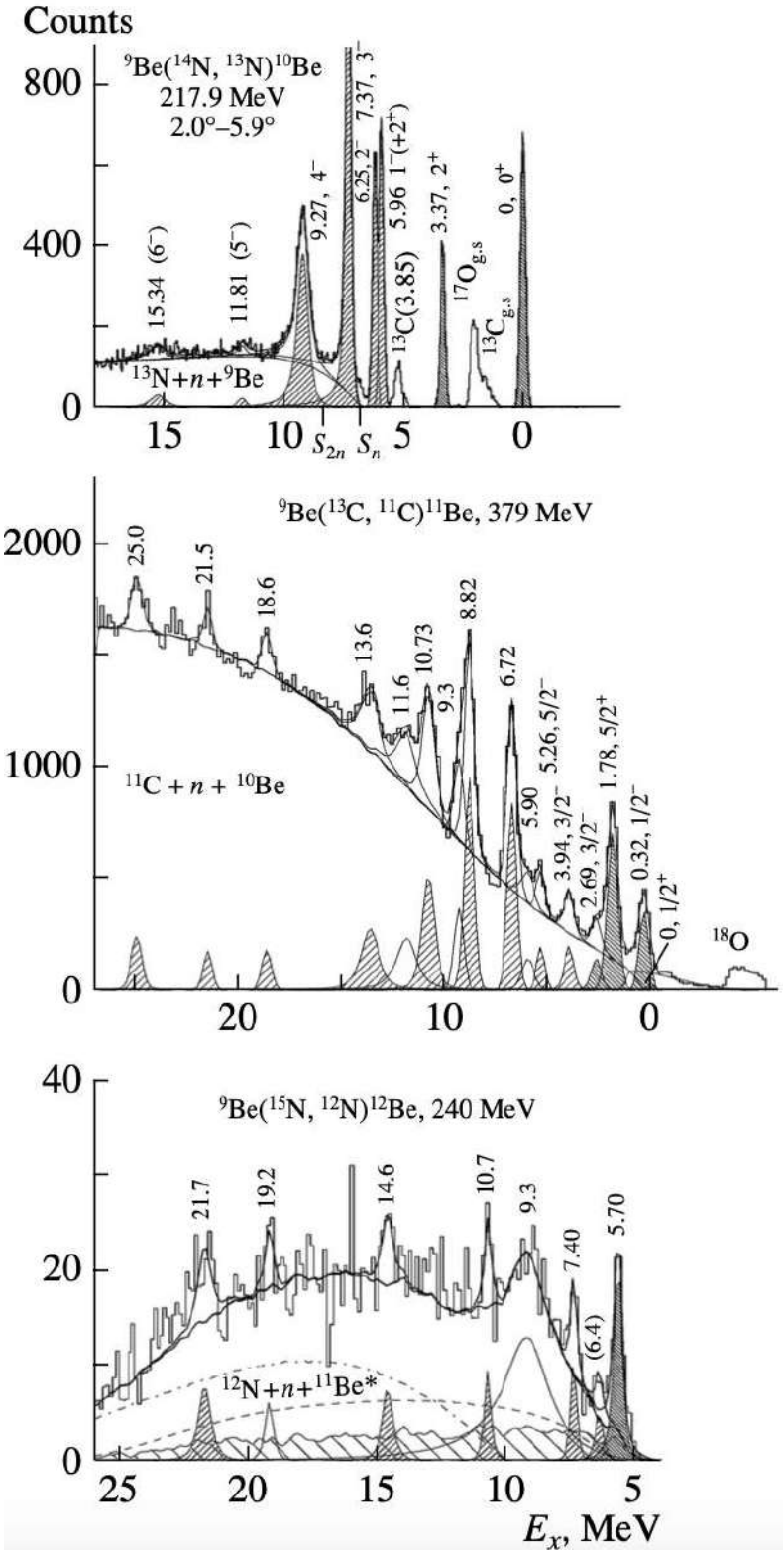


Figure 26. Spectrum of transfer of one, two and three neutrons to the $^{9}$Be nucleus [42].

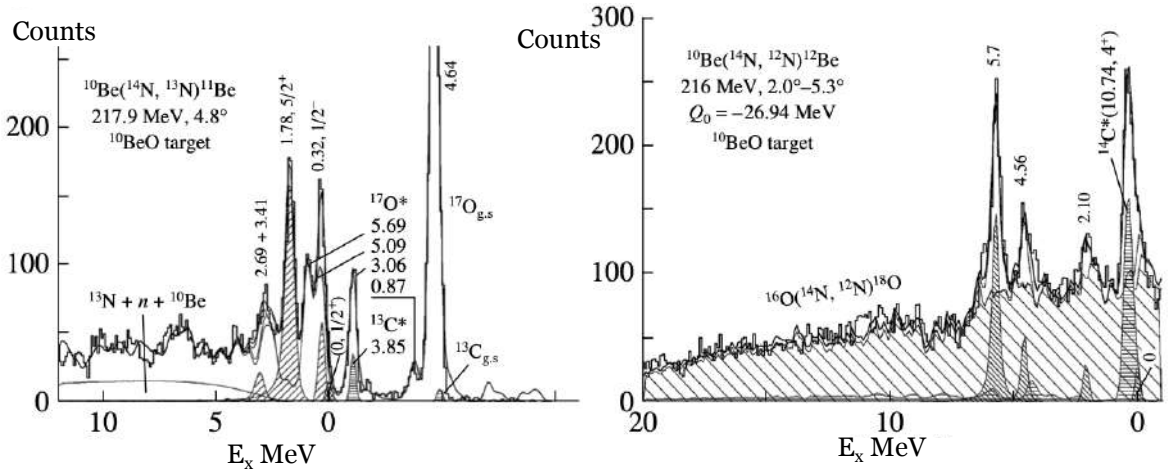


Figure 27. Spectrum of transfer of one and two neutrons to the $^{10}$Be nucleus [42].

of rotational bands. Such states are shaded in Figure 26. Some of the angular momenta have been assigned only estimatively based on the above dependence. The remaining spins were assigned according to the referential sources [155].

We were able to identify the following spin bands:

$^{10}$Be $K^\pi$=$1^-$ : $E_x$=0.25[$J$($J$+1)-1· 2]+5.96 MeV

$^{11}$Be $K^\pi$=$\frac{3}{2}^-$ : $E_x$=0.23[$J$($J$+1)-$\frac{3}{5}\cdot\frac{5}{2}$]+3.96 MeV

$^{12}$Be $K^\pi$=$0^+$ : $E_x$=0.21[$J$($J$+1)]+6.4 MeV

As is clear from the formula (16), the multiplier in front of the square brackets is inversely proportional to the moment of inertia of the rotating configuration. Assuming that, analogous to $^8$Be, there are two $\alpha$-particles rotating, and the neutrons are distributed as shown in Figure 24, we can estimate the distance between the $\alpha$-particles to be on the order of 5 fm! Such a large distance implies very little overlap of $\alpha$-particles, and such bands are almost purely molecular.

Let us compare the results obtained with the spectrum from the experiment for the $^{10}$Be target (Figure 27). Because of the strong background from the oxygen present in the target, it is difficult to estimate the contributions from weakly manifested states. Only the contributions from 0.32 and 1.78 MeV and the doublet of 2.7 and 3.4 MeV in the $^{11}$Be nucleus and 2.1, 4.56, and 5.7 MeV in the $^{12}$Be nucleus were significant. All these states are cor $^{10}$Be + neutrons, with no formation of levels belonging to the rotational band.

The states of the $^{11}$Be nucleus can be considered as single-particle states, with a neutron in the $1p1/2$, $1d5/2$, and $1d3/2$ orbitals, as well as in the 30%-

filled $1p3/2$ occupancy of the $1p3/2$ nucleus $^{10}$Be in the ground state due to mixing configurations. In the $^{12}$Be core, similar states can populate in $^{10}\mathrm{Be}(t,p)$ [156,157]. They have the structure $(1p1/2)^{-1}(sd)^1$ and $(sd)^1$.

As mentioned above, there is uncertainty with the identification of the spins of some low-lying states of the $^{11}$Be nucleus. Thus, the state with energy 3.96 MeV, when analyzing the $^{10}\mathrm{Be}(t,p)$ reaction, was assigned spin $3/2^-$ due to the very characteristic shape of the angular distribution obtained in the experiment for the transfer process with $l$=0. Thus, based on DWBA analysis, the angular spins $3/2^-$, $3/2^+$, and $3/2^-$, respectively [158], were obtained for the low-lying states 3.41, 3.89, and 3.96 MeV.

At the same time, for the $(d,2p)$ and $(t,^3\mathrm{He})$ reactions, the 3.89/3.96 MeV state was assigned spin $5/2^-$ [159, 160] when analyzing the unresolved 3.89/3.96 MeV doublet. In the work [154], the following spins were assigned to the states considered: 3.41, 3.89, and 3.96 MeV – $3/2^-$, $3/2^+$, and $5/2^-$, respectively. This work was based on shell calculations.

To clarify this issue, we performed an angular distribution experiment. The reaction was chosen so that the shape of the distribution would be most sensitive to the determined spins. For this purpose, we used the reactions $^9\mathrm{Be}(^{16}\mathrm{O},^{14}\mathrm{O})$ to study the transfer of two neutrons and $^{13}\mathrm{C}(^{12}\mathrm{C},^{14}\mathrm{O})$ to study the pickup of two protons. Their distinguishing feature is that the transfer is $0^+ \to 0^+$, so that the transferred momentum did not distort the angular distribution. Figure 28 shows the resulting angular distributions.

Comparison of the calculations for different angular momenta clearly indicates that the 3.96 MeV state has negative parity. Considering the referential data, our result supports the assumption of spin $3/2^-$ for this state. The two-proton pickup reaction actively populates states with energies of 0.32, 2.7, and 3.9 MeV. All these states have similar distributions (see Figure 28, right side). Thus, the 3.9 MeV level must have negative parity and spin $5/2^-$ is confirmed for it (instead of the 3.96 MeV state). The 3.41 MeV state is unpopulated (and very weakly populated in two-neutron transfer), which does not allow us to draw conclusions about its properties. However, since it is actively populated in single neutron transfer, we can conclude that it is a $3/2^+$ level.

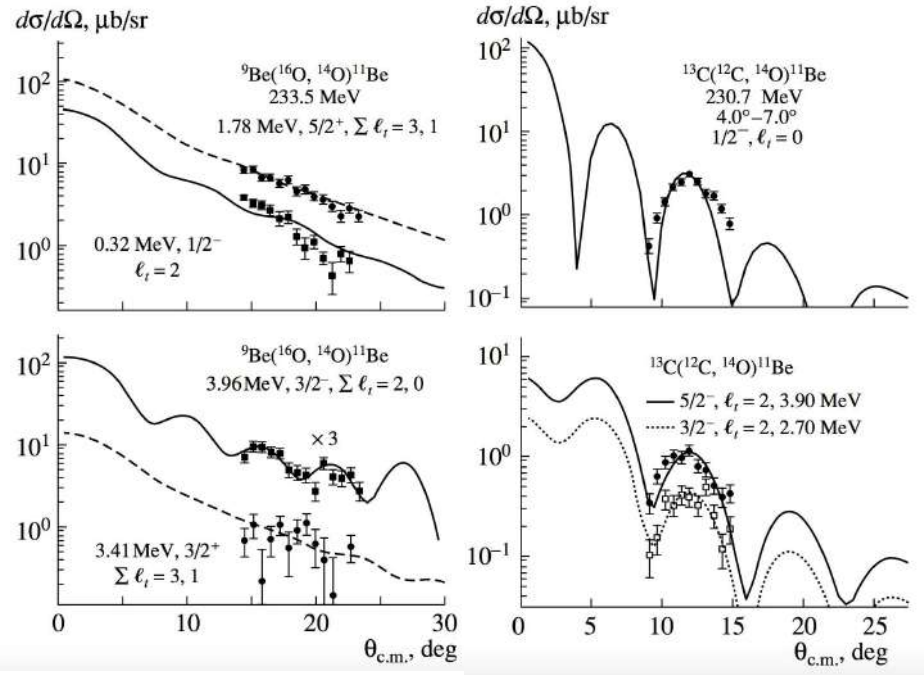


Figure 28. Angular distribution obtained in the reaction $^{9}$Be($^{16}$O,$^{14}$O) (left) and in the reaction $^{13}$C($^{12}$C,$^{14}$O) (right).

### 3.2.2. Results obtained

So, the 3.41, 3.89, and 3.96 MeV states were shown to have spins $3/2^+$, $5/2^-$, and $3/2^-$, respectively.

A summary Table 5 for the spin bands of the beryllium isotopes is presented below. As expected, according to Figure 24, each isotope corresponds to a low-lying rotational band, and the nuclei $^{10}$Be,$^{11}$Be, and $^{12}$Be, also have molecular bands.

## 3.3. Carbon isotopes

The carbon nucleus was listed among the nuclei exhibiting significant cluster properties in the introduction to this chapter because of two well-known facts related to its structure:

1) The existence of states well described by group-theoretic approaches, where the nucleus is viewed as an equilateral triangle with $\alpha$-particles at its vertices [79].

2) The famous "Hoyl's" $0^+$ state at an excitation energy of 7.65 MeV. According to the modern interpretation, it is considered as a pure cluster state, when the three constituent $\alpha$-particles are in a state close to the Bose-Einstein condensate state.

Table 5. Characteristics of rotational bands of beryllium isotopes.

| Isotope | $K^\pi$ | $E_x$ (MeV) | $\hbar^2/(2\Theta)$ (MeV) | Estimation of the distance between $\alpha$-particles (fm.) |
|---|---|---|---|---|
| Molecular bands | | | | |
| $^{10}$Be | $1^-$ | 5.96 | 0.25 | 5.16 |
| $^{11}$Be | $3/2^-$ | 3.96 | 0.23 | 5.16 |
| $^{12}$Be | $0^+$ | (6.4) | 0.21 | 5.16 |
| Low-laying (cluster) bands | | | | |
| $^{8}$Be | $0^+$ | 0.0 | 0.56 | 3.5 |
| $^{9}$Be | $3/2^-$ | 0.0 | 0.55 | 3.22 |
| $^{9}$Be | $1/2^+$ | 1.67 | 0.39 | 4.16 |
| $^{10}$Be | $0^+$ | 0.0 | 0.48 | 3.3 |
| $^{11}$Be | $1/2^+$ | 0.0 | 0.43 | 3.34 |
| $^{11}$Be | $1/2^-$ | 0.32 | 0.58 | 2.56 |
| $^{12}$Be | $0^+$ | 0.0 | 0.21 | 4.18 |

And to date, the study of the spectrum of states of the $^{12}$C nucleus remains an extremely urgent task. It is mainly connected with the search for high-spin states and explanation of their structure. In this sense, the carbon nucleus is very similar to the beryllium nucleus considered in the previous paragraph. But there is a significant difference.

While beryllium isotopes even with a large neutron excess retain the main features of cluster states, carbon nuclei, from a pronounced clustering pass to a shape close to spherical with a neutron "skin".

Nevertheless, as can be seen from Figure 9, at least for theoretical reasons, for the isotope $^{14}$C can still be considered a cluster structure, if not fundamental, at least important. It too contains rotational bands and admits a structure of the form $\alpha$+$^{10}$Be [18].

### 3.3.1. Aims and Methods of the Study

The goal of our experiment was to study the carbon isotope with an even larger neutron excess – $^{16}$C. To do this, the reaction $^{13}$C($^{12}$C,$^{9}$C)$^{16}$C was studied. Using the $^{13}$C nucleus as a target for the three neutron transfer allowed to populate the $^{16}$C states with one hole in the $1p1/2$ shell, and three neutrons located in the ($sd$) shell. In addition, $^{13}$C has a deformed cor as a $^{12}$C nucleus, which allows us to study the effect of cluster structure in the $^{16}$C nucleus at high excitation energies. Like other neutron excess nuclei, the $^{16}$C nucleus also has molecular

states, however, they are located too high.

This experiment was performed using the Q3D magnetic spectrometer of the Hahn-Meitner Institute in Berlin. The $^{12}$C beam energy was 230.7 MeV, the thickness of the $^{13}$C target was 260 $\mu$g/cm$^2$, and the enrichment was 95%. In order to remove the background, additional measurements were performed with $^{12}$C foil with a thickness of 200 $\mu$g/cm$^2$. This reaction was also used to calibrate and test the system.

Figure 29 shows the spectrum obtained from the experiment [43].

This resulted in the discovery of 14 previously unobserved states listed in Table 6. The spins and parities of the new states were assigned based on analysis within the coupled channel method and the random phase [161] method.

.

Table 6. $^{16}$C core levels detected in the experiment performed [43, 45].

| $J^\pi$ | Excitation energy (MeV) | $\Gamma$ (keV) | $J^\pi$ | Excitation energy (MeV) | $\Gamma$ (keV) |
|---|---|---|---|---|---|
| $(3^-)$ | 7.74 | 200 | $(3^-)$ | 11.85 | 220 |
| $(5^-)$ | 8.92 | 100 | - | 12.54 | 200 |
| $(4^+)$ | 9.1 | 50 | $(5^-)$ | 13.12 | 400 |
| $(4^-)$ | 9.42 | 100 | - | 14.26 | 200 |
| $(3^-)$ | 9.98 | 120 | - | 14.9 | 300 |
| $(2^-)$ | 10.39 | 150 | - | 16.44 | 150 |
| $(1^-)$ | 11.08 | 100 | - | 17.4 | 200 |

Most of the currently known levels of the $^{16}$C nucleus have been studied in the two-neutron transfer reaction $t$+$^{14}$C, which predominantly results in the occupation of states with positive parity. In this work, we studied the three-neutron transfer reaction to a nucleus with a hole in a $1p_{1/2}$ shell. Let us consider possible configurations for the $^{16}$C excited levels.

In principle, shell closure with $1p_{1/2}$ state filling and configurations of the form $(2p-0h)$ are possible. However, a configuration with three transferred nucleons filling the *sd* shell is more likely, so that the state can be described as $(sd)^3(1p_{1/2})^{-1}$. From the point of view of the shell model, the states $(1d_{5/2})^3$ and $(1d_{5/2})^2(2s_{1/2})^1$ will populate there most intensively.

Another important factor determining the settlement probability is the large difference between the input and output angular momenta due to the high value of

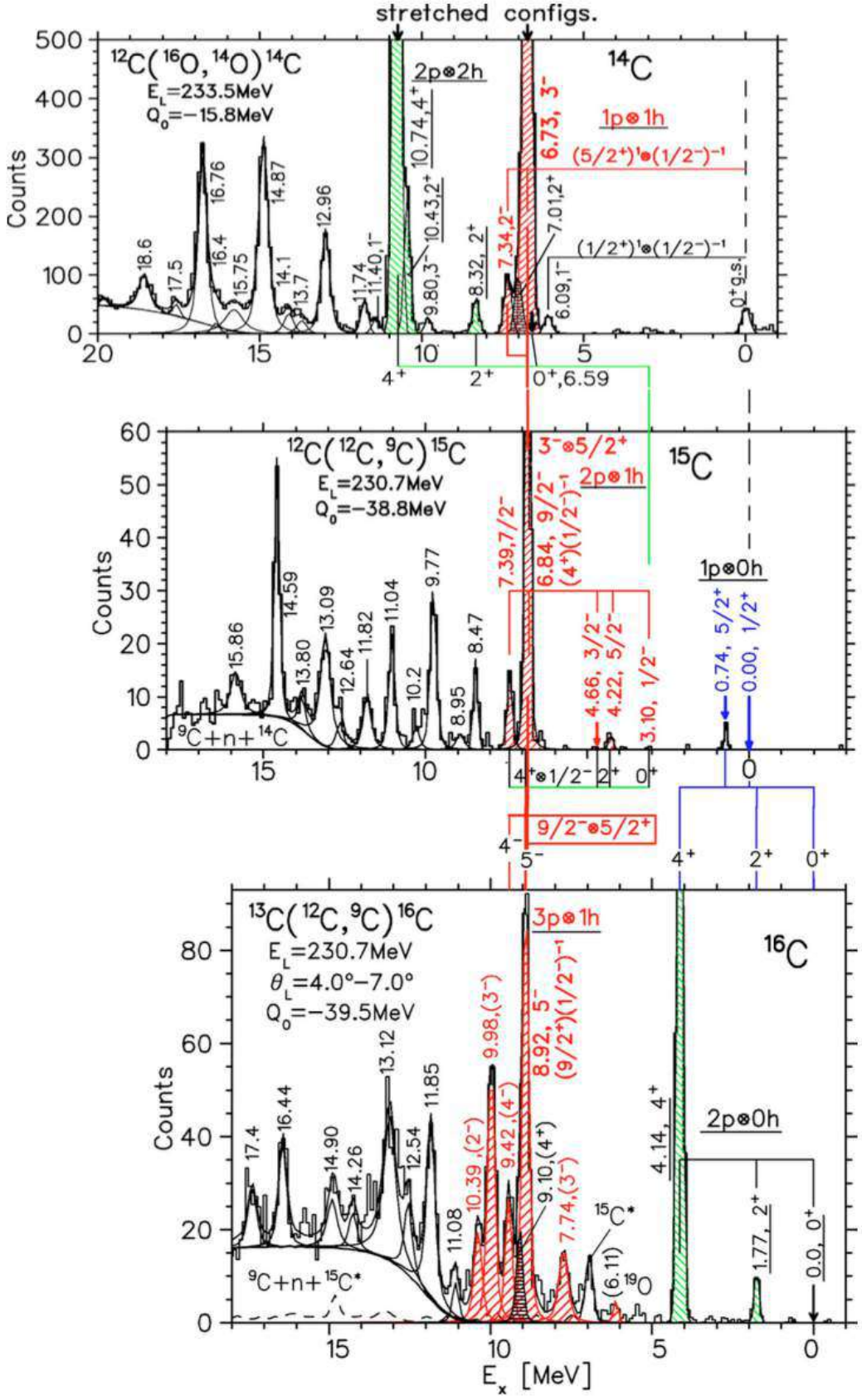


Figure 29. The spectrum of $^{14}$C, $^{15}$C, and $^{16}$C obtained in this experiment [43].

the $Q$-reaction (-39.5 MeV). This leads to an increase in the population probability of high-spin states. The spectrum in Figure 29 shows that the most intensively populated states are $5^-$, $(3p-1h)$ and $4^+$, $(2p-0h)$.

### 3.3.2. Results obtained

The data obtained indirectly confirm the currently existing systematics for light nuclei [18]. The states considered are predominantly of single-particle rather than cluster nature. Nevertheless, as the excitation energy increases, we can expect the populating of more exotic configurations (e.g., with one or two holes in the $1p_{3/2}$ and $1p_{1/2}$ shells), the populating of high-lying states (e.g., $1d_{3/2}$ and $1f_{7/2}$), and finally proton excitations. The latter can lead to the manifestation of $\alpha$-cluster states. The threshold for their manifestation is not too high and is of the order of 14 MeV, but it is not possible to conclude about the presence of such states in the spectrum. At the same time, these neutron-excess carbon isotopes are of special interest from the point of view of cluster degrees of freedom. Detailed calculations in terms of molecular orbitals predict a very high probability of the appearance of a linear configuration, for nuclei with molecular orbitals: $^{16}\mathrm{C}\big((3/2^-_\pi)^2(1/2)^0_\sigma)^2\big)$ [162]. Given the importance of considering molecular orbitals, the information obtained can be used in comparison with theoretical approaches, for example AMD. This will make it possible to identify low-lying levels at the base of quasi-molecular rotational bands in this nucleus.

## 3.4. Oxygen isotopes

As mentioned in the Introduction and the first chapter, the $^{16}$O nucleus can be represented as four $\alpha$-particles (tetrahedral structure), which is reflected in the properties of some excited states (group theory approach to the problem). Another way of solving the problem of describing the spectrum of excited states is to use the potential model. It can be said that the potential model was developed and tested just on the nuclei $^{16}$O and $^{20}$Ne. Unlike neon, the $^{16}$O nucleus is twice magic, so that the rotational band starts from the head level $K^\pi=0^+$ at energy 6.05 MeV. In the "classical" reaction for cluster bands ($^6$Li,$d$), the population of states with negative and positive parity occurs, albeit in a significantly non-uniform [163]. This has led to a discussion of the possible non$\alpha$-particle na-

ture of states with negative parity. Despite the low population intensity of such states in [164], their $\alpha$-particle structure was concluded to be consistent with the predictions of [15] theory. On the other hand, the cluster hypothesis was tested within the [165] potential model, which showed that states with negative parity require a significantly different kind of potential! While for positive parity the potential turned out to be very close (virtually equivalent) to the potential for the convolution of the $\alpha$-particle and the density distribution in the $^{12}$C nucleus (formula (28)), the potential for reproducing negative parity states turned out to be closer to the Woods-Saxon potential, with a flat "bottom". In [55] we showed that the potential for positive parity states can also be well reproduced within the limit $\alpha$-cluster model.

One could have assumed that this behavior of the potential is either a symptom of a poor manifestation of the cluster properties of states with negative parity, or at least may require the introduction of an angular momentum-dependent parameter. However, the problem was solved in the framework of a simple potential model using the $WS + WS^3$ potential (formula (27)).

Experimental confirmation of the cluster nature of the band can be obtained by using a reaction sensitive to the population of $\alpha$-cluster states – the $\alpha$-particle transfer reaction. In spite of the fact that the reaction ($^6$Li,$d$) was used to prove the cluster nature of the rotational bands, the levels with negative parity are populated rather weakly [163]. A different situation is observed for the $\alpha$-particle transfer in the ($^{12}$C,$^8$Be) [166] reaction. We used this result further to analyze the spectrum of $^{18}$O and to discuss the states of the $^{40}$Ca nucleus. The rotational band levels are summarized in Table 7. As can be seen, the population is quite active for negative parity, and this reaction shows better selectivity to cluster states, especially in the high spin region.

Despite the fact that in the case of the $^{16}$O nucleus the band has an excited state as its head level, the doublet considered above can be described in terms of a potential model.

Assuming that the $^{16}$O nucleus has a well-observed doublet of rotational bands, the question arises as to the behavior of the isotopes – will the added neutrons preserve the cluster structure, as they do in beryllium isotopes, or will

Table 7. rotational doublet $^{16}$O [155].

| $J^\pi$ | Excitation Energy (MeV) | Γ (keV) | $J^\pi$ | Excitation Energy (MeV) | Γ (keV) |
|---|---|---|---|---|---|
| $0^+$ | 6.05 | 67 ps | $1^-$ | 9.6 | 420 |
| $2^+$ | 6.92 | 4.7 fs | $3^-$ | 11.6 | 800 |
| $4^+$ | 10.36 | 26 | $5^-$ | 14.7 | 670 |
| $6^+$ | 16.3 | 420 | $7^-$ | 20.9 | 900 |
| $(8^+)$ | 21.7 | - | | | |

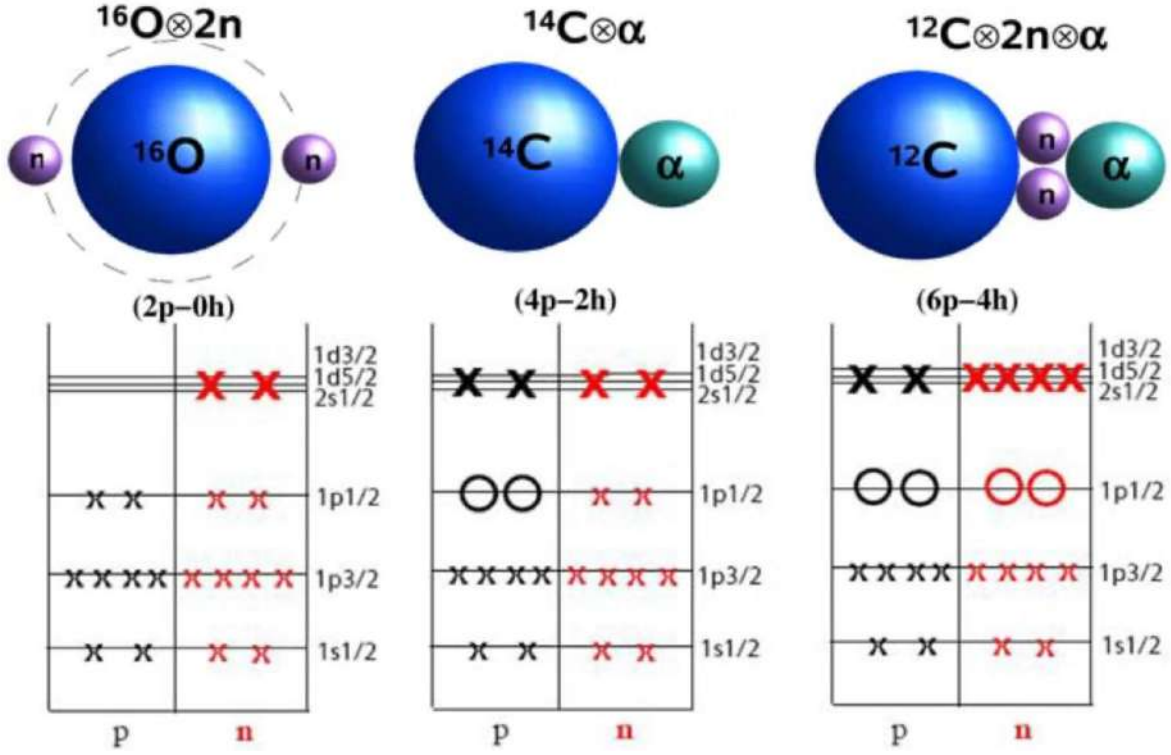


Figure 30. Structure of rotational bands of the $^{18}$O [167] nucleus.

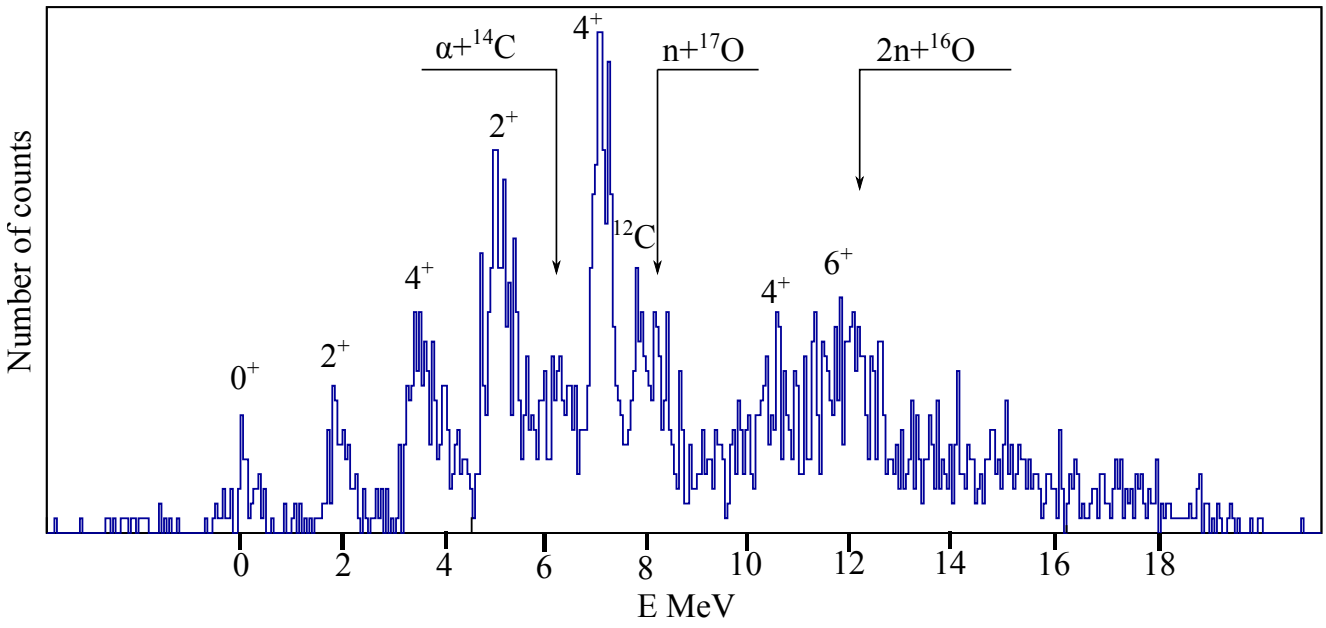


Figure 31. Structure of $^{18}$O nucleus states. Thresholds for the emergence of structures with different configurations are shown. The beam energy is 44 MeV [40].

they destroy it, as they do in carbon isotopes? In terms of cluster structure and covalently bound neutrons, we can expect the following picture for the rotational band structure of the $^{18}$O nucleus (see Figure 30 from the paper [167]). A band of single-particle states is shown on the left, a $\alpha$-cluster doublet in the center, and a molecular doublet on the right. All these states were observed experimentally. Thus, in the $^{18}$O nucleus, the cluster degrees of freedom are fully manifested.

### 3.4.1. Aims and Methods of the Study

The experimental data obtained in our experiments to study the $^{12}$C+$^{14}$C reaction are summarized below.

Our experiment was performed at the cyclotron of the University of Jyvaskyla, Finland. A $^{12}$C beam with an energy of 41-46 MeV was incident on a $^{14}$C target. Figure 31 shows the spectrum from the $^{14}$C($^{12}$C,$^{8}$Be)$^{18}$O reaction. The nuclei were registered by two groups of gas detectors (see Chapter 2), coincidences between neighboring PIN diodes registering $\alpha$-particles allowed $^{8}$Be to be registered. Further selection was performed by imposing appropriate kinematic conditions using the invariant mass method.

As can be seen, there is active population of states associated with the spin alignment of two valence neutrons – $0^+$ – 0.0 MeV, $2^+$ – 1.98 MeV, $4^+$ – 3.56 MeV. These states correspond to the $^{16}$O$\otimes$2n structure in Figure 30 when two neutrons

are arranged in a $d_{5/2}$ shell, which admits a maximum spin of 4. Further, the $0_2^+$-based doublet states with energy 3.64 MeV are clearly visible. In Figure 30, its structure is labeled as $^{14}C \otimes \alpha$. The populated states for this cluster band are $2^+$ – 5.26 MeV, $4^+$ – 7.512 MeV, $6^+$ – 11.7 MeV for the even-numbered band, and $1^-$ – 7.512 MeV for the odd-numbered band. The literature [167, 168] indicates that there is uncertainty with the value of the state energy $8^+$ – 17.6-18.06 MeV. Based on our results, it can be assumed that the second value is correct, since the 17 MeV region is still accessible in our experiment and no significantly populated states are found there. On the other hand, there are indications of a relatively low intensity of the corresponding peak, which is similar to the situation with the $^{16}O$ nucleus.

The analysis of the $^8Be$ yield from the reaction for different energies shows that the excitation cross section of the rotational band states is almost independent of the beam energy, while significant oscillations are observed for the single-particle states.

### 3.4.2. Results obtained

The characteristics of the doublet levels, supplemented with data from the work [167] are summarized in Table 8.

Table 8. Rotational doublet in nucleus of $^{18}O$ [167].

| $J^\pi$ | E exc. (MeV) | Γ (keV) | Presence in this work | $J^\pi$ | E exc. (MeV) | Γ (keV) | Presence in this work |
|---|---|---|---|---|---|---|---|
| $0^+$ | 3.64 | - | yes | $1^-$ | 8.04 | <10 | no |
| $2^+$ | 5.26 | - | yes | $(3)^-$ | 9.71 | 15 | no |
| $4^+$ | 7.12 | <10 | yes | $(5)^-$ | 13.6 | 22 | no |
| $6^+$ | 11.7 | 19 | yes | $(7)^-$ | 18.6 | 100 | no |
| $(8^+)$ | 18.1 | 80 | no | | | | |

According to the data presented in the [167], a molecular doublet with the structure corresponding to the right part of Figure 30 was also found. At the same time, we cannot but note the extreme ambiguity of the situation in this matter. As can be seen from Figure 31, our work, confirming the results [167], demonstrates the cluster character (and, accordingly – belonging to the rotational band) of the states $2^+$, 5.26 MeV, $4^+$, 7.12 MeV for positive parity and $1^-$, 8.04 MeV for

negative parity. However, in a recent paper [169], the authors concluded that there are no cluster states in the $^{18}$O nucleus, except for the $6^+$ 11.7 MeV state. Since the authors studied the $\alpha$-particle transfer reactions in reaction with $^7$Li, a situation similar to the case of the $^{16}$O nucleus emerges. In a recent review on cluster degrees of freedom [33], the authors point out that further careful investigation of this issue is needed. In the following, we will focus on the results obtained in our experiment.

Not long ago, the paper [170] presented data on the rotational bands of the $^{20}$O nucleus. The structure of such states is more complicated; in particular, theoretical consideration of the question tells us that it is possible for both $\alpha$-particles and $^6$He [171] to exist as a cluster in such a nucleus. The cluster structures expected in the $^{20}$O nucleus have been discussed in [170]. The cluster doublet data from this work are summarized in Table 9.

Thus, it can be concluded that the neutron excess in the oxygen nucleus has a much weaker effect than for carbon.

.

Table 9. rotational doublet of nucleus $^{20}$O [170].

| $J^\pi$ | Excitation Energy (MeV) | $\Gamma$ (keV) | $J^\pi$ | Excitation Energy (MeV) | $\Gamma$ (keV) |
|---|---|---|---|---|---|
| $0^+$ | 4.46 | - | $(1^-)$ | 9.92 | 20 |
| $2^+$ | 5.24 | - | $(3)^-$ | 11.95 | 90 |
| $4^+$ | 7.75 | - | $(5)^-$ | 13.96 | 150 |
| $(6^+)$ | 10.93 | 40 | $(7)^-$ | 18.46 | 140 |
| $(8^+)$ | 16.36 | 90 | | | |

## 3.5. Isotopes of neon

As stated earlier, the $^{20}$Ne nucleus is, along with the $^{44}$Ti nucleus, the main "test stone" for testing the cluster approximations. Due to its twice-magic core, as well as the presence of its own rotational bands of cluster nature, this nucleus has always attracted considerable attention. One of the first works on the global systematics of cluster states of light nuclei was Richards' work on the $^{20}$Ne [88] nucleus, which, in many respects, "set the tone" for further studies in this direction. In particular, Richards showed the existence of a number of bands in neon,

the members of which had close values of reduced widths. The bands identified so far have been shown in Figure 11. As in the previous section, the question arises – whether such states can be described within the potential model and how the structure of the nucleus would behave if neutrons were added.

Apparently, the first suggestion of the existence of an inverse doublet for the rotational band in the $^{20}$Ne nucleus was made in [15]. The study of such states, similar to the case of the $^{16}$O nucleus, proceeded preferentially using lithium transfer reactions or the transfer of two $\alpha$-particles in the $^{12}$C($^{12}$C,$\alpha$) [172] reaction, which allowed the study of a large number of high-spin states of neon. In contrast to lithium transfer reactions, where one usually applies an angular distribution analysis within the DWBA framework, the angular correlation method is preferred in this case. In this case, the problem is reduced to the study of the reaction $^{12}$C($^{12}$C,$\alpha_1$)$^{20}$Ne*$\rightarrow^{16}$O+$\alpha_2$. In the case where $\alpha_1$ is registered at 0° (or a very small angle), the angular distribution of $\alpha_2$ obeys the distribution:

$$W(\theta) \sim \frac{2J+1}{4\pi}|P_J(\cos\theta)|^2 \tag{70}$$

where $\theta$ is the angle of registration $\alpha_2$ (or between $\alpha_2$ and $\alpha_1$ in the case where the first particle is not registered under zero). This procedure greatly facilitates the finding of the $J$ angular momenta of the $J$ excited states of the neon nucleus.

Table 10 summarizes the data for the two doublets.

.

Table 10. Rotational doublet of nucleus $^{20}$Ne [155].

| $J^\pi$ | Excitation Energy (MeV) | Γ (keV) | $J^\pi$ | Excitation Energy (MeV) | Γ (keV) |
|---|---|---|---|---|---|
| $0^+$ | 0.0 | - | $(1^-)$ | 5.788 | 0.028 |
| $2^+$ | 1.63 | - | $3^-$ | 7.156 | 8.2 |
| $4^+$ | 4.25 | - | $5^-$ | 10.262 | 145 |
| $6^+$ | 8.776 | 0.11 | $7^-$ | 15.336 | 78 |
| $8^+$ | 11.951 | 0.035 | $9^-$ 22.87 | 225 | |

Whereas for the first band the generally accepted interpretation of the $^{16}$O$\otimes\alpha$ states. For the second, the $8p-4h$ configuration is usually considered, which can be interpreted as $^{12}$C$\otimes 2\alpha$ or $^{12}$C$\otimes^8$Be. The first interpretation admits a symmetric picture of the arrangement of the two $\alpha$-particles with respect to the core.

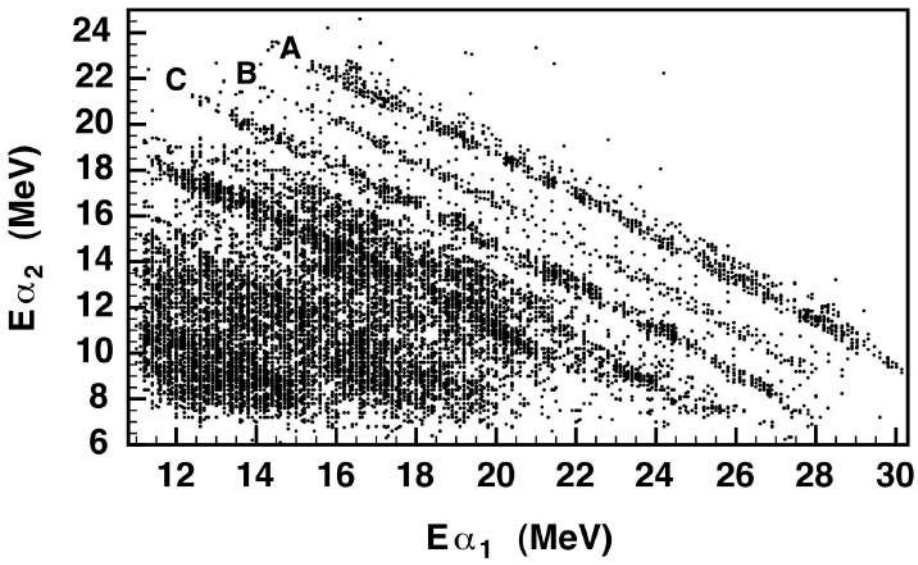


Figure 32. 2D-plot $^{14}$C($^{12}$C,$\alpha_1$)$^{22}$Ne*$\rightarrow^{18}$O+$\alpha_2$. A corresponds to populating the ground state of the $^{18}$O nucleus, B to an excitation energy of 1.98 MeV, and C to an excitation energy of 3.55-3.63 MeV [35].

### 3.5.1. Aims and Methods of the Study

A reaction similar to the above $^{14}$C($^{12}$C,$\alpha_1$)$^{22}$Ne*$\rightarrow^{18}$O+$\alpha_2$ with the angular correlation analysis method was chosen to experimentally study similar high-spin states in the $^{22}$Ne nucleus. Previously, in [173], it was shown that a high-spin $18^+$ resonance exists in the $^{12}$C+$^{14}$C system at energy $E_{cm}$=23.5 MeV. Such a resonance will correspond to an increased probability of populating high-spin states in the exit channels of this reaction.

The experiment was performed at the gas pedal of the University of Jyvaskyla, Finland. The beam of the K-130 cyclotron was directed onto a $^{14}$C 280 $\mu$g/cm$^2$ foil with 90% enrichment. The beam energy was 44 MeV, which corresponded to the above resonance. The reaction products were detected by four groups of detectors – two gas $\Delta E - E$ telescopes and two detectors located at an angle of $\pm 3^\circ$ relative to the beam. To extract $\alpha$-particles, these detectors were switched on using the pulse shape analysis scheme [130] (see Chapter 2). The gas detectors spanned an angle of $34^\circ \geq \theta \geq 74^\circ$ to analyze the angular distributions. The detector positions were chosen so as to capture the angle $90^\circ$ in the center-of-mass system in the investigated energy range, which was previously tested for the case of a $^{12}$C target. A detailed description of the study performed is presented in [35, 36].

The Figure 32 shows the two-dimensional spectrum of the studied reaction. As can be seen from the two-dimensional spectrum, we have a good resolution of the three low-lying levels of the $^{18}$O nucleus (see also Figure 31). The minor contribution from the $^{12}$C impurity (states above the A band) was removed by subtracting the known states from the data we obtained with the $^{12}$C target and analyzing the dependence of the peak intensity position on the excitation energy of the residual nucleus. The resolution in this experiment was assumed to be better than 100 keV. In agreement with [173, 174] the $^{22}$Ne nucleus decays preferentially to the $4^+$ state and slightly to the $2^+$ state of the $^{18}$O residual nucleus in this range of excitation energies.

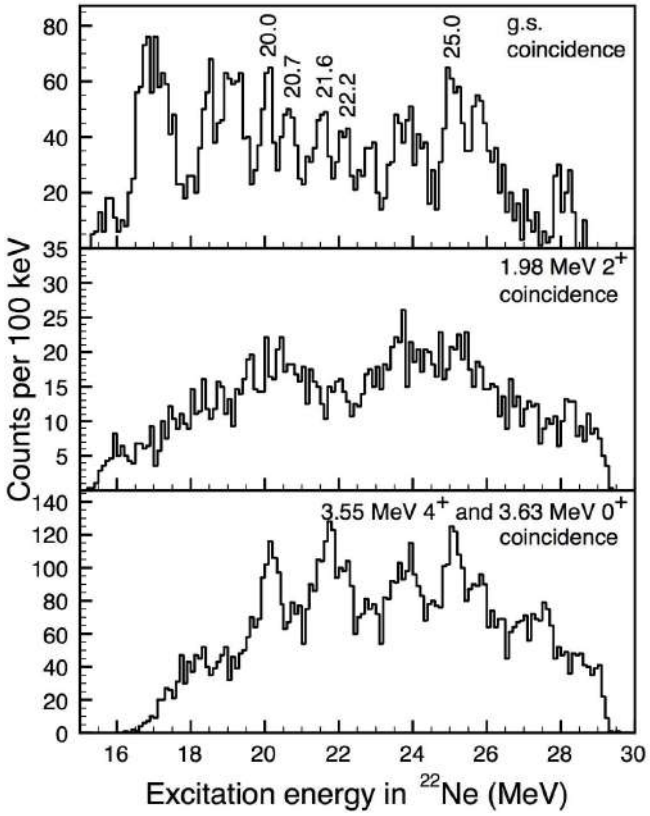


Figure 33. One-dimensional spectra of the reaction $^{14}$C($^{12}$C,$\alpha_1$)$^{22}$Ne*$\rightarrow^{18}$O+$\alpha_2$ for the three states of the residual nucleus [35]. The upper panel corresponds to the ground state of the $^{18}$O nucleus, the middle one to the state with excitation energy 1.98 MeV, and the lower one to the unresolved doublet 3.55-3.63 MeV.

Figure 33 shows the spectrum of the excited states of the $^{22}$Ne nucleus. The upper panel corresponds to the decay of $^{22}$Ne into the ground state $^{18}$O, the middle one, into the $2^+$ state with energy 1.98 MeV, the lower one corresponds to the decay into the insoluble doublet $4^+$ 3.55 MeV and $0^+$ 3.63 MeV. An analysis of the distribution in the intensities of the spectrum perpendicular to the location

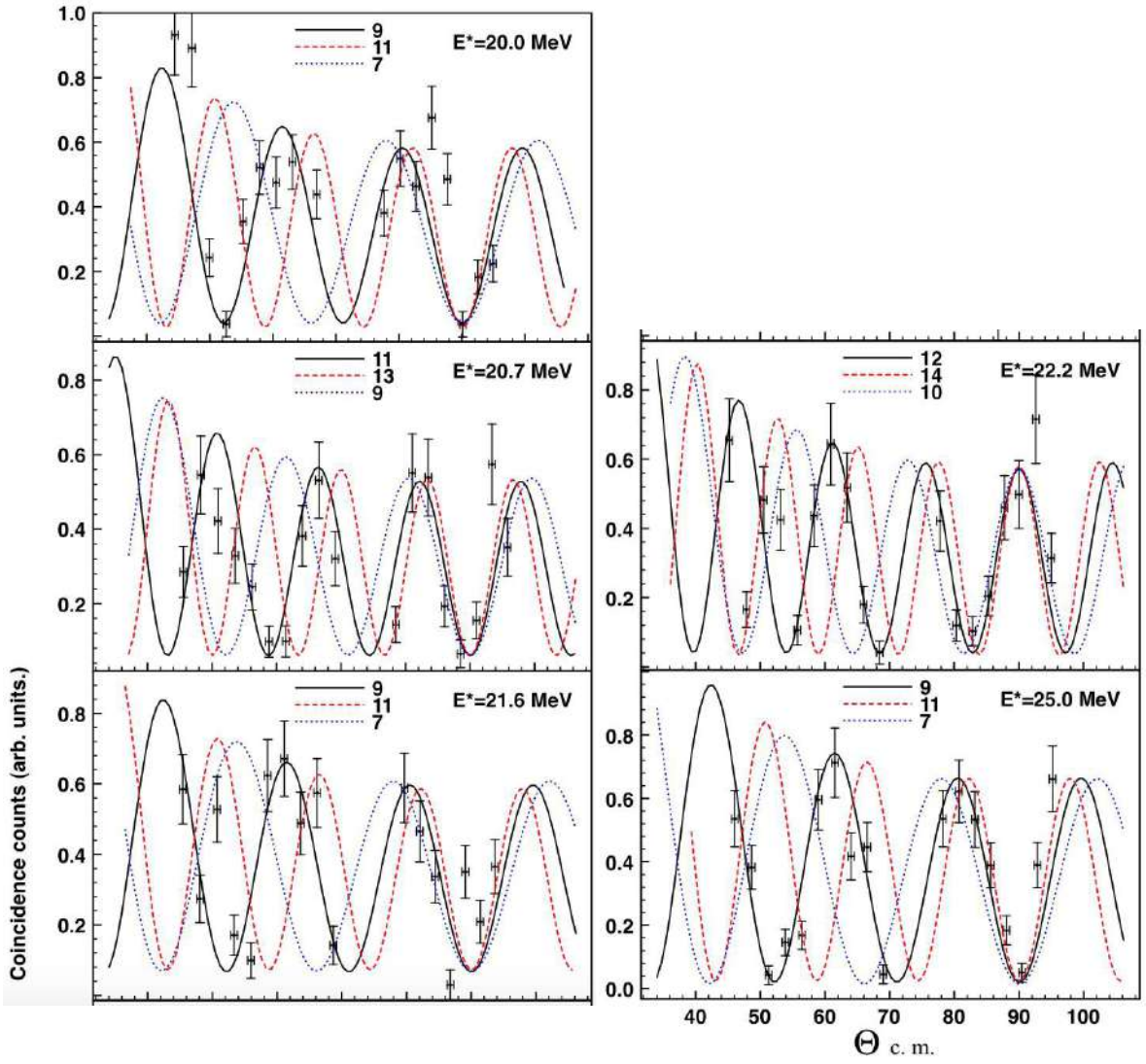


Figure 34. Angular correlations for $\alpha$-decay of $^{22}$Ne* to the ground state of $^{18}$O [35].

of the loci shows that it is the $4^+$ state that gives the largest contribution to the latter spectrum.

In the experiment, the excitation region from 15 to 30 MeV was investigated. As a result, 12 states were investigated, of which 5 were identified as new high-spin states belonging to the rotational bands.

Figure 34 shows correlation plots for the five states detected in this work. The fit to the experimental points was performed by the function $|P_J|^2$+const, which, as can be seen from the formula (70), makes it possible to assign values of the angular momenta to the states considered. The background present due to the coincidence requirement is small and can be removed.

The obtained results and comparison with the reference data are presented in Table 11.

Table 11. $^{22}$Ne nucleus levels.

| Experimental data [35,36] | | | References data | | |
|---|---|---|---|---|---|
| $J^\pi$ | Exc. energy. (MeV) | $\Gamma$ (keV) | $J^\pi$ | Exc. energy. (MeV) | Ref. |
| | 17.0 | non resolved | $(7^-)$ | 17.05 | [177] |
| | 18.45 | 330 | | 18.42 | [174] |
| | 19.13 | non resolved | $7^-$ | 19.28 | [175] |
| $9^-$ | 20.0 | 270 | $(10)^+$ | 19.89 | [176] |
| $11^-$ | 20.7 | 340 | $9^-$ | 20.85 | [175] |
| $9^-$ | 21.6 | 350 | $9^-$ | 21.8 | [175] |
| $12^+$ | 22.2 | 250 | | 22.2 | [174] |
| | 22.9 | 290 | | | |
| | 24.0 | non resolved | | 24.1 | [178] |
| $9^-$ | 25.0 | 350 | | | |
| | 25.9 | non resolved | | | |
| | 27.0 | non resolved | | | |

As indicated above, the reaction we have chosen is particularly efficient in populating cluster states with the structure $\alpha$+Cor and $2\alpha$+Cor. A comparison of the available theoretical and experimental data on the structure of rotational bands in the $^{22}$Ne nucleus with the results obtained allows us to attribute the levels found to rotational bands of different structure . The levels found in the paper and listed in Table 11 are detailed below.

Level $9^-$, 20.0 MeV. In the $^{14}$C($^{18}$O,$^{18}$O+$\alpha$) reaction, levels with close energies of 19.9 MeV [174] and 19.89 MeV [176] were observed. In the latter case, the spin was presumably determined to be $(10^+)$. As follows from the spectra obtained in [173] for the population of the $4^+$ state (3.55 MeV) in $^{18}$O, several closely spaced levels with a strong dependence of the population probability on the beam energy are present in this energy region. The most intense level with energies slightly below 20 MeV appears at beam energy $E_{c.m.}$=20.75 MeV, while at higher energies a peak with energy 20 MeV is observed. Its position coincides well with the predictions for the end of the $K = 0^+$ band

$11^-$ level, 20.7 MeV. In [175], evidence was obtained for the presence of a fragmented rotational band of negative parity in an elastic scattering study of $\alpha$-particles in inverse geometry. Doublets with angular momenta $1^-$,$3^-$,$7^-$,$9^-$ were found and the existence of a state with spin $11^-$ was predicted. On the other hand, in the paper [179], based on the use of a microscopic cluster model, the

breakage of this band at angular momentum $7^-$ is predicted.

The $9^-$ level, 21.6 MeV. In this energy region, the $9^-$ level was observed in [176] (excitation energy 21.96 MeV) and in [175] (excitation energy 21.84 MeV). It presumably belongs to the fragmented molecular rotational band.

Level $12^+$, 22.2 MeV. This level, having a significant spin, may belong only to the yrast line. For the case of the *sd*-region, the maximum spin when the $\alpha$-particle populates the next shell is $8^+$ for the $^{20}$Ne nucleus and $10^+$ for the $^{22}$Ne nucleus. However, in [180, 181] it was shown that there are minima on the potential surface for neon nuclei corresponding to higher angular momenta. As shown in [180], the rotational band corresponding to the yrast line in the $^{22}$Ne nucleus experiences backbending already at spin $10^+$. Thus, this level allows us to test the consistency between cluster models and models based on collective effects [180, 181].

Level $9^-$, 25.0 MeV. In this energy region, states corresponding to the structure $2\alpha(^8\text{Be})+^{14}\text{C}$ should be expected to appear. Then the found state corresponds well to the case when the head level $0^+$ is formed near the decay threshold of the system. Moreover, such a level lies in the region where, according to the work [178], states with high intensity decay of the $^{22}$Ne nucleus into $^{12}\text{C}+^8\text{Be}$ are observed. Two such states, 24.14 MeV and 26.89 MeV, were reported in [178]. Their spins were estimated as $6^+$ and $8^+$ or $8^+$ and $10^+$, assuming an approximate equality of excitation energies for bands of the same structure in $^{20}$Ne and $^{22}$Ne nuclei, corrected for the magnitude of the $Q$-reaction.

The obtained result is illustrated in the Figure 35 of [32], where, in addition to the previously known states of the $^{22}$Ne nucleus, the high-spin states obtained in our [35, 36] (shown in red) are given. As can be seen, the high-spin state $12^+$ belonging to the yrast line may also belong to the band $K^\pi=0_2^+$.

As mentioned above, in the simplest case of the shell model for the $^{22}$Ne nucleus, the 6 nucleons in the *sd* shell assume a ground state band cutoff at spin $10^+$. Theoretical analysis of the properties of the neon isotopes [182,183] predicts a backbanding phenomenon at a spin value of 8 for the $^{22}$Ne nucleus and 6 for $^{20}$Ne. This was confirmed by experimental results in the detection of the high-spin state $10^+$ [180] in $^{22}$Ne. Significant efforts have been made to search for a similar level

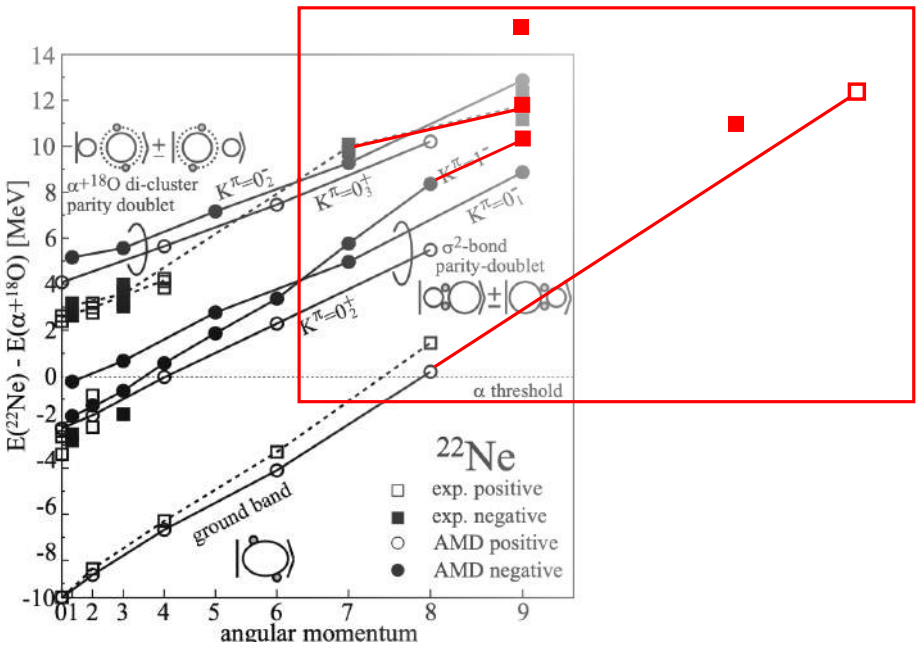


Figure 35. Molecular bands in the $^{22}$Ne nucleus from the paper [32]. Red shows the results of our work [35, 36].

in $^{20}$Ne, since states with spin greater than 8 are allowed and predicted [177, 184] for the high-lying bands. It is now believed that such a state has been found [185], allowing an interesting comparison of $^{20}$Ne and $^{22}$Ne nuclei.

A plot of the effective moment of inertia of the $^{20}$Ne and $^{22}$Ne nuclei as a function of rotational frequency is shown in Figure 36. As indicated in [180], there are two important differences between these nuclei: the moment of inertia for $^{20}$Ne experiences stronger oscillations than in the case of $^{22}$Ne and backbending occurs in $^{22}$Ne two angular momentum units later than in $^{20}$Ne. These effects can be qualitatively understood within the Nilsson-Strutinsky theory approach. The inset Figure 36 shows the trajectory of the minimum on the energy surface of $^{20}$Ne and $^{22}$Ne nuclei obtained in the work [181]. This graph emphasizes the similarity of the backbending processes occurring for these nuclei. The results obtained by us perfectly confirm the theory of energy surface construction, which predicts almost linear (in $J(J+1)$ coordinates) behavior of the yrast line up to the $12^+$ state for the $^{22}$Ne nucleus, in contrast to the sharp jump of the yrast line for the $^{20}$Ne nucleus. The predicted value of the $12^+$ state of 24.5 MeV turns out to be very close to our experimental value of 22.2 MeV.

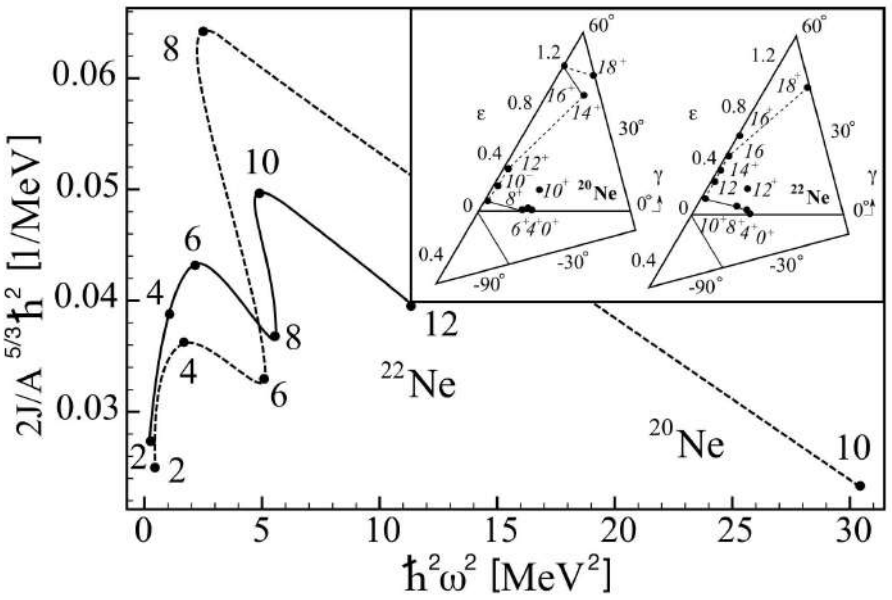


Figure 36. Effective moment of inertia as a function of rotation frequency for the yrast line of $^{20}$Ne and $^{22}$Ne [35, 36]. The inset shows the yrast line trajectories for these nuclei on the energy surface [181]

.

### 3.5.2. Results obtained

The oxygen and neon nuclei considered above can be seen to possess a significant number of states, which can be called cluster or molecular states. An important feature of these nuclei is also that the core and clusters populate different shells – $p$ shell for the core, $sd$ – for the clusters. Before moving on to heavier nuclei, it is interesting to compare the possibility of describing neon isotopes within the potential model.

In [62] we have described the rotational bands in the nuclei $^{16}$O, $^{18}$O, $^{20}$O, $^{20}$Ne, and $^{22}$Ne using the $WS{+}WS^3$ potential with parameters $a$=0. 73 fm, $x$=0.3 (satisfying Buck's systematics), and the potential itself was chosen as $V(r) = 250 \cdot f(r)$, where the form factor was given by the formula (27). We have presented the results obtained in [61, 62]. A comparison of these results with experimental data is presented in Figure 37. The radius values were fitting parameters and the following values were chosen:

$^{16}$O - $R$=2.9 fm.

$^{18}$O - $R$=2.93 fm.

$^{20}$O - $R$=3.21 fm.

$^{20}$Ne - $R$=3.06 fm.

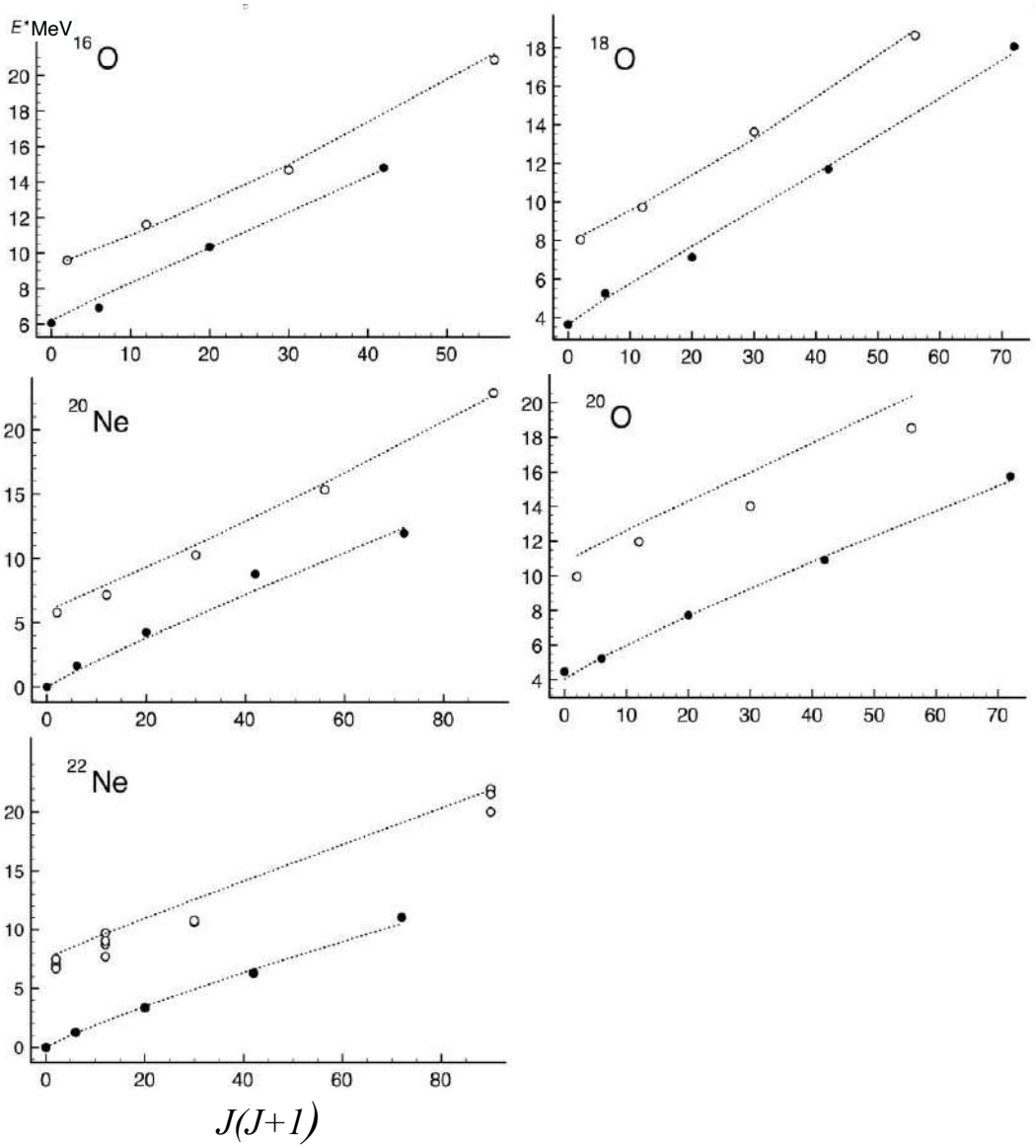


Figure 37. Comparison of potential model predictions for $^{16}$O, $^{18}$O, $^{20}$O, $^{20}$Ne, and $^{22}$Ne nuclei [35]. The dark and light circles are states with positive and negative parity, respectively. For states with negative parity $^{22}$Ne, several candidates are presented

.

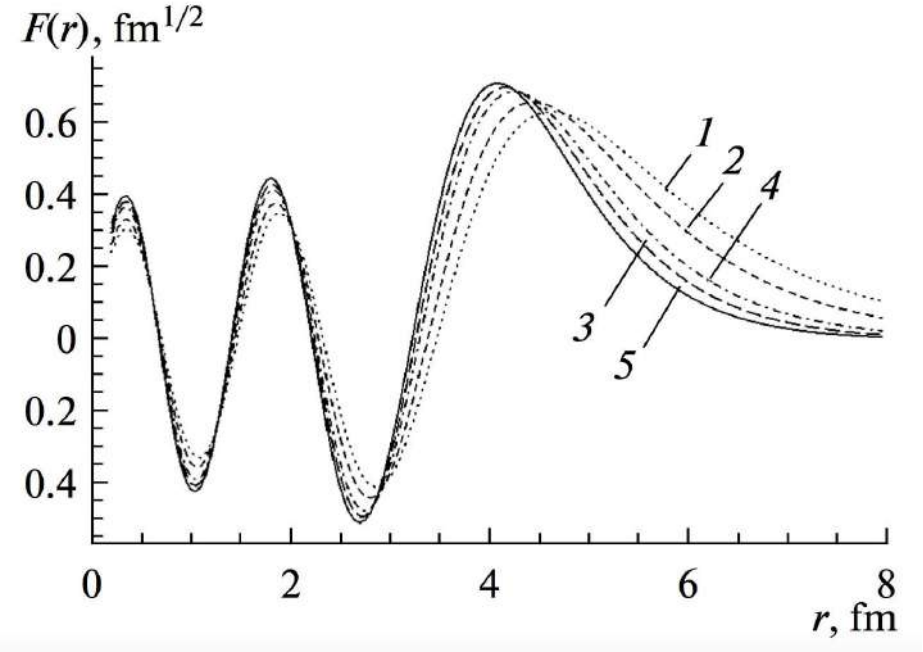


Figure 38. Radial wave functions for $0^+$ states $^{16}$O – 1, $^{18}$O – 2, $^{20}$O – 3, $^{20}$Ne – 4, and $^{22}$Ne – 5 [62].

$^{22}$Ne - $R$=3.21 fm.

For the $^{20}$Ne nucleus, the value we have chosen coincides with the result obtained in [76]. The radius behavior is approximately described as $R = r_0 A^{1/3}$, where $r_0$=1.14 fm.

Figure 38 shows the wave functions for the ground states of the considered nuclei.

### 3.6. Magnesium

One of the most important reactions in which molecular resonances have been and are being studied is the elastic scattering of $^{12}$C+$^{12}$C, i.e., the states in the $^{24}$Mg nucleus. As a result, to date, we have extensive material on this reaction. Let us list the main results obtained indicating the presence of molecular structure.

1) Presence of a well-distinguishable structure in the full cross-section plot.

2) The spectrum contains narrow peaks.

3) The energy of the excited states varies with angular momentum in proportion to $J(J+1)$.

4) The slope of the resulting graph is in good agreement with the "classical" moment of inertia for a system of two closely spaced nuclei with mass number 12.

There is a large number of interesting and relevant problems related to the analysis of molecular states in such a system. At the same time, there are quite a lot of models allowing to describe such interactions from the point of view of quantum mechanics: potential model (Buck potential, convolution potential), model of linear combination of nuclear orbitals (LCNO), model of cluster orbitals, vibrator-rotator model, etc.

Above we have shown that additive neutrons can destroy the cluster structure of carbon nuclei. In this case, how do molecular states behave in scattering and how do they relate to reactions?

Consider the $^{14}$C+$^{12}$C reaction with yields of various beryllium isotopes near the elastic scattering resonance found in the $^{14}$C+$^{12}$C system E$_{cm}$ =23.5 MeV [173, 186]. As found [173], this state corresponds to a quasi-molecular resonance with angular momentum $18^+$ at energy E$_{cm}$ =23.5 MeV, and the excitation function in this region has the same resonance-like structure for a number of output channels, including the $^{12,13,14}$C excited states (see Figure 39). A similar structure is observed for the $^{14}$C($^{12}$C,$^{10}$Be)$^{16}$Ochannel we are considering. The interest in this reaction is due to the significant angular momentum (exceeding the grazing angular momentum) for such a light system, which is in poor agreement with theoretical predictions based on the DWBA approach to describe quasi-molecular resonances [187], leaving even the question of the optical interaction potential in such a system uncertain.

At the same time, the possibility of the existence of a sufficiently high momentum in the considered system is indirectly confirmed by the data obtained earlier in the works [35,36], in which it is shown that the residual $^{22}$Ne nucleus formed in the reaction $^{14}$C($^{12}$C,$\alpha$) can have a spin $12^+$ significant for such a nucleus. In order to study this reaction and to determine its relation to quasi-molecular states, we have obtained angular distributions at energies E$_{cm}$=21.1 MeV and 24.6 MeV – near resonance and at the resonance point at energy 23.5 MeV.

The experiment was performed at the cyclotron of the University of Jyvaskyla (Finland). The $^{12}$C beam was directed onto a self-supported $^{14}$C target (thickness 280 $\mu$g/cm$^2$, enrichment 90%). The detector system for registration of reaction products was located in a scattering chamber with a diameter of 1.5 meters. The

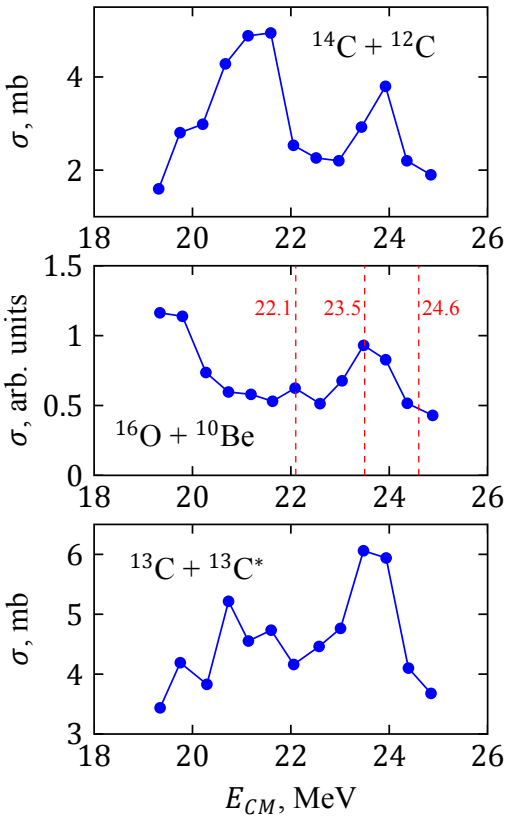


Figure 39. Excitation function for the reaction $^{14}C+^{12}C$. The elastic channel and the channel with $^{16}O+^{10}Be$ output are shown. The dotted line shows the energies chosen in the paper for the study [38].

products were registered by two position-sensitive gas $\Delta E - E$ telescopes (see Chapter 2). The accuracy of the information on the particle registration angle was $\pm 0.2°$. A detailed description of the experiment is presented in [37, 38]

The angular distributions of the $^{10}Be+^{16}O$ yield channel obtained for the three energies shown in Figure 40.

The angular distributions for all considered energies have an oscillatory character with a tendency to increase the cross section at small angles, and the period of their oscillations in the first approximation can be described by a Legendre polynomial. For the case of nonresonant energies, the order of the polynomial cannot be determined unambiguously; however, the best approximations for 21.1 and 24.6 MeV are of order 15 and 16, respectively, which coincides well with the estimates of $L_{gr}$ for these energies [186]. In the case of the 23.5 MeV energy, there is a sharp minimum in the distribution of $\chi^2$ values for the fitting polynomials, corresponding to a 12th-order polynomial. This behavior is characteristic of an isolated resonance. The angular distributions for the excited states of the

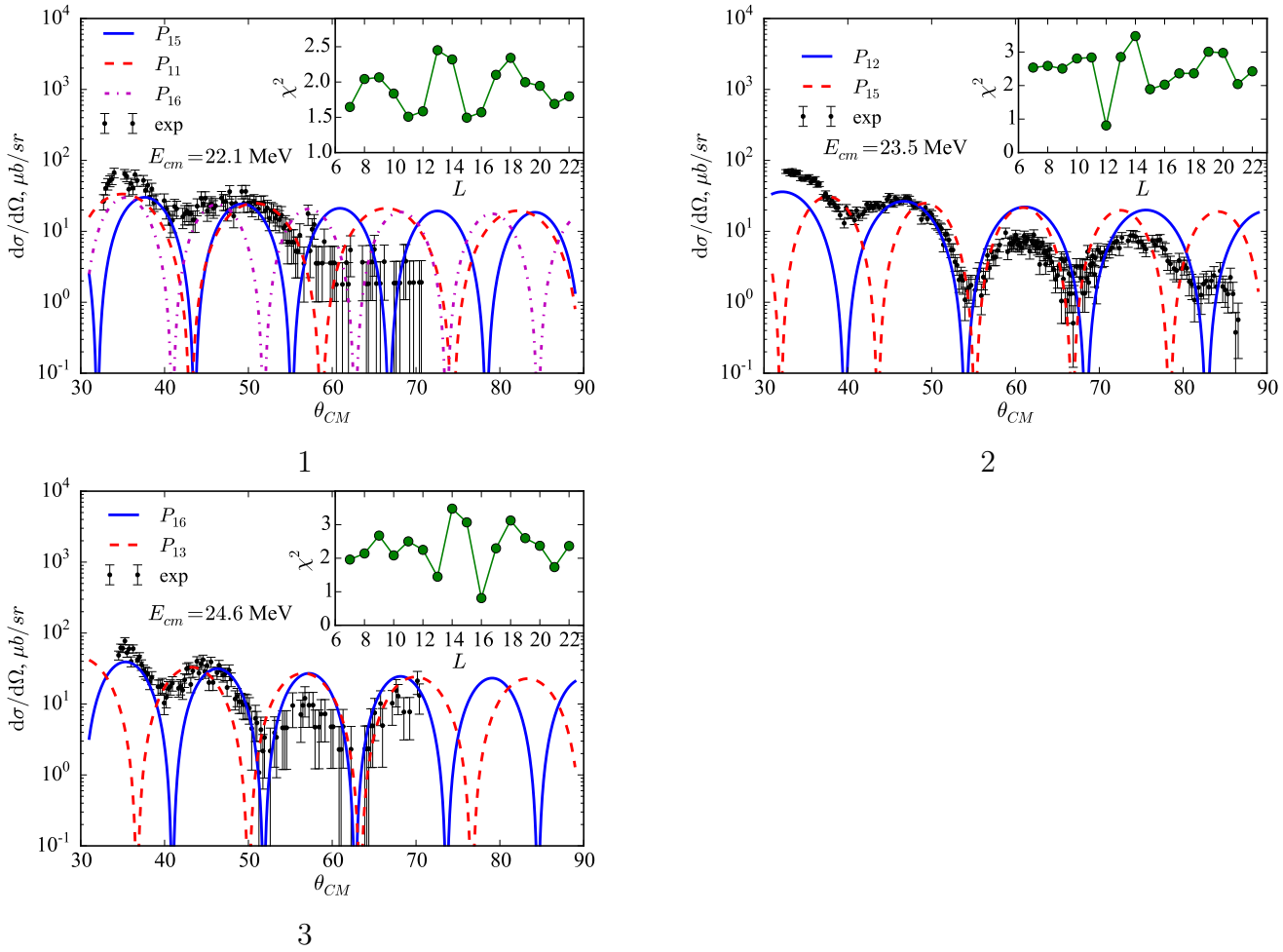


Figure 40. Angular distributions for three energies near resonance [37]. Comparison with Legendre polynomials is shown, the insets give $\chi^2$ values for the polynomials. 1 – 22.1 MeV, 2 – 23.5 MeV, 3 – 24.6 MeV.

$^{16}$O residual nucleus and for the case of the $^{9}$Be yield turned out to be almost structureless, with the cross section falling smoothly with increasing angle.

In the simplest model for resonance states in reactions with heavy ions, the order of the Legendre polynomial describing the angular distribution corresponds to the angular momentum in the system under consideration. The angular momenta determined by this method can be compared with the predictions of quasi-classical models. Figure 41 shows the maximum partial wave orders available in the input and output channels. The calculation was performed using the formula [188]:

$$L_{cr} = r_0(A_1^{1/3} + A_2^{1/3})\sqrt{(2\mu/\hbar^2)(E_{cm} - V_c)}, \qquad (71)$$

where $\mu$ – reduced mass, $V_c$ – height of the Coulomb barrier, $A_{1,2}$ – mass numbers, $r_0$=1.55-0.00125$\eta$, $\eta$ – Sommerfeld parameter.

As can be seen, in our case there is no smooth growth of the angular momen-

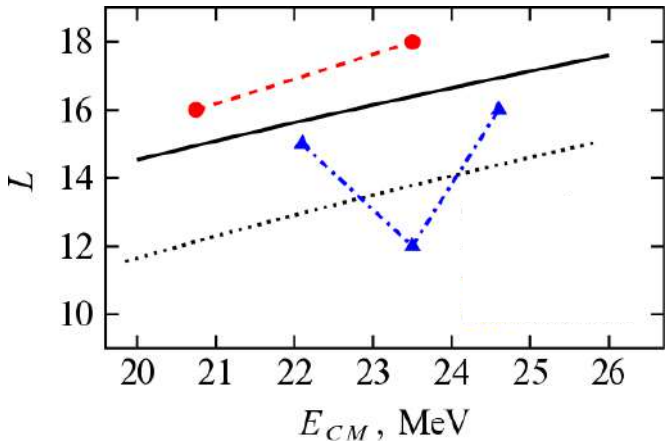


Figure 41. Comparing the maximum angular momenta for the input and output channels for the $^{14}$C($^{12}$C,$^{10}$Be)$^{16}$Oresponse [37]. Triangles–experimental data. Solid line – maximum partial wave order values for the input channel, dashed line – for the output channel. Circles – data for elastic resonances from the paper [173].

tum with energy, as it occurs in the case of nonresonant reactions. Except for the 23.5 MeV energy, the angular momentum growth corresponds well to the change in the maximum order of the partial wave. Taking into account the closeness of the moments obtained from the quasi-classical analysis and the maximum values for the partial wave moments, we can conclude that absorption of waves with maximum momentum plays a significant role in the reactions at energies 21.1 and 24.6 MeV.

It should be noted that there is a significant difference in the angular momenta for the input and output channels of the response under consideration. In the work [173], the $^{12}$C+$^{14}$C states with energies of 20.75 and 23.5 MeV are assigned angular momenta of 16 and 18, respectively, so that the slope of the graph also roughly corresponds to the increase with energy of the $L_{cr}$ value, although the angular momentum values found lie somewhat higher, and the angular momentum value of 12, found by us, lies somewhat below the $L_{cr}$ estimates for the exit channel (see Figure 41). At the same time, for the known resonances in the $^{12}$C+$^{12}$C system, the angular momenta found for the different channels (elastic and $^{8}$Be output) almost coincide. This discrepancy may have the following explanations:

1) The observed distribution is not a consequence of resonance in the system and is due to a direct reaction mechanism in the transfer of a sufficiently heavy cluster. Thus, in the work [189] such a picture arises due to the processes associated with the transfer of the $\alpha$-particle.

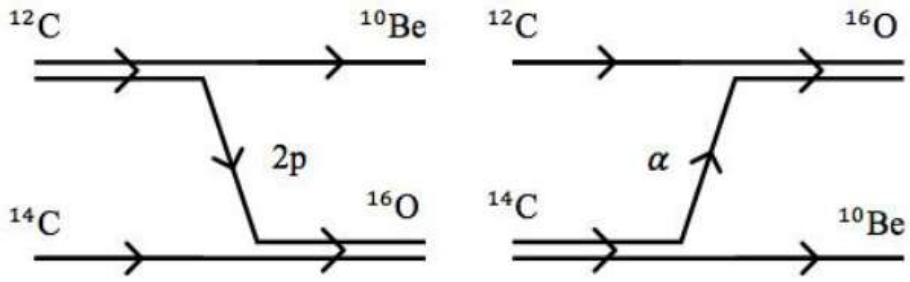


Figure 42. Schematics of single-stage two-proton transfer processes and $\alpha$-cluster transfer [37].

2) In the system under consideration, there are two nearby resonances with angular momenta $18^+$ and $12^+$. The first one is most intense in the elastic channel, while the intensity of the second one is small there, but it becomes prominent in the $^{10}$Be+$^{16}$O channel.

To evaluate the contribution of direct processes, the transmission reactions were calculated within the DWBA model. Two direct reaction channels available in the one-step approximation were considered. Their graphical representation is given in Figure 42.

The core-products are identical but rearranged so that the channels in question dominate at different angular ranges of the $^{14}$C($^{12}$C,$^{10}$Be)$^{16}$Oreaction. The two-proton disruption is maximized in the anterior hemisphere, and the transmission of the $\alpha$-cluster defines the region of larger angles. The intermediate angles are thus formed by the interference of these two processes and from the formula (83) for the differential cross section of the $^{14}$C($^{12}$C,$^{10}$Be)$^{16}$Oreaction can be written:

$$\frac{d\sigma}{d\Omega} \sim \left| f_{2p}\left(\theta, S_{2p}\right) + f_{\alpha}\left(\pi - \theta, S_{\alpha}\right) \right|^2, \tag{72}$$

where $f_i$ – reaction amplitudes, $i = 2p$ – two-proton disruption, $i = \alpha$ – $\alpha$-cluster pickup, $S_{2p,\alpha}$ – coefficients determining the magnitude of the contribution of each mechanism and equal to the product of the corresponding spectroscopic amplitudes. The case of the influence of this mechanism on elastic scattering will be considered below.

The calculation of the response $^{14}$C($^{12}$C,$^{10}$Be)$^{16}$O and the analysis of channel contributions were performed within the DWBA model of the FRESCO [161] pro-

gram, taking into account the cluster approximation to describe the transmission process. The optical potential found from the analysis of the elastic scattering data $^{14}$C + $^{12}$C obtained by us in this study and from comparison with experimental data from the [173] paper was used as the input channel potential. The parameters of the potential used, of the Woods-Saxon type with bulk and surface absorptions, are fixed in energy and equal to:
$V_0 = 135.003$ MeV, $r_0 = 1.200$ fm, $a_0 = 0.440$ fm,
$W_0 = 29.841$ MeV, $r_W = 1.352$ fm, $a_W = 0.114$ fm,
$W_{d0} = 1.699$ MeV, $r_{Wd} = 1.518$ fm, $a_{Wd} = 0.107$ fm.
For all potentials used in this work, the Coulomb radius parameter was chosen to be $r_C = 1.25$ fm, and the radii, as above, are determined by the expression: $R_i = r_i \left( A_t^{1/3} + A_p^{1/3} \right)$. Nevertheless, it should be noted that the use of a simple non-volatile model of the input channel potential can only be considered as a first approximation, since a more correct description of the elastic scattering of $^{14}$C + $^{12}$C requires the elastic transmission of two neutrons to be taken into account. The importance of such a mechanism for scattering is shown, for example, in [190].

Due to the lack of potential parameterization or elastic scattering data for the $^{10}$Be+$^{16}$O output channel, a modified energy-dependent optical potential with bulk absorption for $^{9}$Be+$^{16}$O [191] was used. Its parameters are summarized in Table 12.

.

Table 12. Optical potential parameters $^{10}$Be + $^{16}$O [39].

| $E_{\text{cm.}}$, MeV | 22.1 | 23.5 | 24.6 |
|---|---|---|---|
| $V_0$, MeV | 134.000 | 138.665 | 142.554 |
| $r_0$, fm | 0.964 | 0.940 | 0.925 |
| $a_0$, fm | 0.694 | 0.707 | 0.716 |
| $W_0$, MeV | 11.500 | 11.744 | 11.939 |
| $r_W$, fm | 1.301 | 1.291 | 1.282 |
| $a_W$, fm | 0.694 | 0.707 | 0.716 |

The spectroscopic amplitudes were free parameters of the calculation. From the analysis of the angular distributions, it was obtained that the spectroscopic amplitudes are practically independent of energy and are for $\langle ^{12}\text{C}|^{10}\text{Be}\rangle_{g.s.}$ and $\langle ^{16}\text{O}|^{14}\text{C}\rangle_{g.s.}$ 0.380 ($2p$ breakdown), and for $\langle ^{14}\text{C}|^{10}\text{Be}\rangle_{g.s.}$ and $\langle ^{16}\text{O}|^{12}\text{C}\rangle_{g.s.}$ 0.618

($\alpha$-cluster pickup), as shown in Tables 13, 14, 15, 16, 17.

Table 13. Theoretical spectroscopic amplitudes and quantum numbers of the $\alpha$-cluster [39].

| overlap | $NLj$ $\alpha$-cluster | $A$ |
|---|---|---|
| $\langle^{14}\mathrm{C}\vert^{10}\mathrm{Be}\rangle_{g.s.}$ | $3S_0$ | -0.566 [192] |
| $\langle^{16}\mathrm{O}\vert^{12}\mathrm{C}\rangle_{g.s.}$ | $3S_0$ | 0.544 [193] |

Table 14. Theoretical spectroscopic amplitudes for the two-proton transfer reaction [39].

| overlap | $\left(1p_{\frac{3}{2}}\right)^2$ | $\left(1p_{\frac{1}{2}}\right)^2$ | $2S_0$ [192] |
|---|---|---|---|
| $\langle^{12}\mathrm{C}\vert^{10}\mathrm{Be}\rangle_{g.s.}$ | 0.770 | 0.544 | 0.800 |
| $\langle^{16}\mathrm{O}\vert^{14}\mathrm{C}\rangle_{g.s.}$ | -0.817 | -0.577 | |

Table 15. Spectroscopic amplitudes obtained from the analysis of the $^{14}$C($^{12}$C,$^{10}$Be)$^{16}$O reaction at 41.5 MeV [39].

| overlap | $A$ | overlap | $A$ |
|---|---|---|---|
| $\langle^{14}\mathrm{C}\vert^{10}\mathrm{Be}\rangle$ | 0.618 | $\langle^{12}\mathrm{C}\vert^{10}\mathrm{Be}\rangle$ | 0.374 |
| $\langle^{16}\mathrm{O}\vert^{12}\mathrm{C}\rangle$ | 0.618 | $\langle^{16}\mathrm{O}\vert^{14}\mathrm{C}\rangle$ | 0.374 |

As can be seen from Figure 43, in the angular range of the experimental data obtained, the main contribution is given by the two-proton transfer reaction, and the influence of the $\alpha$-cluster transfer channel is manifested approximately starting from an angle of 60°. Thus, the transmission of the heavy cluster is not, in this case, the cause of the resonance-like structure. Nevertheless, the importance of the contribution from $\alpha$-cluster configurations to the structure of the $^{14}$C+$^{12}$C nuclei formed in the $^{14}$C reaction should be noted, since the relative channel yields for different excitation energies of the $^{18}$O residual nucleus show a suppression of states with the $4p$-$2h$ configuration at 24.6 MeV compared to others.

Figure 44 shows a comparison of the experimental distributions with the DWBA calculation results. A comparison of the experimental data for the reaction $^{14}$C($^{12}$C,$^{10}$Be)$^{16}$O for the case of interference of the two channels considered is presented. As discussed earlier, when considering the elastic transmission response for $^{12}$C+$^{16}$O scattering, the best agreement with the calculation results occurs when we are not at the resonance point. At energy $E_{cm}$ =23.5 MeV, the value of

Table 16. Spectroscopic amplitudes obtained from the analysis of the $^{14}$C($^{12}$C,$^{10}$Be)$^{16}$O reaction at 44 MeV [39].

| overlap | $A$ | overlap | $A$ |
|---|---|---|---|
| $\langle^{14}\mathrm{C}\vert^{10}\mathrm{Be}\rangle$ | 0.618 | $\langle^{12}\mathrm{C}\vert^{10}\mathrm{Be}\rangle$ | 0.391 |
| $\langle^{16}\mathrm{O}\vert^{12}\mathrm{C}\rangle$ | 0.618 | $\langle^{16}\mathrm{O}\vert^{14}\mathrm{C}\rangle$ | 0.391 |

Table 17. Spectroscopic amplitudes obtained from the analysis of the $^{14}$C($^{12}$C,$^{10}$Be)$^{16}$O reaction at 46 MeV [39].

| overlap | $A$ | overlap | $A$ |
|---|---|---|---|
| $\langle^{14}\mathrm{C}\vert^{10}\mathrm{Be}\rangle$ | 0.618 | $\langle^{12}\mathrm{C}\vert^{10}\mathrm{Be}\rangle$ | 0.375 |
| $\langle^{16}\mathrm{O}\vert^{12}\mathrm{C}\rangle$ | 0.618 | $\langle^{16}\mathrm{O}\vert^{14}\mathrm{C}\rangle$ | 0.375 |

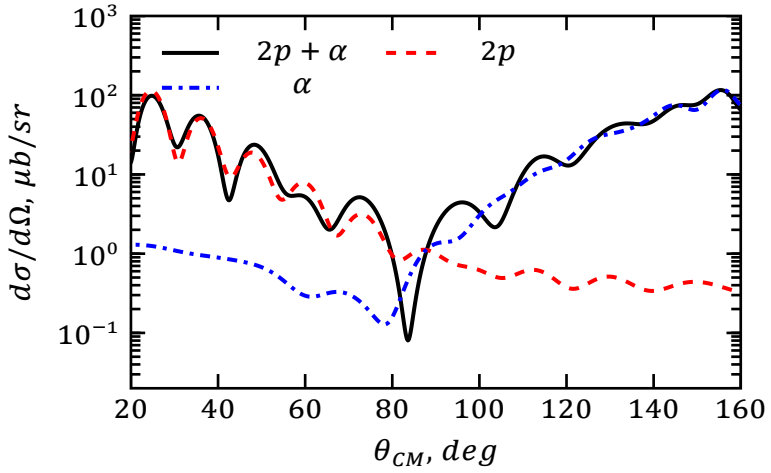


Figure 43. The contributions of the two-proton transmission channels (red dashed line), the $\alpha$-cluster (blue dashed line), and their interference (black solid line) for energy E$_{cm}$ =22.1 MeV [37].

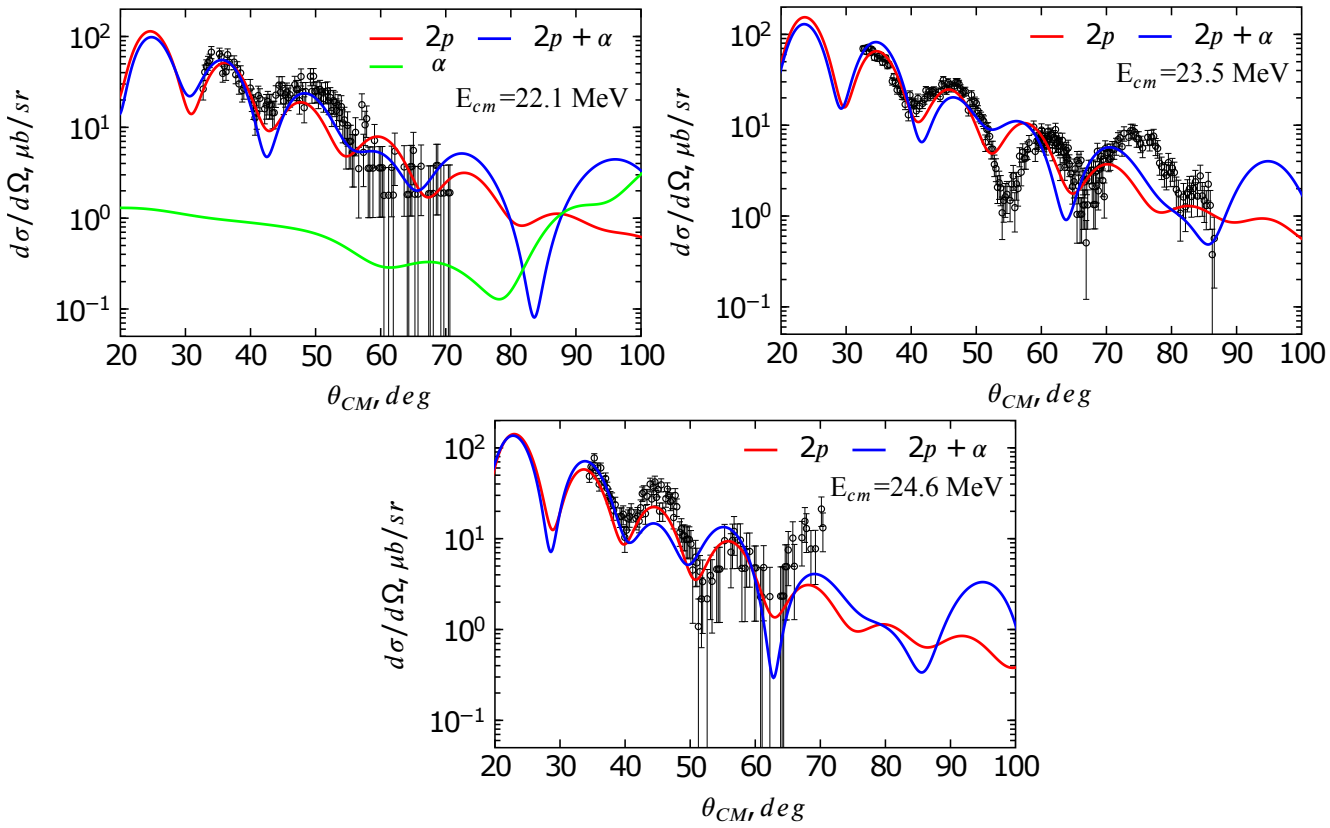


Figure 44. The angular distributions obtained in this paper [37].

$\chi^2$ increases by an order of magnitude, which may indicate the inclusion of other reaction mechanisms, including resonance ones.

In general, as can be seen, there is a good agreement between the calculations and the experimental data. Nevertheless, it should be noted that the obtained integral cross section poorly reproduces the experimental excitation function, predicting a smooth growth of the cross section with energy.

Thus, the results obtained indicate a good description of the angular distribution within the DWBA model at the nonresonant energies $E_{cm}$ =22.1 and 24.6 MeV and, to a first approximation, reproduce the general regularities of the angular dependence at the resonant energy $E_{cm}$ =23.5 MeV. This indicates the applicability of DWBA as a method for describing the nonresonant background in this reaction. The differences appearing in the resonance region may be the result of the existence of an additional $12^+$ resonance weakly manifested in the elastic channel.

Considering that the studied resonance-like structure at energy $E_{cm}$=23. 5 MeV is observed, as mentioned above, in several output channels at once (including those with excited states) we can conclude that there is a complex quasi-

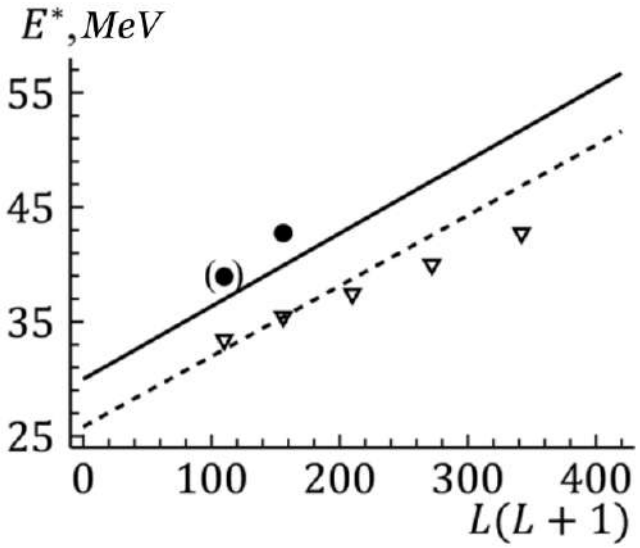


Figure 45. Comparison of the dependence of excitation energy on angular momentum for the system $^{14}$C+$^{12}$C (dashed line) and $^{16}$O+$^{10}$Be (solid line) based on the systematics of the [105] paper. Experimental data are given [38]: triangles – for the reaction $^{14}$C+$^{12}$C from the work [105], dots – the present work. The predicted state $10^+$ is enclosed in brackets.

molecular structure of the compound-core $^{26}$Mg, similar to the detected mixing of configurations $|^{8}\text{Be}\otimes^{16}\text{O}\rangle$ and $|^{12}\text{C}\otimes^{12}\text{C}\rangle$ in the study of decays of high-lying resonances in $^{24}$Mg [194]. A similar situation is observed in the case of the study of the $^{12}$C($^{16}$O,$^{8}$Be)$^{20}$Ne [195] reaction, indicating the importance of the effects discussed at the beginning of this chapter for light nuclei as well. The results also indicate the occurrence of resonance processes in the case of neutron-depleted nuclei, but do not allow us to unambiguously confirm the resonance nature of the case under consideration.

For a better understanding of the nature of the emerging structure, the angular distribution of other channels showing signs of resonance should be studied. Also, from this point of view, it is of interest to study the reaction $^{14}$C($^{12}$C,$^{10}$Be)$^{16}$O in the region of energy $E_{cm}$ =19.7 MeV, where a structure similar to the one considered by us is observed. If the quasi-molecularity hypothesis is confirmed, this point may correspond to a resonance with an angular momentum of $10^+$. This is shown in Figure 45, where a comparison of the results obtained with the systematics is made.

Let us consider the possibility of applying the potential model to our result. Table 18 gives examples of $WS^2$ potential parameters for various combinations of nuclei forming molecular resonances (the case of $^{12}$C+$^{16}$O will be considered

separately). For each potential, the value of the volume integral is given:

$$J_V = \frac{4\pi}{A_1 A_2} \int V(r) r^2 dr. \tag{73}$$

.

Table 18. Examples of potential parameters for reactions with heavy ions obtained in this work.

| | $V_0$ MeV | $R$ fm. | $a$ fm. | $J$ MeV·fm$^3$ |
|---|---|---|---|---|
| $^{12}$C+$^{12}$C | 294 | 3.84 | 1.3 | 367 |
| $^{12}$C+$^{12}$C | 313 | 3.66 | 1.6 | 379 |
| $^{16}$O+$^{16}$O | 413 | 3.97 | 1.46 | 330 |
| $^{16}$O+$^{16}$O | 362 | 3.92 | 1.56 | 288 |
| $^{16}$O+$^{20}$Ne | 241.5 | 4.5 | 1.59 | 221 |
| $^{10}$Be+$^{16}$O | 331.8 | 3.77 | 0.95 | 320 |

In this case, the excitation energy of the $10^+$ state is $E$=14.84 MeV with a width of $\Gamma$=0.508 MeV, and for $12^+$ the energy is $E$=18.66 MeV, with a width of $\Gamma$=0.356 MeV, which is close to the experimental results.

Magnesium isotopes are not "good" representatives of exactly $\alpha$-cluster nuclei, although the very manifestation of clustering is quite strong in them. Our experimental results on this issue will be presented below in the discussion of heavy cluster interactions.

From the point of view of theory, the best approach to describing the cluster structure of this nucleus is precisely the calculations based on the liquid drop method with the Nilsson-Strutinsky corrections [181, 196, 197] to obtain the corresponding energy surface. The $^{24}$Mg nucleus was one of the first to be studied in detail within this model, resulting in the discovery of several minima corresponding to cluster degrees of freedom. The connection between deformed-shell and clustering calculations was well demonstrated in [83,198], where a comparison between the results of the liquid drop model and the pure Brink-Bloch cluster approach was made for the $^{24}$Mg nucleus [5,199]. A comparison of these results with the predictions of the maximal $\alpha$-particle model has been presented in Table 2.

It is the $^{24}$Mg nucleus that has been particularly scrutinized for the detection of chain configurations, bearing a pronounced $\alpha$-cluster [200] character. Nevertheless, the main discussion of cluster degrees of freedom in this nucleus is centered

mainly in the field of molecular resonances associated with heavy ions (such as $^{12}$C+$^{12}$C). This issue will be discussed later in the paper.

In order to investigate cluster and high-spin states in this nucleus, the already mentioned reactions leading to the active population of cluster states have been studied. For example, despite the difficulties of using a $^{20}$Ne gas target, the reactions ($^6$Li,$d$) and ($^7$Li,$t$) [201, 202] were studied. More successful work has been done with the reactions $^{12}$C($^{16}$O,$\alpha$) or $^{16}$O($^{12}$C,$\alpha$) [203–205]. In particular, it has been shown:

1) Existence of levels with sufficiently high settlement efficiency.

2) The existence of high-spin states (with spins $8^+$,$9^-$), which can be considered as a manifestation of rotational bands [205].

In [202], the $^{26}$Mg states in the $^{22}$Ne($^6$Li,$d$) reaction were also investigated.

Despite the limited information it is possible to compare the predictions of the potential model with the obtained result. For the $^{24}$Mg nucleus, the level data were taken from [155, 205], and for $^{26}$Mg, the states forming the yrast line from the [155] data were selected. As suggested in [202], the constraint on the number of nodes from the formula (23) was chosen as $2N + L$=8. The value of the radii was taken from fitting to the experimental data:

$^{24}$Mg - $R$=3.2 fm.

$^{26}$Mg - $R$=3.22 fm.

The results are shown in Figure 46. The obtained result can only be evaluated qualitatively because, due to the rather large detachment energy of the $\alpha$-particle, most of the positive parity levels are located under the threshold, and due to the large splitting, even the low-spin levels are poorly defined and poorly investigated. In particular, for the negative parity states in the $^{24}$Mg nucleus, the closest set of levels with a suitable angular momentum has been used, thus perhaps these states do not belong to the $K^\pi$=$0^-$ band. Thus, in the paper [205] another variant of the states $3^-$, $5^-$ and $8^+$ was proposed.

Using the example of the $^{26}$Mg nucleus, it has been shown that Buck's hypothesis about the possibility of the manifestation of several cluster states in a nucleus also holds for such light nuclei. Even such a nucleus with a complex internal structure as $^{10}$Be (see Figure 24) can be a cluster for the rotational band.

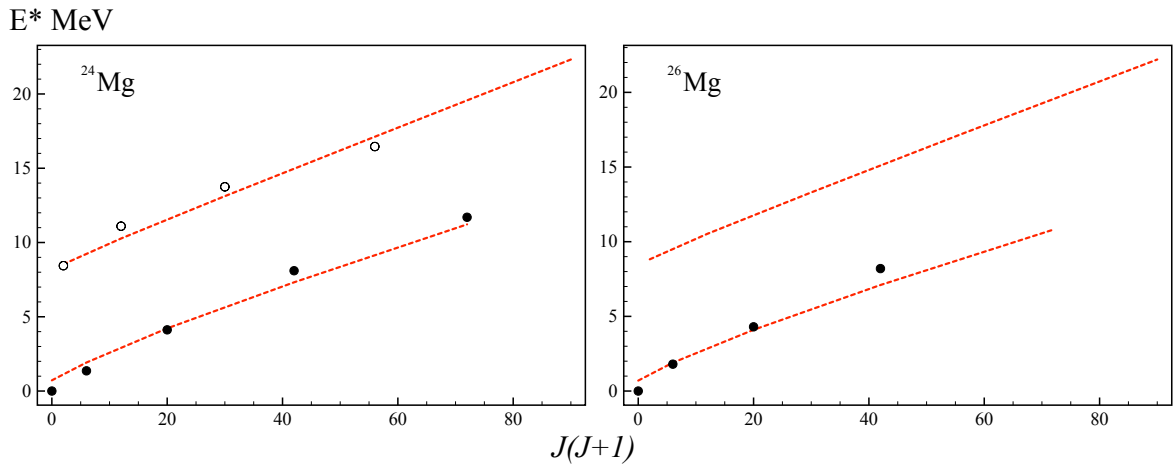


Figure 46. Comparison of potential model predictions for $^{24}$Mg and $^{26}$Mg nuclei [155]. Dark and light circles – states with positive and negative parity, respectively.

## 3.7. Silicon and Sulfur

Silicon and sulfur nuclei do not seem to have low-lying bands with good cluster structure, but these nuclei play an important role in the use of heavy nuclei ($^{12}$C+$^{16}$O and $^{16}$O+$^{16}$O) as clusters, which will be discussed below. Also, when considering the high-lying $\alpha$-cluster states. In contrast to heavier nuclei (with the exception of argon, discussed below), these nuclei have been well studied in resonance scattering of $\alpha$-particles, mostly in inverse geometry with a thick target.

As shown by the performed experiment [206], the high-lying states form well-defined fragmented bands. Within the potential model approach, it is difficult to describe such parity-unfragmented bands. The case of sulfur will be discussed separately in the next paragraph. One could assume that, within the infinite barrier tunneling model, a band is formed in which $\alpha$-particles populate high-lying orbitals. One can only estimate the moment of inertia for such systems, given that the moments of inertia of positive and negative parity bands are approximately the same.

## 3.8. Argon

Like the previous two nuclei, $\alpha$-cluster degrees of freedom are relatively poorly understood for the $^{36}$Ar nucleus. Nevertheless, from the available evidence it can be concluded that this nucleus has rotational bands that can be identified as $\alpha$-cluster bands. And, in addition, a large number of fragmented cluster states are

present.

The first work to study such states was the $\alpha$-particle ($^6$Li,$d$) [207] transmission experiments. Similarly to other self-coupled nuclei, a number of states populated with increased intensity were found in this reaction. The states corresponding to the ground state band, $0^+$ – ground state, $2^+$ – 1.97 MeV, and $4^+$ – 4.41 MeV were weakly populated.

In [207], attention was drawn to the existence of intensely populated levels whose spins had not been determined at that time – 4.95, 6.14, 7.8, 9.9 MeV. The study of the $^{36}$Ar nucleus in $\gamma$-spectroscopy experiments allowed us not only to assign spin to these states, but also to find out that they belong to the band $K^\pi$=$0^+$ (4.33 MeV), which has a sufficiently large moment of inertia and extends to values of $18^+$, which, for this nucleus, is a very high angular momentum. At the same time, the active population of initial states may indicate the importance of the $\alpha$-cluster degree of freedom for all states of this band.

On the other hand, a significant deficit of states with negative parity, which would not be "one-particle" in nature, draws attention. Thus, the observed states $3^-$ 4.18 MeV, $2^-$ 4.97 MeV, and $5^-$ 5.17 MeV, when compared with the results of the reaction $^{35}$Cl($\tau$,d), show their belonging to the $(d_{3/2})^3_{3/2}f^{7/2}$ multiplet, while the states $1^-$ 5. 84 MeV, $3^-$ 6.84 MeV belong to the $(d_{3/2})^3_{3/2}p_{3/2}$ multiplet. While two such $1^-$ states with energies of 9.12 and 10.65 MeV are populated with sufficient efficiency in both the transfer reaction and the ($^{32}$S,$\gamma$) reaction, which may be a sign of the onset of fragmented states.

To obtain information on the high-lying fragmented cluster states, we performed an elastic scattering experiment of $\alpha$-particles on $^{32}$S [66] nuclei. The experiment was performed using the inverse geometry method with a thick target [208]. As a result, 44 new levels with angular momenta from 0 to 6 and located in the excitation energy range from 12 to 16 MeV were identified as active in this reaction. Figure 47 presents a compilation of the data on $\alpha$-cluster levels for comparison with the potential model predictions.

As can be seen, for radius $R$=4.1 fm, there is a good agreement with the data obtained in the transfer reactions and by $\gamma$ spectrometry, but the fragmented states detected in the experiment lie too high, except for the $5^-$ 12.2 MeV level.

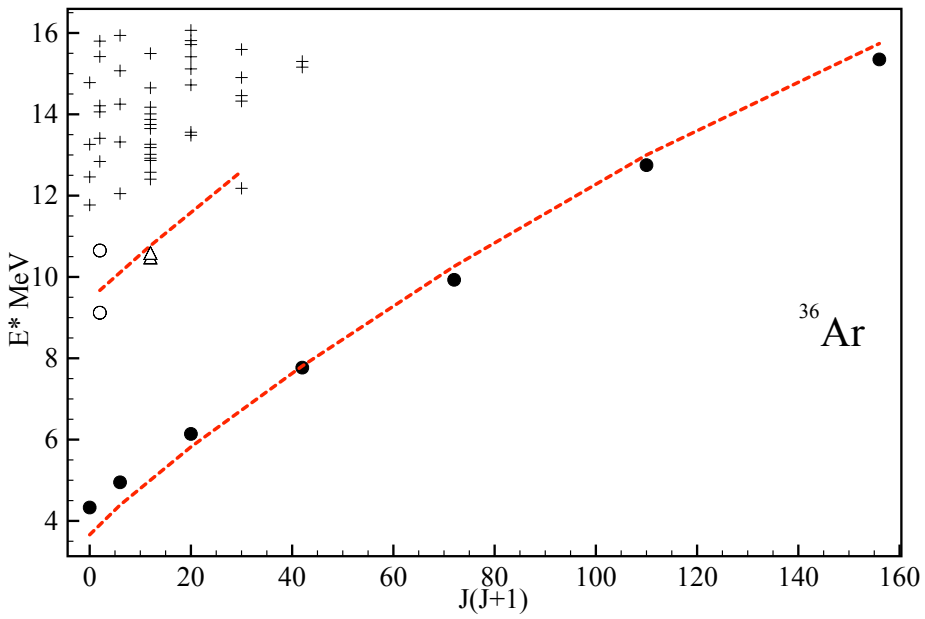


Figure 47. States in the $^{36}$Ar nucleus having cluster character. Black dots – states with positive parity obtained from experiments with transfer reactions and $\gamma$-spectroscopy. Light dots – $1^-$ states that are actively populated in transfer reactions. Triangles – low-lying $3^-$ states from the $\alpha$-particle capture reaction [155]. Crosses – data from our elastic scattering experiment [66].

This level, which has a small width (5 keV) and a large reduced width compared to the other states, was also observed in the transmission reaction in the work [208]. Also shown in the Figure are the $1^-$ levels discussed above that are actively populated in the transmission reaction and the low-lying $3^-$ doublet found in the $^{32}$S$(\alpha,\gamma)$ [155] reaction. However, it is not clear from the results whether these levels are the beginning of a fragmented band.

## 3.9. Calcium

Although we have pointed out a number of cluster properties of the $^{36}$ Ar nucleus, it is the $^{40}$Ca nucleus that turns out to be particularly important in terms of cluster degrees of freedom, now in intermediate nuclei. Since this nucleus is twice magic (the last nucleus of this type of stable self-conjugated nuclei), we should expect the clusters to populate the new $fp$ shell. This approach allowed us to draw an analogy with the well-known cluster nuclei we considered earlier.

$^{16}$O$\Longrightarrow{}^{40}$Ca

$^{20}$Ne$\Longrightarrow{}^{44}$Ti.

Thus, by analogy with the cluster states of $^{16}$O and its isotopes, we might expect cluster states in $^{40}$Ca. Indeed, a number of theoretical studies have pre-

dicted the existence of states characterized by the $4p-4h$ and $8p-8h$ structure. We have performed an experimental study of the levels of $^{40}$Ca and $^{42}$Ca nuclei, which allowed us to detect the predicted states and the bands appearing based on them. The experimental apparatus and procedure have been fairly fully described in [209], and the results obtained are reported in [63].

Let us consider the application of the two models described in Chapter 1 to the case of a rotational doublet in the $^{40}$Ca [63] nucleus. Positive and negative parity states distributed in good agreement with the law $E_{ex} \sim J(J+1)$, where $E_{ex}$ is the energy of the excited level, reach a sufficiently high (for a nucleus of such mass) value of angular momentum. According to [210, 211], the positive parity band based on the $0^+$ state, with energy 3.35 MeV, has a $4p-4h$ structure, which is confirmed by the high probability of its population in $\alpha$-particle transfer reactions. The negative parity band has a moment of inertia close in value to the moment of inertia of the $4p-4h$ band, and its low-lying states are also rather actively populated in $\alpha$-transfer [212] reactions.

More complex tunneling models for octupole strain [213,214] include a parameterization of the barrier between the two configurations describing the decrease in the magnitude of the splitting with increasing angular momentum. In [215], the equation describing the potential entering the Hamiltonian of octupole oscillations contains as parameters the moment of inertia and the octupole deformation of the $\beta$ nucleus, is of the form:

$$U_J(\beta) = \frac{J(J+1)d_2^2(\beta^2-\beta_{min}^2)^2}{2(d_1+d_2\beta_{min}^2)^2(d_1+d_2\beta^2)}. \quad (74)$$

Here $d_{1,2}$ are the parameters determining the moment of inertia, $\beta_{min}$ is the equilibrium octupole deformation parameter. The data obtained in this work for $^{224}$Ra, $^{226}$Ra, $^{224}$Th, $^{226}$Th nuclei allow us to make an estimate of the potential for the deformed $^{40}$Ca nucleus [64]. The value corresponding to the moment of inertia is defined in the paper [215] as $\Theta(\beta) = d_1+d_2\beta^2$. Moreover, the average value of the deformation parameter $d_1$ for the range of nuclear masses considered in [215] is of the order of 0.045 MeV$^{-1}$, and for $d_2$ – of the order of 0.155 MeV$^{-1}$. Considering that, by analogy with the moment of inertia of a solid, both coefficients are proportional to $A^{5/3}$, for the case of the $^{40}$Ca nucleus we obtain, respectively,

$d_1$ ∼0.0025 MeV$^{-1}$, $d_2$ ∼0.0087 MeV$^{-1}$. On the other hand, we can assume that the octupole deformation parameter will be only slightly larger than that found in [215], since the cluster/cor mass ratio for the above heavy nuclei is of the order of the ratio $\alpha$-particle/$^{36}$Ar, viz. i.e., $\beta_{min}$ ∼0.2. Another parameter necessary for the calculation of the band splitting is the effective mass parameter $B_3$ included in the Hamiltonian [216]:

$$H_{osc}^{oct} = \frac{\hbar^2}{2B_3}\frac{d^2}{d\beta^2} + U_J(\beta). \tag{75}$$

As is obvious, this parameter is a function of mass. For the static octupole deformation for the moment of inertia, we can obtain that $\Theta$=$6B_3\beta^2$ [217]. For the simplest kind of dual-core system $\alpha\otimes^{36}$Ar, the moment of inertia parameter $\hbar^2/2\Theta$ is a value on the order of 81 keV [63]. Thus, for our estimate of the octupole deformation, we can, as a first approximation, obtain $B_3 \approx 25\hbar^2$ MeV$^{-1}$.

Let us choose the found parameters as a first approximation for fitting by the expression (74) the experimental data obtained by us [63]. To calculate the energy of octupole oscillations, an expression was proposed in [215]:

$$E_{osc}(J) = E_0 - \frac{1}{2}(-1)^J \delta E(J), \tag{76}$$

where $\delta E(J) = E_J^- - E_J^+$ is the energy difference between the negative and positive parity states, and $E_0$ is a constant. This approach allows us to remove the non-rotational part from the expression. Since in the experiment we observe only states with natural parity, to determine the value corresponding to the parity splitting we write:

$$\delta E(J) = \frac{1}{2}\left[E(J+1) - 2E(J) + E(J-1) - \right. \\ \left. \frac{1}{4}(E(J+2) - 2E(J) + E(J-2))\right]. \tag{77}$$

For the case when $J$=1 the formula (77) is written as $\delta E(1) = E(1) - 0.5(E(0) + E(2))$, which is the first approximation.

The theoretical prediction for the energies $E_J^-$ and $E_J^+$ was obtained by numerically solving the Schrödinger equation with the Hamiltonian from the ex-

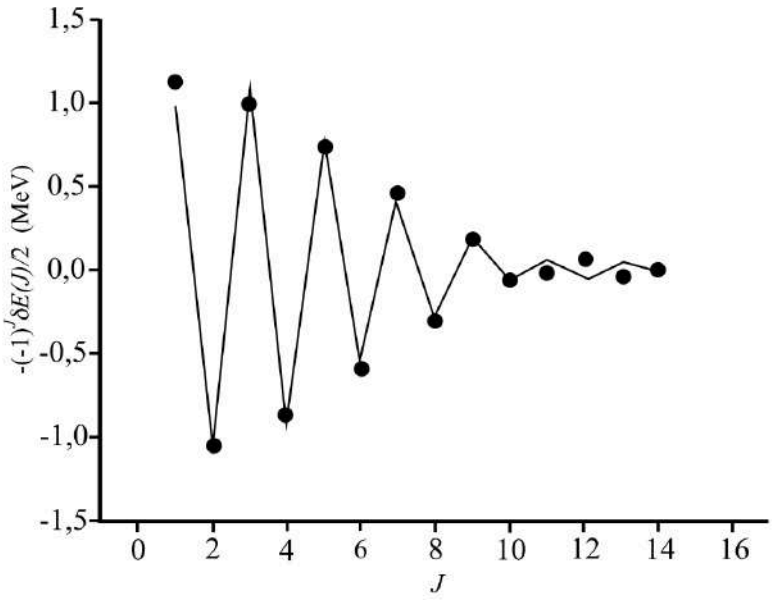


Figure 48. Comparing the experimental parity dependence of the rotational band splitting in the $^{40}$Ca nucleus with the theoretical prediction [64, 65].

pression (75) and the potential $U_J(\beta)$ (formula (74)). The result is shown in Figure 48.

Note that in this case the limit on the number of nodes from the formula (23) is $2N + L$=12, while the Figure 48 shows all states of the observed doublet. Since the splitting for large values of angular momentum is small, only the Hamiltonian (75) was used in the fit; however, assuming a band structure more complex than $2N + L \geq$12, where the allowed angular momentum may exceed the value $J$=12, the quadrupole-octupole rotational model [218] may need to be taken into account to describe the splitting at large values of angular momentum. As can be seen, there is good agreement between the theoretical and experimental values of the splitting. The parameters found, with the exception of $d_2$, deviate slightly from the expected values. The obtained value of the octupole strain also agrees well with the estimate that can be obtained from the analysis of the reduced transition probability between states $2^+ \to 0^+$, which is $B(E2)$=30±4 W.U. [219]. From the approximation for the transition probability:

$$B(E2; 2^+ \to 0^+) = \left(\frac{3}{4\pi} eZR^2\right)^2 \beta_2^2, \tag{78}$$

follows from the value of $\beta_2$ =-0.16 if we take the value of the parameter $r_0$ in determining the radius to be 1.2 fm.

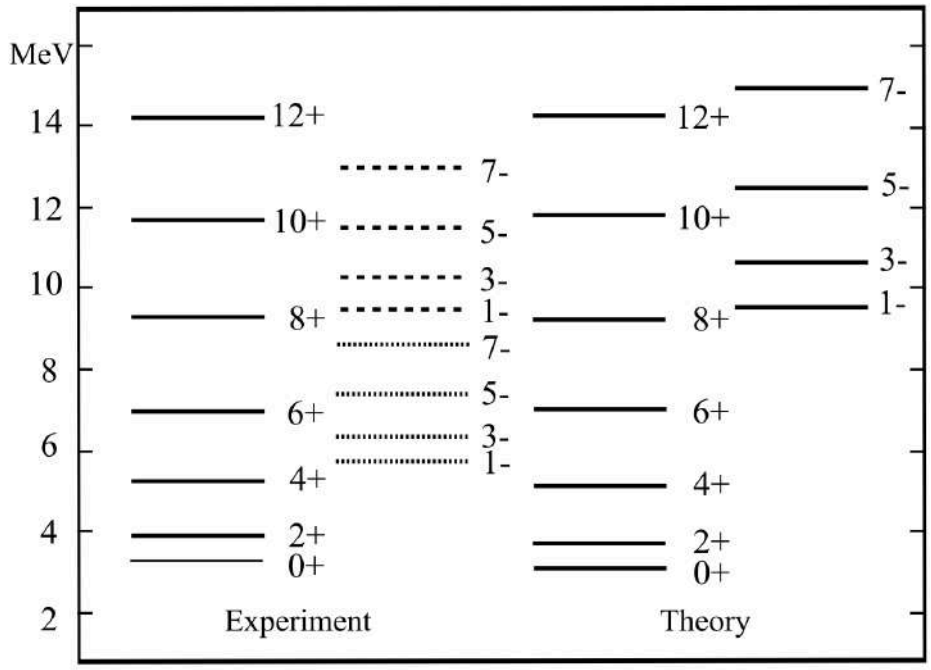


Figure 49. Comparison of experimental and theoretical results for positive and negative parity bands in the $^{40}$Ca nucleus [64, 65]. See text for explanations.

Now let us consider the second variant of the description of the parity-split states in the framework of the potential model using the $WS + WS^3$ potential, formula (27). As mentioned above, this potential has been successfully applied not only to heavy nuclei [220, 221], but also to the above $\alpha$-cluster bands in light nuclei. In [76], it was also used to successfully characterize the states in the $^{44}$Ti nucleus. The parameters $a$=0.73 fm. and $x$=0.33 coincide with the previously chosen parameters for oxygen and neon nuclei. The form factor was normalized by its value at zero radius. The depth of the potential was chosen as $V = -54.0 \cdot A_1 A_2/A$, where $A_{1,2}$ are the mass numbers of the core and cluster, and $A$= 40.

Applying this potential one finds that the band with positive parity in the $^{40}$Ca nucleus is described much better than when the cosh-type potential [219] is applied. Figure 49 shows the results of calculations for the energies of the rotational band levels with positive and negative parity, and Table 19 summarizes the values of $B(E2)$ for the known transitions in comparison with theoretical data obtained by us as well as with results from the work [219]. The value $R$=4.15 fm was chosen as the radius of $^{40}$Ca.

The transition probabilities were calculated using the semiclassical model [222], taking into account the effective charge, the replacement $Z = Z + \epsilon A$

and the factor $\epsilon$= 0.25 [109]. Such good agreement is achieved only under the assumption of population of the $fp$ shell, which corresponds to $2N + L$=12.

Table 19. Comparison of transition intensities in the $^{40}$Ca nucleus for different types of potential [64, 65].

| Transition | Intensity (W.u.) | $WS + WS^3$ (W.u.) | Deep *cosh* (W.u.) [219] | Shallow *cosh* (W.u.) [219] |
|---|---|---|---|---|
| 2→ 0 | 30±4 | 29.7 | 5.7 | 27.0 |
| 4→ 2 | 59±6 | 40.3 | 7.3 | 37.0 |
| 6→ 4 | $16^{+8.8}_{-4.4}$ | 38.5 | 6.4 | 37.5 |
| 8→ 6 | | 31.2 | 4.8 | 34.1 |
| 10→ 8 | | 21.0 | 3.0 | 27.6 |
| 12→ 10 | | 9.9 | 1.3 | 17.2 |

In describing the positive parity bands for self-conjugated nuclei with mass number 36≥ $A$ ≥48, applying a similar potential, one can obtain a very good agreement with experiment for the positions of levels with positive parity, and the value of the radius of the nucleus used as a parameter will have a dependence on the mass:

$$R \approx 0.85(A_{core}^{1/3} + A_{clust}^{1/3}). \tag{79}$$

At the same time, as it was shown in [76], the above potential also describes high-lying negative parity bands found in some nuclei, which, except for the $^{20}$Ne nucleus, appear as a set of nearby levels with the same spin and are actively populated in $\alpha$-transfer reactions [223]. Taking into account that the calculation of the positions of the "weighted average" levels involves certain difficulties, we can give only approximate estimates of the lower bounds for their energies. These are the values indicated for the experimental values of the energies of states with negative parity (Figure 49, dashed line). For these values we used the totality of the data on $\alpha$-transfer reactions available to date [64, 65], so the energies of the levels in Figure 49 are slightly different from those given in the paper [223].

Thus, we are dealing with a set of rotational bands possessing $\alpha$-cluster structure, one with positive parity and two with negative parity. The positive parity band (having a $4p - 4h$ structure) is weakly split with the low-lying negative parity band, with the splitting exponentially decreasing with increasing angular

momentum [63] and is well described by theory. The high-lying band with negative parity appears fragmented and has a moment of inertia close to the moments of inertia of the other two bands. It should be noted that a similar low-lying band with negative parity is also found in the neighboring $^{40}$Ca nuclei ($^{44}$Ti and $^{48}$Cr). Although the absence of clearly distinguished states with low spins and the presence of a band with non-natural parity suggest that this is one band with $K \neq 0$. At the same time, another assumption is possible for the $^{40}$Ca nucleus [63].

This approach can be applied to describe nuclei far from the region of closed shells. Consider again the $^{32}$S nucleus. It is characterized by the absence of well separated $\alpha$-particle bands. By applying the $WS + WS^3$ potential and using the above expression to estimate the radius parameter, we can find that for the number $2N + L$=8 (the case of correlation in the $2s - 1d$ shell) the energy of the $0^+$ state is too low (much smaller than the binding energy). In the case of $2N + L$=12 ($1f - 2p$ shell), the $0^+$ level has an energy of about 7.2 MeV, $2^+$ – about 8 MeV, and $12^+$ lies higher than 22 MeV. Hence, it is possible that similar bands are present in this nucleus, but because of the need to populate a new shell, they are strongly suppressed. To date, we have very little information on both the states of the $^{32}$S nucleus excited at energies above 10 MeV and on the $\gamma$-transitions in the case of reactions with heavy ions [65].

As can be seen, the $WS+WS^3$ potential is well suited for describing states in nuclei having a more complex structure than $4p-0h$. This allows us to better understand the properties of the rotational bands, which, due to their multiparticle character, have too complicated and approximate description in the framework of the shell model [224].

In conclusion, however, it should be noted that, unlike the potential model, the tunneling model cannot be unambiguously accepted for a given nucleus. Similar to the $^{16}$O nucleus described above, there are works [225] pointing to a relatively small deformation of high-spin states having negative parity. As seen in our work [63], we have uncertainty with the choice of the $5^-$ state, and, in particular, the problem of interpreting some states with negative parity in this nucleus [226] has been pointed out. Despite the fact that in this effect of the work, the authors of the paper [225] pointed out a possible consistency with the results of the tunnel-

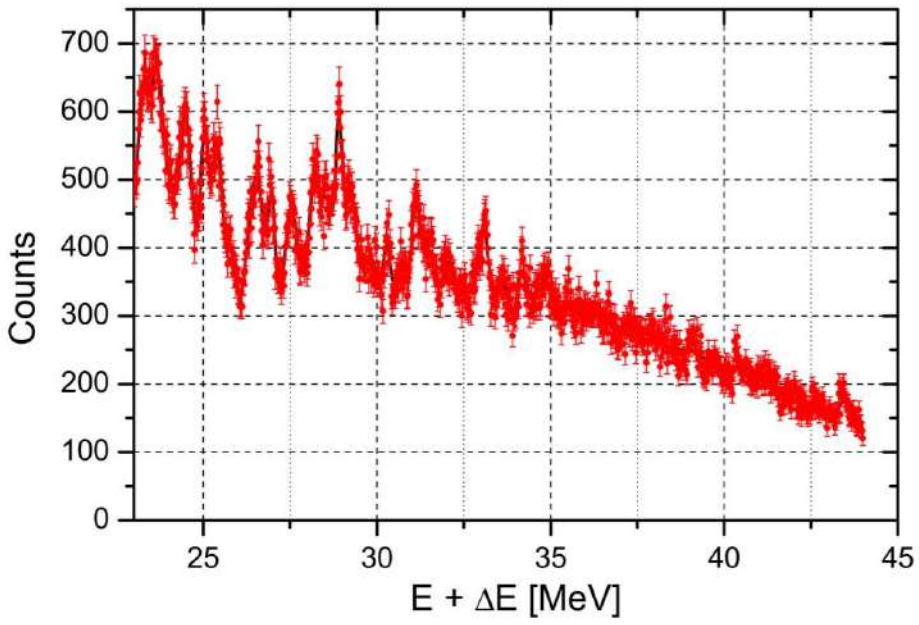


Figure 50. Excitation function obtained by scattering $^{40}$Ar on helium. The spectrum taken from the $\Delta E - E$ detector is shown [228].

ing model, it is nevertheless necessary to exercise some caution and assume that the tested cluster states with negative parity belong mainly to the fragmented band described above.

### 3.10. Heavy nuclei and clusters

An interesting question is the experimental study of analogous states for heavier clusters as well as neutron excess nuclei. Thus, to date, no sufficiently well-confirmed data on molecular resonances in systems heavier than $^{16}$O+$^{16}$O have been obtained. For example, rather controversial results [227] have been obtained [227] when studying the scattering of $^{16}$O+$^{40}$Ca.

Since in this problem we need to study the excitation function over a sufficiently wide interval, the best approach to the solution is to use the inverse kinematics and thick target method discussed in Chapter 1 and applied earlier in our study of $\alpha$-cluster states in the $^{36}$Ar [206, 228] nucleus.

The work was performed at the cyclotron at the University of Warsaw. We investigated elastic scattering reactions of $^{40}$Ar with energy 220 MeV on gas targets – $^{4}$He, $^{20}$Ne, and $CO_2$. A thick carbon target was also used. Excitation functions at 180° for the above targets were obtained. A large number of narrow resonances were found for the $^{40}$Ar+$\alpha$ excitation function. This indicates that the band of

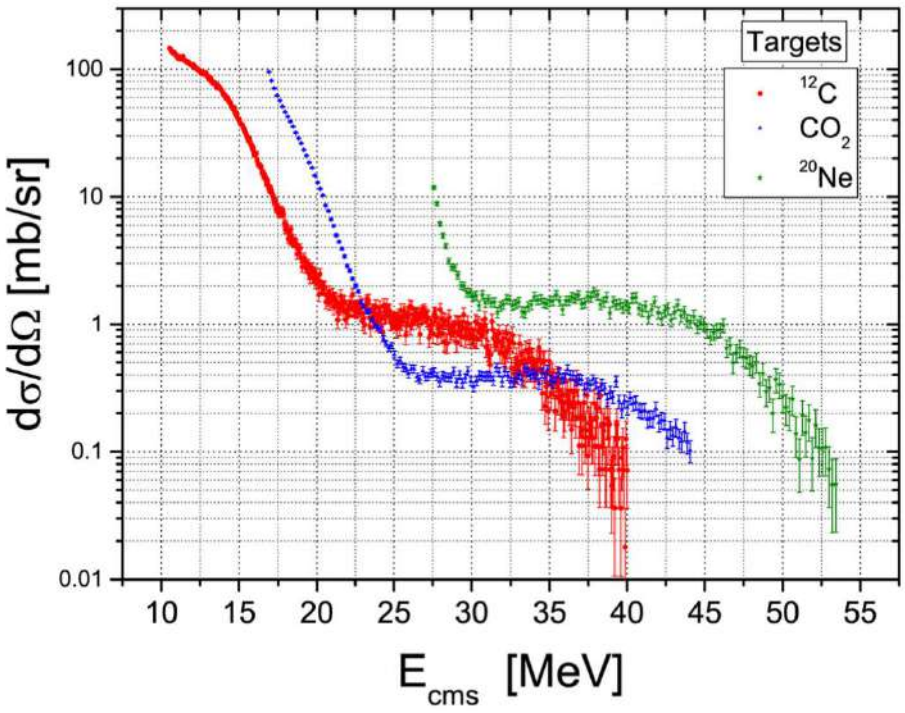


Figure 51. Excitation function obtained by scattering $^{40}$Ar on $^{12}$C, $CO_2$ and $^{20}$Ne [228].

fragmented states is also manifested in the $^{44}$Ca nucleus. The excitation function is shown in Figure 50.

At the same time, we did not obtain a resonance pattern for the case of heavier nuclei (see Figure 51). However, the results show a significant superiority of the yield of the target nuclei over their neighbors.

Thus, to date we have no reliable information on molecular resonances in systems corresponding to $fp$ shell nuclei and above. Given the great interest in such states, their importance, including for astrophysical studies, and the presence of encouraging theoretical predictions, the study of such structures should be continued.

As a conclusion, let us briefly review the situation of heavier nuclei not investigated in this paper. As discussed in the Introduction, one of the most common examples of the application of the potential model in describing $\alpha$-cluster degrees of freedom is the $^{44}$Ti nucleus. The population of the $\alpha$-particle $fp$ shell over a closed magic core leads to the appearance of well-defined rotational bands forming a split doublet. In this case, as indicated in the discussion of the bands in the $^{40}$Ca nucleus, we have a situation analogous to the neon nucleus.

Cluster levels in the $^{44}$Ti nucleus have been studied in the transmission re-

action [223] , elastic scattering of $\alpha$-particles [229], and by $\gamma$-spectrometry [230]. The latter study revealed the presence of several bands of complex structure in $^{44}$Ti. Similar to $^{40}$Ca, titanium does not have a "complete" low-lying negative band; the states observed in it begin at level $3^-$ – the lowest-lying level with negative parity, although the further behavior of the intensities of transitions between states is characteristic of the rotational band. Another important difference from the cluster levels discussed above is the poor fit to the $E^* \approx J(J+1)$ law. For the shell-filling $fp$-shell $\alpha$-particle from the Wildermuth (23) condition we have $2N + L \geq 12$, while the energy difference between $8^+$ and $10^+$ (1.162 MeV) is smaller than the difference between $8^+$ and $6^+$ (2.495 MeV) and this difference is quite small for the transition between $12^+$ and $10^+$ and is only 368 keV. In spite of this, in the $E^*$.vs.$J(J+1)$ plot, the position of the levels will be described by a smooth curve, in the two-particle approximation, corresponding to the growth of the moment of inertia.

The point is that from the point of view of the potential model the moment of inertia is unstable and can both decrease with increasing angular momentum and increase. The first process corresponds to "displacement" of the particle into the peripheral region due to the growing effective angular momentum potential. The second is due to the decreasing number of nodes. Figure 52 shows the change in the wave function with decreasing number of nodes. The presence of a strongly oscillating part in the overlap region (to exclude forbidden states), leads to the fact that when the number of nodes is small, the particle is closer to the nucleus. Thus, if the potential is narrow and deep, the first process is more effective, and for a wide potential the second process is more effective.

In his paper, Pilt [108] chose a narrow *cosh* potential which, although it described the behavior of the graph $E^*$.vs.$J(J+1)$, did not, as Okubo pointed out, combine with Wildermuth [107]'s condition. This error was corrected both in the above work by Okubo (for a potential of type $WS^2$) and by Pal and Lovas [219], who chose a broader potential *cosh*. However, all the above works predicted a quadratic energy growth between levels and described well only states with positive parity. Thus, the potential from [219] gives an estimate for the $1^-$ state of 9.5 MeV.

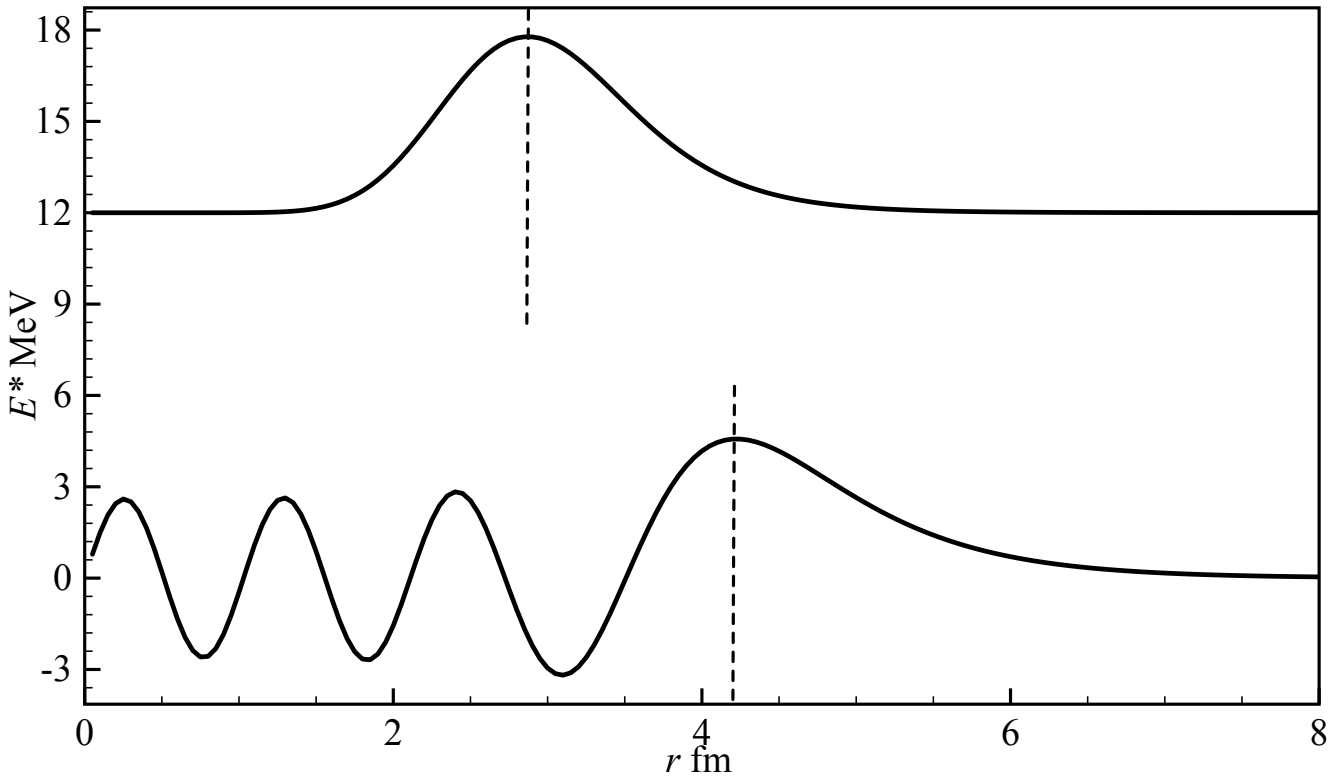


Figure 52. Shown are the wave functions of the ground state $0^+$ (bottom) and state $12^+$ (top) for the band with the condition $2N + L$ =12. The dotted line shows the most probable distance for the cluster-core system.

If we draw an analogy with the neon nucleus, we should observe a negative parity band with a potential that describes states with positive parity. Taking the $^{40}$Ca nucleus discussed above as an example, in the absence of a low-lying "tunneling" band, we should observe a band of fragmented states.

In the [76] paper, the first option was considered. Using the $WS + WS^3$ potential, positive parity states (band from $0^+$ to $8^+$) and low-lying negative parity states actively populated in the reactions $^{40}$Ca($^6$Li,$d$) and $^{40}$Ca($^{16}$O,$^{12}$C) - $1^-$ 6. 25 MeV, $3^-$ 7.37 MeV, and $5^-$ 9.46 MeV. For the radius value $R$=4.33 fm, we were also able to satisfactorily describe the widths and intensities of the known transitions. However, for the $10^+$ and $12^+$ states, the error in the positions of the levels was significant.

In [223], the potential model was applied to the same states with positive parity (also omitting high-spin states because of the large error), and the centers of fragmented states were chosen as the states for the negative parity band, as in [64, 65] – $1^-$ 7.16 MeV, $3^-$ 8.00 MeV, $5^-$ 9.5 MeV.

Summarizing the intermediate conclusion, it can be stated that in the region

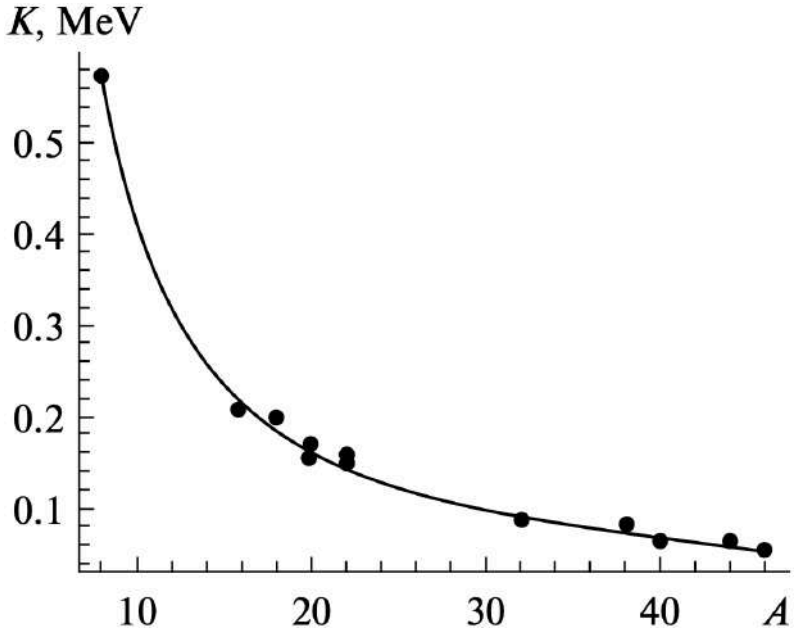


Figure 53. Dependence of the moment of inertia parameter on the mass number [61]. The dots indicate experimental data, the solid line is the fit by the formula (80).

of $fp$ shells the states having the $\alpha\otimes$Cor structure are no less widely represented than for the previous shells. Moreover, in the framework of the Merchant potential model, it was shown that such states also appear for non-self-conjugate nuclei [231].

As shown above, the application of the $WS + WS^3$ potential for $^{16,18,20}$O and $^{20,22}$Ne nuclei allowed a good description of the low-lying rotational bands. The correct value of the theoretically obtained moment of inertia shows that all considered states have a very large contribution of structure of the form $\alpha\otimes$cor. This remains true even for the $^{20}$O nucleus, where the value of the theoretical splitting is slightly larger than the experimental value. This picture suggests a more global manifestation of the cluster structure in nuclei of light and intermediate mass groups with neutron excess [232].

Let us emphasize the currently known low-lying rotational states of $\alpha$-cluster nature, discussed above, in nuclei up to and including titanium. Figure 53 shows the dependence of the moment of inertia parameter $\hbar^2/(2\Theta)$ where $\Theta$ is the moment of inertia of the nucleus, from the mass number for the known low-lying rotational bands with positive and negative parity nuclei $^{8,10,11,12}$Be,$^{12}$C,$^{16,18,20}$O, $^{20,22}$Ne, $^{32}$S, $^{36,38}$Ar, $^{40,42}$Ca, $^{46}$Ti, $^{44,48}$Cr. This result was presented in the paper [61].

If the structure of all the given rotational bands can be represented as $\alpha\otimes$core, the points will be approximately located on the curve corresponding to the following dependence of the moment of inertia on the mass number of the nucleus:

$$\Theta = \Theta_1 + \Theta_2 + \frac{A_1 A_2}{A} R^2 m_0. \tag{80}$$

here $A_{1,2}$ and $\Theta_{1,2}$ are the mass numbers and moments of inertia of the cluster and the core, respectively, $A$ is the mass number of the nucleus, $R$ is the distance between the cluster and the core, and $m$ is the mass of the nucleon. Assuming that the moments of inertia of the cluster and the core are equal to the moments of inertia of spherical nuclei of radius $R_{1,2} = r_0 \cdot A_{1,2}^{1/3}$ and the distance between them is equal to the sum of radii $R = R_1 + R_2$, the equation (80) contains only one free parameter $r_0$, which for nuclei of a given mass group is usually chosen in the range 1-1.2 fm. By fitting the equation (80) to the available experimental data, we can estimate the value of $r_0$, which is 1.134 fm, which corresponds well to the specified range. The correctness of the considered treatment is indicated by the good coincidence between the fitting curve and the point corresponding to the moment of inertia parameter for the $^{8}$Be nucleus. The exception is the $^{12}$Be nucleus, which has a very large moment of inertia due to the large distance between the $\alpha$-particles (see Table 5). By this feature, the rotational band in this nucleus could be categorized as molecular.

The next nuclei when the $\alpha$-particle populates a state above two closed shells are $^{94}$Mo and $^{212}$Po. For both nuclei, the low-lying bands of states with positive parity are well known and they conform very poorly to the $E^* \approx J(J+1)$ law. Attempts to detect states with negative parity that could be identified as a $\alpha$-cluster band were made in the work [223] in the $^{90}$Zr($^{6}$Li,$d$)$^{94}$Mo reaction. However, the result was unsatisfactory - the spectrum was strongly contaminated with $^{16}$O and $^{20}$Ne states and it was not possible to identify any intense levels with negative parity. It should be noted that during the study of $\gamma$-spectra in this nucleus a band with negative parity states reaching angular momenta of order 17 was found and, like the analogous band in the $^{44}$Ti nucleus, it has no low-spin states.

Nevertheless, the bands in $^{94}$Mo and $^{212}$Po were considered in the framework of the potential model in [112, 233] with *cosh* and $WS + WS^3$ potentials. It

was shown that although the distribution of all levels cannot be satisfactorily described, the model predicts the approximate position of some part of the levels and allows us to estimate the half-lives of [234].

It should be noted that, despite the success of the potential used to describe cluster states over a wide mass range, in this case, the analogy between cluster bands in heavy and light nuclei is not complete. As was shown in [232], the rms distance between cluster and core depends strongly on the mass number, so that even for neighboring isotopes the simple correspondence between the moment of inertia and the excitation energy difference that we found in [62] is not satisfied, when the normalized ratio of energies of levels with different spins is proportional to the reduced mass of the considered nuclei. This fact confirms the assumption about the $\alpha$-cluster nature of the low-lying rotational bands of the considered nuclei.

Thus it can be seen that the presence of additional neutrons not only does not reduce the contribution of cluster configurations to the excited states, but leads to an increase in the available combinations due to their different ways of inclusion.

The above examples of the manifestation of cluster degrees of freedom concern firstly only $\alpha$-clusters, and secondly, relate specifically to the problem of the structure of the nucleus. In this chapter we will consider the possibility of the existence of heavier clusters with respect to nuclear reactions.

As it was mentioned in the introduction, one of the objectives of the transition to the cluster consideration of the nucleus structure is to reduce the number of variables and to reduce the problem to a two-particle one. Of course, not any partitioning is suitable and sometimes the process of cluster selection is nontrivial. One interesting and effective approach to solving this problem for heavy nuclei was proposed by Buck [235]. For this purpose, a function on the charge and mass of the core $(Z_1, A_1)$ and cluster $(Z_2, A_2)$ was introduced:

$$D(Z_1, A_1, Z_2, A_2) = [B_A(Z_1, A_1) - B_L(Z1, A_1)] + [B_A(Z_2, A_2) - B_L(Z_2, A_2)] \quad (81)$$

where $B_A$ is the binding energy of the corresponding nucleus and $B_L$ is the binding energy calculated from the liquid drop model. Then the obtained function is averaged over neighboring values and plotted as a function of the averaged charge. When this function reaches a maximum, it means that the nucleus energetically "benefits" from such a partitioning. Often this function has several maxima [109]. By introducing the cluster-core interaction potential (usually $WS + WS^3$), one can calculate the positions of the rotational band levels, transition intensities, and lifetimes. Such a model is applicable only to sufficiently heavy nuclei, so that the use of Wildermuth's rule is already quite difficult. In [236], an alternative expression was proposed to determine the value of $G = 2N + L$:

$$G = \frac{0.88 A_1 A_2}{(A_1 + A_2)^{2/3}} \tag{82}$$

This approach allowed us to describe a large number of rotational bands in the heavy nuclei arising from clustering [237].

Another very important case of clustering in medium and heavy nuclei, mostly belonging to *sd* shells (and above), analogous to the Ikeda diagram, is the appearance of molecular resonances. By definition, a *nuclear molecule* – a system of two nuclei (or more) bound by a quasi-molecular potential [238]. From the microscopic point of view, such systems can arise also if there is a nucleon (nucleons) whose orbitals are arranged around both nuclei, like covalent bonds in molecules. Earlier we described such configurations when a $\alpha$-particle was considered as a cluster. In this section, we are interested in the manifestation of molecular structure arising from the scattering of heavy ions – the phenomenon of *molecular resonances*.

In work [238], it was noted that "nuclear molecules are the most pronounced manifestation of clustering at the moment". Given that we can only observe such states in experiment if there is no strong absorption, the molecular properties are most clearly manifested by studying the scattering of well-connected nuclei, with mass numbers between 12 and 28. For example, $^{12}$C+$^{12}$C, $^{12}$C+$^{16}$O, $^{16}$O+$^{16}$O, $^{16}$O+$^{28}$Si, $^{28}$Si+$^{28}$Si, although there are predictions even for such giant molecules as $^{238}$U+$^{238}$U [239].

To date, quite a large number of resonances in the scattering of self-conjugated nuclei are known, although there is no precise understanding of whether all such

resonances are “molecular”. Purely phenomenologically, they can best be described by the systematics proposed by Abbondanno in [105]. It is with it that we will compare our results.

The above examples of molecular states are well enough studied, and in this section we will describe experimental studies of such states in neutron-deficient nuclei and the manifestation of “heavy” clustering in the decay of excited states.

## Chapter 4. Cluster transfer in elastic scattering

Usually, in heavy-ion interaction reactions, the process of compound-nucleus formation followed by evaporation of light particles and emission of $\gamma$-quanta plays an important role. In the case of light nuclei, especially self-conjugated ones, the picture is somewhat more complicated due to the presence in such systems of molecular resonances, rainbow scattering, and other important and interesting features. One such feature is the elastic transmission response. This issue was mentioned earlier in Chapter 3.

The general approach to transmission reactions was discussed in Chapter 1. Let us restrict ourselves to the case where two nuclei collide and the structure of one can be represented as $A + a$ and the other as $A$. Then a $a$-transfer process is possible, with the same set of nuclei remaining in the output channel as in the input channel, as in the case of simple elastic scattering, as is evident:

$A + (A + a) = A + (A + a)$ - elastic scattering

$A + (A + a) = (A + a) + A$ - elastic transmission

The two cases are schematically illustrated in Figure 54. Because of the indistinguishability of the particles, we cannot conclude whether or not transfer has occurred in this particular case, but to obtain the full amplitude of the process we must consider the amplitude of the transfer as well. Since in the center-of-mass system the angle between the scattered particles is related by the expression $\theta_A = \pi - \theta_B$, where $B$ denotes the $(A + a)$ system, the total amplitude can be written as:

$$|f_{tot}(\theta_B)|^2 = |f_{el}(\theta_B) + (-)^A f_{tr}(\pi - \theta_B)|^2. \tag{83}$$

The situation considered is often encountered in scattering physics when describing interaction processes: electron exchange in molecular scattering, neutron exchange in nuclear scattering, and $\pi$-meson exchange in nuclear particle scattering.

One interesting and verifiable consequence of the presence of well-defined cluster degrees of freedom is the increase of the scattering cross section in the back-angle region due to cluster transfer. Thus, when studying the most important

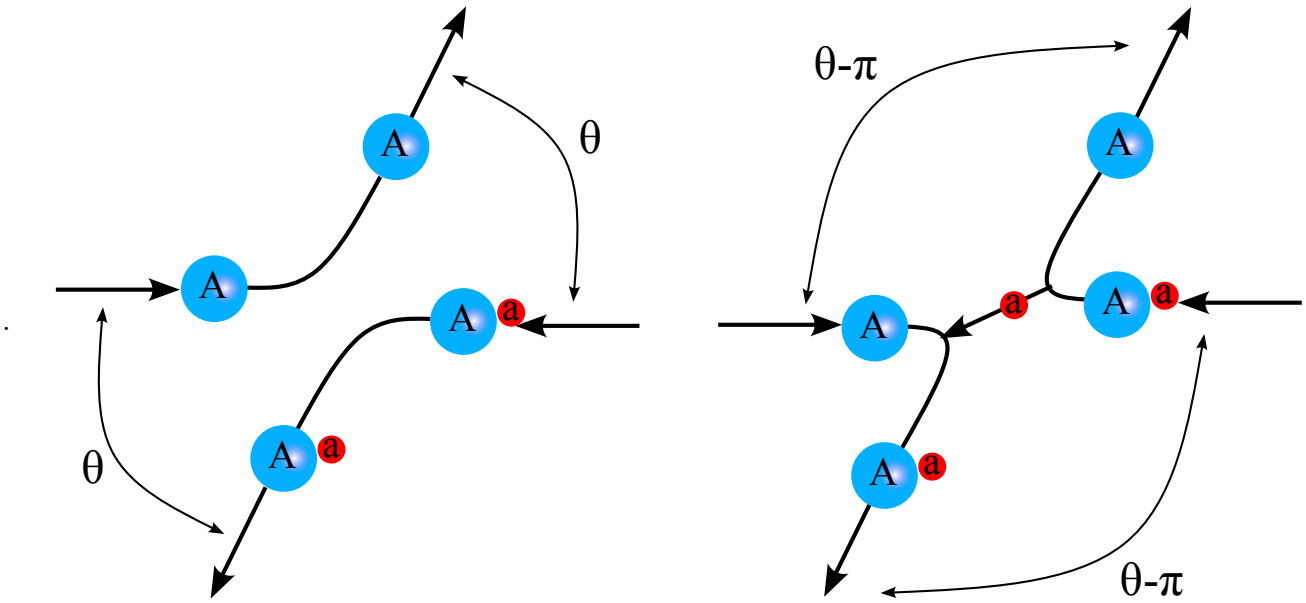


Figure 54. 1 – Elastic dissipation, 2 – Elastic transmission.

reactions that allow us to study the occurrence of molecular resonances ($^{12}$C+$^{16}$O, $^{16}$O+$^{20}$Ne) to describe the elastic scattering angular distribution, we need to take into account the $\alpha$-particle transmission. Given the fact that it is from the analysis of elastic scattering within the optical model that we can extract the interaction potentials important for analyzing reactions related to nucleon redistribution, taking into account the elastic transfer processes is a necessary step for the correct determination of these potentials. In this chapter, we briefly discuss our results from a cluster point of view.

In our work, we have experimentally investigated the reactions associated with the elastic transfer of $\alpha$-particles –$^{16}$O+$^{20}$Ne and $^{10,11}$B+$^{15}$Ne.

### 4.1. Reaction $^{16}$O+$^{20}$Ne

Of interest from the point of view of studying the elastic transfer reaction is the elastic scattering reaction $^{16}$O+$^{20}$Ne, where the $\alpha$-particle exchange also gives a significant increase in cross section at large angles in the posterior hemisphere [240]. This response was first studied in [241] in the $\leq$156° angular range in the center-of-mass system, where a strong increase in cross section at large angles was observed.

Since, from the point of view of studying the elastic transmission response, we are interested specifically in large angles, we performed an experiment to study the elastic scattering of $^{16}$O on $^{20}$Ne in the $\leq$156° range in the center-of-mass system.

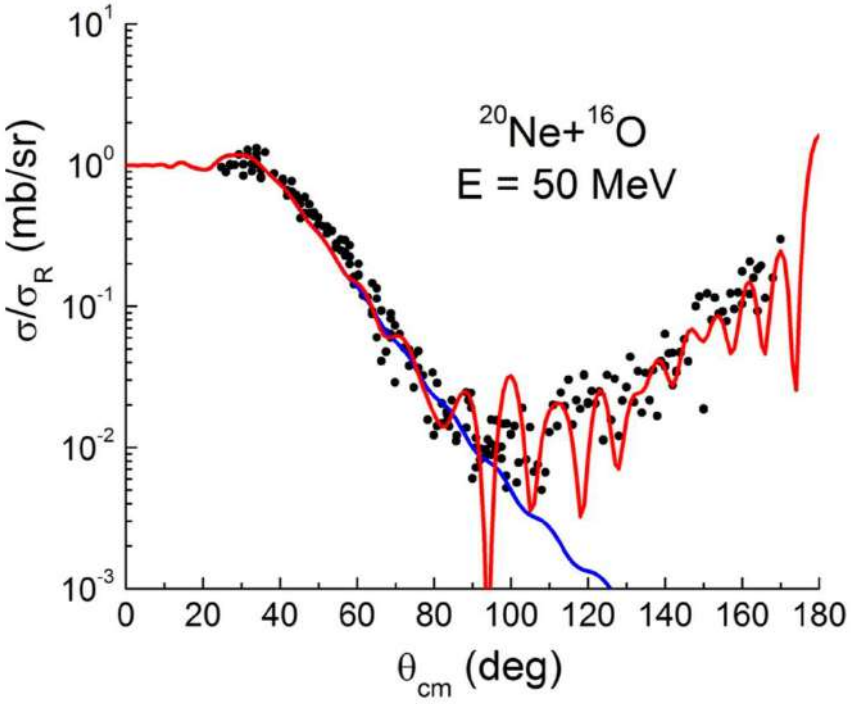


Figure 55. The angular distribution of elastic scattering of $^{16}$O on $^{20}$Ne. Blue and red lines – calculation without and with $\alpha$-particle transmission, respectively.

The measurements were performed on a $^{20}$Ne beam at the cyclotron laboratory of the University of Warsaw. The beam energy was 2.5 MeV/A. The scattered particles were detected by the gas $\Delta E - E$ telescopes of the ICARE system, their resolution was 700 keV. The target was made as a self-supported aluminum oxide foil $Al_2O_3$, 150 mg/cm$^2$ thick. Details of the work are presented in the paper [242].

The measurements showed that the angular distribution has a typical, in terms of the optical model, structure in the anterior hemisphere and a significant increase in cross-section in the posterior hemisphere. The resulting angular distribution is shown in Figure 55.

Experimental data in the anterior hemisphere were analyzed within the optical model as shown in the Figure, while a cross section involving the elastic transmission mechanism was obtained using the FRESCO [161] program. The optical potential values are summarized in Table 20.

Table 20. Potential parameters for the reaction $^{12}$C+$^{20}$Ne.

| $V_0$ MeV | $r_r$ fm. | $a_r$ fm. | $W_0$ MeV | $r_i$ fm. | $a_i$ fm. |
|---|---|---|---|---|---|
| 100.0 | 1.20 | 0.49 | 35.0 | 1.31 | 0.49 |

## 4.2. Reaction $^{10,11}$B+$^{15}$N

As has been shown, the $^{20}$Ne nucleus is a "good" cluster nucleus. However, elastic transfer of $\alpha$-particles can also take place in the case of other nuclei. Let us consider two elastic scattering reactions:

1. $^{15}$N($^{11}$B,$^{11}$B)$^{15}$N
2. $^{15}$N($^{10}$B,$^{10}$B)$^{15}$N

The process of elastic transmission can proceed only in the first case (if we neglect the possibility of transmission of the $^{5}$He cluster) and, accordingly, the cross section of the second reaction at large angles can be described in the first approximation by an optical model, while the first one will require accounting for elastic transmission and addition of amplitudes by the formula (83).

The experiment was performed at the cyclotron laboratory of the University of Warsaw. A $^{15}$N beam with an energy of 43 MeV was incident on $^{10}$B and $^{11}$B targets with densities of 0.15 mg/cm$^2$ and 0.25 mg/cm$^2$, respectively. The particles were recorded by the ICARE gas telescope system. The angular distribution of the scattered $^{15}$N nuclei was measured over the angular range 5° to 40° in the laboratory system. To obtain cross-sectional data at larger angles, the distributions of $^{10}$B and $^{11}$B nuclei were studied. The details of the experiment are outlined in the paper [52].

The Woods-Saxon potentials $WS$ (24) and the double convolution potential $F2$ (29) were used for the analysis within the optical model and DWBA, the imaginary part in both cases being taken into account by Woods-Saxon.

In the case of the double convolution potential for the nucleon-nucleon interaction $V_{NN}(r)$, the CDM3Y6 potential based on the M3Y-Paris [98,243] potential was used. The density distribution in the nuclei was calculated in the MHO (Modified Harmonic Oscillator) [244] approximation:

$$\rho(r) = \rho_0 \left[1 + \alpha \left(\frac{r}{a}\right)^2\right] \exp\left[-\left(\frac{r}{a}\right)^2\right], \tag{84}$$

where the parameters $\rho_0$, $a$, and $\alpha$ are given in Table 21.

The parameters of the Woods-Saxon optical potential for the reaction $^{15}$N($^{11}$B,$^{11}$B)$^{15}$N are given in Table 22. When calculated with the real part as a double convolution, the imaginary part had the same parameterization as for

.

Table 21. Density distribution parameters [244].

| Nucleus | $\rho_0$ | $a$ | $\alpha$ |
|---|---|---|---|
| $^{10}$B | 0.1818 | 1.71 | 0.837 |
| $^{11}$B | 0.1818 | 1.69 | 0.811 |
| $^{15}$N | 0.158 | 1.81 | 1.25 |

the real Woods-Saxon. The parameters of the optical Woods-Saxon potential for the reaction $^{15}$N($^{10}$B,$^{10}$B)$^{15}$N are given in Table 23. In this case, when using the double convolution potential, the imaginary part of the potential is given in the second row of the table. The radius was calculated using the formula $R = r_{r,i}(A_1^{1/3} + A_2^{1/3})$, where $A_{1,2}$ are the mass numbers of the colliding nucleus and target.

.

Table 22. Potential parameters for the reaction $^{15}$N($^{11}$B,$^{11}$B)$^{15}$N.

| $V_0$ MeV | $r_r$ fm. | $a_r$ fm. | $W_0$ MeV | $r_i$ fm. | $a_i$ fm. |
|---|---|---|---|---|---|
| 200.0 | 0.79 | 0.75 | 11.0 | 1.25 | 0.75 |

.

Table 23. Potential parameters for the reaction $^{15}$N($^{10}$B,$^{10}$B)$^{15}$N.

| $V_0$ MeV | $r_r$ fm. | $a_r$ fm | $W_0$ fm | $r_i$ MeV | $a_i$ fm. | fm. |
|---|---|---|---|---|---|---|
| 205.7 | 0.79 | 0.831 | 8.48 | 1.25 | 0.95 | |
| . - | - | - | 9.94 | 1.25 | 0.97 | |

The angular distributions obtained in the experiment and the model calculations are shown in Figures 56 and 57.

For the DWBA analysis of the elastic transmission response, the spectroscopic amplitude was chosen to be 0.435. The wave functions of the relative motion of the $\alpha$-particle were calculated for the $WS$ potential when the radius was calculated for a value of $r_0$=1.25 fm and diffusivity $a = 0.65$ fm. The depth of the potential was chosen from the condition of reproducing the binding energy. The number of wave function nodes was chosen according to the Wildermuth condition, formula 23.

From the results obtained, we can conclude that it is important to take

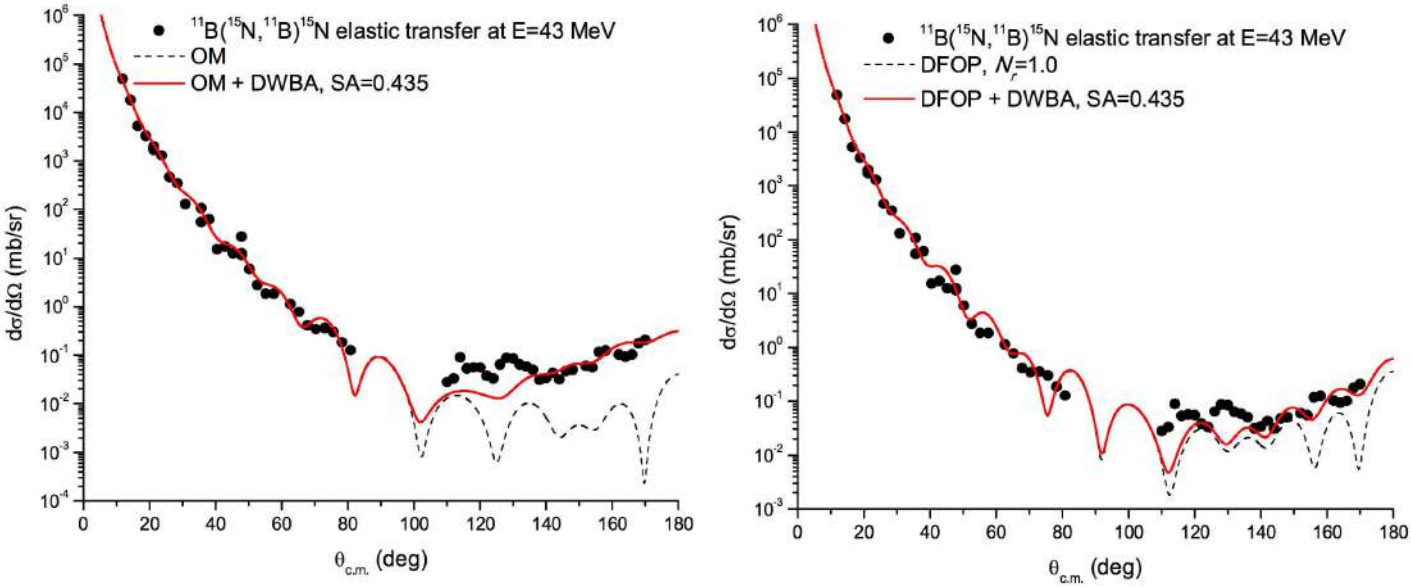


Figure 56. The angular distribution of elastic scattering $^{15}$N($^{11}$B,$^{11}$B)$^{15}$N. The case of the $WS$-potential is shown on the left and the folding-potential is shown on the right [52].

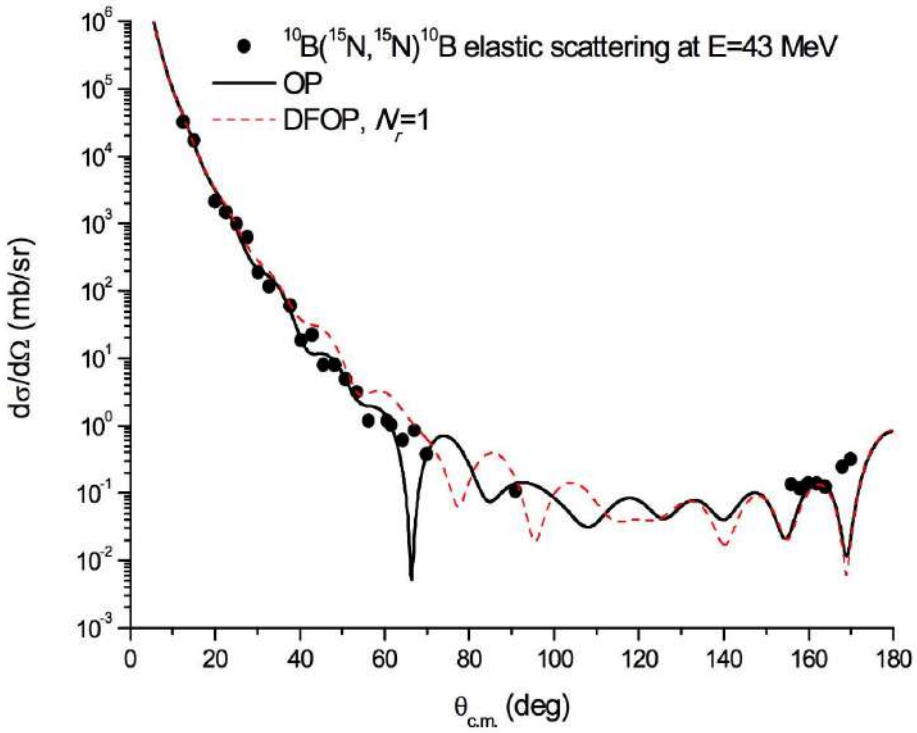


Figure 57. Elastic scattering angular distribution $^{15}$N($^{10}$B,$^{10}$B)$^{15}$N [52].

into account the transfer process when extracting the optical potential parameters from the elastic scattering reaction in order to use them in more complicated cases involving nucleon redistribution processes. This remains true even if the nuclei are not self-conjugated. For example, the elastic scattering reaction $^{15}$N($^{11}$B,$^{11}$B)$^{15}$N [52] considered is important for extracting the interaction potential of $^{11}$B and $^{15}$N. This will allow us to study the inelastic channels $^{15}$N($^{11}$B,$^{16}$O)$^{10}$Be and $^{15}$N($^{11}$B,$^{14}$C)$^{12}$C. And these reactions, in turn, allow us to evaluate the processes of proton capture by the nuclei $^{15}$N and $^{14}$C, which are important, from the astrophysical point of view, for the correct analysis of the CNO cycle reactions.

# Chapter 5. Reactions with heavy cluster escape

As already mentioned in the discussion of cluster states in the $^{40}$Ca nucleus, one important way to investigate the structure of nuclei is to study the formation of compound systems followed by evaporation of light particles (protons, neutrons, and light ions) and spectrometry of $\gamma$-transitions. However, to analyze the properties of the resulting structures, it is necessary to have at least a qualitative description of the reactions taking place. To date, quite a large number of decay species with manifestation of cluster degrees of freedom are known, ranging from the familiar $\alpha$-decay to heavy exotics. However, accurate quantum mechanical calculations are difficult in some cases. Given the great importance of such processes, one can conclude that experimental study is necessary for subsequent theoretical evaluation. Thus, to study exactly the cluster component in the output channels of reactions, in addition to the obvious and quite well experimentally studied case of the $\alpha$-particle output, one should consider nuclei in which the contribution to the structure of the cluster configuration is very large. As can be seen from the list of "good" cluster nuclei (not too heavy for high intensity of their observation in the exit channel), these are $^{8}$Be nuclei in the ground state and $^{12}$C in the "Hoyl" $0^+$ state with an excitation energy of 7.65 MeV.

The importance of studying such exit channels is, in addition, due to the fact that the residual, nucleus, in this case, may be in a state that is unattainable when observing exit channels with only light particles. This is essential in the study of high-spin states, since, for example, the proton, carrying away a relatively large energy, carries away a small momentum, so that the channel will be "closed" if the residual nucleus is under the yrast line. A wide range of experimental approaches are now available to study such reactions. For example, our work described above on $^{8}$Be registration in the study of $^{18}$O levels was based on the selection of events by an invariant mass spectrum, which allowed us to efficiently isolate $\alpha$-particles from the decay of the $^{8}$Be nucleus (as described earlier in the study of the $^{18}$O nucleus.

This experiment was performed at the Accelerator Laboratory of Legnaro, Italy. The experimental setup consisted of a system of silicon $\Delta E - E$ detec-

tors covering 64% of the full surface in $4\pi$ steradian and protected from heavy fragments by a $14\mu$m aluminum foil and a $\gamma$ spectrometer based on ultrapure germanium detectors. A detailed description of the experimental setup is given in [245]. The main feature of this work was the geometry of the experiment, which allows the registration of exotic channels with heavy ion output. For both output channels considered ($^8$Be and $^{12}$C$^*$), the nuclei were in states only slightly above the decay energy, so that the cluster dispersal was performed at a very small solid angle, so that the reaction products predominantly fell into a single telescope.

For our purposes, two reactions were chosen:

1) $^{13}$C($^{18}$O,$^8$Be)$^{23}$Ne. The beam energy was 100 MeV. Both the study of channels with $\alpha$-particle yields and the spectroscopy of states of neon nuclei were allowed. Due to the low energy of the first excited state of beryllium, its small impurity could be observed in the spectrum.

2) $^{24}$Mg($^{28}$Si,$^{12}$C$^*$)$^{40}$Ca. The beam energy was 130 MeV. The $^8$Be was also allowed to be registered in this experiment.

Due to the foil shielding of the telescopes, nuclei heavier than lithium did not reach the detector. However, since $^{12}$C* and $^8$Be decay in flight, individual particles of these nuclei could be registered. On the other hand, the relative momenta of these particles are so small that the detector "perceives" their hits as a single event, placing them at the appropriate locus. The spectra obtained in the $\Delta E - E$ work for both reactions are shown in Figure 58. The loci corresponding to protons, deuterons, tritons, and $\alpha$-particles, as well as the obtained loci for the registered unbound states $^8$Be and $^{12}$C$^*$ are clearly visible.

Let's compare the intensities of several $\alpha$-particles hitting one detector with their intensities hitting different detectors. Suppose we have $N$ identical detectors and their efficiency is $\Omega$. Let us denote by $M$ the number of uncorrelated $\alpha$-particles hitting $p$ detectors. If several particles hit one detector, it is considered as a common event. Then the probability of triggering $p$ of $N$ detectors is:

$$P_N^p = \sum_{k=p}^{N} P_N^k \cdot P(kp). \tag{85}$$

The first multiplier, the probability that each particle hits some detector, is $N\Omega$ -

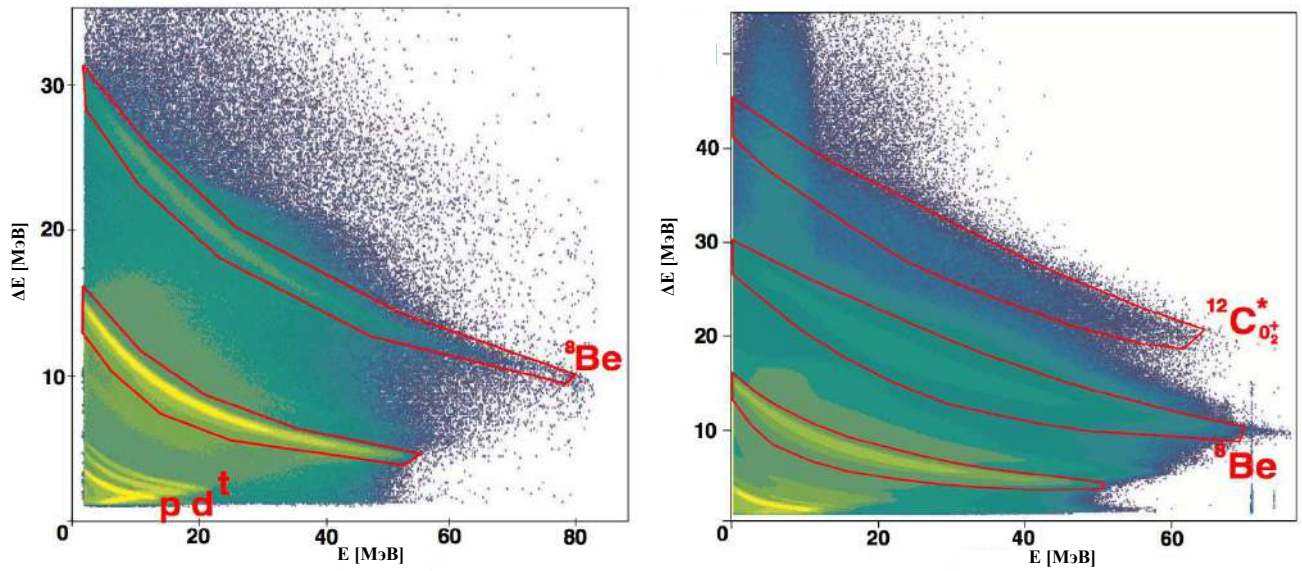


Figure 58. $\Delta E - E$ spectra for the reactions $^{13}$C($^{18}$O,$^{8}$Be)$^{23}$Ne (left) and $^{24}$Mg($^{28}$Si,$^{12}$C$^{*}$)$^{40}$Ca (right) [47]. The corresponding loci are shown. The shadowing at low particle energies is due to instrument overloading due to high intensities of light particles.

the total efficiency. The second multiplier denotes the distribution of $k$ particles to $N$ detectors. The probability that $k$ of $M$ particles will hit any detector is [246]:

$$P_N^k = \binom{M}{k} (N\Omega)^k (1 - N\Omega)^{M-k}. \tag{86}$$

To account for the full efficiency, we need to move from the center-of-mass system to the laboratory system, which is provided by multiplying it by the Jacobian, a kinematic transformation often used to transition between reference systems in determining the cross section. Since the Jacobian is different for different channels, we will denote the obtained efficiencies with the corresponding reaction product.

In this paper, we evaluated the ratio of yields for different channels. We give the corresponding calculations for the channels of interest.

**Channel 2$\alpha$**

Probability of detecting two $\alpha$:

$$P_2^2 = (N\Omega_\alpha)^2. \tag{87}$$

Probability of two $\alpha$-particles hitting different detectors:

$$(P_2^2)_s = N(N-1)\Omega_\alpha^2. \tag{88}$$

Then the probability of registration of two particles in one detector is:

$$(P_2^2)_d = P_2^2 - (P_2^2)_s = N\Omega_\alpha^2, \tag{89}$$

and the ratio of the probability of registering two $\alpha$-particles in one detector to the probability of their hitting in different detectors is:

$$\frac{(P_2^2)_d}{(P_2^2)_s} = \frac{1}{N-1}. \tag{90}$$

**Channel $^8$Be**

Similarly, the probability of registering $^8$Be is:

$$P_{^8Be} = N\Omega_{^8Be}. \tag{91}$$

Its ratio to the probability of registering two $\alpha$-particles in two detectors will be:

$$\frac{P_{^8Be}}{(P_2^2)_s} = \frac{\Omega_{^8Be}}{(N-1)\Omega_\alpha^2}. \tag{92}$$

**Channel 3$\alpha$**

For channel $^{12}$C$^*$, we have a registration of three $\alpha$-particles out of three. So:

$$P_3^3 = (N\Omega_\alpha)^3. \tag{93}$$

And for the probability of three $\alpha$-particles hitting different detectors:

$$(P_3^3)_s = N(N-1)(N-2)\Omega_\alpha^3, \tag{94}$$

, so for three $\alpha$-particles to hit one detector:

$$(P_3^3)_d = P_3^3 - (P_3^3)_s = N(3N-2)\Omega_\alpha^3. \tag{95}$$

The ratio of the probability of three $\alpha$-particles hitting one and three different detectors is:

$$\frac{(P_3^3)_d}{(P_3^3)_s} = \frac{3N-2}{(N-1)(N-2)}. \tag{96}$$

**Channel $^{12}$C$^*$**

In this case, three $\alpha$-particles hit one detector.

$$P_{^{12}C} = N\Omega_{^{12}C}. \tag{97}$$

and the ratio of probabilities of hitting $\alpha$-particles from the decay of $^{12}$C into one detector to the number of $\alpha$-particles hitting three detectors will be:

$$\frac{P_{^{12}C}}{(P_3^3)_s} = \frac{\Omega_{^{12}C}}{(3N-2)\Omega_\alpha^3}. \tag{98}$$

One more important feature of the kinematics of this experiment should be noted. Since the relative momentum of the particles in the center-of-mass system is small, it is these particles that fill the corresponding locus ($^8$Be or $^{12}$C$^*$). In other words, the energies of all alpha particles are equal and are half or one third of the total, depending on the channel. For random particles hitting one detector, this equality is no longer satisfied and the particle "leaves" the corresponding locus. If, as in the case of two $\alpha$-particles, the probabilities of such events are not too small, this will result in a background that distorts the locus. Figure 59 illustrates this fact in a Monte Carlo simulation. The "ideal" beryllium locus (black circles) and random $\alpha$-particles (white circles) are shown. The resulting "hump" is clearly visible above the beryllium locus on the left in Figure 58.

A detailed description of the experimental procedure of this study is given in our paper [47]. Let us review the most interesting results.

To compare the yields of $^8$Be or $^{12}$C nuclei, an energy spectrum was constructed containing events corresponding to the registration of two or three $\alpha$-particles, respectively. The number of events and energies were normalized for these spectra. The results are presented in Figures 60 and 61. To compare the $^8$Be spectrum, kinematic calculations were performed to account for the differences in the $^{13}$C($^{18}$O,$^8$Be)$^{23}$Ne reaction and the $^{13}$C($^{18}$O,$\alpha$)$^{27}$Mg reaction. The Jacobian value was used for the calculations:

Yield $\alpha\mathcal{J}$=1.9, yield $^8$Be $\mathcal{J}$=2.7 (reaction $^{13}$C+$^{18}$O).

The yield of $\alpha\mathcal{J}$=2.1, the yield of $^{12}$C $\mathcal{J}$=3.0 (reaction $^{28}$Si+$^{24}$Mg).

We will use the formula (92) to compare the spectra, then we can write:

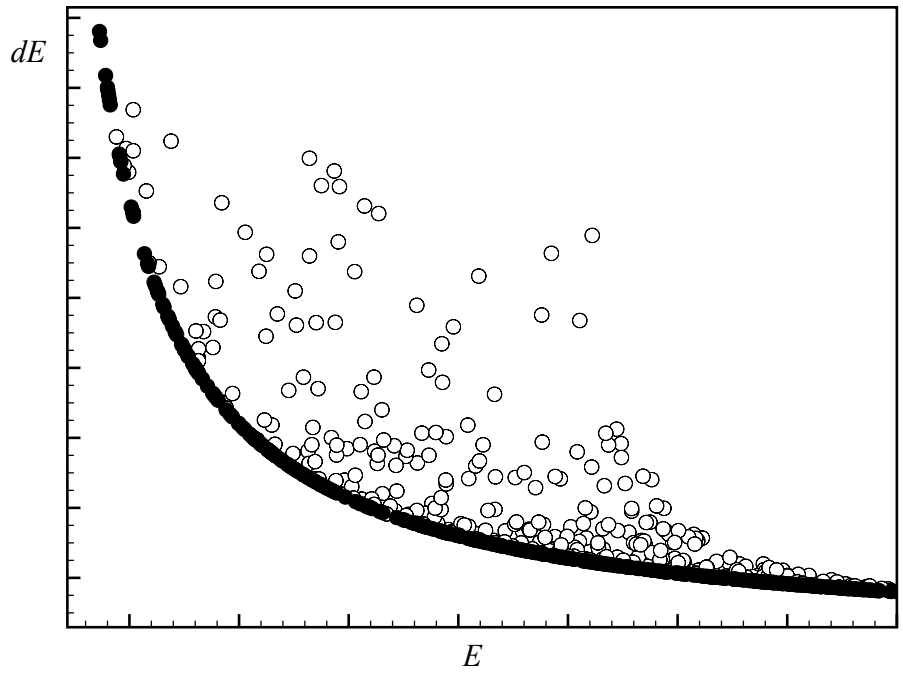


Figure 59. Position of the kinematic $\Delta E - E$ locus for $^8$Be (black circles) and random matches (white circles).

$$\frac{N^*_{^8Be}}{N^*_{2\alpha}} = \frac{N_{^8Be}}{N_{2\alpha}} \frac{1}{(N-1)} \frac{\mathcal{J}_{^8Be}}{\epsilon^* \mathcal{J}^2_\alpha}, \tag{99}$$

here $\epsilon^*$ is the geometry-adjusted detector efficiency, $N^*_{^8Be}$ and $N^*_{2\alpha}$ are the experimental intensities in the corresponding channels given the detector efficiency in the laboratory reference frame, and $N_{^8Be}$ and $N_{2\alpha}$ are the true intensities. Similarly for the comparison with three $\alpha$-particles:

$$\frac{N^*_{^{12}C^*}}{N^*_{3\alpha}} = \frac{N_{^{12}C^*}}{N_{3\alpha}} \frac{1}{(3N-2)} \frac{\mathcal{J}_{^{12}C^*}}{\epsilon^{*2} \mathcal{J}^3_\alpha}, \tag{100}$$

where the values are chosen similarly to the previous formula. Thus, we can compare the energy spectra for the departure of heavy clusters with the $\alpha$-particle exit channels. For example, for the $2\alpha$ channel, a factor of two arises due to the addition of the intensities of the registered particles, which allows us to take into account the case of their different energies. A similar procedure was performed for the channel with three $\alpha$-particles.

When analyzing the spectra (Figures 60, 61), one should take into account the loss of events in the low-energy part, since the particle must overcome the protective foil and the $\Delta E$ part of the detector. In our case, the clipping for

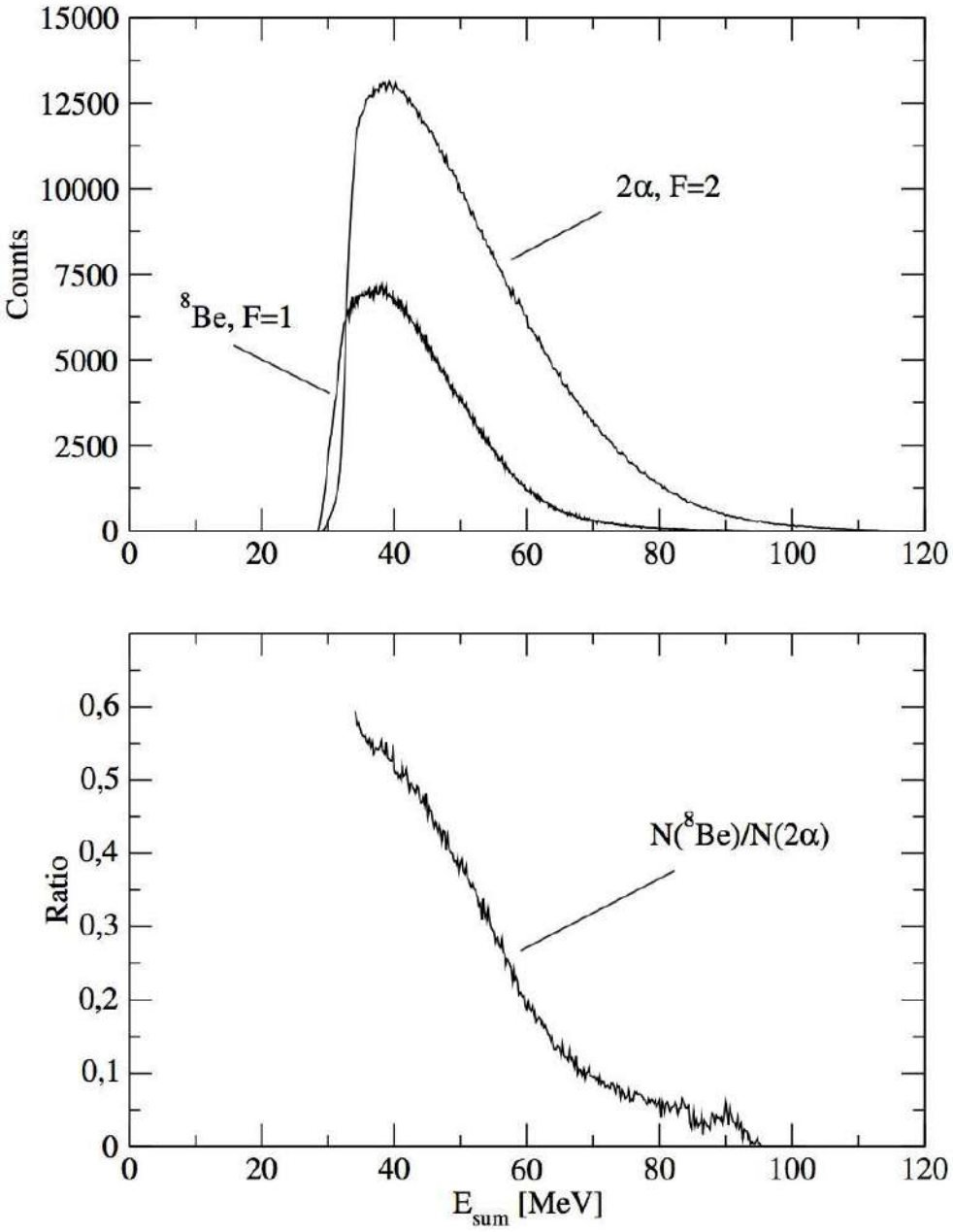


Figure 60. The spectra of the uncorrelated two $\alpha$-particles and $^8$Be nuclei are compared at the top. The ratio of their intensities is shown at the bottom [47].

$\alpha$-particles occurred at an energy of 14.9 MeV.

When comparing with the 90 and 96 formulas, one must take into account possible inaccuracies due to the possibility of high intensities in channels with heavy cluster escape (which obviously gives a contribution to the events detected by different detectors), the possibility of other particles escaping, and the energy dependence of the Jacobian. In both cases of decay, we observe a shift of the emission intensity to small values where its probability becomes maximal. An important consequence of this is the increased excitation energy of the residual

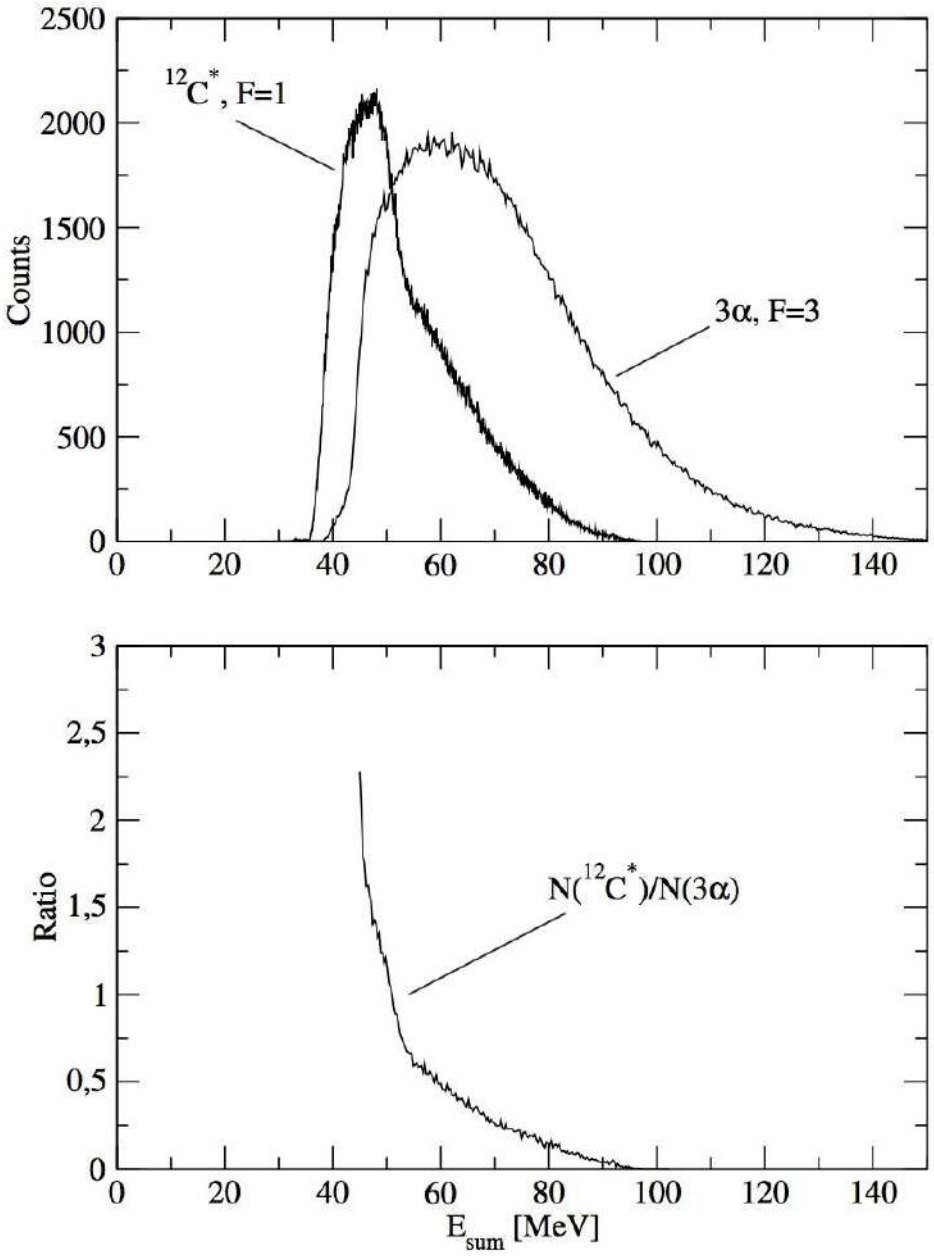


.

Figure 61. The spectra of the uncorrelated three $\alpha$-particles and $^{12}C^*$ nuclei are compared at the top. The ratio of their intensities is given at the bottom [47].

nucleus compared to the escape of uncorrelated particles.

Let us consider the allowed angular momenta for such residual nuclei in both cases on the example of the escape of two $\alpha$-particles and $^8$Be. The dependence of the angular momentum $L$ carried away by the particle on its kinetic energy $E$ is given by the formula:

$$L = R\frac{\sqrt{2m(E - V_C)}}{\hbar}, \tag{101}$$

where R is the radius of the nucleus, $V_C$ is the height of the Coulomb barrier,

$m$ is the mass of the particle. For two $\alpha$-particles of the same energy $E$ and a $^{8}$Be nucleus with twice the energy $2E$, the values of the angular momenta are equal. However, it is necessary to take into account the two-stage process – in the one-stage process the smaller angular momentum is carried away. In addition, the value of the channel radius may change.

Thus, we need to determine experimentally the values of the entrained energies and angular momenta in the reactions under consideration. This can be done by analyzing the $\gamma$-spectra of the residual nuclei. The spectrum of the $^{18}$O+$^{13}$C reaction was analyzed with one of two output channel conditions:

1) 2$\alpha$-particles

2) $^{8}$Be nucleus.

For the reaction spectrum of $^{28}$Si+$^{24}$Mg, one of three options was allowed:

1) 3$\alpha$-particles

2) $^{8}$Be nucleus and $\alpha$-particle

3) $^{12}$C$^{*}$ nucleus

In addition, since the analysis was based on the obtained $\gamma$-spectra, with sufficient excitation energy it was possible to distinguish channels with the departure of an additional $\alpha$-particle, proton or neutron. Because of the high velocity of the residual nucleus, the $\gamma$-spectrum was subjected to a Doppler shift, which allowed the width of the $\gamma$-lines to be significantly reduced. Figure 62 shows the $\gamma$-spectrum of the reaction of $^{24}$Mg($^{28}$Si,$^{12}$C$^{*}$)$^{40}$Ca with conditions 3$\alpha$ (upper part) and $^{12}$C$^{*}$ (lower part). The previously mentioned difference in the excitation energy of the $^{40}$Ca residual nucleus depending on the channel is clearly seen - the $^{36}$Ar residual nuclei appear as a result of the departure of an additional $\alpha$-particle and their number is negligibly small in the upper spectrum. In addition, the $^{39}$K levels appear more intensely on the lower spectrum (the departure of an additional proton), and some transitions corresponding to high-lying $^{40}$Ca levels are very strongly suppressed.

The relative intensities for the above three output channels of the $^{28}$Si+$^{24}$M reaction, which include the possible departure of light particles, are shown in Figure 63. The difference in the excitation energy of the residual nucleus is well demonstrated by the ratio of the formation intensities of $^{40}$Ca and $^{39}$K nuclei. The

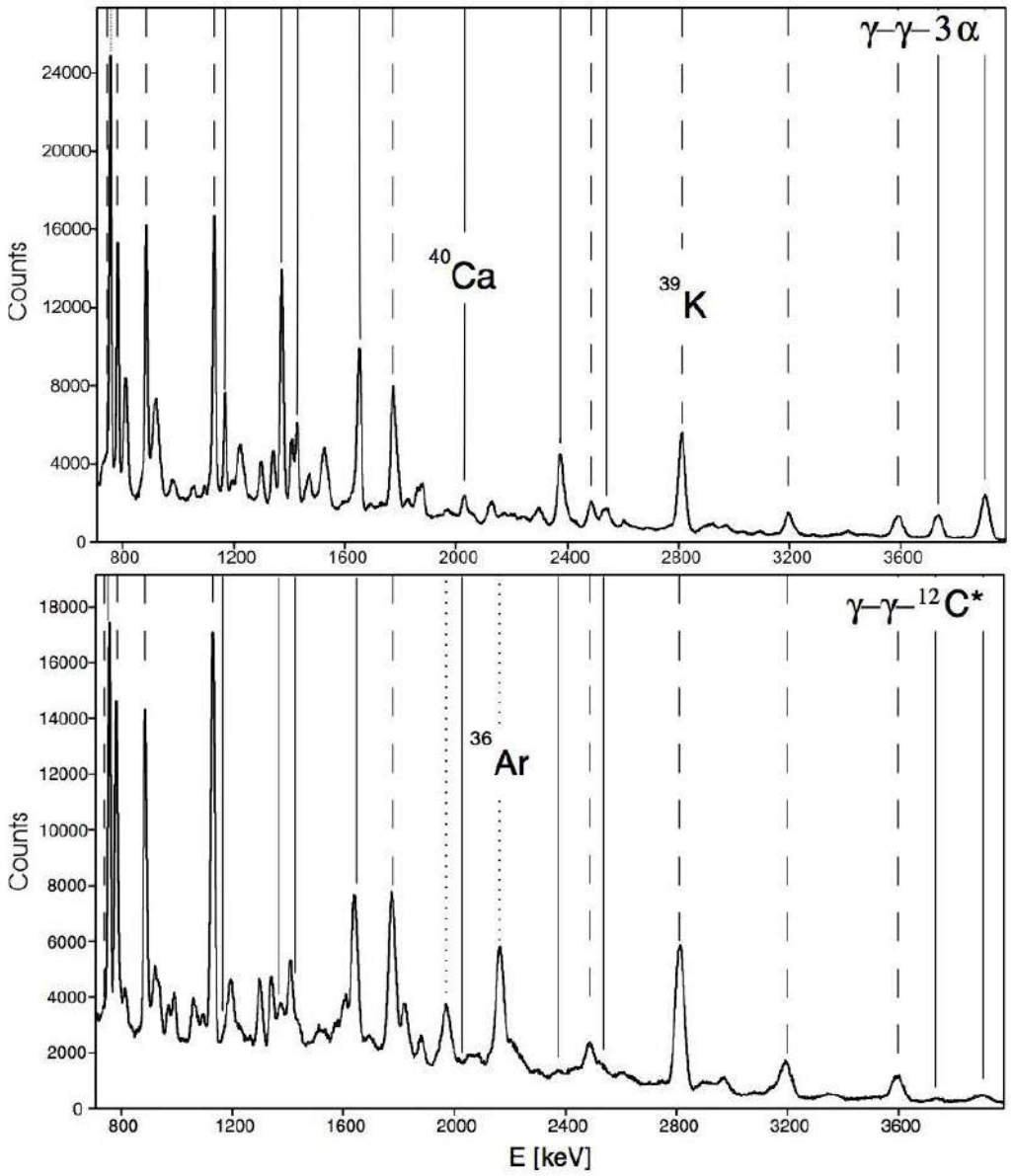


Figure 62. Dependence of the $\gamma$-spectrum on the type of decay [63]. The lines indicate the residual nuclei corresponding to the peaks.

following conclusions can be drawn from this result:

1) At the departure of two $\alpha$-particles, the probability of the subsequent departure of a $\alpha$-particle is approximately equal to the probability of the departure of two protons.

2) The joint departure of a $^{8}$Be $\alpha$-particle nucleus has about three times less probability than the departure of three $\alpha$-particles.

3) The $^{12}C^{*}$ nucleus flies out almost 14 times less often than three $\alpha$-particles, while the probability of an additional proton flying out increases about 16 times.

Consider the reaction $^{13}$C+$^{18}$O, in which the comparison is made for the

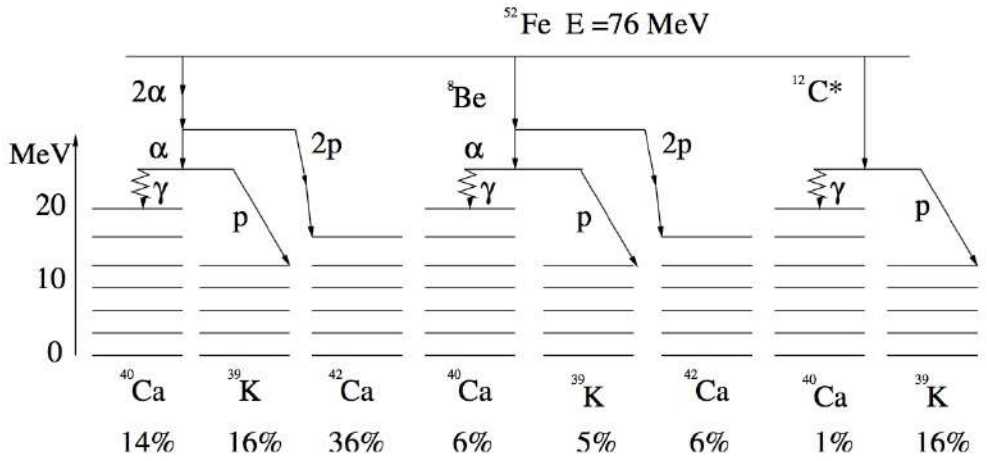


.

Figure 63. Ratio intensities for different reaction channels $^{28}$Si+$^{24}$Mg [209].

escape channels of two $\alpha$-particles and the $^{8}$Be nucleus. If the residual nucleus has sufficient excitation energy, one or two neutrons can be ejected. The result of the comparison is shown in Figure 64. The $^{8}$Be locus shown in Figure 58 overlaps strongly with the locus of the $^{8}$Li nucleus, which can overcome the protective foil and the $\Delta E$ part of the detector. This leads to the appearance of a residual $^{23}$Na nucleus, which is clearly visible when comparing the $\gamma$ spectra. The intensity ratio of $2\alpha/^{8}$Be is of the order of 4 for the $^{22}$Ne residual nucleus and of the order of 1.5 for $^{21}$Ne. As can be seen from the Figure 64, the yield of $^{8}$Be is almost 2.5 times higher than that of lithium (results for lithium isotopes with mass numbers 7 and 6 and subsequent escape of one or two neutrons, respectively, are included here).

As shown in Figure 65, the beryllium yield events belong predominantly to the low-energy range, which is in perfect agreement with the spectrum in Figure 60. Consequently, the two approaches, comparison of particle spectra and analysis of $\gamma$-spectra, are equivalent.

Thus, it can be concluded from this work that heavy clusters carry away less energy from the composite nucleus than the constituent particles individually. On the other hand, a much higher probability of sequential emission of $\alpha$-particles than of heavy clusters was observed, which is consistent with statistical models. The residual nuclei formed after the emission of light clusters appear closer to the yrast line than in the case of heavy clusters.

Calculations within the framework of the models developed by us [40] for the extended Hauser-Feshbach method allow us to obtain very good agreement with

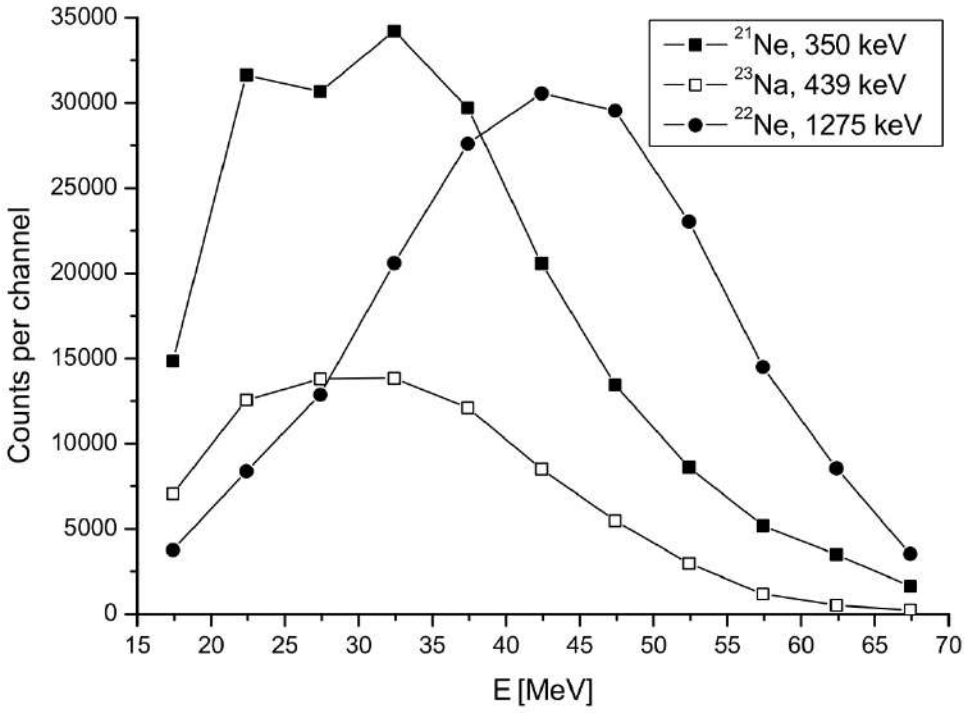


.

Figure 64. Distribution of ground state transition intensities for various residual nuclei after emission by the compound nucleus $^{8}$Be [47].

the experimental data on the intensities of occupancy of different levels. The potential from the paper [247], in the form $WS$ with parameters:
$V_0 = 51.5$ MeV, $r_0 = 1.175$ fm, $a_0 = 0.645$ fm, $W_0 = 27.5$ MeV, $r_I = 1.09$ fm, $a_I = 0.659$ fm,

with radius parameter $r_C = 1.2$ fm. The radius value was determined from the formula $R_x = r_x(A_1^{1/3} + A_2^{1/3})$, where $x = 0, I, C$, and $A_1$, $A_2$ are the mass numbers of the heavy ions. It is interesting to note that this potential was chosen in the work [247] to reproduce the resonance-like structure in the $^{24}$Mg+$^{28}$Si system. It was shown that at interaction energies of 50-53 MeV there is a strong dominance of partial waves, of the order $l$=33-38$\hbar$. This agrees very well with our assumptions on the flow of compound processes.

The permeability coefficients for $\alpha$-particles were calculated based on the modified parabolic Hill-Wheeler model [40], and for the other channels within the systematics [248] framework

The level density parameter was chosen in a core temperature-dependent form as proposed in [249]:

$$\sigma^2 = 0.0145A^{5/3}t, \tag{102}$$

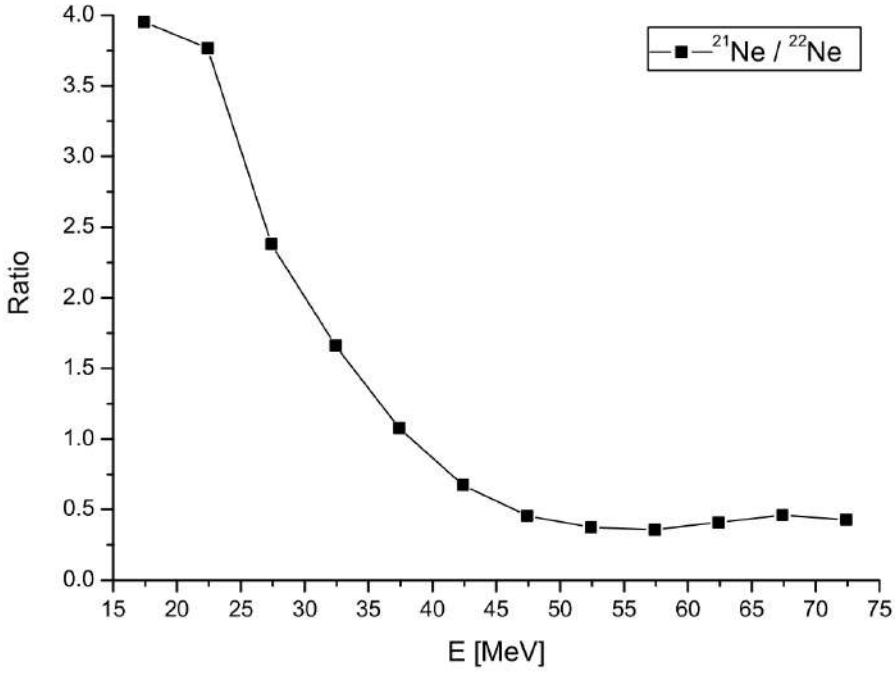


Figure 65. Ratio between the intensities of transitions to the ground states of $^{21}$Ne and $^{22}$Ne [47].

where the nuclear temperature is given by the formula:

$$t = \sqrt{\frac{E_x - \delta}{a}}. \tag{103}$$

The level density parameter was chosen from the work [249], and the energy shift value was calculated based on the drop model with Pearson parameterization [250].

The simplified approach is chosen in order to obtain estimates of the occupancy probabilities of states with different angular momenta in the cluster decay. For a more accurate description it is necessary to use the extended Hauser-Feshbach version, when the excitation energy of the corresponding fragments is taken into account for the resulting partial widths:

$$P_J^{(c)} = \sum_{(I_L,I_H)I} \sum_{(L,I)J} \int\int\int \rho_{I_L}(\epsilon_L)\rho_{I_H}(\epsilon_H)T_L(E)$$

$$\times \delta(\epsilon_L + \epsilon_H + E + Q - E_x)d\epsilon_L d\epsilon_H dE. \tag{104}$$

Here $T_L(E)$ is the permeability coefficient for the case of angular momentum $L$. The delta function provides the energy conservation law, $\epsilon$ is the excitation

energy of the corresponding nucleus, the indices $L$ and $H$ correspond to the cases of light and heavy fragments, and $Q$ is the reaction energy. The summation is performed over all final states of the daughter nucleus $i$, as well as over the angular momenta of the heavy and light fragments and the angular momentum of the compound nucleus available in the system. $\rho(\epsilon_H)$ is the density of levels of the heavy fragment. In this case, the excitation of the light fragment will correspond to the Hoyl state. The calculation showed an increased probability of populating states with angular momentum $L$=10, approximately reproducing the spectrum obtained for $\alpha$-particles

The above observed decrease in the energy carried away by the heavy cluster can lead to very interesting conclusions. The explanation may be based on the representation of the $^{12}\mathrm{C}(0_2^+)$ state with excitation energy 7.65 MeV as a Bose-Einstein condensate state. [96, 251]. As was pointed out in Chapter 1, the condensation process of $\alpha$-particles in nuclei, is associated with a strong increase of the rms radius and, accordingly, a decrease of the density (including the charge density). In this case, tunneling at low energies will not be so strongly suppressed by the Coulomb barrier as in the case of tunneling by a compact particle. The calculations agree well with the experimental data, so that the obtained result is not only a new proof of the existence of the Bose condensate in nuclei, but also provides an additional method for its search and experimental investigation.

In this chapter we considered the cases when nuclei heavier than $\alpha$-particles were considered as a cluster. It was shown that, although such states are not detected in resonance scattering for $fp$-shell nuclei, nevertheless, for $sd$-shell nuclei they show up well in experiment even in the case of neutron-excess nuclei. At the same time as for such sufficiently heavy nuclei, the existence of fragmented $\alpha$-cluster states forming a rotational band is observed.

It has been shown that heavy clusters are not necessarily strongly bound nuclei. We have considered cases where even the unbound $^8$Be and $^{12}\mathrm{C}(0_2^+)$ nuclei were considered as clusters. It was shown that the pattern observed in the experiment with the emission of these nuclei is related to another, extremely important manifestation of cluster degrees of freedom, the Bose-Einstein condensation in the nuclei.

# Chapter 6. Systematics of interaction of heavy clusters within the framework of a potential model

## 6.1. Elastic interaction

As mentioned in the Introduction, the description of cluster states in nuclei using the potential model allows one to simplify the calculations considerably by introducing some effective interaction potential. In the previous chapters, within the framework of this approach, several ways of introducing the "cluster-core" potential were considered, differing, among others, in the method of eliminating forbidden states in the overlap region of the cluster and the core. The introduction of a surface potential was considered in Chapter 1, in the description of states associated with Bose-Einstein condensation in nuclei. In this case, the wave function decreased rapidly in the overlap region of the nuclei. The volume potential close to the convolution potential was considered in the description of the $\alpha$-particle+core structure, and the forbidden states arising in it were excluded by the appropriate choice of the global quantum number on the basis of the formulas (23) or (82). The advantages of the second approach stem from the possibility of using a potential related, as it is assumed, to the potential used in the analysis of angular distributions in the optical model. This issue has been investigated in [252], but a good reproduction of the energies arising in the nucleus of states, was not achieved. A similar approach was used in the work [76]. Potential, as a sum of $WS + WS^3$, was used to describe the states in the nuclei $^{20}$Ne and $^{44}$Ti and was discussed earlier in Chapter 3. Note that this approach also allowed us to correctly describe the intensities of $\gamma$-transitions and angular distributions in the energy range of $\alpha$-particles 20-40 MeV. The depth of the imaginary potential (surface $WS$ for the $^{20}$Ne nucleus and $WS^3$ for $^{44}$Ti) was used as a free parameter. In the present work, this approach was used to describe the states in the $^{40}$Ca nucleus, and, in this case, the cor was not a doubly magic nucleus.

Let us consider the case of the interaction of heavier nuclei that can nevertheless be considered as clusters (i.e., structureless objects). For this purpose, we considered the interaction of $^{12}$C and $^{16}$O nuclei. On the one hand, for this reaction there is a large amount of available experimental data (including those

obtained in the present work), which allows us to carry out a systematization. On the other hand, in contrast to similar reactions $^{12}$C+$^{12}$C and $^{16}$O+$^{16}$O, there is an interaction of non-identical particles, so that the existence of states with negative parity is allowed in the system. The occurrence of quasi-molecular states with the structure $^{12}$C+$^{16}$O was previously considered in [253], and the optical potential was obtained from the analysis of elastic scattering of $^{12}$C on $^{16}$O nuclei at an energy of 75 MeV [254]. It was shown that a number of resonances in such can be described as quasi-bound states forming rotational bands with different values of the global quantum number $G$. In addition, the authors of this work concluded that the contribution to the elastic transmission cross section of the $\alpha$-particle at low energies is negligible, which allows us to simplify the problem of finding the potential. We have proposed an approach to analyze the interaction of heavy clusters in the framework of the potential model [53].

## 6.2. Model

Several methods are currently available for determining the angular momentum of resonances arising in heavy ion scattering reactions. However, most of the angular momenta of resonances, which are presented as possible quasi-molecular states, were determined by comparing the angular distributions with Legendre polynomials. In this case, the angular distribution in the posterior hemisphere, where oscillations of the cross section are clearly manifested, was compared with a function of the form $A \cdot |P_L(\cos\theta)|^2$ and the angular momentum corresponding to the best match with the polynomial was assigned to the resonance.

Let us consider a complex potential of two-particle interaction, which allows us to describe in a first approximation the angular distribution of elastic scattering in the energy region containing states that may belong to rotational bands having a quasi-molecular (cluster) configuration. We will limit ourselves to potentials with the depth of the real part independent of energy, and we will use the depth of the imaginary part as a free parameter. According to [76] and [253], states with different values of global quantum numbers and fragmentation of states can arise in the scattering of heavy ions. Then, for regions with sufficiently high excitation energy of the composite nucleus, one can expect the presence of a significant

number of resonances.

Within the framework of the optical model, we obtain angular distributions with a given potential for different energies, comparing the result in the region of angles 90°-180° with Legendre polynomials of different orders from the region of expected values of angular momenta (less than the value of the critical angular momentum). The differential cross section of elastic scattering, in general, has a complex character of dependence on the angle, but there are cases when we can talk about the recovery of a polynomial structure and in this case there is a set of maxima that can be identified with the maxima of a function of the form $P_L^2(\cos\theta)$ (where $P_L(x)$ is a Legendre polynomial corresponding to the order of $L$) with a fixed value of $L$. Even in these cases, the structure cannot be described only by a given polynomial of degree $L$. However, to determine the dominant order of the polynomial, the cross section can be approximated by a function:

$$f_L(\theta) = \begin{cases} a_1 P_L^2(\cos\theta), & 0 \le \theta < \theta_1 \\ a_2 P_L^2(\cos\theta), & \theta_1 \le theta < \theta_2 \\ \dots \\ a_L P_L^2(\cos\theta), & \theta_L \le theta < \pi, \end{cases} \tag{105}$$

where $a_i$ are the free parameters. Here, two cases were considered as bounds for the angular intervals: $\theta_i$ – positions of zeros or maxima for the function $P_L^2(\cos\theta)$. It should be noted that both cases of angular range partitioning give rather close results.

During the approximation procedure, we fixed the value of $L$. At the same time, the differential cross section was divided into intervals $[0, \theta_1)$, $[\theta_1, \theta_2)$, $\dots$,$[\theta_i, \theta_{i+1})$, $\dots$, $[\theta_L, \pi)$. Depending on the chosen angular range of our experimental data, there can be at most $L$ intervals. Each such interval $i$ will correspond to a different function $a_i P_L^2(\cos\theta)$ of (105). The magnitude of the coefficients $a_i$ was determined from the minima in the expression:

$$\chi_i^2 = \frac{1}{N_i - 1} \sum_{\theta_j \in i\text{-th interval}} \frac{\left(\sigma(\theta_j) - a_i P_L^2(\cos\theta_j)\right)^2}{\Delta\sigma^2(\theta_j)}, \tag{106}$$

where $N_i$ is the number of points falling into the given interval $i$. In general, the

quality of such approximation by the function $f_L(\theta)$ is given by the expression:

$$\bar{\chi}^2_L = \frac{1}{M}\sum_{k=1}^{M}\chi^2_k, \tag{107}$$

where $M$ is the number of intervals in which we perform the analysis. Thus, the dominant value from the contribution of the polynomial $L_{\text{opt}}$ in the analysis of the experimental elastic scattering distribution is defined as follows:

$$L_{\text{opt}} = \underset{L\in[L_{min},L_{max}]}{\arg\min}\ \bar{\chi}^2_L, \tag{108}$$

where $[L_{min}, L_{max}]$ is the interval for the powers of the Legendre polynomial we used in the analysis.

In addition to analyzing for the whole angular range of differential sections available to us, we can take only the part of interest, for example, in our case it will be the interval from 90° to 180°.

It is convenient to consider the value (107) obtained in this case as a function of energy. In this case, the minimum on the graph of such a function will correspond to the energy for which the modeled distribution best coincides with a polynomial of order $L$. When analyzing such a function, it would be interesting to obtain answers to the following questions:
1) Do such minima appear in the region of resonances with different global quantum numbers found within the potential two-particle model?
2) How do the regions in which experimentally detected resonances are present relate to the minima obtained for polynomials of different orders?
3) What are the contributions for partial waves of different orders to the regions of such minima?

Since this formulation of the problem allows strong ambiguity in the choice of a possible potential, we have considered two possible potentials that allow us to describe well the experimental angular distribution for the elastic scattering of $^{12}$C+$^{16}$O nuclei.

In the experiment we performed, we chose a narrow region of energies $E_{cm}$=17.28-18 MeV [256, 257] corresponding to two consecutive narrow peaks in the $^{12}$C+$^{16}$O excitation function was chosen. The first peak is identified as

$l$=11 [256]. By making measurements over a wide angular range for intermediate energy, the contribution from extraneous processes can be reduced to analyze the elastic transfer response. The work was performed at the cyclotron of the University of Warsaw, Poland. A $^{16}$O beam with an energy of 41.3 MeV (which corresponded to an energy value of 17.7 MeV in the center-of-mass system) was incident on a self-supported $^{12}$C target (35 $\mu$/cm$^2$). The registration was carried out with the gas $\Delta E - E$ telescopes of the ICARE system, covering an angle from 8° to 153° in the laboratory system. The result is shown in Figure 66 together with the adopted data.

The first potential ($WS1$) was used in [253] to determine the position of quasi-bound states for the potential model, and was also used in [254] to describe the experimental angular distribution of elastic scattering at energies of 75 MeV. The second potential used ($WS2$) was obtained by us from the condition to reproduce the experimental angular distribution of elastic scattering in the energy region from 10 to 30 MeV and the quasi-bound states that were obtained in [253], but with the condition that the wave function for the corresponding levels contains one additional node more. The form factors for both potentials were chosen as the quadratic Woods-Saxon ($WS^2$), the formula (25), their parameters, and the values of the corresponding volume integrals (73) are given in Table 24.

Table 24. Parameters of the real part of optical potentials [53].

| Parameter | Value |
|---|---|
| $WS1$ | |
| $V_0$ | 305 MeV |
| $R_v$ | 4 fm. |
| $a_v$ | 1.4 fm. |
| $J_v$ | 326 MeV fm$^3$ |
| $WS_2^2$ | |
| $V_0$ | 320 MeV |
| $R_v$ | 4.184 fm. |
| $a_v$ | 1.3 fm. |
| $J_v$ | 378 MeV fm$^3$ |

Figure 66 compares the experimental elastic scattering angular distributions with calculations based on the proposed potentials $WS1$ and $WS2$. We chose the imaginary part as the bulk Woods-Saxon $WS$ (24), for the $WS1$ potential the used radius and diffusivity parameters were taken from the paper [254], and for the

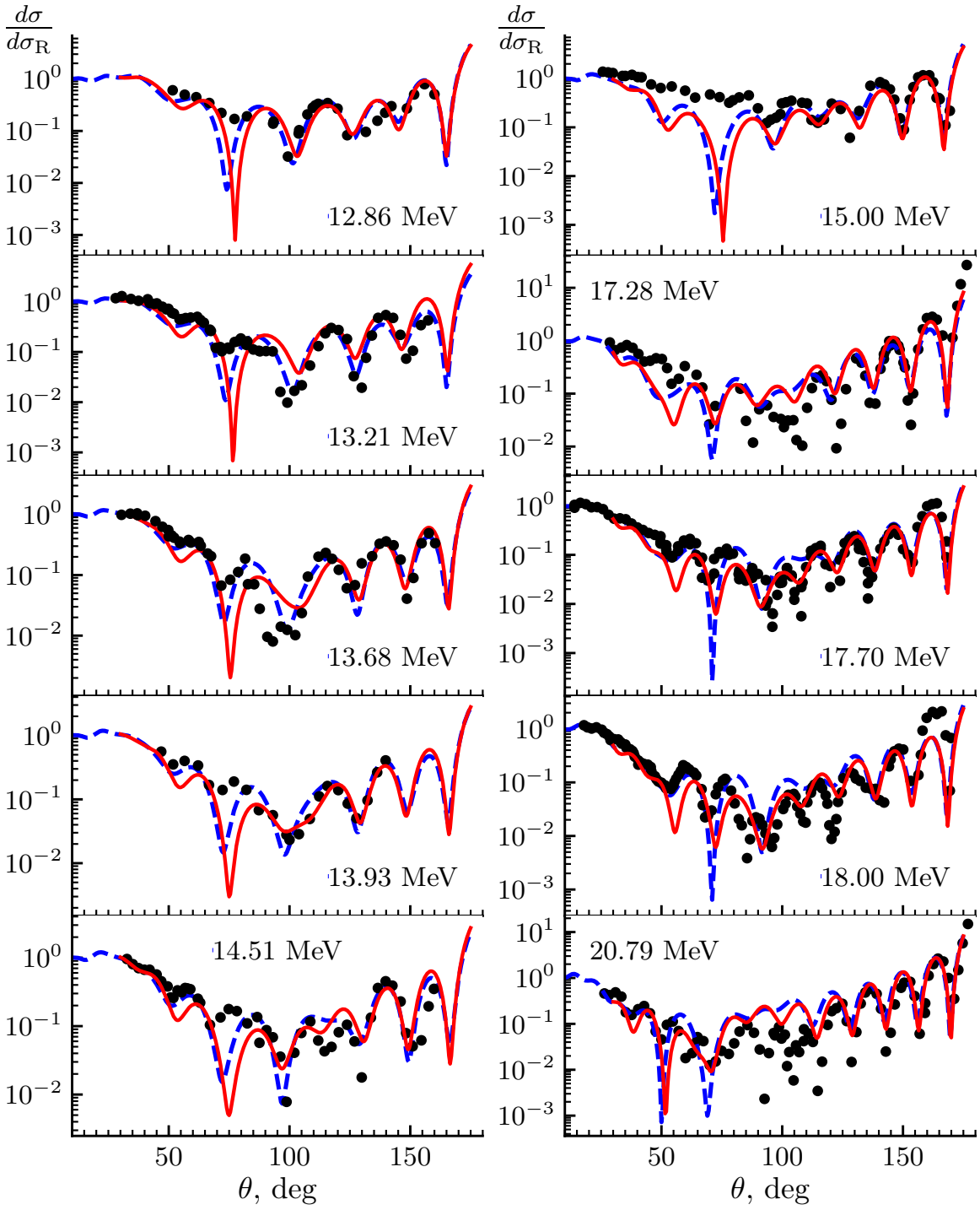


Figure 66. Angular distributions of elastic scattering of nuclei are shown $^{12}C+^{16}O$. Black dots – experimental data (from NNDC [155] database and [255]), blue dashed curve – calculation with $WS1$ potential, red solid curve – calculation with $WS2$ potential.

$WS2$ potential they were chosen as $R_w$=4.81 fm, $a_w$=0.26 fm. The depth for the imaginary part in both cases was taken from the best fit to the experimental data at a given energy. As can be seen from Figure 66, there is good agreement between the model angular distributions and the experimental data for angles larger than 90° for the chosen energy range. At the same time, calculations for quasi-bound

states within the potential model lead to an almost identical dependence for the energy of levels on their angular momentum, but the global quantum number for the potential $WS2$ is one more than for $WS1$.Note that the values of the global quantum number used in our work exceed the value of $G$ obtained on the basis of the phenomenological formula 82. The FRESCO [161] program was used for calculations based on the optical model. The program GAMOW [258] was used to calculate the positions of quasi-bound states.

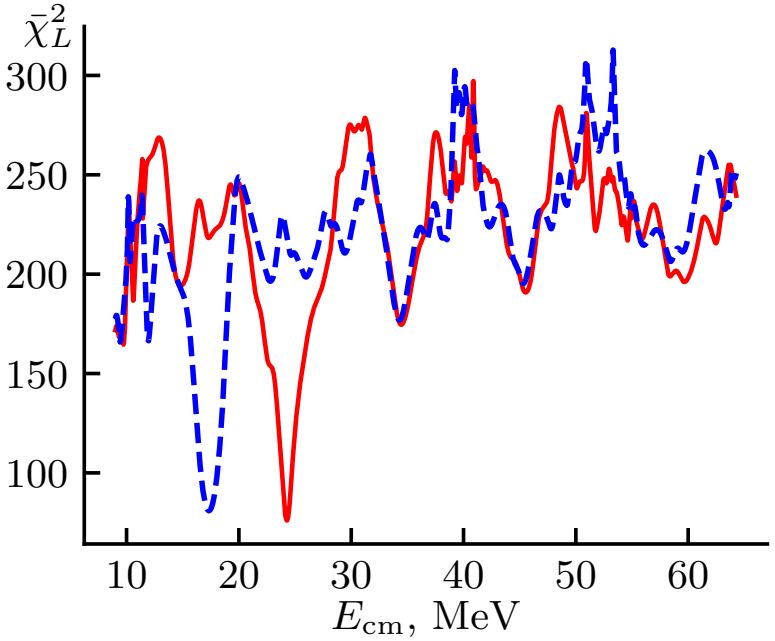


Figure 67. Graph of $\bar{\chi}^2_L$ dependence on energy for polynomials $L = 11$ (blue dashed curve) and $L = 14$ (red solid curve) [53]. The minima correspond to the values of energy $E_{\rm cm} = 17.3$ MeV and $E_{\rm cm} = 24.2$ MeV.

Let us consider the procedure of comparing the model angular distributions with Legendre polynomials of different orders. Figure 67 shows the energy dependence of the value $\bar{\chi}^2_L$ calculated by the formula (107) for the values of angular momenta $L = 11$ and $L = 14$. Similar dependencies were obtained for other angular momenta. Thus, for the range of energies ($E_{cm}$=10-30 MeV) and allowable angular momenta ($L$=8-18) considered in this work, we observe well-marked minima corresponding to the best fit of the model angular distribution to the Legendre polynomial of the corresponding order. Figure 68 shows a comparison of the obtained positions of the minima with the positions of the quasi-bound states for even (odd) angular momenta calculated in the framework of the potential model with values of the global quantum number $G$=22(23) for the potential $WS1$ and

$G$=24(25) for the potential $WS2$. As can be seen, for small values of angular momenta ($L \leq 10$) the obtained plots almost coincide. In addition, the Figure shows the phenomenological dependence for the cluster rotational bands derived from the Abbondanno [105] systematics. Note that up to values of angular momenta of order $L$=9, all three plots almost coincide.

### 6.3. Analysis

Let us consider the result obtained above from the point of view of the possibility of unambiguously determining the angular momenta of the states when comparing the experimental angular distribution of elastic scattering with Legendre polynomials. The excitation function for the $^{12}$C+$^{16}$O reaction was obtained in a number of papers [259–261], and it was found that there are fairly strong oscillations of the cross section values with energy. However, examination of the correlations showed [262] that only the state with energy 19.7 MeV has a significant deviation in the excitation function. From comparison with the Legendre polynomials, the angular momentum $L$=14 was assigned to this state. Note that this state coincides well with the $G$=22 [253] band levels. However, based on the analysis of experimental angular distributions, it was shown [263] that the excitation function must, in addition, also contain a rather significant number of resonances forming rotational bands. This led to the comparison of some rather narrow and sparse peaks of the excitation function to states with a certain angular momentum only on the basis of comparison with Legendre polynomials.

Figure 68 shows the currently available data on resonances with known angular momentum observed in elastic scattering of $^{12}$C+$^{16}$O. As can be seen, most of these states (with the exception of low-lying states) cluster near the systematics line and do not show a splitting that allows us to assign states to bands with specific values of $G$. It is also possible to identify a few states lying above the systematics. These states, in the case of combining them into a rotational band, have a smaller moment of inertia than the potential model allows (even with increasing values of $G$). On the other hand, their positions correspond well to the regions of the excitation function where the angular momentum corresponds to the order of the Legendre polynomial, which best describes the angular distribution. The

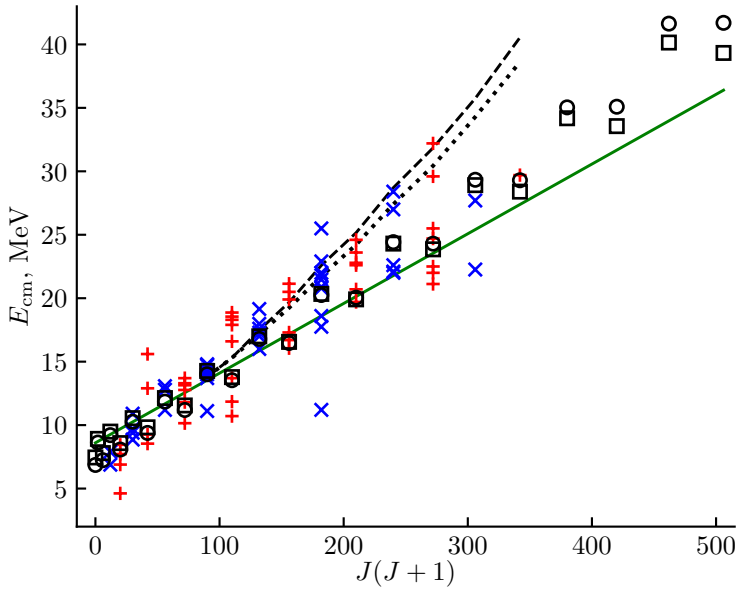


Figure 68. Dependence of the energy of states in elastic scattering of $^{12}$C+$^{16}$O in the center-of-mass system on the angular momentum of the states $J(J+1)$ [53]. Red and blue crosshairs – states with positive and negative parity, respectively. Squares and circles, states obtained within the potential model with potentials $WS1$ and $WS2$, respectively. Solid line, parameterization [105]. Dotted line and dots – values of the minima of the function as shown in Figure 67 for potentials $WS1$ and $WS2$, respectively.

main candidates for these states are: $9^-$, 14.8, 14.4,14.35 MeV [264, 265], $10^+$, 18.3, 18.55,18.87 MeV [266–268], $11^-$, 17. 29, 17.98, 19.15, MeV [267, 268], $12^+$, 19.9, 20.5, 21.4 MeV [260, 268, 269], $13^-$, 22. 0, 22.9, 25.5 MeV [260, 270, 271], $14^+$, 22.79,23.6,24.6, MeV [259,272], $15^-$, 25.5,27.0,28.4, MeV [259,270,272], $16^+$, 29.6,32.2, MeV [261, 272]. All the above states correspond to sufficiently large cross sections of the excitation function. Levels $11^-$, $14^+$ and with higher values of angular momentum were obtained from experimental data for the angular distributions of elastic scattering at large angles, $12^+$ – from the angular distribution of the reaction $^{12}$C($^{16}$O,$^{8}$Be), $9^-$ and $13^-$ – from analysis of the reaction and elastic scattering cross sections. The remaining states were investigated in reactions for both the elastic and inelastic scattering cases, including from the analysis of compound-core decay correlations. The distinguishing feature of these states is their increased energy with respect to the predictions based on systematics and the potential model.

As can be seen from the position of the minima for the $\bar{\chi}^2_L(E)$ function, there is a coincidence with both the states discussed above and the lower-spin resonances. When a fluctuation or resonance with small angular momentum and

small reduced width coincides with a region for which the angular distribution has a polynomial structure at large angles, there may be an error in determining the angular momentum of the state. For example, consider the cross section behavior for the energy corresponding to the minimum with $L$=14 in Figure 67. Figure 69 shows its corresponding angular distribution for the scattering of $^{12}$C+$^{16}$O nuclei with an interaction potential as $WS_2^2$, compared to a 14th-order Legendre polynomial. However, while matching the polynomial well, this model state not only cannot be unambiguously described as a resonance with angular momentum $L$=14, but may not contain a partial wave of this order at all, as can be seen in Figure 69. This leads to the need for a more careful approach in determining the positions and quantum characteristics of resonances in elastic scattering reactions of heavy ions.

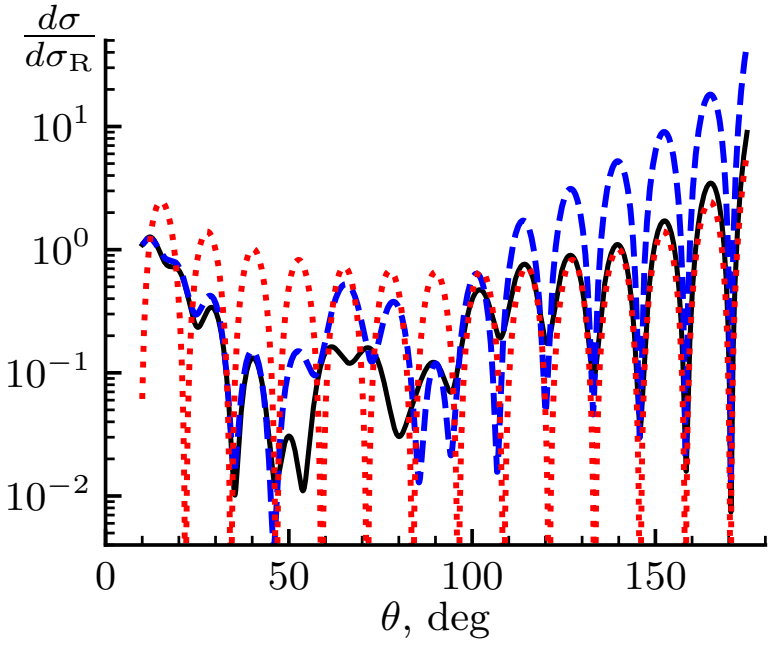


Figure 69. Angular distribution, in the region of the minimum (see Figure 67) for $L$ = 14 [53]. Black solid and blue dashed curves – calculations within the optical model, for the full set of partial waves and with the exclusion of the $L$=14 partial wave, respectively. The red dashed curve is the square of the 14th order Legendre polynomial.

Thus, we see that the selected potentials reproduce well the experimental angular distributions in the region of small interaction energies. This allows us to raise the question about the applicability of these potentials to the problems of astrophysics.

# Chapter 7. Fusion reactions in the cluster approximation

The application of the ideas of the cluster description of nuclei can be useful not only for the case of elastic (quasi-elastic) scattering, but also when considering nuclear fusion processes. Indeed, the initial approach to the description of the fusion cross section assumed complete structurelessness of nuclei and was determined only by the permeability coefficient. The development of this approach led to the appearance of the method of coupled channels and the consideration of the internal structure of interacting nuclei (excitations, deformation), but, at the same time, the uncertainty associated with the phenomenological parameters describing the process - first of all, with the parameters of the potential - increased. At the same time, in the region of low interaction energies there are a number of processes manifested in fusion reactions, which probably have a cluster nature and their qualitative explanation is preferable to be given within the framework of the simplest approach, avoiding unnecessary parameterization. In this paper we will consider two examples – the resonance-like behavior of the excitation function of the $^{12}C+^{16}O$ nuclear fusion reaction (which will allow us to use the results of the previous section) and the systematics of the excitation function of reactions at energies below the Coulomb barrier. Since both cases correspond to small interaction energies, their consistent description is of paramount importance for nuclear astrophysics. The results are reported in the articles [48–50]

## 7.1. Cluster states in astrophysics problems

Nuclear reactions play a key role in the evolution of the Universe, from the Big Bang epoch to the description of stellar evolution. For this reason, it is crucial to estimate the contributions of different reactions to the energy balance of burning elements, which not only gives a deeper understanding of stellar evolution, but also allows us to evaluate the efficiency of different nucleosynthesis variants and compare the results with the data on the abundance of elements in nature. According to modern concepts, we have three types of nuclear transformation processes, the course of which requires a detailed analysis of the reactions accompanying them:

1) Processes accompanying the Big Bang and occurring after the epoch of baryogenesis.
2) Nuclear reactions occurring in stars and stellar atmospheres.
3) Processes occurring in the interstellar medium during the interaction of nuclei with high-energy cosmic rays.

The most important reactions occurring during the Big Bang lead mainly to the formation of helium nuclei, although some models may also consider the formation of nuclei up to and including oxygen [273]. A key feature of this stage is the presence of neutrons, which allows the efficient formation of deuterons in the $p + n \rightarrow d + \gamma$ reaction. Despite the importance of this reaction in understanding the initial nucleosynthesis, it is relatively poorly studied experimentally in the energy range of interest, $0.02 < E < 0.2$ MeV, and we have the main information about it from a detailed equilibrium analysis for the $d + \gamma \rightarrow p + n$ reaction. Further processes are mainly related to the formation of helium isotopes, which allows the subsequent formation of heavier elements.

Despite this, it can be assumed with good accuracy that the expanding Universe immediately after the Big Bang consisted of 75 percent hydrogen and 25 percent helium. Thus, it is these two nuclei that would play a significant role at the very beginning of stellar nucleosynthesis. In addition, $\alpha$-particles are produced as "ash" as a result of hydrogen burning in the *pp*-cycle. Subsequent reactions suggest the participation of carbon, oxygen, and up to and including silicon nuclei as fuel for stellar nucleosynthesis, up to and including the formation of iron nuclei. A good opportunity to clearly demonstrate the processes occurring in stars was the introduction by Kubono in 1994 of the CND Cluster Nucleosynthesis Diagram, which allows us to take into account the basic processes within the cluster approximation [274]. The proposed diagram was a modification of the Ikeda diagram discussed above, which allows us to take into account cluster states in nuclei near the threshold for the cluster+core system. The proposed diagram is shown in Figure 70. The first step considered in this approach is the synthesis of $^{12}$C by capturing the $\alpha$-particle by a resonant (unstable) $^{8}$Be state, thus overcoming the so-called "beryllium gap". The next step is the capture of the $\alpha$-particle in the $^{12}\mathrm{C}(\alpha, \gamma)^{16}\mathrm{O}$ reaction. Thus, the $^{12}$C and $^{16}$O nuclei, well known from the point

of view of the cluster approach, are formed as "ash", besides $\alpha$-particles. Further, the formed nuclei also participate in the combustion process, in turn being sources of $\alpha$-particles and leading to the appearance of even-even *sd*-region nuclei. The next step – reactions with $^{20}$Ne are strongly suppressed due to structural (exactly cluster!) features of the $^{20}$Ne nucleus. Gradually, photodesintegration reactions to clusters become important, according to CND.

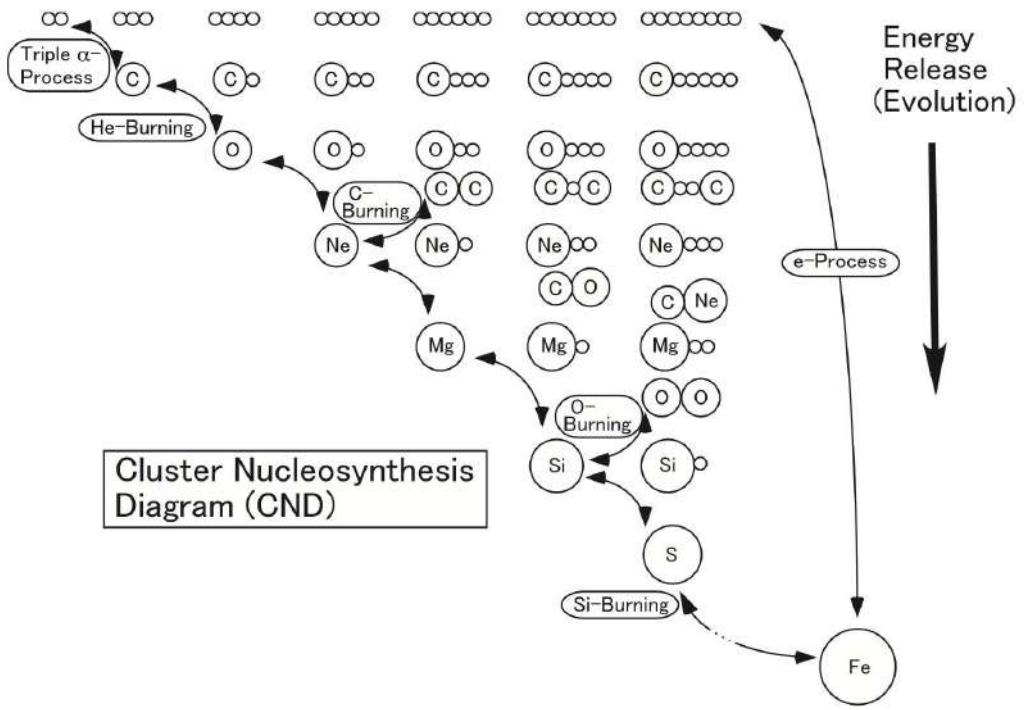


.

Figure 70. Diagram of cluster nucleosynthesis proposed in the paper [274]

It should be noted that the class of reactions considered in this approach is much broader than given in the Figure, so that the only requirement for an appropriate description is a significant overlap of the states considered in a particular reaction with the cluster configurations. Examples of reactions considered in [274, 275] under this approach are

$^{8}$Li($\alpha$,n)$^{11}$B,

$^{14}$O($\alpha$,p)$^{17}$F,

$^{18}$Ne($\alpha$,p)$^{21}$Na,

$^{13}$C($\alpha$,n)$^{16}$O,
and there is also an influence of CND on the reactions associated with $\nu - p$ processes important for understanding the evolution of supernovae of the second type.

## 7.2. Reactions in Nuclear Astrophysics

As stated above, the area of interest of this work is limited to the consideration of reactions described within the CND approach or related reactions with $\alpha$-particles or other clusters in the entrance channel. Thus, there is a significant effect of the Coulomb barrier for energies characteristic of nucleosynthesis reactions at temperatures on the order of $10^7$ K. The Coulomb barrier tunneling probability $P$ can be written in the form:

$$P = \exp(-2\pi\eta), \tag{109}$$

where $\eta$ is the Sommerfeld constant. For particles with charge $Z_1$ and $Z_2$ moving with relative velocity $v$, it is:

$$\eta = \frac{Z_1 Z_2 e^2}{\hbar v}. \tag{110}$$

If the particle energy is expressed in keV and $\mu$ is the reduced mass in AEM, we can write:

$$2\pi\eta = 31.29 Z_1 Z_2 \left(\frac{\mu}{E}\right)^{\frac{1}{2}}. \tag{111}$$

Then, the probability of tunneling through the Coulomb barrier is proportional to:

$$\sigma(E) \propto \exp(-2\pi\eta). \tag{112}$$

On the other hand, the proportionality of the cross section to the de Broglie wavelength must be taken into account:

$$\sigma(E) \propto \pi\lambda^2 \propto \frac{1}{E}. \tag{113}$$

Then from the expressions (112) and (113), for the reaction cross section with

charged particles we can write:

$$\sigma(E) = \frac{1}{E}\exp(-2\pi\eta)S(E), \tag{114}$$

where the function $S(E)$ is called the astrophysical $S$-factor. This value is usually used instead of the reaction cross section, including for reactions with heavy ions at low energies. In most cases it is obtained directly from the formula (114) in the form:

$$S(E) = \sigma(E)E\exp(2\pi\eta), \tag{115}$$

although there are also its modifications.

When studying the processes occurring in supernovae and at the late stages of development of supermassive stars, it is necessary to take into account the combustion of carbon and oxygen and heavier nuclei. For this purpose, it is necessary to study the fusion reactions of such nuclei at low energies characteristic of stars. The energy region of the most intense occurrence of these processes has been called the "Gamov window". We have closely approached this energy region for the interaction of light and heavy nuclei [276, 277], but for intermediate masses the situation is still ambiguous. In recent years, progress in experimental work on the study of nuclear fusion at sufficiently low energies has allowed us to obtain reliable estimates of the astrophysical $S$-factor for reactions with $^{12,13}$C,$^{16}$O nuclei. One interesting feature for the derived excitation functions was the appearance of a resonance-like structure for $^{12}$C+$^{12}$C+$^{12}$C fusion reactions at energies $E_{cm}$¡6 MeV [278]. Several models have been proposed to explain the behavior of the cross section, including those treating the observed structure as a manifestation of molecular resonances coupled to fragmentation by overlapping compound states [282]. On the other hand, an explanation within the framework of isolated compound states [278] has been proposed. In this work, it was shown that this structure can be explained within the framework of the cross-sectional fluctuation model, when the width of resonances in a system of nuclei becomes comparable to the average distance between them. This approach made it possible to satisfactorily describe the expected regions of the resonance-like structure in the $^{12}$C+$^{12}$C reaction and to predict the energy region for its observation in other

reactions, for example, with oxygen and carbon nuclei. Thus, for the $^{12}C+^{16}O$ fusion reaction, this region will be limited to energies of the order of 2 MeV, but experimental results indicate its presence up to energies of about 7.5 MeV or even higher. Thus, the reaction mechanism described in [278] probably has only limited application to the $^{12}C+^{16}O$ fusion reaction, at least in the energy region of 3-7.5 MeV. In the work [279], the manifestation of such states was also considered from the position of the AMD model. The existence of several rotational bands was predicted and data on the possible position of low-lying resonances with positive parity near the Gamowindow were obtained. On the other hand, as discussed above, the $^{12}C+^{16}O$ nuclei system is known to have a large number of resonances, which are regarded as members of rotational bands and are of molecular [253] character.

### 7.3. Interaction Potential

In the present work we have considered the processes of the appearance of suprathreshold and subthreshold molecular resonances in the $^{28}Si$ nucleus at interaction energies $^{12}C+^{16}O$ near the Gamow window. These reactions are essential for the processes occurring during the formation of type Ia supernovae and in massive [280] stars. One of the distinguishing features of these reactions is the manifestation of a resonance-like structure in the excitation function of the fusion reaction for energies below $E_{CM}<10$ MeV, so that, in the case of the presence of a resonance near the Gamow window, the nuclear interaction cross section can increase by a factor of several. Such resonance-like structure was most strongly observed in the $^{12}C+^{12}C$ reaction and, to a lesser extent, in the $^{12}C+^{16}O$ reaction, while for the $^{16}O+^{16}O$ reaction such structure was hardly observed [278]. The applicability of the cluster approach to these reactions allows their sequential inclusion in the cluster nucleosynthesis diagram (DNC) [274], which implies the possibility of molecular states leading to strong fluctuations in the fusion cross section. Significant success in the experimental study of the excitation function for fusion reactions has provided experimental data for the deep sub-barrier interaction in the region around 3 MeV [281]. Several models have been proposed to explain the behavior of the cross section, including those treating the observed

structure as a manifestation of molecular resonances coupled to fragmentation by overlapping compound states [282]. On the other hand, an explanation within the framework of isolated compound states [278] was proposed. A boundary energy below which the occurrence of structure can be explained by the fluctuation of the cross section due to the presence of non-overlapping compound states was obtained. The value of the boundary for the $^{12}$C+$^{12}$C fusion reaction was of the order of 7.3 MeV, which almost completely covers the range of the observed structure, while for $^{12}$C+$^{16}$O this value was of the order of 1.8 MeV. This is well below the energies available for experimental studies to date [281]. Thus, the $^{12}$C+$^{16}$O reaction was chosen to determine the contribution of molecular states, on the one hand having a low threshold for the manifestation of fluctuations from compound states, and on the other hand exhibiting a well-observed structure in the cross section of the fusion reaction.

To eliminate the ambiguity mentioned in [279] related to the choice of the model describing the $^{12}$C+$^{16}$O reaction, the following conditions were imposed on the interaction potential:

1) Qualitative description of the angular distribution of elastic scattering in the energy region corresponding to the small probability of quasi-elastic transmission of the $\alpha$-particle.

2) Description within the potential model [11] of the observed resonances attributed to the rotational band near the Abbondanno [105] systematics.

3) Agreement of the fusion cross section calculations with the experimental value of the astrophysical $S$-factor at energies on the order of 7.5 MeV.

An additional condition may be the requirement to reproduce the widths of states and the probabilities of transitions between them, as we have done, for example, for the case of rotational bands in the $^{40}$Ca nucleus. However, for heavy nuclei this information is usually missing, which may lead to the use of potentials that allow anomalously broad “unphysical” states [253].

These conditions are well met by the potentials we used earlier in Table 24. However, this approach requires the introduction of a global quantum number, which can be determined by the Wildermuth formula (23) not for all potentials [107] and not for all cluster-cor [109] combinations, especially in the case

of approximate equality of their masses.

Figure 71 shows the energy dependence of the fusion cross section for the considered potentials, and the experimental data [283–286]. The theoretical value of the cross section was determined in a model with a boundary condition on the wave function defining the absorption of the incident wave [287]. As can be seen, both potentials give good agreement with the experimental results up to the minimum values known to date, near the Gamow window. It should be noted that similar results are observed for a rather wide class of potentials, such as the deep double convolution potential [288] or the shallow potential of the rectangular potential well [289]. However, in the low energy region, the deep potential, as well as the barrier passage [290] model, give deviations from the experimental values of the $S$-factor. On the other hand, the application of the rectangular pit may be associated with certain difficulties in interpreting the results obtained [291]. This issue will be discussed in detail below.

.

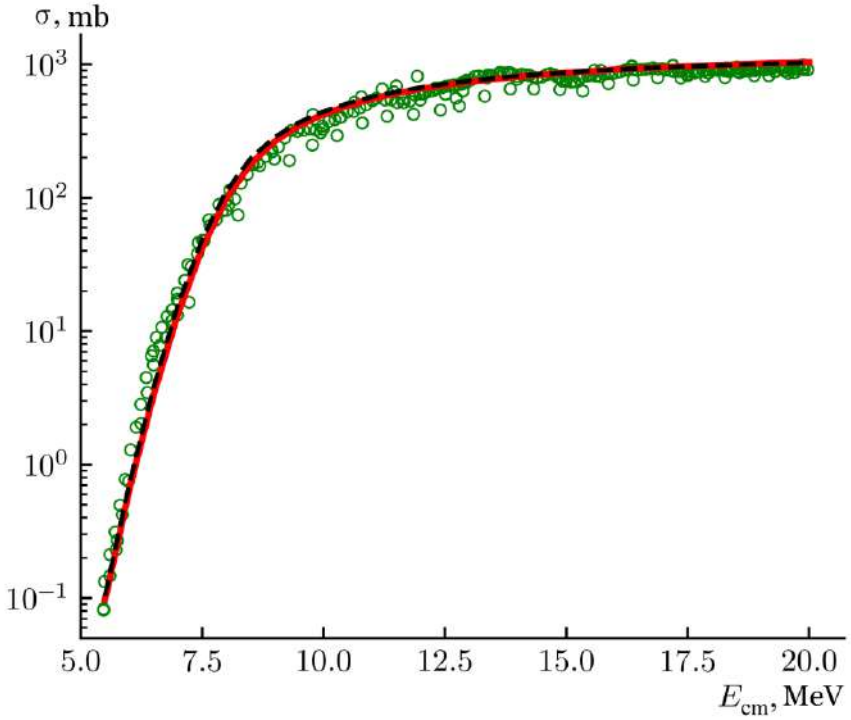


Figure 71. Fusion cross section $^{12}$C+$^{16}$O. Circles – experimental data [155]. Solid line – calculation for $WS2$ potential, dashed line – for $WS1$ potential [49].

Following the approach of describing the interaction of nuclei within the potential model developed in [11, 253], we consider the resonance and bound states arising for these potentials. The numerical solution was obtained using the pro-

gram GAMOW [258]. Since, as mentioned above, the choice of the global quantum number for the considered system is difficult, we should be guided by the description of the existing resonances. For the potential $WS1$ [253], most of the resonances observed in the system $^{12}C+^{16}O$ are well described by the rotational band $G$=22(23) for even (odd) states. Similar results are obtained for the $WS2$ potential when $G$=24(25). The moment of inertia for such rotational bands as well as the value for the average energy of the ($0^+$-$0^-$) states E(0) agree well with the systematics of the work [105]. The averaging data for the resulting parity splitting are presented in Table 25.

.

Table 25. Bands parameters [49].

| Parameter | $WS1$ | $WS2$ | Systematics [105] |
|---|---|---|---|
| $E(0)$ MeV | 6.9 | 7.5 | 8.6 |
| Moment of inertia parameter | 71.3 | 67.2 | 55.0 |

Thus, we can assume that these potentials equivalently describe high-lying rotational bands with large angular momentum values. If a low-lying band exists, it should have a close moment of inertia parameter, and its head level should be located either near the binding energy of -16.76 MeV or near the threshold.

This leads to the need to consider bands of several types. For the first-type band, both potentials predict states with strong parity splitting (on the order of 7 MeV), with $G$=18(20) for WS1 and 20(21) for WS2. The positive parity levels form a ground state band in the $^{28}Si$ core with flattened strain, having a much smaller moment of inertia [292]. Note that the states with negative parity, which can be considered as candidates for this band, despite a very good energy match, are not expected to belong to a particular band.

The bands of the second type $G$=20(21) for WS1 and $G$=22(23) for WS2 in both cases have a moment of inertia parameter on the order of 600 keV and a parity splitting on the order of 5 MeV. Since the average value of $E(0)$ is of the order of 1 MeV, some of the low-spin states ($0^+$,$2^+$ and $4^+$ for WS1 and $0^+$,$2^+$ for WS2) are located below the threshold.

Figure 72 shows a comparison of the positions of the resonances obtained from the potential model with the referential data for which the boundaries of

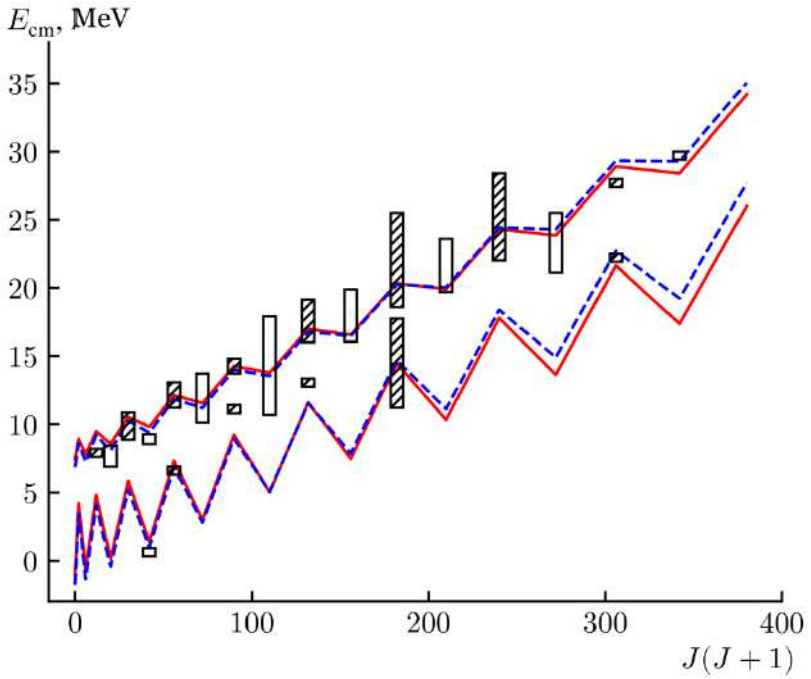


Figure 72. Position of resonances in the system $^{12}$C+$^{16}$O. Rectangles indicate fragmentation regions obtained from experimental data (shaded, unshaded – negative and positive parity, respectively). The solid line is the calculation within the potential model for $WS2$, the dashed line is for the potential $WS1$.

the fragmented states [293–296]. As can be seen, there are several states near the predicted resonances for the low-lying bands. The states $1^-$-$7^-$ are located directly above the threshold and, on the one hand, already have high enough excitation energies for their experimental detection. On the other hand, these states do not overlap with the states of the overlying band and with states of positive parity.

As in the case of high-lying states, such quasi-molecular resonances can lead to oscillations of the fusion cross section. Figure 73 shows the energy dependence of the $S$-factor. The solid line and dashed line show the calculations for the $WS2$ and $WS1$ potentials. Both curves describe the experimental result well under the assumption that the cross section in this region can be represented as:

$$\sigma_r = \sigma_{res} + \sigma_{non}, \tag{116}$$

where $\sigma_{res}$ is the cross section of resonant processes and $\sigma_{non}$ is the cross section of non-resonant interaction, which can be reproduced in the framework of the coupled channel model [287].

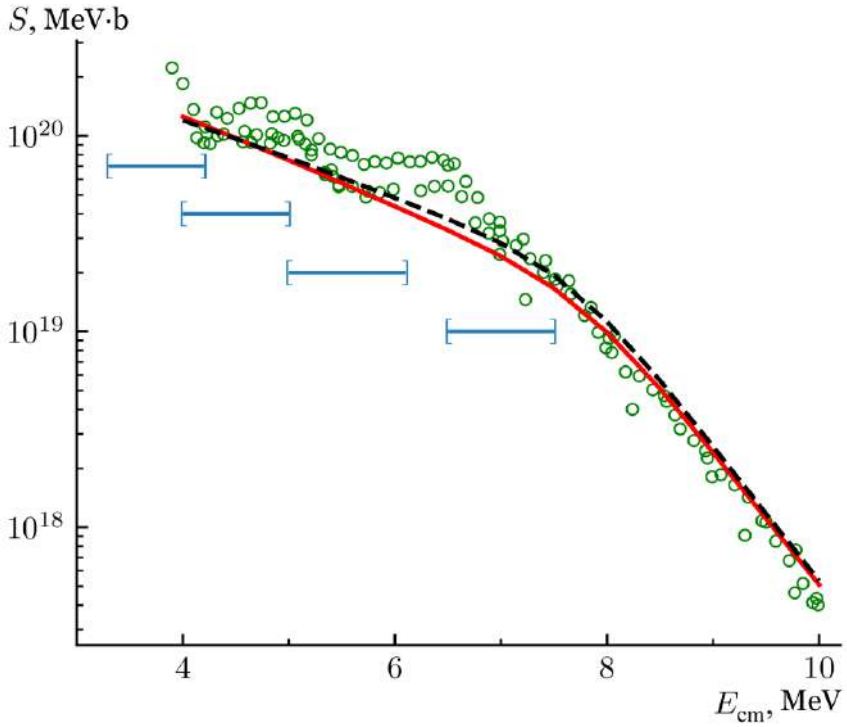


Figure 73. Astrophysical S-factor for the $^{12}C+^{16}O$ reaction [49]. Solid line – calculation for the $WS2$ potential, dashed line – for the $WS1$ potential. The horizontal lines indicate the interval for the states (from left to right) $1^-$, $3^-$, $5^-$, $7^-$.

Thus, if for the system $^{12}C+^{16}O$, the resonance-like states predicted in the paper [278] should be observed up to energies of the order of $E_{cm}$=2 MeV, the existence of the corresponding structure in the region 3-7.5 MeV [281,297] can be explained by the contribution from states with molecular nature. As can be seen from the figures, low-lying resonance states with negative parity are located in this region. It should be noted that the model used does not allow us to unambiguously identify the positions of the resonances. In the excitation energy region under consideration, the difference between the predictions for the two potentials is of the order of 700 keV, which is comparable to the expected distance between the levels. Table 26 summarizes the results of calculations of the energies of low-lying states with approximate positions of possible maxima of the experimental cross section.

The present results indicate only an approximate region of the appearance of molecular states, both because of the ambiguity in the choice of potential parameters discussed in this work and the possible energy dependence of the potential.

.

Table 26. Band parameters [49].

| Experiment [281, 297] MeV | $WS1$ MeV, $J^\pi$ | $WS2$ MeV, $J^\pi$ |
|---|---|---|
| | 3.4, $1^-$ | |
| 3.9 | 4.1, $3^-$ | 4.2, $1^-$ |
| 4.9 | 5.2, $3^-$ | 4.8, $3^-$ |
| 6.1 | | 5.9, $5^-$ |
| 6.6 | 6.8, $7^-$ | |
| 7.2 | | 7.3, $7^-$ |

## 7.4. Description of quasi-bound states in the framework of the potential model

To date, there have been a significant number of papers considering one or another aspect of potential models to calculate cross sections, the astrophysical $S$-factor, or the possible position of resonances in reactions with heavy ions [76, 291, 298, 299]. Depending on the goals of the work, potentials from the simplest case of a rectangular pit, allowing an analytical solution [291], to a potential with a large number of parameters, taking into account the dependence on the angular momentum [298] or constructed on the basis of a semi-microscopic description [299], can be used. Let us briefly consider the manifestation of the ambiguity in the choice of potential mentioned in the previous section. We will proceed from the three positions we have established.

The potential model gives a good description of the arising molecular states belonging to rotational doublets for the case of $\alpha$-particle+cor [76], but in the case of heavy nuclei, as it was indicated, there is a problem of experimental identification of such states [253]. The strong sensitivity of the calculations to the potential parameters leads to difficulty in identifying unknown resonances in order to determine their angular momentum. In the cluster approximation, the rotational band (doublet) is defined by a condition on the wave function in the form of the parameters $G$ – global quantum number, $N$ – number of nodes of the wave function in the cluster approximation, $L$ – angular momentum of the state under consideration. For the case of the $1s0d$ shell, $G \geq 24$. The application of such a formula assumes that the integral of the overlap of the wave functions for the single-particle states in the considered potential and the corresponding oscillator

wave functions is close to unity. For the system of $^{12}$C+$^{16}$O nuclei, despite the closed oxygen shells, the use of this formula may be insufficiently justified. A variant of the phenomenological assignment of the number $G$ was also considered, but its definition was limited to the potential proposed in the paper [300]. For the studied system of carbon and oxygen nuclei, the phenomenological value was $G \geq$18. Also, the ambiguity in the choice of the $G$ value within the RGM, OCM, and SU(3) model approaches, is discussed in paper [253]. Thus, the parameter $G$ cannot be determined unambiguously. In addition, according to [76, 253] one can expect the appearance of several rotational bands with different global quantum numbers.

Using the data known to date on the manifestation of resonances corresponding to rotational doublets in nuclei, we can assume that the head state $0^+$ of the first band will be located near the binding energy $^{16}$O and $^{12}$C in the $^{28}$Si nucleus (-16.8 MeV). We will denote it as $L$ – the band. The band of resonances close to the maximum angular momenta allowed in this system should also be observed. Let us denote it as the $H$-band. According to the systematics of the [105] paper, this should be a weakly split band with a mean value of $0^+$-$0^-$ of the order of 8.6 MeV and a slope of the rotational band of about 0.055 MeV.

Using the methods proposed in [49], several optical potentials suitable for describing the $^{12}$C+$^{16}$O interaction were considered in this work. Various parameterizations of the quadratic Woods-Saxon potential and a potential derived from a semi-microscopic approach, the Sao Paulo potential (SPP), taking into account the nucleon density calculated on the basis of the Dirac-Hartree-Fock [301] model, have been considered. This potential was successfully used by us earlier in the description of angular scattering of $\alpha$-particles on the $^{14}$C [51] nucleus.

1. The deep potential for elastic scattering in the energy range ECM = 10 - 30 MeV obtained using Bayesian analysis [302].

2. SPP potential with a normalization factor equal to one.

3. The phenomenological potential from the previous section $WS2$.

4. The phenomenological potential from the previous section $WS1$.

5. Potential derived from systematics data for optical potentials (previous 4 items), with a requirement to reduce the number of wave function nodes.

The characteristics of the potentials under consideration are summarized in Table 27.

Table 27. Potential parameters [48]. The radius value is defined as $R = r_0(A_P^{1/3} + A_T^{1/3})$. Potential 2 was the SPP potential with a normalization factor equal to one. Potential parameters 3 and 4 were taken from Table 24.

| Potential | $V$ MeV | $r_0$ fm. | $a$ fm. |
|---|---|---|---|
| 1 | 390.6 | 0.902 | 1.11 |
| 2 | SPP | | |
| 3 | 320.0 | 0.87 | 1.3 |
| 4 | 305.0 | 0.83 | 1.4 |
| 5 | 295.9 | 0.75 | 1.5 |

## 7.5. Rotational bands in the heavy ion system

The positions of the resonances were obtained with the condition of reproducing the energies given for the $L$ and $H$ bands. The calculation was carried out within the model proposed in [258]. For all potentials considered, the gap between two neighboring doublets was of a magnitude much smaller than the required energy difference for the $L$ and $H$ bands (25.4 MeV). This suggests that another band exists between them. Let us denote it by the $M$-band. The existence of such a band for states with positive parity was predicted within the AMD model in [279]. Estimates for the position of the $0^+$ head level give a value in the region of – 6 MeV, so that the doublet should form near the threshold.

.

Table 28. Positions of the head levels $E(0^+)$ and $E(1^-)$ of the considered doublets and the corresponding global quantum numbers $G$ [48].

| Potential | 1 | 2 | 3 | 4 | 5 |
|---|---|---|---|---|---|
| Band | $H$ | | | | |
| $E(0^+)/E(1^-)$ MeV | 6.84/9.12 | 5.34/8.27 | 7.41/8.90 | 6.91/8.62 | 7.82/9.03 |
| $G(+)/G(-)$ | 28/29 | 26/27 | 24/25 | 22/23 | 20/21 |
| Band | $M$ | | | | |
| $E(0^+)/E(1^-)$ MeV | -4.60/2.15 | -5.85/0.55 | -1.07/4.22 | -1.77/3.42 | 0.81/5.32 |
| $G(+)/G(-)$ | 26/27 | 24/25 | 22/23 | 20/21 | 18/19 |
| Band | $L$ | | | | |
| $E(0^+)/E(1^-)$ MeV | -21.4/-12.4 | -21.4/-13.1 | -14.5/-7.20 | -14.9/-7.70 | -11.2/-4.53 |
| $G(+)/G(-)$ | 24/25 | 22/23 | 20/21 | 18/19 | 16/17 |

Table 28 lists the values of the $0^+$ and $1^-$ states for all $G$ values considered

for the $G$ values corresponding to the formation of the $L$, $M$, and $H$ bands. The question of the ambiguity of the potentials used to describe elastic scattering was considered earlier in [49]. We next consider the issue of ambiguity in the definition of the potential to describe the fusion cross section by analogy with the ambiguity arising in the analysis of elastic scattering.

In our determination of the potential parameters, the following ambiguities arose: for phenomenological potentials, there was an almost linear decrease in the depth of the real part of the potential with increasing radius value. When extracting the potential on the basis of Bayesian methods, a stable correlation of the kind of proportionality of the imaginary potential to the value $1/\sqrt{W}$, where $W$ is the depth of the imaginary potential, appeared. Thus, for the description of the fusion cross section we have an ambiguity similar to that arising in the description of elastic scattering. The ambiguity in the choice of potential can also be seen in Figure 74, which shows the value of the astrophysical $S$-factor for the considered potentials and comparison with available experimental data and their fitting within the framework of the phenomenological model [290].

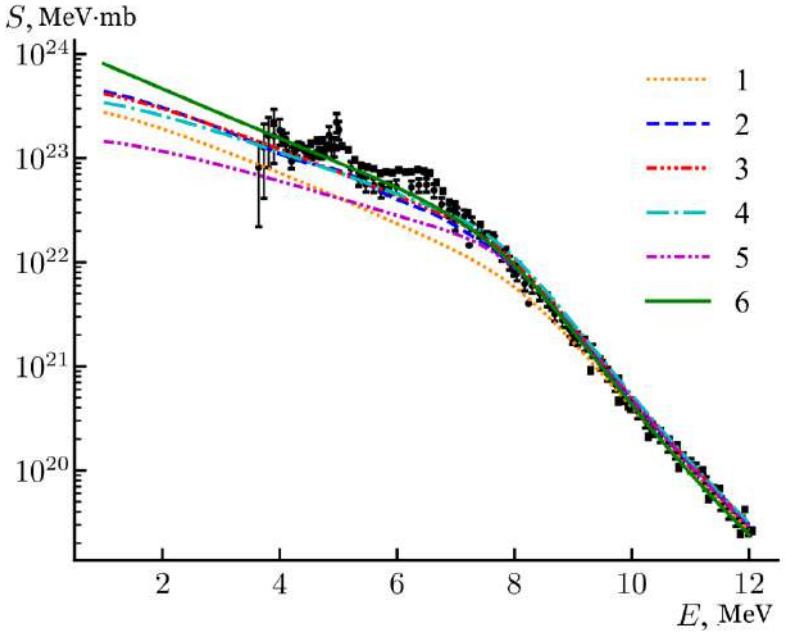


Figure 74. The value of the astrophysical $S$-factor as a function of energy [48]. Shown are the experimental values [281] and cross sections obtained from the coupled channel model with potentials 1 - 5 from Table 27. Curve 6 corresponds to a fit of the cross section to the experimental data from the paper [290].

As can be seen, the results, for potentials 2,3 and 4 are almost identical and close to the fitting curve. The method with the condition of strong absorption

under the Coulomb barrier [287] was used to obtain the fusion cross section.

As can be seen from Figure 74, if there is a cross section hindrance effect in the low energy region in a given reaction, it is observed only for the last point. Additionally, it should be noted that a number of proposed models allow the $S$-factor to drop with decreasing interaction energy in the framework of the potentially [303] model, which will be used in the next chapter.

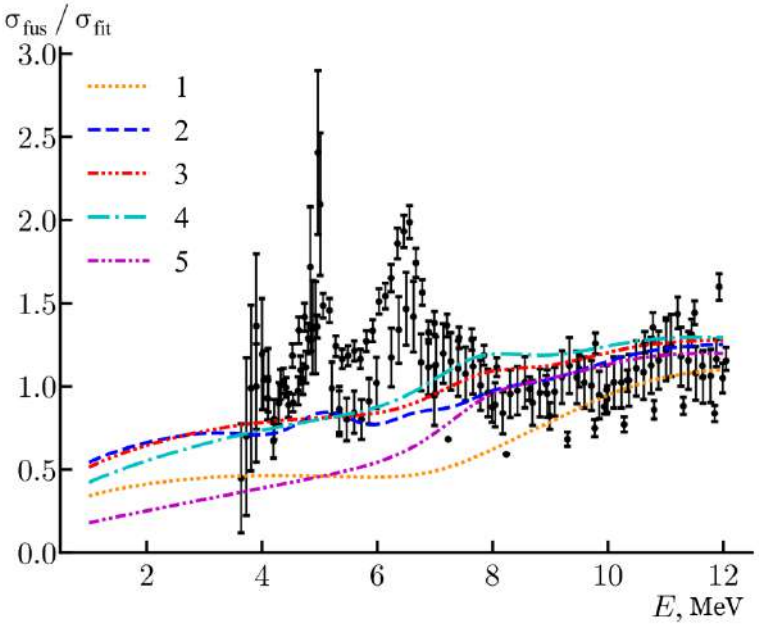


Figure 75. Normalization of the experimental and theoretical cross section for potentials 1 – 5 from Table 27 [48] to the fitted cross section values from the paper [290].

.

Table 29. Parameters of rotational band [48].

| Angular momentum of the state with energy 3.92 MeV | Energy of the state $1^-$ MeV | MeV slope parameter |
|---|---|---|
| $3^-$ | 3.31 | 0.06 |
| $5^-$ | 2.47 | 0.05 |
| $7^-$ | 1.81 | 0.04 |

Next, we consider the positions of resonances in the low-energy region from the viewpoint of the potential model. According to the data given in Table 28, one can expect the appearance of low-spin resonances of negative parity in the energy region up to 12 MeV. For clarity, this is demonstrated in Figure 75, where we normalize the experimental data by the value of the fit [290]. The resonance structure with sharp maxima in the energy region of 3.92 MeV, 5 MeV, 6.5 MeV,

and 8.6 MeV is clearly visible in the plot. In [281], the possibility of describing the first two peaks within the framework of R-matrix theory was shown. There are several possibilities for including these peaks in the sequence of states with negative parity belonging to the $M$ band. Depending on the choice of the angular momentum of the initial state (3.92 MeV), the band will be characterized by the parameters ($1^-$ level energy and band slope) listed in Table 29. The band for potential 4 has the closest characteristics, predicting for the $3^-$ state an energy of 4.1 MeV and a slope parameter of 0.05 MeV. At the same time, it should be noted that the condition of reproducing the positions of the resonances has the strongest sensitivity to the parameters of the potential, so the requirement for an exact match between the molecular resonances and the experimental data does not seem reasonable. It should be noted that in such an approach no obvious connection between the spin of the considered state and the number $G$ is observed (see Table 29). Thus, in potential 2, a state appears at energy 3.85 MeV with angular momentum $7^-$, and in potential 3, at energy 4.2 MeV with angular momentum $1^-$. Thus, to remove the ambiguity, it is necessary to experimentally determine the value of the angular momentum of the states under consideration.

As a conclusion, we compare the results obtained in this work and in the framework of the AMD model. The result is presented in Figure 76. The presented result is similar to Figure 68, but in this case, potential 2 from Table 27 was chosen for comparison, resulting in an additional node in the wave function. As can be seen, for the band $G$=26-27 there is a good agreement with both the experimental results and the calculations AMD performed in [279].

Thus, it is shown that there is ambiguity in the choice of potential for each of the processes under consideration, but all three processes can be described simultaneously by a single potential, and specifying the angular momentum of the low-energy states can remove the ambiguity. As can be seen from Table 29, all the considered potentials predict the existence of resonances for the $M$-band in the energy region below three MeV, which corresponds to temperatures below $10^9$ K attainable in hot stars. Thus, these resonances can significantly affect the intensity of element formation in heavy ion fusion reactions in stellar nucleosynthesis, and their consideration provides important information for analyzing stellar evolution

.

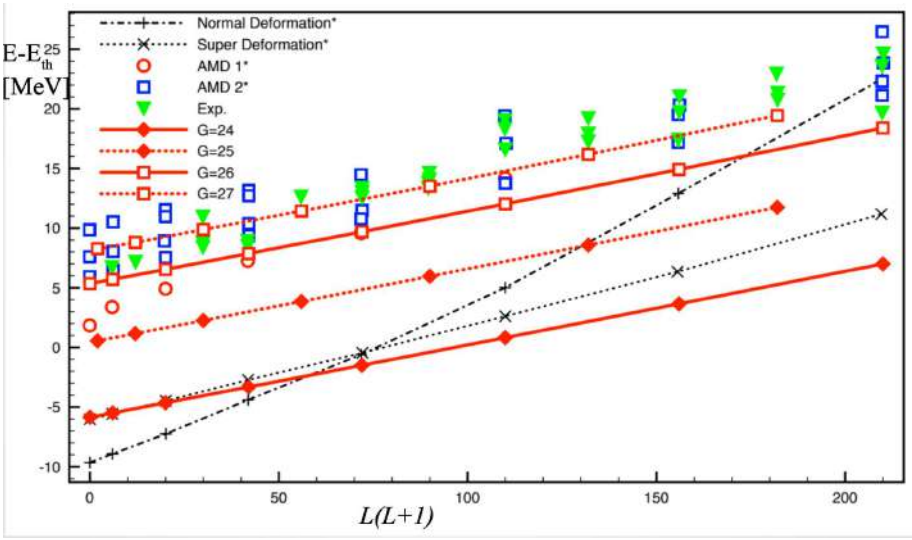


Figure 76. Comparison of $G$=26-27 band position [48] with experimental data [155] and AMD calculations from the paper [279].

processes.

## 7.6. Determination of the astrophysical $S$-factor for the cluster approximation in the framework of the rectangular potential well model

.

Conventionally, all the reactions considered in the CND framework can be categorized into two groups – reactions with $\alpha$-particles and heavy ion fusion reactions. The first group of reactions can be considered directly within the potential model, taking into account possible resonances, e.g., as suggested in [304]. Unfortunately, this approach does not always allow one to describe the occurrence of narrow resonances. It is convenient to consider the second group in the framework of an approximate optical model by introducing a complex potential and determining the corresponding fusion cross section. This was done in the last chapter, but the systematics is complicated by the presence of a large number of parameters. In this chapter we will consider the simplest quantum model of a rectangular hole, which allows, at the same time, to describe very well the fusion cross section with a minimum number of free parameters. The results were presented by us in the paper [50].

In recent years, a large number of experimental works have appeared devoted to the study of fusion reactions at energies below the Coulomb barrier [305].

Special interest in such works arises because of their importance for analyzing the processes of stellar nucleosynthesis, studying the formation of superheavy elements and exotic states of nuclear matter. To describe the observed excitation functions in fusion reactions (FRs), a number of approaches have been proposed, relying both on phenomenological models [306] and on various approximations within the potential model. In the simplest case, the cross section for the MS can be estimated by setting a boundary condition for the wave function and introducing some value of the radius at which complete absorption occurs. Taking into account the coupled channels in this case, it is possible to describe the MS cross section more effectively in a wide range of masses and energies [287]. The uncertainty arising in this case can be reduced by taking into account the known resonances in the system under study. Approaches involving convolution-based potentials [307] and unified potentials [301] reduce the number of parameters, but this approach is difficult for the imaginary part of the potential.

An interesting way to account for the real and imaginary potentials with a small number of parameters is to use the simplest version of the potential – a rectangular pit, with the radii of the imaginary and real parts coinciding. This was one of the first models with which to analyze FRs important for astrophysical purposes [308]. In a paper [291] on the validity of such a model, a number of artifacts arising in the process of describing the MS cross section were considered and it was concluded that such a description was acceptable. One of the main consequences of such a model is the presence of a core – the real part of the potential is taken with a plus sign [289], so that this type of potential is labeled "small". At the same time, it was noted in [291] that this behavior of the potential is not due to a manifestation of its microscopic nature (e.g., the Pauli prohibition). For a correct systematics, it is necessary to clarify this issue.

We have addressed the question of the parameter systematics of the rectangular potential model that has been used to describe the sub-barrier fusion of nuclei from CND. So far, this approach has been applied to single nuclei, not allowing us to obtain the dependence of the potential parameters on the charge and mass numbers of the nuclei involved in the reaction. In the present work, we analyzed the RS between spinless nuclei, which play an important role in stellar

nucleosynthesis processes, at energies below the Coulomb barrier, in the mass range $A$=2-28 [50].

Calculations were performed within the formalism proposed in [309] for a rectangular pit of radius $R$ and a potential with real and imaginary parts ($V$+i$W$) equation (30). The permeability coefficient for the partial wave $l$, in this case, can be written as:

$$T_l = \frac{4P_l \mathrm{Im}(f_l)}{(1 - S_l \mathrm{Re}(f_l) + P_l \mathrm{Im}(f_l))^2 + (P_l \mathrm{Re}(f_l) + S_l \mathrm{Im}(f_l))^2}. \tag{117}$$

The functions $P_L$ and $S_L$ are defined in terms of the regular and irregular Coulomb wave functions $F$ and $G$. Unfortunately, in the literature, the value of $P_L$ denotes both the barrier permeability (formula 34) and the *permeability parameter* used in the calculation of the reduced level width (formula 47). In this section, the second option will be used:

$$P_l = \frac{kR}{F_l^2 + G_l^2}, \tag{118}$$

$$S_l = kR \frac{F_l F_l' + G_l G_l'}{F_l^2 + G_l^2}, \tag{119}$$

where the wave vector of the free particle $k = \sqrt{2\mu E/\hbar^2}$. The wave vector inside the hole can be written in the form:

$$K = \sqrt{2\mu(E - V + \mathrm{i}W)/\hbar^2}. \tag{120}$$

Here $\mu$ is the reduced mass, $E$ is the energy in the center-of-mass system, $V$ is the real part of the potential, and $W$ is the imaginary part. $f_l$ is the complex logarithmic derivative of the wave function in the region of the potential well. As stated in [291], such a wave function can be considered proportional to $\exp(-\mathrm{i}Kr)$. Our comparison of this approximation with the wave function obtained by numerical solution of the Schrödinger equation with the considered potential described by means of splines [310] has shown the correctness of the chosen approach. In this case, the logarithmic derivative at the boundary of the potential can be written as $f_l = \mathrm{i}/(KR)$. To estimate the cross section of the RS from the formula (33) we have [291]:

$$\sigma_{fus} = \frac{\pi}{k^2} \sum_l w_l (2l+1) T_l. \tag{121}$$

The multiplier $w_l = 1 + (-1)^l$ applies to the case of merging identical nuclei.

Using the obtained formulas one can calculate the values of the astrophysical $S$-factor. Since in this work it was assumed to consider only energies below the Coulomb barrier, it is convenient to carry out the corresponding normalization of $E/V_C$ when comparing the theoretical results with the experiment. The value of the Coulomb barrier was assumed to be equal to:

$$V_C = \frac{Z_T Z_P e^2}{1.36(A_T^{1/3} + A_P^{1/3}) + 0.5}. \tag{122}$$

In this work we considered the fusion processes of combinations of nuclei: $^{12}$C, $^{16,18}$O, $^{20}$Ne, $^{24}$Mg, $^{28,30}$Si. The experimental data were taken from the EXFOR [311] database. The potential parameters $V, W, R$ were determined by minimizing the value $\chi^2$, which, in turn, characterizes the discrepancy between the values of the $S$-factor theoretically calculated by the formula (119) and its experimental values. The fit was limited to the region of energies below the Coulomb barrier. The obtained values of $V, W, R$ are given in Table 30.

Table 30. Parameters of the potential of a rectangular well from the work [50].

| Reaction | $V$ MeV | $W$ MeV | $R$ fm |
|---|---|---|---|
| $^{12}$C+$^{12}$C | 3.9 | 1.16 | 6.8 |
| $^{12}$C+$^{16}$O | 5.7 | 1.01 | 7.5 |
| $^{12}$C+$^{18}$O | 4.8 | 3.70 | 7.8 |
| $^{16}$O+$^{16}$O | 9.2 | 1.92 | 8.1 |
| $^{12}$C+$^{20}$Ne | 7.8 | 2.01 | 7.7 |
| $^{16}$O+$^{18}$O | 7.9 | 2.22 | 8.2 |
| $^{12}$C+$^{30}$Si | 11.2 | 0.72 | 7.9 |
| $^{12}$C+$^{24}$Mg | 9.8 | 0.56 | 7.6 |
| $^{24}$Mg+$^{24}$Mg | 20.8 | 6.8 | 8.9 |
| $^{28}$Si+$^{28}$Si | 27.4 | 1.4 | 9.0 |

A comparison of the obtained astrophysical $S$-factor with the experimental data is shown in Figure 77. As can be seen, in the whole range of masses and energies considered, there is such a set of parameters $R, V, W$ that allows us to satisfactorily describe the energy dependence of the $S$-factor. Nevertheless, there

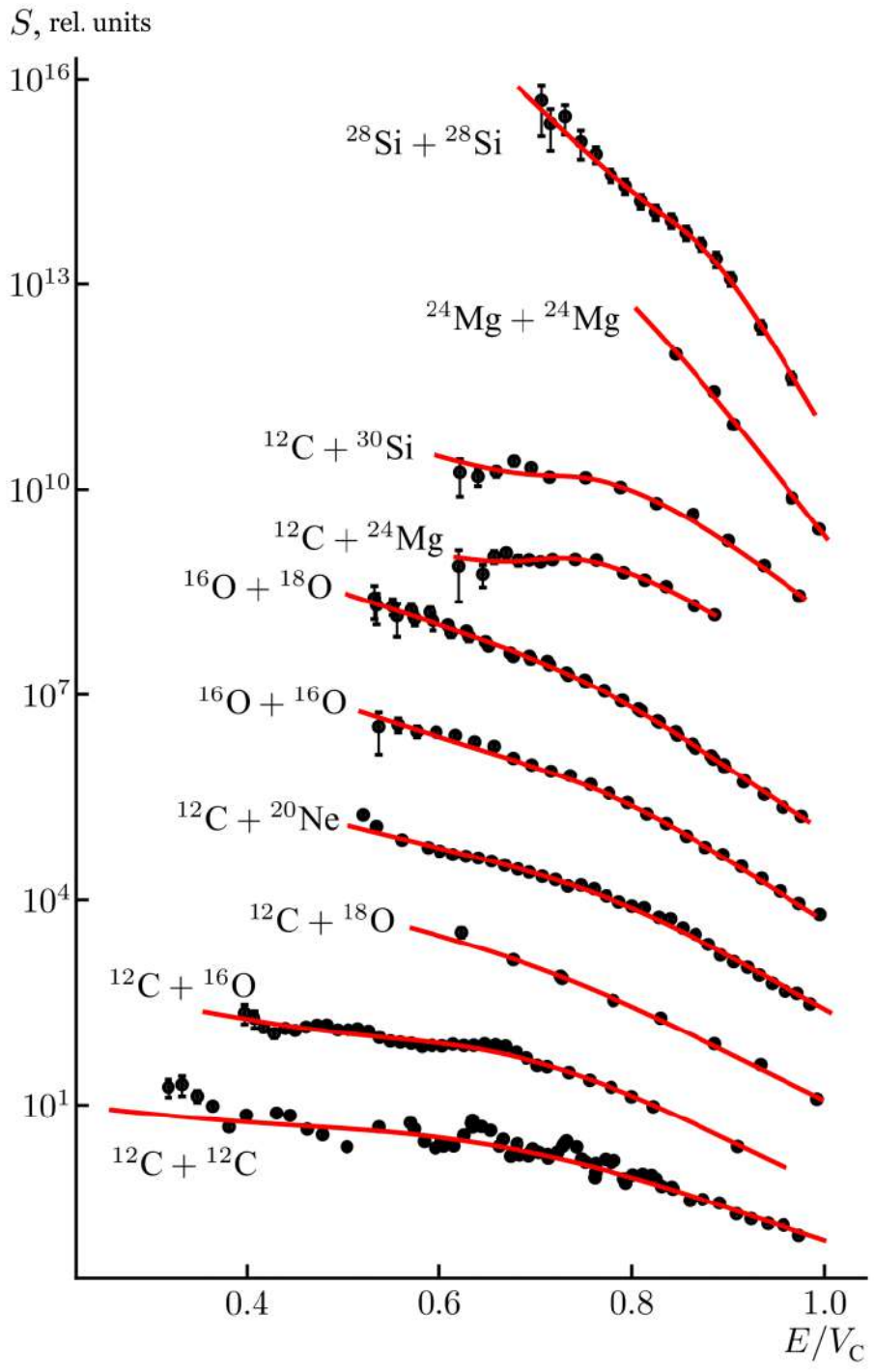


Figure 77. The dependence of the astrophysical $S$-factor on the energy normalized by the height of the Coulomb barrier. Dots are experimental results [311]. The solid line is the fitting data [50].

is uncertainty for all parameters, since small changes in their values do not lead to a significant change in the resulting $S$-factor and, in addition, it would be incorrect to require a perfect description of the experimental data within such a simple model. We should emphasize the possibility of describing the recently discovered phenomenon of cross section hindrance at low energies in comparison with calculations based on optical potentials [312, 313]. As indicated in [312],

the hindrance leads to the presence, at some energy, of a maximum value of the astrophysical $S$-factor, and then, for lower energies, it is assumed to fall smoothly. In numerical experiments, such behavior of the $S$-factor for a rectangular potential well in the region of the considered nuclei turns out to be irreproducible. However, it is possible to describe the existence of a local maximum for the $S$-factor, with the presence of a local minimum at lower energies and a smooth growth of the $S$-factor as the energy tends to zero. In Figure 77, this behavior of the excitation functions (presence of a local maximum) can be observed for the reactions $^{12}$C+$^{30}$Si and $^{12}$C+$^{24}$Mg.

Of particular interest is the possible systematics of the parameters obtained, summarized in Figure 78.

For all reactions considered, an increased value of the reaction channel radius is observed (Figure 78 a). The magnitude dependence of the obtained parameter can be approximated by a linear function:

$$R = 1.35(A_p^{1/3} + A_t^{1/3}) + 0.92, \tag{123}$$

which agrees well with the value of the Coulomb radius in such systems. On the other hand, according to [291], the increased value of the radius is due to the presence of a potential jump and is an artifact of the model. This, due to the equality of the radii of the real and imaginary parts of the potential, leads to an increased absorption at large distances compared to the Woods-Saxon potential. Taking this effect into account may help to explain the significant difference in the values of the astrophysical $S$-factor for the systems of the considered mass range.

As shown in Figure 78 b, the real part of the potential is determined mainly by the Coulomb contribution, and has a well-defined linear dependence on the magnitude of , leading to a repulsive core.

$$V = 0.98\frac{Z_p Z_t}{A_p^{1/3} + A_t^{1/3}} - 4.0. \tag{124}$$

The observed small negative contribution turns out to be almost constant for all the nuclei considered in the paper.

At the same time, for the depth of the imaginary part of the potential (Fig-

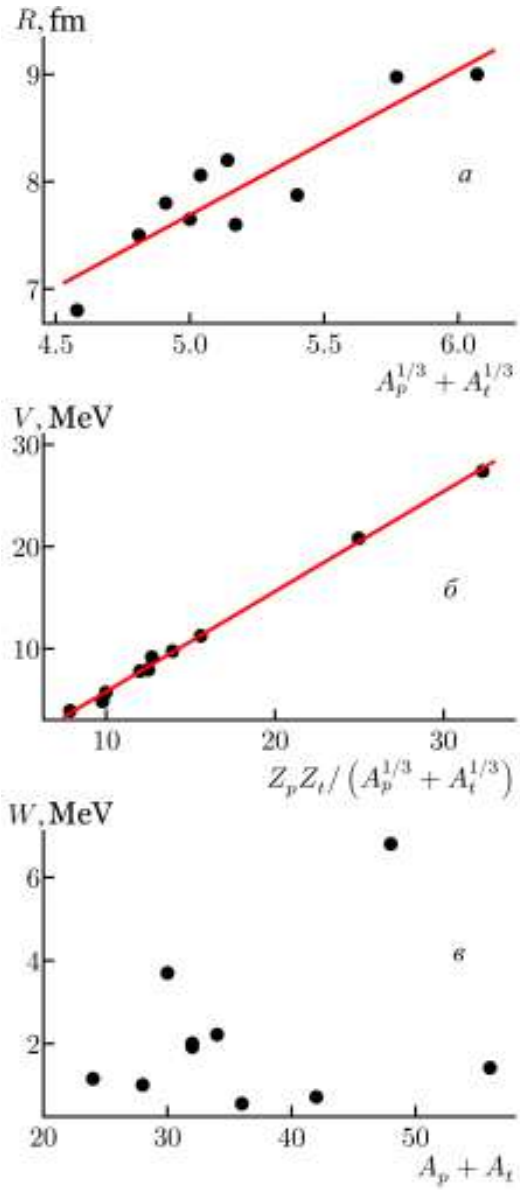


Figure 78. Potential parameters obtained in the paper [50]. Dots – fitting values, solid line – approximation by a linear function (see explanations in the text). Top figure – dependence of the radius $R$ on the value $(A_T^{1/3} + A_P^{1/3})$. Center figure – dependence of the real part of the potential $V$ on the value $\frac{Z_T Z_P e^2}{A_T^{1/3} + A_P^{1/3}}$. Bottom figure – dependence of the imaginary part of the potential $W$ on the mass of the compound core.

ure 78 c), there is a rather wide scatter of values that does not show any strict systematic dependence. As can be seen from Figure 78 c, small values of the imaginary potential are found for heavy nuclei, while for light nuclei, on average, an increase proportional to the mass of the compound nucleus is observed. It should be noted that in some cases it was possible to achieve a satisfactory description of the value of the $S$-factor and at zero depth of the imaginary potential.

As a conclusion to this section, the results obtained in this work are illustrated in Figure 79, which shows the experimental values of $S$-factors normalized to the

.

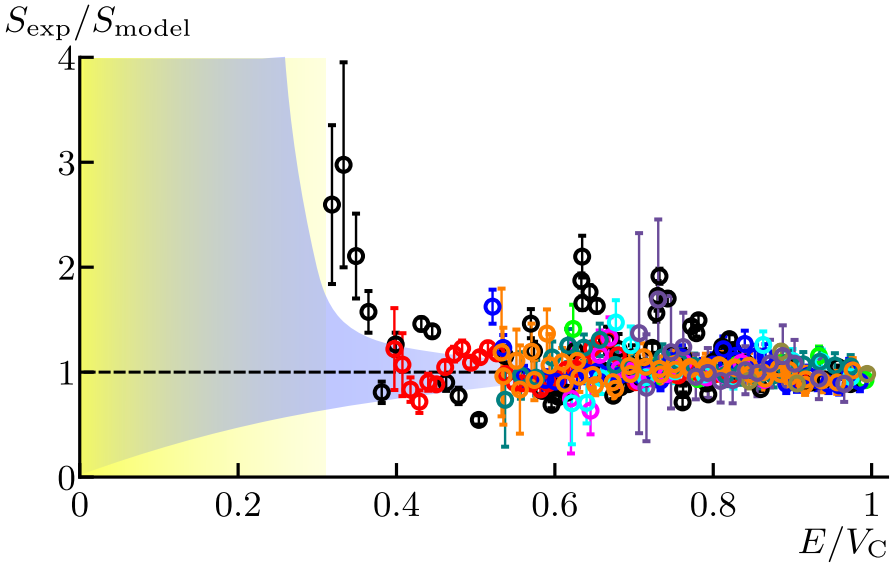


Figure 79. The ratio of the experimental $S$-factor to the one obtained within the considered model [50], as a function of the energy of the nuclei divided by the height of the Coulomb barrier (colors correspond to different combinations of nuclei). The purple region corresponds to the scatter of theoretical predictions, and the yellow region to the conditions occurring in the stars

.

values obtained in the framework of the proposed approach. As can be seen, there is a very good agreement, which allows us not only to predict the value of the cross section for low energies, but also to better understand the mechanism of the fusion reactions taking place.

# Conclusion

.

In conclusion, we summarize the results of the research work on the thesis topic.

The manifestation of cluster degrees of freedom is associated with a wide range of experimentally verifiable phenomena related both to the structure of atomic nuclei and to questions related to the mechanism of nuclear reactions.

From the point of view of structure, we have considered the maximal $\alpha$-cluster model, when the whole nucleus is represented as a system of interacting $\alpha$-particles. In spite of the quasi-classical approach, it was shown that the consequences of this model allow us to describe not only the ground states of self-conjugated nuclei (in the whole mass range known to date), but also exotic excited states. For example – possessing such a strong deformation that they can be considered as an analog of chain states, when several $\alpha$-particles line up one after another. Or the emergence at a certain excitation energy of a Bose-Einstein condensate of $\alpha$-particles constituting the nucleus.

Further we considered the manifestation of cluster degrees of freedom in nuclei of a broad mass group.

Using the example of $^{6,8}$He nuclei, we considered the cases when the function of the core is performed by the $\alpha$-particle nucleus, $^{6}$He, and when one can presumably speak of neutron clusters. The structure of such nuclei is a challenge for both experimental and theoretical studies. The momentum distributions of the clusters comprising these halo nuclei have been obtained.

For light nuclei – beryllium, carbon, oxygen and neon, magnesium, and argon – experiments to study the interaction of $\alpha$-particles with the core were considered. It was shown that in the considered nuclei neutron excess does not always lead to a decrease in the contribution of cluster configurations to the structure of excited states.

Adopted data for heavier nuclei were considered. Despite their lack of well-identified low-lying cluster states, they nevertheless possess high-lying fragmented states. For argon nuclei, an elastic scattering experiment has been considered to study the fragmented states. The detected states agree well with the predictions

of the potential model.

A detailed consideration (both experimental and theoretical) of the next nucleus – $^{40}$Ca allowed us not only to detect low-lying cluster states, but also to apply a unified model to describe them – both potential and tunneling models. This makes it possible to relate the data for such intermediate-mass nuclei to nuclei in the uranium region, for which such behavior is characteristic. This conclusion extends the notion of shape isomerism.

Finally, heavy clusters were considered. The most interesting manifestation of this form of clustering is the observation of molecular resonances in heavy ion scattering.

Exotic clusters in the form of unbound nuclei were considered, which made it possible to conclude about the transition arising in such nuclei leading to condensation, thus linking these states with the limit $\alpha$-cluster model considered at the very beginning.

The potential model approach to the description of states in the carbon-oxygen system at energies close to the Gamow window has been considered. A satisfactory description of the fusion cross section and the positions of the observed resonances was obtained. A systematics in the cluster approximation for reactions important from the point of view of astrophysics was obtained.

The author expresses his great gratitude to all those who helped him in his scientific work and in the process of writing this paper.

First of all, I would like to thank my supervisor, K. A. Gridnev, who, unfortunately, has not lived to this day. Without his constant attention to the work, help in setting problems and finding solutions, this work would never have been written.

I express my gratitude to my Russian and foreign colleagues:

W. von Oertzen, G. Bohlen and Tz. Kokalova, as well as all the staff of the SF7 group of HMI, Berlin, Germany.

K. Rusek, N. Burtebayev, S. B. Sakuta and the staff of the Cyclotron Laboratory, University of Warsaw, Poland.

W. Trzaska, S. V. Khlebnikov, Y. G. Sobolev, B. G. Novatsky, G. P. Tyurin, M. Mutterer, T. Lonnroth, V. A. Rubchenya and I. Slotte for their help in per-

forming experiments at the University of Jyvaskyla, Finland.

V. Z. Goldberg and G. V. Rogachev A&M University, USA.

Y. A. Litvinov, L. V. Chulkov, and T. Aumann GSI, Germany.

I. A. Mitropolsky PNPI NRC “Kurchatov Institute”, Russia.

I would like to thank all my colleagues in the department and especially V. I. Zherebchevsky and N. A. Maltsev and G. A. Feofilov whose help in the work was very significant.

I also express my gratitude to my family.

**Bibliography**

[1] Wheeler J. A. Molecular Viewpoints in Nuclear Structure // Phys. Rev.–1937.–Vol.52.–P.1083–1106. DOI: https://doi.org/10.1103/PhysRev.52.1083

[2] Teller, E., Wheeler, J. A. On the Rotation of the Atomic Nucleus // Phys. Rev.–1938.–Vol.53.–P.778–789. DOI: https://doi.org/10.1103/PhysRev.53.778

[3] Hafstad, L. R., Teller, E. The Alpha-Particle Model of the Nucleus // Phys. Rev.–1938.–Vol.54.–P.681–692. DOI: https://doi.org/10.1103/PhysRev.54.681

[4] Wheeler J. A. On the Mathematical Description of Light Nuclei by the Method of Resonating Group Structure // Phys. Rev.–1937.–Vol.52.–P.1107–1122. DOI: https://doi.org/10.1103/PhysRev.52.1107

[5] Brink D. M. The Alpha-Particle Model of Light Nuclei // Proceedings of International School of Physics. “Enrico Fermi” 1966.–Vol.36.–P.247.

[6] Saito S. Interaction between Clusters and Pauli Principle // Progress of Theoretical Phys.–1969.–Vol.41.–P.705–722. DOI: https://doi.org/10.1143/PTP.41.705

[7] Ikeda K., Tagikawa N., Horiuchi H. The Systematic Structure-Change into the Molecule-like Structures in the Self-Conjugate 4n Nuclei // Progress of Theoretical Phys.–1968.–Vol.E68.–P.464–475. DOI: https://doi.org/10.1143/PTPS.E68.464

[8] https://badge.dimensions.ai/details/id/pub.1063145694/citations

[9] von Oertzen W. Two-center molecular states in $^{9}$B,$^{9}$Be,$^{10}$Be, and $^{10}$B // Z. Phys. A – Hadrons and Nuclei–1996.–Vol.354.–P.37–43. DOI: https://doi.org/10.1007/s002180050010

[10] von Oertzen W. Covalently bound molecular structures in the $\alpha + {}^{16}O$ system // Eur. Phys. J.–2001.–Vol.A11–P.403–411. DOI: 10.1007/s100500170052

[11] Buck, B., Dover, C. B., Vary, J. P. Simple potential model for cluster states in light nuclei // Phys. Rev. C.–1975.–Vol.11.–P.1803–1821. DOI: https://doi.org/10.1103/PhysRevC.11.1803

[12] Buck B., Pilt A.A. Alpha-particle and triton cluster states in $^{19}$F // Nucl. Phys. A.–1977.–Vol.280.–P.133–160. DOI: https://doi.org/10.1016/0375-9474(77)90300-1

[13] Buck B., Friedrich H., Pilt A.A. Alpha-particle cluster states in $^{18}$F and $^{18}$O // Nucl. Phys. A.–1977.–Vol.290.–P.205–217. DOI: https://doi.org/10.1016/0375-9474(77)90675-3

[14] Vary J.P., Dover C.B., Simple potential model for nucleus-nucleus interactions // Phys. Rev. Lett.–1973.–Vol.31.–P.1510–1513. DOI: https://doi.org/10.1103/PhysRevLett.31.1510

[15] Horiuchi H., Ikeda K. A Molecule-like Structure in Atomic Nuclei of $^{16}$O* and $^{20}$Ne // Progress of Theoretical Phys.–1968.–Vol.40.–P.277–287. DOI: https://doi.org/10.1143/PTP.40.277

[16] Horiuchi H., Ikeda K., Suzuki Y. Molecule-Like Structures in Nuclear System // Progress of Theoretical Phys (Suppl.).–1972.–Vol.52.–P.89–172 DOI: https://doi.org/10.1143/PTPS.52.89

[17] Kanada-En'yo Y., Kimura M., Ono A. Antisymmetrized molecular dynamics and its applications to cluster phenomena // Progress of Theoretical and Experimental Physics.–2012.– Vol.2012.–P.01A202. DOI: https://doi.org/10.1093/ptep/pts001

[18] von Oertzen, W., Freer, M., Kanada-En'yo Y. Nuclear clusters and nuclear molecules // Physics Reports.–2006.–Vol.432.–P.43–113. DOI: https://doi.org/10.1016/j.physrep.2006.07.001

[19] Beck C. Ed. Clusters in Nuclei // Lecture Notes in Physics (Springer-Verlag, Berlin).–2014.–Vol.3.

[20] Horiuchi H., Ikeda K., Kato K. Recent Developments in Nuclear Cluster Physics // Progress of Theoretical Physics Supplement.–2012.–Vol.192.–P.1–238, https://doi.org/10.1143/PTPS.192.1

[21] Freer M., Horiuchi H., Kanada-En'yo Y. et al. Microscopic clustering in light nuclei // Rev. Mod. Phys.–2018.–Vol.90.–P.035004. DOI: https://link.aps.org/doi/10.1103/RevModPhys.90.035004

[22] Kanada-En'yo, Y., Horiuchi, H. Coexistence of cluster and shell-model aspects in nuclear systems // Front. Phys.–2018–Vol.13.–P.132108. DOI: https://doi.org/10.1007/s11467-018-0830-y

[23] Nemets O. F., Neudachin V. G., Rudchik A. T. et al. Nucleon associations in atomic nuclei and nuclear reactions of multinucleon transfers. Kiev.–1988.

[24] Artemenkov D. A., Bradnova V., Chernyavsky M. M. et al. Unstable states in dissociation of relativistic nuclei // Eur. Phys. J. A.–2020.–Vil.56.–P.250. DOI: https://doi.org/10.1140/epja/s10050-020-00252-3

[25] Artemenkov D. A., Bradnova V., Kashanskaya O.N. et al. Prospects of Searches for Unstable States in Relativistic Fragmentation of Nuclei // Phys. Atom. Nuclei.–2022.–Vol.85.–P.528–539. DOI: https://doi.org/10.1134/S1063778822060035

[26] Zaitsev A. A., Artemenkov D. A., Glagolev V. V. Correlation in formation of $^{8}$Be nuclei and $\alpha$-particles in fragmentation of relativistic nuclei // Phys. Lett. B.–2021.–Vol.820.–P.136460. DOI: https://doi.org/10.1016/j.physletb.2021.136460

[27] Zaitsev A. A., Marimuthu N., Artemenkov D. A. et al. Cosmophysical Aspects of Relativistic Nuclear Fragmentation // Phys. Atom. Nuclei.–2023.–Vol.86.–P.1101–1106. DOI: https://doi.org/10.1134/S1063778824010617

[28] Yang Z., Huang S. Clustering in nuclear systems: from finite nuclei to neutron stars // Science Bulletin.–2021.–Vol.66.–P.2054-2056. DOI: https://doi.org/10.1016/j.scib.2021.07.009

[29] Roca-Maza X., Paar N. Nuclear equation of state from ground and collective excited state properties of nuclei // Progress in Particle and Nuclear Physics.–2018.–Vol.101.–P.96-176. DOI: https://doi.org/10.1016/j.ppnp.2018.04.001

[30] Duer, M., Aumann, T., Gernhuser, R. et al. Observation of a correlated free four-neutron system // Nature.–2022.–Vol.606.–P.678–682. DOI: https://doi.org/10.1038/s41586-022-04827-6

[31] Wei K., Ye,Y. L., Yang Z. H. Clustering in nuclei: progress and perspectives // NUCL SCI TECH.–2024.–Vol.35.–P.216 DOI: https://doi.org/10.1007/s41365-024-01588-x

[32] Kimura M., Suhara T., Kanada-En'yo, Y. Antisymmetrized molecular dynamics studies for exotic clustering phenomena in neutron-rich nuclei // Eur. Phys. J. A.–2016.–Vol.52.–P.373. DOI: https://doi.org/10.1140/epja/i2016-16373-9

[33] Lombardo I., Dell'Aquila D. Clusters in light nuclei: history and recent developments // La Rivista del Nuovo Cimento.–2023.–Vol.46.–P.521–618. DOI: https://doi.org/10.1007/s40766-023-00047-4

[34] Kahl D., Yamaguchi H., Hayakawa S. Alpha clustering in nuclear astrophysics and topology // Front. Phys.–2023.–Vol.11.–P.1189040. DOI: https://doi.org/10.3389/fphy.2023.1189040

[35] Torilov S.Y., Brenner M., Goldberg V.Z. et al. High-spin states in $^{22}$Ne populated in the $^{14}$C($^{12}$C,$\alpha$) reaction // Eur. Phys. J. A.–2011.–Vol.47.–P.158. DOI: https://doi.org/10.1140/epja/i2011-11158-4

[36] Torilov S.Y., Gridnev K.A., Zherebchevsky V.I. et al. Cluster states in the neutron excess nucleus $^{22}$Ne // Jetp Lett.–2011.–Vol.94.–P.6–10. DOI: https://doi.org/10.1134/S0021364011130170

[37] Torilov S.Y., Maltsev N.A., Goldberg V.Z. et al. Quasimolecular states in a reaction with carbon isotopes // Jetp Lett.–102, 69–72 (2015). https://doi.org/10.1134/S0021364015140118

[38] Torilov S.Y., Maltsev N.A., Goldberg V.Z. et al. Decay of quasimolecular states in $^{26}$Mg // Bull. Russ. Acad. Sci. Phys.–2016.–Vol.80.–P.871–874. DOI: https://doi.org/10.3103/S1062873816080384

[39] Torilov S.Y., Maltsev N.A., Zherebchevsky V.I. et al. Resonant and non-resonant yield from the reaction with neutron excess carbon isotopes // Vestnik SPBGU.–2015.–Ser.4.–Vol.2–P.319.

[40] Torilov S. Yu., Zherebchevsky V. I., Gridnev K. A., Lazarev V. V. Modeling the decay of nuclear systems formed in reactions with heavy ions // Vestnik SPBGU.–2011.–Ser.4.–Vol.2–P.49.

[41] Bohlen H.G., Kalpakchieva R., von Oertzen W. et al. Structure studies of neutron-rich beryllium and carbon isotopes // Nuc. Phys. A.–2003.–Vol.722.–P.c3–c9. DOI: https://doi.org/10.1016/S0375-9474(03)01327-7

[42] Bohlen H.G., von Oertzen W., Kalpakchieva R. et al. Structure of neutron-rich Be and C isotopes // Phys. Atom. Nuclei.–2003.–Vol.66.–P.1494–1500. DOI: https://doi.org/10.1134/1.1601755

[43] Bohlen H.G., Kalpakchieva R., Gebauer B. et al. Spectroscopy of particle-hole states of $^{16}$C // Physical Rev. C.–2003.–Vol.68.–P.054606. DOI: https://doi.org/10.1103/PhysRevC.68.054606

[44] Bohlen H.G., von Oertzen W., Kalpakchieva R. et al. Structure studies of neutron-rich beryllium and carbon isotopes. // APH N.S., Heavy Ion Physics.–2003.–Vol.18.–P.179–184. DOI: https://doi.org/10.1556/APH.18.2003.2-4.10

[45] Bohlen H.G., Kalpakchieva R., von Oertzen W. et al. Particle-hole structures of neutron-rich Be- and C-isotopes // Nuclear Phys. A.–2004.–Vol.734.–P.345–348. DOI: https://doi.org/10.1016/j.nuclphysa.2004.01.063

[46] Chulkov L.V., Aksouh F., Bleile A. et al. Quasi-free scattering with $^{6,8}$He beams // Nucl. Phys. A.–2005.–Vol.759.–P.43–63. DOI: https://doi.org/10.1016/j.nuclphysa.2005.05.148

[47] Kokalova T., von Oertzen W., Torilov S. et al. Emission of unbound $^{8}$Be and $^{12}$C* (0+2) clusters in compound nucleus reactions // Eur. Phys. J. A–2005.–Vol.23–P.19–31. DOI: https://doi.org/10.1140/epja/i2004-10071-3

[48] Torilov S.Y., Maltsev N.A., Zherebchevsky Analyzing Resonance States in Describing the Astrophysical $S$-Factor for Heavy Ion Fusion Reaction $^{16}$O+$^{12}$C // Bull. Russ. Acad. Sci. Phys.–2022.–Vol.86.–P.966–970. DOI: https://doi.org/10.3103/S106287382208024X

[49] Torilov S.Yu., Maltsev N.A., Zherebchevsky V.I. Studying Low-Energy Resonances in the $^{16}$O+$^{12}$C System // Bull. Russ. Acad. Sci. Phys.–2021.–V.85.–P.548–551. DOI: https://doi.org/10.3103/S1062873821050233

[50] Torilov S.Y., Maltsev N.A., Zherebchevsky V.I. Astrophysical $S$-Factor in the Model of a Square Potential Well // Bull. Russ. Acad. Sci. Phys.–2023–Vol.87.–P.1217–1220 DOI: https://doi.org/10.3103/S1062873823703124

[51] Zherebchevsky V.I., Torilov S.Y., Andronenkov A. N. et al. Elastic scattering of alpha particles by a neutron-rich nucleus $^{14}$C // Vestnik SPBGU.–2013.–Ser.4.–Vol.1–P.233.

[52] Burtebayev N., Amangeldi N., Alimov D. et al. Scattering of $^{15}$N Ions by $^{10,11}$B Nuclei at the Energy of 43 MeV // Acta Phys. Polon. Supp.–2018.–Vol.11.–P.99. DOI: https://doi.org/10.5506/APhysPolBSupp.11.99

[53] Torilov S.Y., Maltsev N.A., Zherebchevsky V.I. et al. A Study of Resonance States in Nuclear Systems Formed in Reactions with Heavy Ions // Phys. Part. Nuclei–2022.–Vol.53.–P.403–408. DOI: https://doi.org/10.1134/S1063779622020836

[54] Gridnev K.A., Torilov S. Yu., Gridnev D.K., Kartavenko V.G., Greiner W. Model of binding alpha-particles and applications to superheavy elements // Int. Journal Mod. Phys. E.–2005.–Vol.14.–P.635–643. DOI: https://doi.org/10.1142/S0218301305003387

[55] Gridnev K.A., Torilov S. Yu., Kartavenko V.G., Greiner W. Model of binding alpha-particles and structure of the light nu-

clei // Int. Journal Mod. Phys. E.–2007.–Vol.16.–P.1059–1063. DOI: https://doi.org/10.1142/S0218301307006502

[56] Torilov S.Yu., Gridnev K.A., Greiner W. Chain configuration in light nuclei // Int. Journal Mod. Phys. E.–2007.–Vol.16.–P.1757–1764. DOI: https://doi.org/10.1142/S0218301307006927

[57] Gridnev K.A., Torilov S.Y. Ikeda diagram within the model of binding alpha particles // Phys. Atom. Nuclei.–2006.–Vol.69–P.1204–1206. DOI: https://doi.org/10.1134/S1063778806070179

[58] Gridnev K. A., Torilov S. Y., Gridnev D. K. et al. Model of binding alpha-particles and applications to superheavy elements // Eur. Phys. J. A.–2005.–Vol.25.–Suppl.1.–P.609–610. DOI: https://doi.org/10.1140/epjad/i2005-06-020-6

[59] Torilov S. Yu., Gridnev K. A., Greiner W. New insight on the chain states and Bose-Einstein condensate in light nuclei // Int. Journal Mod. Phys. E.–2008.–Vol.17.–P.2150–2154. DOI: https://doi.org/10.1142/S0218301308011252

[60] Gridnev K.A., Torilov S.Yu. Superdeformation in light alpha-particle nuclei // Theor. phys. Samara University.–2007.–Vol.8.–P.9–16.

[61] Torilov S. Y., Gridnev K. A., Korovitskaya T. V. Cluster states in neutron-rich nuclei // Bull. Russ. Acad. Sci. Phys.–2013,–Vol.77.–P.849–851. DOI: https://doi.org/10.3103/S1062873813070253

[62] Torilov S. Yu., Gridnev K. A., Korovitskaya T. V. Rotational bands in light neutron-rich nuclei // Bull. Rus. Acad. Sci. Phys.–2012.–Vol.76.–P.854–856. DOI: https://doi.org/10.3103/S1062873812080278

[63] Torilov S. Thummerer S. von Oertzen W. et al. Spectroscopy of $^{40}$Ca and negative-parity bands // Eur. Phys. J. A.–2004.–Vol.19.–P.307–317. DOI: https://doi.org/10.1140/epja/i2003-10126-y

[64] Torilov S.Yu. Energy splitting of the states in the rotational bands in $^{40}$Ca // Eur. Phys. J. A –2014.–Vol.50.–P.3. DOI: https://doi.org/10.1140/epja/i2014-14003-4

[65] Torilov S.Yu.The alpha-particle structure of rotational bands in $^{40}$Ca // Vestnik SPBGU.–2009.–Ser.4.–Vol.2–P.156.

[66] Goldberg V.Z., Rogachev G.V., Brenner M. et al. Observation of an $\alpha$-cluster structure in $^{36}$Ar // Phys. Atom. Nuclei.–2000.–Vol.63.–P.1518–1526. DOI: https://doi.org/10.1134/1.1312885

[67] Hodgson, P. E. Alpha-particle clustering in nuclear reactions // Contemporary Physics.–2002.–Vol.43.–P.461–472. DOI: https://doi.org/10.1080/00107510210164011

[68] Bernal J.D. Geometry of the Structure of Monatomic Liquids // Nature.–1960.–Vol.–185.–P.68–70.

[69] Marumori T., Suzuki K. Four-body correlations in light nuclei: (I). First excited $0^+$ states in $^{16}$O and $^{40}$Ca // Nucl. Phys. A.–1968.–Vol.106–P.610–640. DOI: https://doi.org/10.1016/0375-9474(68)90519-8

[70] Dussel G. G., Liotta R. J., Perazzo R. P. J. Cluster of nucleons as elementary modes of excitation in nuclei // Nucl. Phys. A.–1982.–Vol.388.–P.606–620. DOI: https://doi.org/10.1016/0375-9474(82)90479-1

[71] Gambhir Y. K. Ring P. Schuck P. Nuclei: A Superfluid Condensate of $\alpha$ Particles? A Study within the Interacting-Boson Model // Phys. Rev. Lett.–1983.–Vol.51–P.1235–1238. DOI: https://link.aps.org/doi/10.1103/PhysRevLett.51.1235

[72] Hasegawa M., Tazaki S., Okamoto R. Condensed structure of $J = T = 0$ $\alpha$-like clusters in $f_{7/2}$-shell even-even nuclei with $N = Z$ // Nucl. Phys. A.–1995.–Vol.592.–P.45-58. DOI: https://doi.org/10.1016/0375-9474(95)00296-D

[73] Koh S. Many-Body Approach to the Alpha-Correlation inside of the Heavy Nuclei // Progr. Theor. Phys. Suppl.–1998.–Vol.132.–P.197–212. DOI: https://doi.org/10.1143/PTP.132.197

[74] Kallunkathariyil J., 20th Nuclear Physics Workshop “Marie and Pierre Curie” Kazimierz 2013.

[75] Nesbet R. K. Localized Orbitals in Nuclear Structure // Phys. Rev.–1955.–Vol.100.–P.228–234. DOI: https://link.aps.org/doi/10.1103/PhysRev.100.228

[76] Buck B. Johnston J. C.Merchant A. C. Perez S. M. Unified treatment of scattering and cluster structure in $\alpha$+closed shell nuclei: $^{20}$Ne and $^{44}$Ti Phys. Rev. C.–1995.–Vol.52–P.1840–1844. DOI: https://link.aps.org/doi/10.1103/PhysRevC.52.1840

[77] Drouart A. et al. Evidence of $Z$=120 Compound Nuclear Formation from Lifetime Measurements in the $^{238}$U+Ni Reaction at 6,62 MeV/Nucleon // Proceedings of the Int. Symp. on Exotic Nuclei EXON2004 World Scientific–2004–P.192.

[78] Bijker R., Iachello F. Evidence for Tetrahedral Symmetry in $^{16}$O // Phys. Rev. Lett.–2014.–Vol.112.–P.152501. DOI: https://link.aps.org/doi/10.1103/PhysRevLett.112.152501

[79] Bijker R., Iachello F. Cluster states in nuclei as representations of a U($\nu$ + 1) group // Phys. Rev. C.–1982.–Vol.61.–P.067305. DOI: https://link.aps.org/doi/10.1103/PhysRevC.61.067305

[80] Itagaki N., Otsuka T., Ikeda K., Tanihata I. Equilateral-Triangular Shape in $^{14}$C // Phys. Rev. Lett.–2004.–Vol.92–P.142501. https://link.aps.org/doi/10.1103/PhysRevLett.92.142501

[81] Morinaga H. Interpretation of Some of the Excited States of $4n$ Self-Conjugate Nuclei // Phys. Rev.–1956.–Vol.101.–P.254–258. DOI: https://link.aps.org/doi/10.1103/PhysRev.101.254

[82] Ring P., Schuck P. The Nuclear Many-Body Problem, Springer, 1980.

[83] Leander G., Larsson S.E. Potential-energy surfaces for the doubly even $N = Z$ nuclei // Nucl. Phys. A.–1975.–Vol.239.–P.93–113. DOI: https://doi.org/10.1016/0375-9474(75)91136-7

[84] Dennison D. M. Excited States of the $^{16}$O Nucleus // Phys. Rev.–1940.–Vol.57.–P.454–456. DOI: https://doi.org/10.1103/PhysRev.57.454

[85] Galindo-Uribarri A., Andrews H. R., Ball G. C. et al. First evidence for the hyperdeformed nuclear shape at high angular momentum // Phys. Rev. Lett.–1993.–Vol.71.–P.231–234. DOI: https://link.aps.org/doi/10.1103/PhysRevLett.71.231

[86] Boucenna A., Madjber S., Bouketir A. Isomeric and hyperdeformed states at high spin for light nuclei // arXiv nucl-th/0305026.

[87] Freer M., Horiuchi H., Kanada-En'yo Y. et al. Microscopic clustering in light nuclei // Rev. Mod. Phys.–2018.–Vol.90.–P.035004. DOI: 10.1103/RevModPhys.90.035004

[88] Richards, H. T. Rotational bands in $^{20}$Ne // Phys.Rev. C.–1984–Vol.29.–P.276–283. DOI: https://link.aps.org/doi/10.1103/PhysRevC.29.276

[89] Tilley D. R., Cheves C.M., Kelley J. H. et al. Energy levels of light nuclei, $A = 20$ // Nucl. Phys. A.–1998.–Vol.636.–P.249–364. DOI: https://doi.org/10.1016/S0375-9474(98)00129-8

[90] Freer M. The clustered nucleus – cluster structures in stable and unstable nuclei // Rep. Prog. Phys.–2007.–Vol.70.–P.2149. DOI: https://doi.org/10.1088/0034-4885/70/12/R03

[91] von Oertzen W. Dynamics of $\alpha$-clusters in $N = Z$ nuclei // Eur. Phys. J. A.–2006.–Vol.29.–P.133–139. DOI: https://doi.org/10.1140/epja/i2006-10076-x

[92] Tohsaki A., Horiuchi H., Schuck P., Röpke G. Alpha Cluster Condensation in $^{12}C$ and $^{16}O$ // Phys. Rev. Lett.–2001.–Vol.87–P.192501. DOI: https://link.aps.org/doi/10.1103/PhysRevLett.87.192501

[93] Schuck P., Funaki Y., Horiuchi H., et al. Alpha-particle condensation in nuclei // Nucl. Phys. A.–2004.–Vol.738–P.94–100. DOI: https://doi.org/10.1016/j.nuclphysa.2004.04.075

[94] Yamada T., Schuck P., Dilute multi-$\alpha$ cluster states in nuclei // Phys. Rev. C.–2004.–Vol.69–P.024309. DOI: https://link.aps.org/doi/10.1103/PhysRevC.69.024309

[95] Ohkubo S., Hirabayashi Y. Bose-Einstein condensation of $\alpha$ particles and Airy structure in nuclear rainbow scattering // Phys. Rev. C.–2004.–Vol.70–P.041602. DOI: https://link.aps.org/doi/10.1103/PhysRevC.70.041602

[96] Kokalova Tz., Itagaki N., von Oertzen W., Wheldon C. Signatures for Multi-$\alpha$-Condensed States // Phys. Rev. Lett.–2006.–Vol.96.–P.192502. DOI: https://link.aps.org/doi/10.1103/PhysRevLett.96.192502

[97] Schuck P., Funaki Y., Horiuchi H. et al. Alpha particle clusters and their condensation in nuclear systems // Phys. Scr.–2016.–Vol.91.–P.123001. DOI: https://link.aps.org/doi/10.1088/0031-8949/91/12/123001

[98] Satchler G. R., Love W. G. Folding model potentials from realistic interactions for heavy-ion scattering // Phys. Rep.–1979.–Vol.55.–P.183–254. DOI: https://doi.org/10.1016/0370-1573(79)90081-4

[99] Neudatchin V. G., Kukulin V. I., Korotkikh V. L., Korennoy V. P. A microscopically substantiated local optical potential for $\alpha$-$\alpha$-scattering // Phys. Lett.–1975.–Vol.348.–P.581–583. DOI: https://doi.org/10.1016/0370-2693(71)90142-0

[100] Kukulin V. I., Ncudatchin V. G., Smirnov Yu. F. Microscopically substantiated local optical potentials for scattering of light nuclei // Nucl. Phys.–1975.–Vol.245.–P.429–443. DOI: https://doi.org/10.1016/0375-9474(75)90619-3

[101] Buck B., Friedrich H., Wheatley C. Local potential models for the scattering of complex nuclei // Nucl. Phys. A.–1977.–Vol.275–P.246–268. DOI: https://doi.org/10.1016/0375-9474(77)90287-1

[102] Marquez L. Alpha-alpha potential // Phys. Rev. C.–1983.–Vol.28.–P.2525–2527. DOI: https://link.aps.org/doi/10.1103/PhysRevC.28.2525

[103] Ali S., Bodmer A.R. Phenomenological $\alpha$-$\alpha$ potentials // Nucl.Phys. A.–1966.–Vol.80.–P.99–112. DOI: https://doi.org/10.1016/0029-5582(66)90829-7

[104] Kanada-En'yo Y. Tetrahedral $4\alpha$ and $^{12}C + \alpha$ cluster structures in $^{16}O$ // Physical Rev. C.–2017.–Vol.96.–P.034306. DOI: https://link.aps.org/doi/10.1103/PhysRevC.96.034306

[105] Abbondanno U., Cindro N. Resonances in Heavy-Ion Reactions: An overview of current models // Int. J. Mod. Phys. E.–1993.–Vol.2.–P.1–37. DOI: https://link.aps.org/doi/10.1142/S0218301393000029

[106] Baz A. I., Goldberg V. Z. Darwisch N. Z. et al. A potential for alpha-particle-nucleus scattering // Lett. Nuovo Cimento–1977.–Vol.18.–P.227–232. DOI: https://doi.org/10.1007/BF02909678

[107] Ohkubo S. Local potential alpha-cluster model and the Wildermuth condition // Phys. Rev. C.–1989.–Vol.39.–P.1186–1187. DOI: https://doi.org/10.1103/PhysRevC.39.1186

[108] Pilt A. A. Alpha-particle cluster states in $^{44}Ti$ // Phys. Lett. B.–1978.–Vol.73.–P.274–276. DOI: https://doi.org/10.1016/0370-2693(78)90512-9

[109] Buck B., Merchant A. C., Horner M. J., Perez S. M. Normal and superdeformed cluster bands in heavy nuclei // Nucl. Phys. A.–2000.–Vol.673.–P.157–170. DOI: https://doi.org/10.1016/S0375-9474(00)00130-5

[110] Horiuchi H. in: H. Kamitsubo, et al. (Eds.) // Proc. of the INS-ICPR Symposium on Cluster Structure of Nuclei and Transfer Reactions Induced by Heavy-Ions, Tokyo, IPCR Cyclotron Progress Report Suppl.–1975.–Vol.4.–P.41.

[111] Suzuki Y. in: H. Kamitsubo, et al. (Eds.) // Proc. of the INS-ICPR Symposium on Cluster Structure of Nuclei and Transfer Reactions Induced by Heavy-Ions, Tokyo, IPCR Cyclotron Progress Report Suppl.–1975.–Vol.4.–P.58.

[112] Buck B., Merchant A. C., Perez S. M. Systematics of alpha-cluster states above double shell closures // Phys. Rev. C.–1995.–Vol.51.–P.559–565. DOI: https://link.aps.org/doi/10.1103/PhysRevC.51.559

[113] Schultheis H. Schultheis R. Prediction of shape-isomeric bands in light nuclei // Phys. Rev. C.–1983.–Vol.27.–P.1367–1370. DOI: https://link.aps.org/doi/10.1103/PhysRevC.27.1367

[114] Iachello F. Algebraic approach to nuclear quasimolecular spectra // Phys. Rev. C.–1981.–Vol.23.–P.2778–2780. DOI: https://link.aps.org/doi/10.1103/PhysRevC.23.2778

[115] Cindro N., Greiner W. Anharmonic vibration-rotation approach to quasimolecular spectra // J. Phys. G.–1983.–Vol.9.–P.L175. DOI: https://link.aps.org/doi/10.1088/0305-4616/9/8/006

[116] Arai T., Horiuchi W., Baye D. Analyzing supersymmetric transformed $\alpha$-nucleus potentials with electric-multipole transitions // Nucl. Phys. A.–2018.–Vol.977.–P.82–100. DOI: https://doi.org/10.1016/j.nuclphysa.2018.06.004

[117] Bai D., Ren Z. Repulsive four-body interactions of $\alpha$ particles and quasistable nuclear $\alpha$-particle condensates in heavy self-conjugate nuclei // Phys. Rev. C.–2018.–Vol.97.–P.054301. DOI: https://link.aps.org/doi/10.1103/PhysRevC.97.054301

[118] Billen J. H. $^{20}$Ne states observed via $^{16}$O($\alpha$,$\alpha_i$)$^{16}$O // Phys. Rev. C.–1979.–Vol.20.–P.1648–1672. DOI: https://link.aps.org/doi/10.1103/PhysRevC.20.1648

[119] John J., Aldridge J. P., Davis R. H. Phase-Shift Analysis of $^{16}$O$(\alpha, \alpha)^{16}$O Scattering from 5 to 10 MeV // Phys. Rev.–1969.–Vol.181.–P.1455-1465. DOI: https://link.aps.org/doi/10.1103/PhysRev.181.1455

[120] Ames L. L. Natural parity levels in $^{16}$O // Phys. Rev. C.–1982.–Vol.25.–P.729–755. DOI: https://link.aps.org/doi/10.1103/PhysRevC.25.729

[121] Riedhauser S. R. $^{20}$Ne states observed via $^{16}$O$(\alpha, \alpha_0)^{16}$O and $^{16}$O$(\alpha, \alpha_1)^{16}$O // Phys. Rev. C.–1984.–Vol.29.–P.1961–1979. DOI: https://link.aps.org/doi/10.1103/PhysRevC.29.1961

[122] Blatt J. M., Weisskopf V. F. Theoretical nuclear physics // Dover Books on Physics 1979.

[123] Kubono S. Experimental determination of astrophysical reaction rates with radioactive nuclear beams // Nucl. Phys. A.–2001.–Vol.693.–P.221–248. DOI: https://doi.org/10.1016/S0375-9474(01)01140-X

[124] Nurmukhanbetova A. K., Goldberg V.Z., Nauruzbayev D. K. et al. Implementation of TTIK method and time of flight for resonance reaction studies at heavy ion accelerator DC-60 // Inst. Meth. Phys. Res. A.–2017.–Vol.847.–P.125–129. DOI: https://doi.org/10.1016/j.nima.2016.11.053

[125] Freer M., Merchant A.C. Developments in the study of nuclear clustering in light even - even nuclei // J. Phys. G.–1997.–Vol.23.–P.261. DOI: https://doi.org/10.1088/0954-3899/23/3/002

[126] Kumbartzki G. J., Benczer-Koller N., Burcher S. et al. Transition from collectivity to single-particle degrees of freedom from magnetic moment measurements on $^{82}_{38}Sr_{44}$ and $^{90}_{38}Sr_{52}$ // Phys. Rev. C.–2014.–Vol.89.–P.064305. DOI: https://link.aps.org/doi/10.1103/PhysRevC.89.064305

[127] Bazzacco D. Proc. Int. Conf. on nuclear Structure at HighAngular momentum, Ottawa 1992.

[128] https://www.slcj.uw.edu.pl/en/icare-2/

[129] Knoll G.F. Radiation Detection and Measurement Wiley 2010.

[130] Mutterer M., Trzaska W.H., Kopatch Yu.N. et al. Nuclear Instruments and Methods in Physics Research Section A: Accelerators, Spectrometers, Detectors and Associated Equipment // Nucl. Instrum. Methods Phys. Res. A.–2009.–Vol.608.–P.275–286. DOI: https://doi.org/10.1016/j.nima.2009.06.060

[131] Bohlen H.G. The magnetic spectrometer at VICKSI // Preprint HMI 83/1 R 1983.

[132] https://root.cern/

[133] Zhukov M. V., Korsheninnikov A. A., Smedberg M. H. Simplified $\alpha$+4n model for the $^{8}$He nucleus // Phys. Rev. C.–1994.–Vol.50–P.R1–R4. DOI: https://link.aps.org/doi/10.1103/PhysRevC.50.R1

[134] Sakamoto Y., Cüer P., Takéutchi F. Interpretation of quasifree scattering in the $^{6}$Li$(p, pd)$ and $(p, p^{3}$He) reactions // Phys. Rev.–1974.–Vol.9.–P.2440–2443. DOI: https://link.aps.org/doi/10.1103/PhysRevC.9.2440

[135] Sakamoto Y., Cüer P., Takéutchi F. Quasifree scattering on clustering particles and separation energies // Phys. Rev.–1975.–Vol.11.–P.668–684. DOI: https://link.aps.org/doi/10.1103/PhysRevC.11.668

[136] Giot L., Roussel-Chomaz P., Demonchy C. E. et al. Investigation of $^{6}$He cluster structures // Phys. Rev. C.–2005.–Vol.71.–P.064311. DOI: https://link.aps.org/doi/10.1103/PhysRevC.71.064311

[137] Direkci M., Kucuk Y., Boztosun I. Analysis of Elastic Scattering of 8He+208Pb System at around the Coulomb Barrier Energies // Journal of Physics: Conference Series.–2015.–Vol.590.–P.012058. DOI: https://link.aps.org/doi/10.1088/1742-6596/590/1/012058

[138] Keeley N., Alamanos N., Kemper K.W., Rusek K. Elastic scattering and reactions of light exotic beams // Progr. Part. Nucl. Phys.–2009.–Vol.63.–P.396–447. DOI: https://doi.org/10.1016/j.ppnp.2009.05.003

[139] Wolski R., Sidorchuk S. I., Ter-Akopian G. M. *et al.* Elastic scattering of $^{8}$He on $^{4}$He and $4n$ system // Nucl. Phys. A.–2003–Vol.722.–P.55c–60c. DOI: https://doi.org/10.1016/S0375-9474(03)01335-6

[140] Cugnon J. Computation of $S$-state binding energy and wave functions in a Saxon-Wood potential // Computer Physics Communications.–1973.–Vol.6.–P.17–23. DOI: https://doi.org/10.1016/S0010-4655(84)82446-7

[141] Marqués F. M., Labiche M., Orr N. A. et al. Detection of neutron clusters // Phys. Rev. C.–2002.–Vol.65.–P.044006. DOI: https://link.aps.org/doi/10.1103/PhysRevC.65.044006

[142] Hagino K., Takahashi N., Sagawa H. Strong dineutron correlation in $^{8}$He and $^{18}$C // Phys. Rev. C.–2008.–Vol.77.–P.054317. DOI: https://link.aps.org/doi/10.1103/PhysRevC.77.054317

[143] Wolski R., Roussel-Cliomaz P., Sidorchuk S. I., Ter-Akopian G. M., Search for extremely neutron rich systems // Nuc. Phys. A.–2004.–Vol.738.–P.431–435. DOI: https://doi.org/10.1016/j.nuclphysa.2004.04.080

[144] Novatsky B.G., Nikolsky E.Y., Sakuta S.B. et al. Possible observation of light neutron nuclei in the alpha-particle-induced fission of $^{238}$U // Jetp Lett.–2012.–Vol.96.–P.280–284. DOI: https://doi.org/10.1134/S0021364012170110

[145] von Oertzen W. Dimers based on the $\alpha$+$\alpha$ potential and chain states of carbon isotopes // Z. Phys. A. - Particles and Fields.–1977.–Vol.357.–P.355–365. DOI: https://doi.org/10.1007/s002180050255

[146] Wiringa R. B., Pieper, S. C., Carlson J., Pandharipande V. R. Quantum Monte Carlo calculations of $A = 8$ nuclei // Phys. Rev. C.–2000.–Vol.62.–P.014001. DOI: https://link.aps.org/doi/10.1103/PhysRevC.62.014001

[147] Scharnweber D., Greiner W., Mosel U. The two-center shell model // Nucl. Phys. A.–1971.–Vol.164.–P.257–278. DOI: https://doi.org/10.1016/0375-9474(71)90212-0

[148] Ajzenberg-Selove F. Energy levels of light nuclei $A$ =11-12 // Nucl. Phys. A.–1990.–Vol.506–P.1–158. DOI: https://doi.org/10.1016/0375-9474(90)90271-M

[149] Descouvemont P. Microscopic three-cluster study of the low-energy $^{9}$Be photodisintegration // Eur. Phys. J. A.–2001.–Vol.12.–P.413–419 DOI: https://doi.org/10.1007/s10050-001-8665-1

[150] Bohlen H. G., Blazevic A., Gebauer B. et al. Spectroscopy of exotic nuclei with multi-nucleon transfer reactions // Prog. Part. Nucl. Phys.–1999.–Vol.42.–P.17–26. DOI: https://doi.org/10.1016/S0146-6410(99)00056-3

[151] Freer M., Angélique J. C., Axelsson L. et al. Exotic Molecular

States in $^{12}$Be // Phys. Rev. Lett.–1999.–Vol.82.–P.1383–1386. DOI: https://link.aps.org/doi/10.1103/PhysRevLett.82.1383

[152] Freer M., Angelique J. C., Axelsson L. et al. Helium breakup states in $^{10}$Be and $^{12}$Be // Phys. Rev. C.–2001.–Vol.63.–P.34301. DOI: https://link.aps.org/doi/10.1103/PhysRevC.63.034301

[153] Kanada-En'yo Y., Horiuchi H. Structure of Light Unstable Nuclei Studied with Antisymmetrized Molecular Dynamics // Prog. Theor. Phys.–2001–Vol.142.–P.205–263. DOI: https://doi.org/10.1143/PTPS.142.205

[154] Millener D.J. Structure of unstable light nuclei // Nucl. Phys. A.–2001.–Vol.693.–P.394-410. DOI: https://doi.org/10.1016/S0375-9474(01)00589-9

[155] https://www.nndc.bnl.gov

[156] Fortune H. T., Liu, G.-B., Alburger D. E. $(sd)^2$ states in $^{12}$Be // Phys. Rev. C.–1994.–Vol.50.–P.1355–1359. DOI: https://link.aps.org/doi/10.1103/PhysRevC.50.1355

[157] Alburger D. E., Balamuth D. P., Lind J. M. et al. Core excited $T = 2$ levels in $A = 12$ from studies of $^{12}$Be // Phys. Rev. C.–1978.–Vol.17.–P.1525–1530. DOI: https://link.aps.org/doi/10.1103/PhysRevC.17.1525

[158] Liu G.-B., Fortune H. T. $^{9}$Be(t,p)$^{11}$Be and the structure of $^{11}$Be // Phys. Rev. C.–1990.–Vol.42.–167–173. DOI: https://link.aps.org/doi/10.1103/PhysRevC.42.167

[159] Inomata T., Akimune H., Daito I. et al. Particle decays from $^{12}$B and $^{12}$N mirror nuclei // Phys. Rev. C.–1998.–Vol.57.–P.3153–3166. DOI: https://link.aps.org/doi/10.1103/PhysRevC.57.3153

[160] Daito I., Akimune H., Austin S. M. et al. Gamow-Teller strengths from (t,$^{3}$He) charge-exchange reactions on light nuclei // Phys. Lett. B.–1998.–Vol.418.–P.27–33. DOI: https://link.aps.org/doi/10.1016/S0370-2693(97)01393-2

[161] Thompson I. P. Coupled reaction channels calculations in nuclear physics // Comput. Phys. Rep.–1988.–Vol.7.–P.167–212. DOI: https://doi.org/10.1016/0167-7977(88)90005-6

[162] Itagaki N., Okabe S., Ikeda K., Tanihata I. Molecular-orbital structure in neutron-rich C isotopes // Phys. Rev. C.–2001.–Vol.64.–P.014301. DOI: https://link.aps.org/doi/10.1103/PhysRevC.64.014301

[163] Bassani G., Pappalardo G., Sauner N., Traore B.M. The $^{16}$O first rotational band from the $^{12}$C($^{6}$Li, $d$)$^{16}$O reaction // Phys. Letters B.–1971.–Vol.34.–P.612–614. DOI: https://doi.org/10.1016/0370-2693(71)90152-3

[164] Artemov K.P., Goldberg V.Z., Petrov I.P. et al. Negative-parity states in $^{16}$O populated in the $^{12}$C($^{6}$Li, $d$)$^{16}$O reaction // Phys. Letters B.–1971.–Vol.37.–P.61–64. DOI: https://doi.org/10.1016/0370-2693(71)90571-5

[165] Buck B., Rubio J. A. Revised calculation of alpha-cluster rotational states in $^{16}$O // J. Phys. G: Nucl. Phys.–1984.–Vol.10.–P.L209. DOI: https://doi.org/10.1088/0305-4616/10/9/004

[166] Wozniak G. J., Harney H. L., Wilcox K. H., Cerny J. $\alpha$-Particle Transfer Via the ($^{12}$C, $^{8}$Be // Phys. Rev. Lett.–1972.–Vol.28.–P.1278–1281. DOI: https://link.aps.org/doi/10.1103/PhysRevLett.28.1278

[167] von Oertzen W., Dorsch T., Bohlen H.G. et al. Molecular and cluster structures in $^{18}$O // Eur. Phys. J. A.–2010.–Vol.43.–P.17. DOI: https://doi.org/10.1140/epja/i2009-10894-2

[168] Cunsolo A., Foti A., Imme G. et al. On the $^{18}$O positive-parity rotational band // Phys. Lett. B.–1982.–Vol.112.–P.121–123. DOI: https://doi.org/10.1016/0370-2693(82)90310-0

[169] Pirrie S., Wheldon C., Kokalova T., Bishop J., Faestermann T., Hertenberger R. et al. Search for evidence of rotational cluster bands in $^{18}$O // Physical Review C.–2020.–Vol.102.–P.064315. DOI: https://doi.org/10.1103/physrevc.102.064315 P.064315

[170] Bohlen H.G., von Oertzen W., Milin M. et al. Structures in $^{20}$O from the $^{14}$C($^{7}$Li, $p$) reaction at 44 MeV // Eur. Phys. J. A.–2011.–Vol.47.–P.44. DOI: https://doi.org/10.1140/epja/i2011-11044-1

[171] Furutachi N., Kimura M., Dote A. et al. // Prog. Theor. Phys.–2008.–Vol.119.–P.403–420. DOI: https://doi.org/10.1143/PTP.119.403

[172] Panagiotou A. D., Gove H. E., Harar S. High-Spin States in $^{20}$Ne and Their Possible Classification into Rotational Bands // Phys. Rev. C.–1972.–Vol.5.–P.1995–2006. DOI: https://link.aps.org/doi/10.1103/PhysRevC.5.1995

[173] Freeman R. M., Basrak Z., Haas F. et al. Resonant and nonresonant behavior of the heavy-ion reaction $^{14}$C+$^{12}$C // Phys. Rev. C.–1992.–Vol.46.–P.589–596. DOI: https://link.aps.org/doi/10.1103/PhysRevC.46.589

[174] Curtis N., Caussyn D. D., Chandler C et al. Evidence for a molecular rotational band in the $^{14}$C + $\alpha$ decay of $^{18}$O and the $\alpha$ decay of $^{22}$Ne // Phys. Rev. C.–2002.–Vol.66.–P.024315. DOI: https://link.aps.org/doi/10.1103/PhysRevC.66.024315

[175] Rogachev G. V., Goldberg V. Z., and Lönnroth T. et al. Doubling of $\alpha$-cluster states in$^{22}$Ne // Phys. Rev. C.–2001.–Vol.64.–P.051302. DOI: https://link.aps.org/doi/10.1103/PhysRevC.64.051302

[176] Yildiz S., Freer M., Soić N. et al. $\alpha$-decaying states $^{18}$O, $^{20}$Ne and $^{22}$Ne in $^{18}$O beam induced reactions // Phys. Rev. C.–2006.–73.–P.034601. DOI: https://doi.org/10.1103/PhysRevC.73.034601

[177] Artemov K.P., Goldberg V. Z., Golovkov M. S. et al. Investigation of $\alpha$-Cluster Structure of $^{18}$O Nucleus in the Reaction $^{14}$C($^{6}$Li, $d$)$^{18}$O($\alpha$)$^{14}$C // Yad. Fiz.–1983.–Vol.37.–P.1351.

[178] Freer M., Ahmed S., Ashwood N. I. et al. $^{8}$Be+ $^{14}$C break-up of $^{22}$Ne // J. Phys. G (London).–2006.–Vol.32.–P.2235. DOI: https://dx.doi.org/10.1088/0954-3899/32/11/015

[179] Dufour M., Descouvemont P. Microscopic study of $\alpha$-cluster

states in $^{22}$Ne // Nucl. Phys. A.–2003.–Vol.726.–P.53–66. DOI: https://doi.org/10.1016/j.nuclphysa.2003.07.004

[180] Szanto E. M., de Toledo A. Szanto, Klapdor H. V. et al. Backbending in $^{22}$Ne // Phys. Rev. Lett.–1979.–Vol.42.–P.622-626. DOI: https://link.aps.org/doi/10.1103/PhysRevLett.42.622

[181] Ragnarsson I., Aberg S., Sheline R. K. A new formalism for high spin states applied to the *sd*-shell region // Phys. Scr.–1981.–Vol.24.–P.215–235. DOI: https://link.aps.org/doi/10.1088/0031-8949/24/1B/017

[182] Arima A., Sakakura M., Sebe T. Electromagnetic properties of *sd*-shell nuclei // Nucl. Phys. A.–1971.–Vol.170.–P.273–308. DOI: https://doi.org/10.1016/0375-9474(71)90636-1

[183] Akiyama Y., Arima A., Sebe T. The structure of the sd shell nuclei: (IV). $^{20}$Ne, $^{21}$Ne, $^{22}$Ne, $^{22}$Na and $^{24}$Mg // Nucl. Phys. A.–1969.–Vol.138.–P.273–304. DOI: https://doi.org/10.1016/0375-9474(69)90336-4

[184] Allcock S. C., Rae W. D. M., Keeling P.R. et al. $10^+$ states in $^{20}$Ne // Phys. Lett.–1988.–Vol.138.–P.201–205. DOI: https://doi.org/10.1016/0370-2693(88)90212-2

[185] Betts R.R. Invited Paper Presented at CLUSTER 94 - Clusters in Nuclear Structure and Dynamics, ed. by F. Haas, Strasbourg, France, 1994.

[186] D. Konnerth, W. Trombik, K. G. Bernhardt *et al.* Scattering and reactions of $^{14}$C+$^{14}$C and $^{12}$C+$^{14}$C // Nucl. Phys. A.–1985.–Vol.36.–P.538–560. DOI: https://doi.org/10.1016/0375-9474(85)90085-5

[187] Tanimura O. Distorted wave approach to heavy ion molecular resonance // Z Physik A.–1984.–Vol.319.–P.227–234. DOI: https://doi.org/10.1007/BF01415637

[188] Huizenga J. R. UR-NSRL-90 report, Rochester, 1974.

[189] Filho R. L., Lépine-Szily A., Villari A. C. et al. Effect of $\alpha$-transfer polarization potential in the $^{24}$Mg+$^{16}$O system // Phys. Rev. C.–1989.–Vol.39.–P.884–890. DOI: https://link.aps.org/doi/10.1103/PhysRevC.39.884

[190] Gridnev K.A., Maltsev N.A., Leshakova N.V. Effect of elastic and inelastic cluster transfer on elastic $^{16}$O+$^{12}$C and $^{16}$O+$^{16}$O scattering // Bull. Russ. Acad. Sci. Phys.–2013.–Vol.77.–P.852–856. DOI: https://doi.org/10.3103/S1062873813070113

[191] Rudchik A. T., Stepanenko Yu. M., Kemper K. W., et al. The $^{7}$Li($^{18}$O, $^{16}$N)$^{9}$Be reaction and optical potential of $^{16}$N+$^{9}$Be versus $^{16}$O+$^{9}$Be // Nucl. Phys. A.–2011.–Vol.860.–P.8–21. DOI: https://doi.org/10.1016/j.nuclphysa.2011.05.003

[192] Kyryanchuk V. M., Rudchik A. T., Budzanowski A. et al. One-nucleon transfer reaction $^{9}$Be($^{11B}$,$^{10}$B)$^{10}$Be and optical potential for the $^{10B}$+$^{10}$Be interaction // Nucl. Phys. A.–2003–Vol.726.–P.231–247. DOI: https://doi.org/10.1016/S0375-9474(03)01623-3

[193] Rudchik A. T., Kemper K. W., Rudchik A. A. et al. Tensor analyzing powers and energy dependence of the $^{7}$Li+$^{16}$O interaction // Phys. Rev. C.–2007.–Vol.75.–P.024612. DOI: DOI: https://doi.org/10.1103/PhysRevC.75.024612

[194] Xu Chen, Qi Chong, Liotta, R. J. et al., Molecular structure of highly excited resonant states in $^{24}$Mg and the corresponding $^{8}$Be +$^{16}$ O and $^{12}$C +$^{12}$ C decays // Phys. Rev. C.–2010.–81.–P.054319. DOI: https://link.aps.org/doi/10.1103/PhysRevC.81.054319

[195] Sugimitsu T., Koga K., Ikeda N. et al. The $^{8}$Be+$^{20}$Ne molecular resonances in the $^{16}$O+$^{12}$C collision // Nucl. Phys. A.–1995.-Vol.586.–P.190–200. DOI: https://doi.org/10.1016/0375-9474(94)00489-A

[196] Brack M., Damgard J., Jensen A.S., Pauli H.C., Strutinski V.M., Wong C.Y. Funny Hills: The Shell-Correction Approach to Nuclear Shell Effects and Its Applications to the Fission Process // Rev. Mod. Phys.–1972.–Vol.44.–P.320–405. DOI: https://link.aps.org/doi/10.1103/RevModPhys.44.320

[197] Ragnarsson I., Nilsson S.G., Sheline R.K. Shell structure in nuclei // Phys. Rep.–1978.–Vol.45.–P.1-87. DOI: https://doi.org/10.1016/0370-1573(78)90004-2

[198] Fulton B.R., Rae W.D.M. Fission of light nuclei // J. Phys. G.–1990.–Vol.16.–P.333. DOI: https://dx.doi.org/10.1088/0954-3899/16/3/007

[199] Marsh S., Rae W.D.M. The structure of $^{24}$Mg using the cranked cluster model // Phys. Lett. B.–1986.–Vol.180.–P.185–190. DOI: https://doi.org/10.1016/0370-2693(86)90293-5

[200] A.H. Wuosmaa, In: Anagnostatos G.S., von Oertzen W. (eds) Atomic and Nuclear Clusters. Springer, Berlin, Heidelberg 1995.

[201] Lepareux M., Saunier N., Gerardin C. et al. States at high excitation energies in $^{24}$Mg obtained from Li-induced reactions on $^{20}$Ne // Lett. Nuovo Cimento.–1973.–Vol.8.–P.725–728. DOI: https://doi.org/10.1007/BF02725355

[202] Anantaraman N., Gove H.E., Toke J., Draayer J.P. Alpha particle spectroscopic strengths for levels populated in the $20, 21, 22$Ne($^{6}$Li, $d$)$^{24,25,26}$Mg reactions // Nucl. Phys. A.–1977.–Vol.279.–P.474–492. DOI: https://doi.org/10.1016/0375-9474(77)90581-4

[203] Middleton R., Garrett J. D., Fortune H. T. Selective Population of Highly Excited States Observed in the Reaction $^{16}$O($^{12}$C, $\alpha$)$^{24}$Mg // Phys. Rev. Lett.–1970.–Vol.24.–1436–1438. DOI: https://link.aps.org/doi/10.1103/PhysRevLett.24.1436

[204] Branford D., Gardner N., Wright I.F. Evidence for negative parity rotational bands in $^{24}$Mg // Phys. Lett. B.–1971.–Vol.36.–P.456–458. DOI: https://doi.org/10.1016/0370-2693(71)90528-4

[205] Fifield L. K., Zurmühle R. W., Balamuth D. P. High-Spin States in the Continuum. II. $^{24}$Mg // Phys. Rev. C.–1973.–Vol.8.–P.2217–2231. DOI: https://link.aps.org/doi/10.1103/PhysRevC.8.2217

[206] Lonnroth T., Goldberg V.Z., Guttormsen M. et al. New observation methods for alpha-particle elastic scattering. Microscopic properties of alpha-cluster states // Proc.7th Intern.Conf.on Clustering Aspects of Nuclear Structure and Dynamics, Rab, Island of Rab, Croatia,1999.

[207] Lindgren R.A., Trentelman J.P., Anantaraman N. et al. Odd-parity levels excited in $^{32}$S and $^{36}$Ar via"alpha-particle" transfer // Phys. Lett. B.–1974.–Vol.49.–P.263–265. DOI: https://doi.org/10.1016/0370-2693(74)90429-8

[208] Artemov K. P., Belyanin O. P., Vetoshkin A. L. et al. Effective Method of Study of $\alpha$-cluster states // Sov. J. Nucl. Phys.–1990.–Vol.52.–P.408. **52** (1990) 408.

[209] S. Yu. Torilov Dissertation for the degree of candidate of physical and mathematical sciences "Study of quasi-molecular states of nuclei $^{40,42}$Ca by gamma spectroscopy", St. Petersburg, 2003.

[210] Zheng D. C., Berdichevsky D., Zamick L. Calculations of many-particle–many-hole deformed state energies: Near degeneracies, deformation condensates // Phys. Rev. C.–1988.–Vol.38.–P.437–443. DOI: https://link.aps.org/doi/10.1103/PhysRevC.38.437

[211] Gerace W. J., Green A.M. $K$-band mixing and 8p-8h states in $^{40}$Ca // Nucl. Phys. A.–1969.–Vol.123.–P.241–249. DOI: https://doi.org/10.1016/0375-9474(69)90498-9

[212] Fortune H. T., Al-Jadir M. N. I., Betts R. R. et al. $\alpha$-spectroscopic factors in $^{40}$Ca // Phys. Rev. C.–1979.–Vol.19.–P.756. DOI: https://doi.org/10.1103/PhysRevC.19.756

[213] Jolos R., von Brentano P. Angular momentum dependence of the parity splitting in nuclei with octupole correlations // Phys. Rev. C.–1995.–Vol.49.–P.R2301. DOI: https://doi.org/10.1103/PhysRevC.49.R2301

[214] Jolos R., von Brentano P. Rotational spectra and parity splitting in nuclei with strong octupole correlations // Nucl. Phys. A.–1995.–Vol.587.–P.377. DOI: https://doi.org/10.1016/0375-9474(95)00008-O

[215] Minkov N., Yotov P., Drenska S., Scheid W. Parity shift and beat staggering structure of octupole bands in a collective model for quadrupole – octupole-deformed nuclei // J. Phys. G: Nucl. Part. Phys..–2006.–Vol.32.–P.497. DOI: https://doi.org/10.1088/0954-3899/32/4/008

[216] Leander G.A., Sheline R.K., Moller P. et al. The breaking of intrinsic reflection symmetry in nuclear ground states // Nucl. Phys. A.–1982.–Vol.–388.–P.452–476. DOI: https://doi.org/10.1016/0375-9474(82)90471-7

[217] J.P. Davidson, Collective Models of the Nucleus, Academic, New York, 1968.

[218] Minkov,N., Drenska S. B., Raychev P. P. et al. "Beat" patterns for the odd-even staggering in octupole bands from a quadrupole-octupole Hamiltonian // Phys. Rev. C.–2001.–Vol.63.–P.044305. DOI: https://link.aps.org/doi/10.1103/PhysRevC.63.044305

[219] Pál K.F., Lovas R.G. Local-potential $\alpha$-cluster model for $^{40}$Ca and $^{44}$Ti // Phys. Lett. B.–1980.–Vol.96.–P.19–22. DOI: https://doi.org/10.1016/0370-2693(80)90202-6

[220] Buck B., Merchant A. C., Perez S. M. Theory of band comparison in even-even nuclei // Phys. Rev. C.–2003.–Vol.68.–P.024313. DOI: https://link.aps.org/doi/10.1103/PhysRevC.68.024313

[221] Buck B., Merchant A. C., Perez S. M. Evidence of nuclear clustering throughout a major shell // Phys. Rev. C.–2005.–Vol.71.–P.014311. DOI: https://link.aps.org/doi/10.1103/PhysRevC.71.014311

[222] Buck B., Plit A.A. Alpha-particle and triton cluster states in $^{19}$F // Nucl. Phys. A.–1977.–Vol.280.–P.133–160. DOI: https://doi.org/10.1016/0375-9474(77)90300-1

[223] Yamaya T., Katori K., Fujiwara M. et al. Alpha-Cluster Study of $^{40}$Ca and $^{44}$Ti by the ($^{6}$Li,$d$) Reaction // Progr. Theor. Phys. Suppl.–1998.–Vol.132.–P.73–102. DOI: https://doi.org/10.1143/PTP.132.73

[224] Caurier E., Menéndez J., Nowacki F., Poves A. Coexistence of spherical states with deformed and superdeformed bands in doubly magic $^{40}$Ca: A shell-model challenge // Phys. Rev. C.–2007.–Vol.75.–P.054317. DOI: https://link.aps.org/doi/10.1103/PhysRevC.75.054317

[225] Lyutorovich N., Tselyaev V. Multiphonon structure of high-spin states in

$^{40}$Ca, $^{90}$Zr and $^{208}$Pb // International Journal of Modern Physics E.–2023.–Vol.32.–P.2350025. DOI: https://doi.org/10.1142/S0218301323500258

[226] Chen J. Nuclear Data Sheets for $A$=40 // Nuclear Data Sheets.–2017.–Vol.140.–P.1-376. DOI: https://doi.org/10.1016/j.nds.2017.02.001

[227] Groeneveld K. O., Meyer-Schützmeister L., Richter A., Strohbusch U. Backward - Angle Elastic Scattering of $^{16}$O on $^{40}$Ca and $^{48}$Ca // Phys. Rev. C.–1972.–Vol.–6.–P.805–. DOI: https://link.aps.org/doi/10.1103/PhysRevC.6.805

[228] Goldberg V.Z., Golovkov M.S., Ivanov I. et al. Search for quasi molecular states in the interaction of $^{40}$Ar with light nuclei // Univ.Warsaw, Heavy Ion Lab, Poland–2014.–P.69.

[229] Delbar Th., Grégoire Gh., Paic G. et al. Elastic and inelastic scattering of alpha particles from $^{40,44}$Ca over a broad range of energies and angles // Phys. Rev. C.–1978.–Vol.18.–P.1237–1248. DOI: https://link.aps.org/doi/10.1103/PhysRevC.18.1237

[230] O'Leary C. D., Bentley M. A., Brown B. A. et al. Nonyrast high-spin states in $N = Z^{44}$Ti // Phys. Rev. C.–2000.–Vol.61.–P.064314. DOI: https://link.aps.org/doi/10.1103/PhysRevC.61.064314

[231] Merchant A. C. Alpha particle cluster states in $fp$-shell nuclei // Phys. Rev. C.–1987–Vol.36.–P.778–784. DOI: https://doi.org/10.1103/PhysRevC.36.778

[232] Buck B., Merchant A. C., Perez S. M., Seals H.E. Core-cluster partitions of rare-earth nuclei // Phys. Rev. C.–2007.–Vol.76.–P.014310. DOI: https://link.aps.org/doi/10.1103/PhysRevC.77.017301

[233] Buck B., Merchant A. C., Perez S. M. Alpha-cluster structure in $^{212}$Po // Phys. Rev. Lett.–1994.–Vol.72.–P.1326–1328. DOI: https://link.aps.org/doi/10.1103/PhysRevLett.72.1326

[234] Buck B., Johnston J. C., Merchant A. C., Perez S. M. Cluster model of $\alpha$ decay and $^{212}$Po // Phys. Rev. C.–1996.–Vol.–53.–P.2841–2848. DOI: https://link.aps.org/doi/10.1103/PhysRevC.53.2841

[235] Buck B., Merchant A. C., Horner M. J., Perez S. M. Choosing cluster and core in cluster models of nuclei // Phys. Rev. C.–2000.–Vol.61.–P.024314. DOI: https://link.aps.org/doi/10.1103/PhysRevC.61.024314

[236] Buck B., Merchant A. Perez S. Cluster Selection in Binary Nuclear Models. // Few-Body Systems.–2000.–Vol.29.–P.53–60 DOI: https://doi.org/10.1007/s006010070008

[237] Buck B., Merchant A. Perez S. Coexistence of very dissimilar cluster bands in $^{212}$Po // J. Phys. G: Nucl. Part. Phys.–2004.–Vol.30.–P.65. DOI: https://doi.org/10.1088/0954-3899/30/2/006

[238] Greiner W., Park J.Y., Scheid W. Nuclear Molecules // World Scientific, Singapore 1995.

[239] Hess P. O., Greiner W., Pinkston W. T. Structure of Giant Nuclear Molecules // Phys. Rev. Lett.–1984.–Vol.53.–P.1535–1538. DOI: https://link.aps.org/doi/10.1103/PhysRevLett.53.1535

[240] Hamada Sh., Burtebayev N., Gridnev K.A., Amangeldi N. Analysis of alpha-cluster transfer in $^{16}$O+$^{12}$C and $^{12}$C+$^{16}$O at energies near Coulomb barrier // Nucl. Phys. A.–2011.–Vol.859.–P.29–38. DOI: https://doi.org/10.1016/j.nuclphysa.2011.04.006

[241] Stock R., Jahnke U., Hendrie D. L. et al. Contribution of alpha cluster exchange to elastic and inelastic $^{16}$O + $^{20}$Ne scattering // Phys. Rev. C.–1976.–Vol.14.–P.1824–1831. DOI: https://link.aps.org/doi/10.1103/PhysRevC.14.1824

[242] Burtebayev N., Duisebayev A., Burtebayeva J. et al. Alpha Cluster transfer in the elastic scattering of $^{20}$Ne on $^{16}$O nuclei at an energy of 50 MeV // Univ.Warsaw, Heavy Ion Lab, Poland.–2014.–P.67.

[243] Khoa D.T., Satchler G.R., Von Oertzen W. Nuclear incompressibility and density dependent NN interactions in the folding model for nucleus-nucleus potentials // Phys. Rev. C.–1997.–Vol.56.–P.954–969. DOI: https://link.aps.org/doi/10.1103/PhysRevC.56.954

[244] De Vries H., De Jager C. W., De Vries C. Nuclear charge-density-distribution parameters from elastic electron scattering // Atomic Data Nucl. Data Tables.–1987.–Vol.36.–P.495–536. DOI: https://doi.org/10.1016/0092-640X(87)90013-1

[245] Farnea E., de Angelis G., de Poli M. et al. A $4\pi$ light-charged particle Si detector as a trigger device for in-beam $\gamma$-ray spectroscopy // Nucl. Instrum. Methods Phys. Res. A.–1997.–Vol.400.–87–95. DOI: https://doi.org/10.1016/S0168-9002(97)00906-6

[246] Van der Werf S.Y. On the formalism of multiplicity measurements // Nucl. Instrum. Methods Phys. Res. A.–221.–Vol.153.–P.221–228. DOI: https://doi.org/10.1016/0029-554X(78)90641-9

[247] Wuosmaa A.H., Saini S., Kutt P.H. et al. Resonance behavior in the $^{24}$Mg+$^{28}$Si system // Phys. Rev. C.–1987.–Vol.36.–P.1011–1015. DOI: https://link.aps.org/doi/10.1103/PhysRevC.36.1011

[248] Murthy K. H. N., Gupta S. K., Chatterjee A. Transmission coefficients for light projectiles. // Z Physik A.–1982.–Vol.305.–P.73–79. DOI: https://doi.org/10.1007/BF01415082

[249] Huang P., Grimes S.M., Massey T.N. Level densities for nuclei with 20<A<41 // Phys. Rev.C.–2000.–Vol.62.–P.044311. DOI: https://link.aps.org/doi/10.1103/PhysRevC.62.024002

[250] Pearson J.M. The Quest for a Microscopic Nuclear Mass Formula // Hyperfine Interactions.–2001.–Vol.132.–P.59–74. DOI: https://doi.org/10.1023/A:1011973100463

[251] von Oertzen W. Clusters in Nuclei // Lecture Notes in Physics–Vol.1– ed. C. Beck Berlin: Springer 2011.

[252] Michel F., Albinski, J., Belery P., Delbar Th., Gregoire Gh., Tasiaux B., Reidemeister G. Optical Model Description of $\alpha$+$^{16}$O Elastic Scattering and Alpha-Cluster Structure in $^{20}$Ne, // Phys. Rev. C.–1983.–Vol.28.P.1904-1917. DOI: https://doi.org/10.1103/PhysRevC.28.1904

[253] Ohkubo S., Yamashita K. Parity-doublet $^{16}$O+$^{12}$C cluster bands in $^{28}$Si // Physics Letters B.–2004.–Vol.578.–P. 304–309. DOI: https://doi.org/10.1016/j.physletb.2003.10.076

[254] Nicoli M. P., Haas F. , Freeman R. M., Szilner S., Basrak Z., Morsad A., Satchler G. R., Brandan M. E. Detailed Study and Mean Field Interpretation of $^{16}$O+ $^{12}$C Elastic Scattering at Seven Medium Energies // Phys. Rev. C.–2000.–Vol.61.–P.034609. DOI: https://doi.org/10.1103/PhysRevC.61.034609

[255] Burtebayev N., Batyrbekov E. G., Baktybayev M. K. et al. Alpha cluster transfer in $^{16}$O+ $^{12}$C at energy 41.3MeV // International Journal of Mathematics and Physics Quarterly Journal of al-Farabi Kazakh National University.–2012.–Vol.3–P.189.

[256] Malmin R. E., Siemssen R. H., Sink D. A., Singh P. P. Resonance in $^{12}$C + $^{16}$O Scattering at $E_{\text{c.m.}} \approx 19.7$ MeV // Phys. Rev. Lett.–1972.–Vol.28.–P.1590–1593. DOI: https://link.aps.org/doi/10.1103/PhysRevLett.28.1590

[257] Voos U.C., von Oertzen W., Bock R. Optical-model analysis of the elastic scattering of complex nuclei at low energies // Nucl. Phys. A.–1969.–Vol.135.–P.207–224. DOI: https://doi.org/10.1016/0375-9474(69)90159-6

[258] Vertse T., Pal K.F., Balogh Z. Gamow, a program for calculating the resonant state solution of the radial Schrödinger equation in an arbitrary optical potential // Comput. Phys. Commun.–1982.–Vol.27.–P.309–322. DOI: https://doi.org/10.1016/0010-4655(82)90178-3

[259] Charles P., Auger F., Badawy I., Berthier B., Dost M., Gastebois J., Fernandez B., Lee S.M., Plagnol E. Resonant behaviour of the $^{16}$O-$^{12}$C elastic scattering cross section // Phys. Lett. B.–1976.–Vol.62.–P.289–292. DOI: https://doi.org/10.1016/0370-2693(76)90077-0

[260] Branford, D., Nagorcka, B. N., Newton, J. O. Further evidence for resonance anomalies in the $^{16}$O+$^{12}$C system // J. Phys. G: Nucl. Phys.–1977.–Vol.3.–P.1565–1575. DOI: https://doi.org/10.1088/0305-4616/3/11/012

[261] Jachcinski C. M., Braun-Munzinger P., Berkowitz G. M., Freifelder R. H., Gai M., Renner T. R., Uhlhorn C. D., $^{16}$O+$^{12}$C resonances within the strong

absorption region for $E_{c.m.}$ ≥23 MeV// Phys. Rev. C.–1980.–Vol.22.–P.101–103. DOI: https://doi.org/10.1103/PhysRevC.22.101

[262] Malmin, R .E., Siemssen, R. H., Sink, D. A., Singh, P. P. Resonance in $^{16}$O+$^{12}$C scattering at $E_{c.m.}$ ≈19.7 MeV // Phys. Rev. Lett.–1972.–Vol.28.–P.1590–1593. DOI: https://doi.org/10.1103/PhysRevLett.28.1590

[263] Fröhlich, H., Dück, P., Treu, W., Voit, H. Experimental evidence for dinuclear structure of $^{16}$O+$^{12}$C resonances in the Coulomb barrier region // Phys. Rev. C.–1983.–Vol.27.–P.578–583. DOI: https://doi.org/10.1103/PhysRevC.27.578

[264] Frawley A. D., Roy A., Fletcher N. R., Transparency to the $l$=9 partial wave in the region of the 14.7-MeV resonance in $^{12}$C+$^{16}$O // Phys. Rev. Lett.–1980.–Vol.44.–P.1377–1380. DOI: https://doi.org/10.1103/PhysRevLett.44.1377

[265] Soga F., Schimizu J., Kamitsubo H., Takahashi N., Takimoto K., Wada R., Fujisawa T., Wada T. Intermediate Structures in $^{12}$C+$^{16}$O System Through Alpha-Induced Reactions on $^{24}$Mg // Phys. Rev. C.–1978.–V.18.–P.2457–2464. DOI: https://doi.org/10.1103/PhysRevC.18.2457

[266] Eberhard K. A., Bohn H., Bernhardt K. G. Narrow $I^{\pi} = 10^{+}$ Resonance for $^{12}$C+$^{16}$O in the Region of Strong Absorption // Phys. Rev. Lett.–1979.–Vol.42.–P.432–436. DOI: https://doi.org/10.1103/PhysRevLett.42.432

[267] Hurd J. R., Fletcher N. R., Frawley A. D. Mateja J. F. Intermediate Structures and Their Dominant $l$ Values in $^{16}$O($^{12}$C, $^{8}$Be)$^{20}$Ne Reactions, $E_{c.m.}$=11.5 to 18.6 MeV // Phys. Rev. C.–1980.–Vol.22.–P.528–539. DOI: https://doi.org/10.1103/PhysRevC.22.528

[268] James D. R., Fletcher R. N. Energies and $J$ values of resonances in $^{16}$O($^{12}$C, $^{8}$Be)$^{20}$Ne reactions // Phys. Rev. C.–1979.–Vol.20.–P.560–568. DOI: https://doi.org/10.1103/PhysRevC.20.560

[269] Kato N., Anai K., Tachikawa T., Fujita H., Kimura K., Sugimitsu T., Nakajima Y. Spin alignment in resonant $^{12}$C+$^{16}$O inelastic scattering // Phys.

Lett. B.–1983.–Vol.120.–P.314–318. DOI: https://doi.org/10.1016/0370-2693(83)90452-5

[270] Chapuran T., Balamuth D. P., Wells W. R., Laymon C. M. Bybell D. P. Angular momenta of intermediate width structures in $^{12}$C+$^{16}$O // Phys. Rev. C.–1986.–V.34.–P.2358–2361. DOI: https://doi.org/10.1103/PhysRevC.34.2358

[271] Fröhlich, H., Dück, P., Galster W., Treu W., Voit H., Witt H., Kuhn W., Lee S.M. Oscillations in the excitation function for complete fusion of $^{16}$O+$^{12}$C at low energies // Phys. Lett. B.–1976.–V.64.–P.408–410. DOI: https://doi.org/10.1016/0370-2693(76)90107-6

[272] Katori K., Furuno K., Ooi T. Enhancement of the excitation function for the $0^+$, 6.049-MeV state of $^{16}$O in the reaction $^{12}$C($^{16}$O,$^{12}$C)$^{16}$O // Phys. Rev. Lett.–1978.Vol.40.–P.1489–1493. DOI: https://doi.org/10.1103/PhysRevLett.41.138

[273] Pisanti O., Cirillo A., Esposito S. et al. PArthENoPE: Public algorithm evaluating the nucleosynthesis of primordial elements // Computer Physics Communications.–2008.–Vol.178.–P.956–971. DOI: https://doi.org/10.1016/j.cpc.2008.02.015

[274] Kubono S, Binh D. N., Hayakawa S. et al. Nuclear Clusters in Astrophysics // Nucl. Phys. A.–2010.–Vol.834.–P.647c–650c. DOI: https://doi.org/10.1016/j.nuclphysa.2010.01.113

[275] S Kubono Binh D. N., Hayakawa S. et al. Role of clusters in nuclear astrophysics with Cluster Nucleosynthesis Diagram (CND) // J. Phys.: Conf. Ser.–2013.–Vol.436.–P.012071. DOI: https://doi.org/10.1088/1742-6596/436/1/012071

[276] Glorius J., Langer C., Slavkovska Z. et al. Proton and $\alpha$ capture studies for nuclear astrophysics at GSI storage rings // J. Phys.: Conf. Ser.–2017.–Vol.875.–P.092015. DOI: https://doi.org/10.1088/1742-6596/875/10/092015

[277] Lestinsky M., Andrianov V., Aurand B. et al. Physics book: CRYRING@ESR. // Eur. Phys. J. Spec. Top.–2016.–Vol.225.–P.797–882. DOI: https://doi.org/10.1140/epjst/e2016-02643-6

[278] Jiang C. L., Back B. B., Esbensen H. et al. Origin and Consequences of $^{12}C$ $+^{12}$ $C$ Fusion Resonances at Deep Sub-barrier Energies // Phys. Rev. Lett.–2013.–Vol.110.–P.072701. DOI: https://doi.org/10.1103/PhysRevLett.110.072701

[279] Taniguchi Y., Kimura M. $^{16}$O+$^{12}$C molecular resonances at deep sub-barrier energy // Phys. Lett. B.–2020.–Vol.800.–P.135086. DOI: https://doi.org/10.1016/j.physletb.2019.135086

[280] Rolfs C.E., Rodney W.S. // Cauldrons in the Cosmos University of Chicago Press, 2005.

[281] Fang X., Tan W. P., Beard M. et al. Experimental measurement of $^{12}$C+$^{16}$O fusion at stellar energies // Phys. Rev. C.–2017.–Vol.96.–P.045804. DOI: https://doi.org/10.1103/PhysRevC.96.045804

[282] Diaz-Torres, A., Wiescher, M. Characterizing the astrophysical $S$ factor for $^{12}$C $+^{12}$ C fusion with wave-packet dynamics // Phys. Rev. C.–2018.–V.97.–P.055802. DOI: https://doi.org/10.1103/PhysRevC.97.055802

[283] Christensen P. R., Switkowski Z. E., Dayras R. A. Sub-barrier fusion measurements for $^{16}$O+$^{12}$C // Nucl. Phys. A.–1977.–Vol.280.–P.189–204. DOI: https://doi.org/10.1016/0375-9474(77)90303-7

[284] Cujec B., Barnes C. A. Total reaction cross section for/sup $^{16}$O+$^{12}$C below the Coulomb barrier // Nucl. Phys. A.–1976.–Vol. 266.–P.461–493. DOI: https://doi.org/10.1016/0375-9474(76)90370-5

[285] deSouza R. T., Hudan S., Oberacker V. E. Confronting measured near- and sub-barrier fusion cross sections for $^{20}$O+$^{12}$C with a microscopic method // Phys. Rev. C.–2013.–Vol.88.–P.014602. DOI: https://doi.org/10.1103/PhysRevC.88.014602

[286] Patterson J. R., Nagorcka., Symons G., Zuk W. Extrapolation of the $^{12}$C+$^{12}$C and $^{16}$O+$^{12}$C Reaction Cross Sections to Astrophysical Energies // Nucl. Phys. A.–1971.–Vol.165.–P.545–549. DOI: https://doi.org/10.1038/physci231017a0

[287] Hagino K., Rowley N., Kruppa A T. A Program for coupled channels calculations with all order couplings for heavy ion fusion reactions // Comput. Phys. Commun.–1999.–Vol.123.–P.143–152. DOI: https://doi.org/10.1016/S0010-4655(99)00243-X

[288] Kocak G. Analysis of the fusion cross sections for $^{16,18,20}$O+$^{12}$C systems at low energies // Can. J. Phys.–2019.–Vol.97.–P.803–807. DOI: https://doi.org/10.1139/cjp-2018-0665

[289] Fowler W. A., Caughlan G. R., Zimmerman B. A. Thermonuclear Reaction Rates //Annu. Rev. Astron. Astrophys.–1967.–Vol.5.–P.525–570. DOI: https://doi.org/10.1146/annurev.aa.05.090167.002521

[290] Yakovlev D. G., Gasques L. R., Afanasjev A. V. et al. Fusion reactions in multicomponent dense matter // Phys. Rev. C.–2006.–Vol.74.–P.035803. DOI: https://doi.org/10.1103/PhysRevC.74.035803

[291] Ogura R., Hagino K., Bertulani C. A. Potential model for nuclear astrophysical fusion reactions with a square-well potential // Phys. Rev. C.–2019.–Vol.99.–P.065808. DOI: https://link.aps.org/doi/10.1103/PhysRevC.99.065808

[292] Jenkins D. G., Lister C. J., Carpenter M. P. et al. Candidate superdeformed band in $^{28}$Si // Phys. Rev. C.–2012.–Vol.86.–P.064308. DOI: https://doi.org/10.1103/PhysRevC.86.064308

[293] Shawcross M., Curtis N., Catford W. N. et al. Angular Correlations from the $^{16}$O+$^{12}$C Breakup of $^{28}$Si and $^{12}$C+$^{12}$C Breakup of 24Mg // Phys. Rev. C.–2001.–Vol.63.–P.03431. DOI: https://doi.org/10.1103/PhysRevC.63.034311

[294] Kubono S., Morita K., Tanaka M. H. et al. Highly excited high spin states in 28Si populated through the $^{12}$C($^{20}$Ne,$\alpha$) reaction // Nucl. Phys. A.–1986.–Vol.457.– P.461–476. DOI: https://doi.org/10.1016/0375-9474(86)90389-1

[295] Ashwood N. I., Murgatroyd J. T., Clarke N. M. et al. Evidence for a highly deformed band in $^{12}$C+$^{16}$O breakup of $^{28}$Si // Phys. Rev. C.–2001.–V.63.–P. Art.034315. DOI: https://doi.org/10.1103/PhysRevC.63.034315

[296] Cindro N. The resonant behaviour of heavy-ion systems // Riv. Nuovo Cimento.–1981.–Vol.4.–P.1–64. DOI: https://doi.org/10.1007/BF02740698

[297] Patterson J. R., Nagorcka B. N., Symons G. D et al. Experimental investigation of $^{16}O+^{12}C$ nuclear burning at stellar energies // Nucl. Phys. A.–1971.–Vol.165.–P.545–559. DOI: https://doi.org/10.1016/0375-9474(71)90469-6

[298] Gao C., Kondo K. A deep optical potential and gross resonant structures in low energy $^{16}O+^{12}C$ scattering // Phys. Lett. B.–1997.–V.408.–P.7–11. DOI: https://doi.org/10.1016/S0370-2693(97)00768-5

[299] Gasques, L.R., Afanasjev, A.V., Beard, M. et al. São Paulo potential as a tool for calculating $S$ factors of fusion reactions in dense stellar matter // Phys. Rev. C.–2007.–V.76.–P.045802. DOI: https://doi.org/10.1103/PhysRevC.76.045802

[300] Buck B., Merchant A. C., Perez S. M. Mass-symmetric form for cluster-core potentials // Nucl. Phys. A.–1997.–Vol.614.–P.–129–136. DOI: https://doi.org/10.1016/S0375-9474(96)00448-4

[301] Chamon L. C., Carlson B. V., Gasques L. R. Sao Paulo potential version 2 (SPP2) and Brazilian nuclear potential (BNP) // Comput. Phys. Commun.–2021.–Vol.267.–P.108061. DOI: https://doi.org/10.1016/j.cpc.2021.108061

[302] Rasmussen C. E., Williams C. K. I. Gaussian Processes for Machine Learning // MIT Press. 2006.

[303] Moghadasi A. Study of $^{12}C+^{12}C$ reaction using the new optimized potential // New Astronomy.–2021.–Vol.89.–P.101649. DOI: https://doi.org/10.1016/j.newast.2021.101649

[304] Bertulani C.A. RADCAP: A potential model tool for direct capture reactions // Computer Physics Communications.–2003.–Vol.156.–P.123–141. DOI: https://doi.org/10.1016/S0010-4655(03)00441-7

[305] JiangC. L., Back B. B., Rehm K. E. et al. Heavy-ion fusion reactions at extreme sub-barrier energies // Eur. Phys. J. A.–2021.–Vol.57.– Art.P.235. DOI: https://doi.org/10.1140/epja/s10050-021-00536-2

[306] Jiang C. L. A modified-Wong formula for heavy-ion fusion reactions // Eur. Phys. J. A.–2022.–Vol.58.–P. Art.72. DOI: https://doi.org/10.1140/epja/s10050-022-00703-z

[307] Kocak G., Karakoc M., Boztosun I., Balantekin A.B. Effects of $\alpha$-cluster potentials for the $^{16}$O $+^{16}$ O fusion reaction and $S$ factor // Phys. Rev. C.–2010.–Vol.81.–P024615. DOI: https://link.aps.org/doi/10.1103/PhysRevC.81.024615

[308] Michaud G., Fowler W. A. Thermonuclear-Reaction Rates at High Temperature // Phys. Rev. C.–1970.–Vol.2.–P.2041-2049. DOI: https://doi.org/10.1103/PhysRevC.2.2041

[309] Michaud G., Scherk L., Vogt E. Nuclear Optical Model and Wave Properties: Barrier Penetration, Reflection, Absorption, and Resonance // Phys.Rev.C.–1970.–Vol.1.– P.864–. DOI: https://doi.org/10.1103/PhysRevC.1.864

[310] Salvat F., Fernndez-Varea J. M. radial: A Fortran subroutine package for the solution of the radial Schrödinger and Dirac wave equations // Comput. Phys. Commun.–2019.–Vol.240.–P.165–177. DOI: https://doi.org/10.1016/j.cpc.2019.02.011

[311] https://www-nds.iaea.org/exfor/

[312] Gasques L. R., Brown E. F., Chieffi A. et al. Implications of low-energy fusion hindrance on stellar burning and nucleosynthesis // Phys. Rev. C.–2007.–Vol.76.–P.035802. DOI: https://doi.org/10.1103/PhysRevC.76.035802

[313] Montagnoli G., Stefanini A. M., Jiang C. L. et al. Fusion of $^{12}$C $+^{24}$ Mg far below the barrier: Evidence for the hindrance effect // Phys. Rev. C.–2020.–Vol.101.–P.044608. DOI: https://doi.org/10.1103/PhysRevC.101.044608

**Appendix**

List of publications on the topic of the dissertation

1. Gridnev K.A., Torilov S. Yu., Gridnev D.K., Kartavenko V.G., Greiner W. Model of binding alpha-particles and applications to superheavy elements // Int. Journal Mod. Phys. E.–2005.–Vol.14.–P.635–643. DOI: https://doi.org/10.1142/S0218301305003387

2. Gridnev K.A., Torilov S. Yu., Kartavenko V.G., Greiner W. Model of binding alpha-particles and structure of the light nuclei // Int. Journal Mod. Phys. E.–2007.–Vol.16.–P.1059–1063. DOI: https://doi.org/10.1142/S0218301307006502

3. Torilov S.Yu., Gridnev K.A., Greiner W. Chain configuration in light nuclei // Int. Journal Mod. Phys. E.–2007.–Vol.16.–P.1757–1764. DOI: https://doi.org/10.1142/S0218301307006927

4. Gridnev K.A., Torilov S.Y. Ikeda diagram within the model of binding alpha particles // Phys. Atom. Nuclei.–2006.–Vol.69–P.1204–1206. DOI: https://doi.org/10.1134/S1063778806070179

5. Gridnev K. A., Torilov S. Y., Gridnev D. K. et al. Model of binding alpha-particles and applications to superheavy elements // Eur. Phys. J. A.–2005.–Vol.25.–Suppl.1.–P.609–610. DOI: https://doi.org/10.1140/epjad/i2005-06-020-6

6. Gridnev K.A., Torilov S.Yu., Kartavenko V.G.et al. The threshold states in the frame of the model of binding alpha particles // Proc. 5-th Conference on nuclear and particle physics Cairo, Egypt 2005.

7. Gridnev K.A., Torilov S.Yu., Kartavenko V.G.et al. Nuclear model of binding alpha-particles// arXiv:nucl-th/0408031 [nucl-th] 2004.

8. Torilov S.Yu., Gridnev K.A., Greiner W. New insight on the chain states and Bose-Einstein condensate in light nuclei // Int. Journal Mod. Phys. E.–2008.–Vol.17.–P.2150–2154. DOI: https://doi.org/10.1142/S0218301308011252

9. Gridnev K.A., Torilov S.Yu. Superdeformation in light alpha-particle nuclei // Theor. phys. Samara University.–2007.–Vol.8.–P.9–16.

10. Kumbartzki G. J., Benczer-Koller N., Burcher S. et al. Transition from collectivity to single-particle degrees of freedom from magnetic moment measurements on $^{82}_{38}Sr_{44}$ and $^{90}_{38}Sr_{52}$ // Phys. Rev. C.–2014.–Vol.89.–P.064305. DOI: https://link.aps.org/doi/10.1103/PhysRevC.89.064305

11. Chulkov L.V., Aksouh F., Bleile A. et al. Quasi-free scattering with $^{6,8}$He beams // Nucl. Phys. A.–2005.–Vol.759.–P.43–63. DOI: https://doi.org/10.1016/j.nuclphysa.2005.05.148

12. Bohlen H.G., Kalpakchieva R., von Oertzen W. et al. Structure studies of neutron-rich beryllium and carbon isotopes // Nuc. Phys. A.–2003.–Vol.722.–P.c3–c9. DOI: https://doi.org/10.1016/S0375-9474(03)01327-7

13. Bohlen H.G., von Oertzen W., Kalpakchieva R. et al. Structure of neutron-rich Be and C isotopes // Phys. Atom. Nuclei.–2003.–Vol.66.–P.1494–1500. DOI: https://doi.org/10.1134/1.1601755

14. Bohlen H.G., Kalpakchieva R., Gebauer B. et al. Spectroscopy of particle-hole states of $^{16}$C // Physical Rev. C.–2003.–Vol.68.–P.054606. DOI: https://doi.org/10.1103/PhysRevC.68.054606

15. Bohlen H.G., von Oertzen W., Kalpakchieva R. et al. Structure studies of neutron-rich beryllium and carbon isotopes. // APH N.S., Heavy Ion Physics.–2003.–Vol.18.–P.179–184. DOI: https://doi.org/10.1556/APH.18.2003.2-4.10

16. Bohlen H.G., Kalpakchieva R., von Oertzen W. et al. Particle-hole structures of neutron-rich Be- and C-isotopes // Nuclear Phys. A.–2004.–Vol.734.–P.345–348. DOI: https://doi.org/10.1016/j.nuclphysa.2004.01.063

17. Zherebchevsky V.I., Torilov S.Y., Andronenkov A. N. et al. Elastic scattering of alpha particles by a neutron-rich nucleus $^{14}$C // Vestnik SPBGU.–2013.–Ser.4.–Vol.1–P.233.

18. Torilov S. Yu., Brenner M., Goldberg V. Z. et al. High-spin states in $^{22}$Ne // arXiv:1001.4285v1 [nucl-ex] 2010.

19. Torilov S.Y., Brenner M., Goldberg V.Z. et al. High-spin states in $^{22}$Ne populated in the $^{14}$C($^{12}$C,$\alpha$) reaction // Eur. Phys. J. A.–2011.–Vol.47.–P.158. DOI: https://doi.org/10.1140/epja/i2011-11158-4

20. Torilov S. Yu., Zherebchevsky V. I., Gridnev K. A., Lazarev V. V. Modeling the decay of nuclear systems formed in reactions with heavy ions // Vestnik SPBGU.–2011.–Ser.4.–Vol.2–P.49.

21. Torilov S.Y., Gridnev K.A., Zherebchevsky V.I. et al. Cluster states in the neutron excess nucleus $^{22}$Ne // Jetp Lett.–2011.–Vol.94.–P.6–10. DOI: https://doi.org/10.1134/S0021364011130170

22. Torilov S.Y., Maltsev N.A., Goldberg V.Z. et al. Quasimolecular states in a reaction with carbon isotopes // Jetp Lett.–102, 69–72 (2015). https://doi.org/10.1134/S0021364015140118

23. Torilov S.Y., Maltsev N.A., Zherebchevsky V.I. et al. Resonant and non-resonant yield from the reaction with neutron excess carbon isotopes // Vestnik SPBGU.–2015.–Ser.4.–Vol.2–P.319.

24. Torilov S.Y., Maltsev N.A., Goldberg V.Z. et al. Decay of quasimolecular states in $^{26}$Mg // Bull. Russ. Acad. Sci. Phys.–2016.–Vol.80.–P.871–874. DOI: https://doi.org/10.3103/S1062873816080384

25. Lonnroth T., Goldberg V.Z., Guttormsen M. et al. New observation methods for alpha-particle elastic scattering. Microscopic properties of alpha-cluster states // Proc.7th Intern.Conf.on Clustering Aspects of Nuclear Structure and Dynamics, Rab, Island of Rab, Croatia,1999.

26. Goldberg V.Z., Rogachev G.V., Brenner M. et al. Observation of an $\alpha$-cluster structure in $^{36}$Ar // Phys. Atom. Nuclei.–2000.–Vol.63.–P.1518–1526. DOI: https://doi.org/10.1134/1.1312885

27. Nurmukhanbetova A. K., Goldberg V.Z., Nauruzbayev D. K. et al. Implementation of TTIK method and time of flight for resonance reaction studies at

heavy ion accelerator DC-60 // Inst. Meth. Phys. Res. A.–2017.–Vol.847.–P.125–129. DOI: https://doi.org/10.1016/j.nima.2016.11.053

28. Goldberg V.Z., Golovkov M.S., Ivanov I. et al. Search for quasi molecular states in the interaction of $^{40}$Ar with light nuclei // Univ.Warsaw, Heavy Ion Lab, Poland–2014.–P.69.

29. Torilov S., Thummerer S., von Oertzen W. et al. Spectroscopy of $^{40}$Ca and negative-parity bands // Eur. Phys. J. A.–2004.–Vol.19.–P.307–317. DOI: https://doi.org/10.1140/epja/i2003-10126-y

30. Torilov S., Thummerer S., von Oertzen W. et al. $\gamma$-spectroscopy of $^{40}$Ca and $^{42}$Ca // Ann. Rep. Lab. Nazionali di Legnaro.–2001.–P.8.

31. Torilov S.Yu.The alpha-particle structure of rotational bands in $^{40}$Ca // Vestnik SPBGU.–2009.–Ser.4.–Vol.2–P.156.

32. Torilov S.Yu. Energy splitting of the states in the rotational bands in $^{40}$Ca // Eur. Phys. J. A –2014.–Vol.50.–P.3. DOI: https://doi.org/10.1140/epja/i2014-14003-4

33. Torilov S. Yu., Gridnev K. A., Korovitskaya T. V. Rotational bands in light neutron-rich nuclei // Bull. Rus. Acad. Sci. Phys.–2012.–Vol.76.–P.854–856. DOI: https://doi.org/10.3103/S1062873812080278

34. Torilov S.Y., Gridnev K.A., Korovitskaya T.V. Cluster states in neutron-rich nuclei // Bull. Russ. Acad. Sci. Phys.–2013,–Vol.77.–P.849–851. DOI: https://doi.org/10.3103/S1062873813070253

35. Burtebayev N., Duisebayev A., Burtebayeva J. et al. Alpha Cluster transfer in the elastic scattering of $^{20}$Ne on $^{16}$O nuclei at an energy of 50 MeV // Univ.Warsaw, Heavy Ion Lab, Poland.–2014.–P.67.

36. Burtebayev N., Batyrbekov E. G., Baktybayev M. K. et al. Alpha cluster transfer in $^{16}$O+ $^{12}$C at energy 41.3MeV // International Journal of Mathematics and Physics Quarterly Journal of al-Farabi Kazakh National University.–2012.–Vol.3–P.189.

37. Burtebayev N., Amangeldi N., Alimov D. et al. Scattering of $^{15}$N Ions by $^{10,11}$B Nuclei at the Energy of 43 MeV // Acta Phys. Polon. Supp.–2018.–Vol.11.–P.99. DOI: https://doi.org/10.5506/APhysPolBSupp.11.99

38. Kokalova T., von Oertzen W., Torilov S. et al. Emission of unbound $^{8}$Be and $^{12}$C* (0+2) clusters in compound nucleus reactions // Eur. Phys. J. A–2005.–Vol.23–P.19–31. DOI: https://doi.org/10.1140/epja/i2004-10071-3

39. Torilov S.Y., Maltsev N.A., Zherebchevsky V.I. et al. A Study of Resonance States in Nuclear Systems Formed in Reactions with Heavy Ions // Phys. Part. Nuclei–2022.–Vol.53.–P.403–408. DOI: https://doi.org/10.1134/S1063779622020836

40. Lestinsky M., Andrianov V., Aurand B. et al. Physics book: CRYRING@ESR. // Eur. Phys. J. Spec. Top.–2016.–Vol.225.–P.797–882. DOI: https://doi.org/10.1140/epjst/e2016-02643-6

41. Glorius J., Langer C., Slavkovska Z. et al. Proton and $\alpha$ capture studies for nuclear astrophysics at GSI storage rings // J. Phys.: Conf. Ser.–2017.–Vol.875.–P.092015. DOI: https://doi.org/10.1088/1742-6596/875/10/092015

42. Torilov S.Y., Maltsev N.A., Zherebchevsky Analyzing Resonance States in Describing the Astrophysical $S$-Factor for Heavy Ion Fusion Reaction $^{16}$O+$^{12}$C // Bull. Russ. Acad. Sci. Phys.–2022.–Vol.86.–P.966–970. DOI: https://doi.org/10.3103/S106287382208024X

43. Torilov S.Yu., Maltsev N.A., Zherebchevsky V.I. Studying Low-Energy Resonances in the $^{16}$O+$^{12}$C System // Bull. Russ. Acad. Sci. Phys.–2021.–V.85.–P.548–551. DOI: https://doi.org/10.3103/S1062873821050233

44. Torilov S.Y., Maltsev N.A., Zherebchevsky V.I. Astrophysical $S$-Factor in the Model of a Square Potential Well // Bull. Russ. Acad. Sci. Phys.–2023–Vol.87.–P.1217–1220 DOI: https://doi.org/10.3103/S1062873823703124